

**Effect of Compaction Parameters and
Sintering Configurations on the
Performance of ZnO Varistor**

A N Mustafizul Karim

Ph.D.


1996

Dublin City University

To
my parents

Declaration

I hereby certify that this material, which I now submit for assessment on the programme of study leading to the award of *Doctor of Philosophy* is entirely my own work and has not been taken from the works of others save and to the extent that such work has been cited and acknowledged within the text of my work.

Signed 
A N Mustafizul Karim

ID No. 92700624

Date: September 25, 1996

ACKNOWLEDGEMENTS

The author wishes to express his sincere appreciation and gratitude to Prof. M. S. J. Hashmi, D. Sc., Head of the School of Mechanical and Manufacturing Engineering for his supervision, guidance and his constructive suggestion and encouragement during the course of this study. I would like to take the opportunity to extend my gratitude to Dr. M A El-Baradie of the same School for his supervision, advice and encouraging suggestions.

I am greatly indebted to Dr. Ramon Puyane, Harris Ireland Limited for the continued assistance, support, valuable advice and supervision in different phases of the project work. I would like to thank Professor B. Mills of Liverpool John Moores University to agree to act as my external examiner.

There are a number of people without whose direct and indirect support and co-operation the investigation would become difficult. I would like to acknowledge the help from Tom Walsh, Liam Domican, Lesley Lawlor of the School.

It should be mentioned here that the substantial part of the project work had been conducted in Harris Ireland Limited and the author is highly indebted to the authority for extending the support in various ways. I must appreciate Sean Corbally for making the technical support available from the tool room.

My appreciation is due to Pat Bellew of Harris Ireland for his help at various stages of the experiment and to James Blaney for his help in drawing the floating die set. Sincere thanks are also extended to Sean Moynihan for his guidance in computer applications and to Brendan Mulholland, Peter O'Connell, Liam Cravan for their help in conducting the experiment. I must remember the names of the BRITE team members with whom I had frequent interactions during the three year period.

The works contained in the thesis have been performed as part of the DOCERPO project under BRITE/EURAM programme, the acronym of which is Basic Research for Industrial Technology in Europe/European Research on Advanced Materials. The author gratefully acknowledges the financial support provided by the European Commission under the contract number: BRE2.CT92.0148.

I would like to offer my sincere thanks to all the Bangladeshi families and friends for their love and care through these years. In this regard I am specially thankful to M Ahemd and his family.

I would like to express my sincere thanks and gratitude to my friends here in Ireland and relatives back at home for their good wishes. In this respect I remember Prof. Anwarul Haque whose past advice and encouragement have kept my morale up during the course of this tedious task.

Last but not least, I must gratefully remember the patient support, encouragement from my wife, Shahida, throughout this long process.

Effect of Compaction Parameters and Sintering Configurations on the Performance of ZnO Varistor

A N Mustafizul Karim

ABSTRACT

Zinc oxide varistors are electronic ceramic devices processed through conventional ceramic technique. Its primary function is to protect an electrical circuit by limiting transient surges repeatedly without failing thereby enhancing the system reliability. There are various critical parameters of varistors, defined to evaluate the performance characteristics. Investigating the influence of the compaction and other processing variables and their optimization in terms of the performance characteristics were the primary objectives of this project.

Enhanced energy absorption capability of the varistor is highly beneficial either in increasing the reliability of the device and of the system or in reducing its volume providing the same level of protection. Varistor discs capable of absorbing more energy will aid in reducing the cost or be suitable for more demanding applications. Evaluation of the effect of compaction parameters was carried out by varying the pressing load and speed. The influence of holding times in pressing cycle was also studied. In addition to the energy absorption capability, some other important properties of the varistor were also investigated.

Statistical approaches such as the response surface methodology and factorial design of experiments were adopted to develop necessary mathematical models on the basis of the experimental data. The reliability of the models were also verified.

A correlation of the physical property and the electrical performance of the ZnO varistor with the sintering orientation was established. The analysis by extensive measurement of the microhardness revealed a relationship between the hardness and grindability of varistor. The tensile strength measured on the disc shaped sections of the arrester block was also found to differ significantly. The density gradient of the sintered disc shows a remarkable influence of the sintering orientation of the disc. By microstructural analysis the observed difference was confirmed.

A few alternative methods have been suggested to overcome the adverse effects arising from the sintering orientation. In this regard horizontal sintering on Vee-groove support was found to be advantageous. Influence of the surface to volume ratio was evaluated by converting the cylindrical discs into hexagonal shape by grinding. A new design with a hexagonal shape has been proposed.

The fracture mechanism of the varistor in a high amplitude short duration (HASD) test was studied and a significant role of the stress wave was observed. The celerity measured by a laser beam based technique through the varistor material was found to be in good agreement with the theoretical prediction. An experimental study also revealed the effect of the stress wave. This understanding will lead to a new approach in combating the fracture from the high current pulse.

CONTENTS

	Page
ACKNOWLEDGEMENTS	i
ABSTRACT	ii
Chapter 1 INTRODUCTION	
1.1 General Overview of Varistor	1
1.2 Sources of Transient Surges	2
1.2.1 Repeatable Transient	3
1.2.2 Random Transients	6
1.3 Transient Protection Technology	9
1.3.1 Voltage Clamping Devices	10
1.3.2 Comparative Scenario of Different Suppressors	12
1.4 Basic Properties of Zinc Oxide Varistor	14
1.4.1 The I-V Characteristics	15
1.4.2 Microstructure of ZnO Varistor	18
1.4.3 Principle of Operation	21
1.5 Application of Zinc Oxide Varistor	24
1.5.1 Functional Parameters of Varistor	27
1.6 Scope of the Present Study	30
Chapter 2 LITERATURE SURVEY	
2.1 Introduction	34
2.2 Brief Description of Ceramic Processing	34
2.2.1 Manufacturing Process of Zinc Oxide Varistor	35
2.2.2 General Phenomena of Compaction Process	38
2.2.3 Factors Influencing Compaction	41
2.3 Objective of the study	50
Chapter 3 EXPERIMENTAL PROCEDURE AND EQUIPMENT	
3.1 Introduction	51
3.2 Preparation of Samples	52
3.2.1 Small Size Arrester disc	53
3.2.2 Standard Arrester Block	54
3.3 Electrical Characterization	56
3.3.1 Current-Voltage Characterization	56
3.3.2 Energy Absorption Capability	58
3.3.3 High Current Performance	60
3.4 Mechanical Characterization	63
3.4.1 Density Gradient	64
3.4.2 Microhardness	64
3.4.3 Diametral Compression Test	64

3.4.4	Microstructural Analysis	65
3.5	Electrical Equipment	66
3.5.1	High Voltage Test System	66
3.5.2	Watt Loss High Temperature Tester	67
3.5.3	Classifier	67
3.5.4	Electrical Strength Tester	68
3.5.5	High Current Tester	69
3.6	Mechanical Tools and Equipment	70
3.6.1	Uniaxial Floating Die	70
3.6.2	Microhardness Tester	71
3.6.3	Instron Machine	71
3.6.4	Hydramet Compacting Press	71
Chapter 4	COMPACTION PARAMETERS - STRESS, SPEED AND DURATION OF DWELL	
4.1	Introduction	73
4.2	Stress and Speed-Effect on Physical Property	74
4.2.1	Brief Description of the Physical Parameters	75
4.2.2	Observation and Analysis of the Effects	77
4.2.3	Summary of the Effects on Physical Properties	84
4.3	Compacting Stress and Speed- Effect on the Electrical Property	85
4.3.1	Investigated Electrical Characteristics	87
4.3.2	Energy Absorption Capability	91
4.4	Microstructural Analysis	96
4.5	Dwell in Pressing Cycle	101
4.5.1	Investigated Physical and Electrical Properties	104
4.5.2	Investigated I-V Characteristics	106
4.5.3	Energy Absorption Capability	113
4.5.4	High Current Performance	119
4.5.5	Replicate Experiment with Dwell Time	122
Chapter 5	FORMULATION OF A MATHEMATICAL MODEL	
5.1	Introduction	124
5.1.1	Factorial Design	124
5.1.2	Response Surface Methodology	125
5.2	Mathematical Modeling	126
5.2.1	Factorial Design with Duration of Dwell	126
5.2.2	RSM with Compacting Stress and Speed	129
Chapter 6	SINTERING CONFIGURATION AND THE PROPERTIES OF ARRESTER DISCS	
6.1	Introduction	139
6.1.1	Sintering Configuration	140
6.2	Microhardness and Grindability	140
6.2.1	Need for Grinding Operation	141

6.2.2	Results	147
6.2.3	Discussion	152
6.3	Sintering Orientation and Tensile Strength	153
6.4	Sintering Orientation and Density Gradient	154
6.5	Microstructural Analysis	156

Chapter 7 ALTERNATIVE SINTERING CONFIGURATION, DESIGN AND ANALYSIS OF FRACTURE

7.1	Introduction	160
7.2	Alternative Sintering Configuration	161
7.2.1	Experimental Procedure	162
7.2.2	Performance in Grinding Operation	164
7.2.3	Energy Absorption Capability	166
7.2.4	High Current Performance	169
7.3	Assessment of Unground Face and Liner Material	170
7.3.1	Energy Absorption Capability	171
7.3.2	Observation and Discussion	172
7.4	Effect of Margin on Electrode	174
7.4.1	Energy Absorption Capability	175
7.4.2	Spin-off Observation on Bismuth Contamination	176
7.5	Hexagonal Discs- Effect of Modified Geometry	178
7.5.1	Sample Preparation and Evaluation of Energy	179
7.5.2	Effect of Higher S/V Ratio on Varistor Life	181
7.5.3	Scope of Versatility in Application	183
7.6	Stress Wave in High Current Impulse	184
7.6.1	Brief Overview of Stress Waves in Solid	185
7.6.2	Comparison of Fracture Originated by a Stress Wave and High Current Pulse	187
7.6.3	Speed of Stress Wave in ZnO Varistor Material	189
7.6.4	Reflection of Stress Waves and Observed Influence in High Current Pulse	192

Chapter 8 CONCLUSIONS AND RECOMMENDATION

8.1	Conclusions	196
8.2	Thesis Contribution	202
8.3	Recommendation for Future Work	203

REFERENCES		206
-------------------	--	-----

APPENDIX A	ASSEMBLY DRAWING OF FLOATING DIE
APPENDIX B	CALCULATION PROCEDURE FOR RSM
APPENDIX C	LIST OF PUBLICATIONS

Chapter 1

INTRODUCTION

1.1 GENERAL OVERVIEW OF VARISTOR

The name varistor, for a variable resistor, is broadly used to cover a variety of devices whose electrical resistance is a non-linear function of the applied voltage. They are non-ohmic in nature as their electrical characteristics do not follow Ohm's law. These devices can be either bidirectional or unidirectional depending upon whether they are capable of carrying current in two or in one direction. However, varistors used for transient overvoltage suppression are commonly bidirectional or symmetrical devices. They are composed of polycrystalline semiconductor materials generally packaged in a sandwich fashion providing a terminal on both surfaces of the semiconductive material. The material choice, its cross-sectional area and thickness and its processing parameters during manufacture determine the electrical characteristics of a varistor.

Zinc oxide varistors are electronic ceramic devices, the primary function of which is to protect the electrical systems by sensing and limiting transient surges and to do so repeatedly without being destroyed¹. In general, electrical properties of varistors are controlled by the physical dimensions of the varistor body which is sintered in various forms such as discs, chips and tubes. The energy rating is determined by volume, voltage rating by thickness or the current flow path length, and current capability by area measured normal to the direction of current flow. However, considerable variation in electrical properties is possible by microstructural changes obtained through altering the chemical formulation and/or the sintering parameters.

In recent years the surge arrester with metal-oxide varistors has become the standard for overvoltage protection at all power system voltage levels²⁻⁶. Traditional arresters with spark gaps and silicon carbide resistors are hardly used now-a-days. Zinc Oxide

varistors have been experiencing a growing demand because of their superior features. Present day telecommunication and automotive systems are being increasingly equipped with electronic circuit having modern miniaturized solid state devices which are more sensitive to voltage surges (spikes and transients). The recent trend of such growth can be visualized by an example of ever increasing use of electronic circuits in the automotive industry⁷ as shown in Figure 1.1.

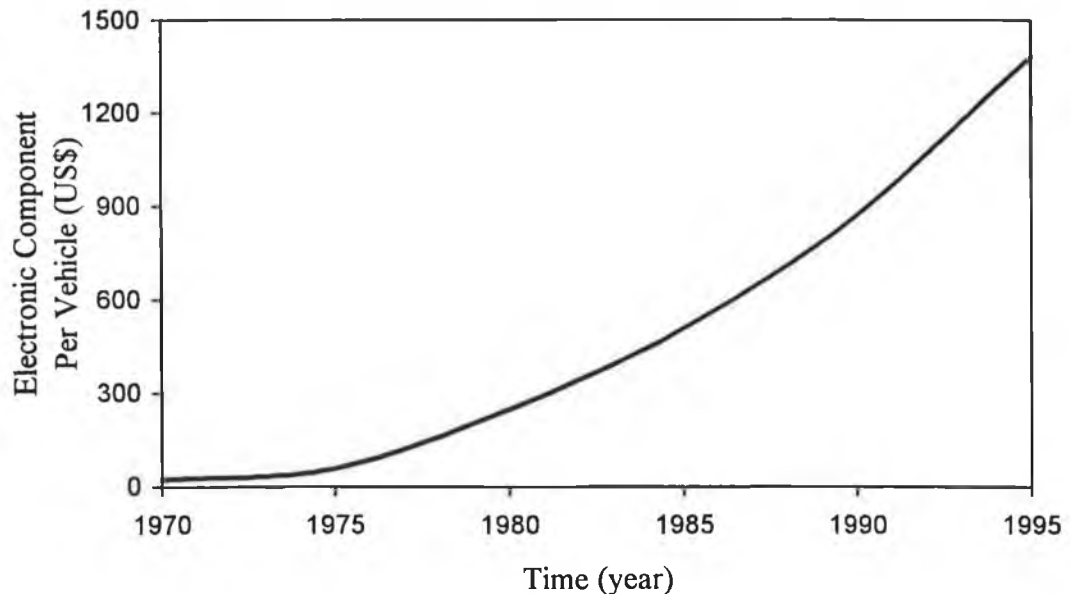


Figure 1.1 Trend of electronic component cost integrated in an automobile

To secure the functional reliability of such sensitive electronic components, transient protection technology is progressing rapidly introducing the ZnO varistor with new configurations to fit the requirements of the wide range of applications.

1.2 SOURCES OF TRANSIENT SURGES

There are numerous sources of transient surges which occur in electrical circuits. These may result from the sudden release of previously stored energy. This energy can be accumulated within the circuit and released by a voluntary or controlled switching action or it can be stored outside the circuit and be injected or coupled into the circuit of interest by some action beyond the control of the circuit designer.

Transient problems arise frequently from the power source feeding the circuit. These transients create the most consternation because it is difficult to define their amplitude, duration and energy content. They can also originate from switching parallel loads on the same branch of a distribution system.

Lightning is another major source of severe transient surges. For millions of years, our planet has experienced continuous activity of atmospheric electrical disturbances. The extent of this activity is enormous and it is estimated that about 2000 thunderstorms are always in progress throughout the world and about 100 lightning flashes strike the earth every second⁸.

The estimated average energy dissipated per unit length of channel, in a single lightning stroke is 10^5 joules per meter. On the average lightning stroke is 3 km long delivering a total expected energy of 3×10^8 joules per stroke. There are usually multiple strokes in a lightning flash the average being four. Thus a huge quantity of electrical energy (more than a trillion kwh per year) is being dissipated to the earth through the lightning stroke.

Transients may occur either in a repeatable fashion or as random impulses. Repeatable transients such as communication voltage spikes, inductive load switching, etc. are more commonly observed. These transients are less dangerous as they can be defined and suppressed without much difficulty. Random transients are more problematic as they may occur at unpredictable times and at remote locations. Gathered data and experience can provide the necessary guidelines of the transient environments in low voltage AC power circuits, telecommunications equipment and automotive electrical systems.

1.2.1 REPEATABLE TRANSIENTS

There are a few recognized sources of repeatable transients. A sudden change in the electrical conditions of any circuit causes a transient voltage to be generated from the energy stored in the circuit inductance and capacitance. The rate of change in current

in an inductor generates a voltage. It is this effect that accounts for most switching-induced transient overvoltages. On switching loads and under fault conditions the overvoltage occurs as commutating spikes in power conversion circuits. But the effect of one switching operation can be repeated several times as arcing may occur at the contact gap of the switch. Some examples of the repeatable transients are briefly described.

Energizing the Transformer Primary

When a transformer is energized at the peak of the supply voltage, the coupling of this voltage step function to the stray capacitance and inductance of the secondary winding can generate an oscillatory transient voltage. The peak amplitude of the transient can be up to twice the normal peak secondary voltage⁹ as shown in Figure 1.2. Subsequent oscillations depend on the inductance (L) and capacitance (C) of the circuit.

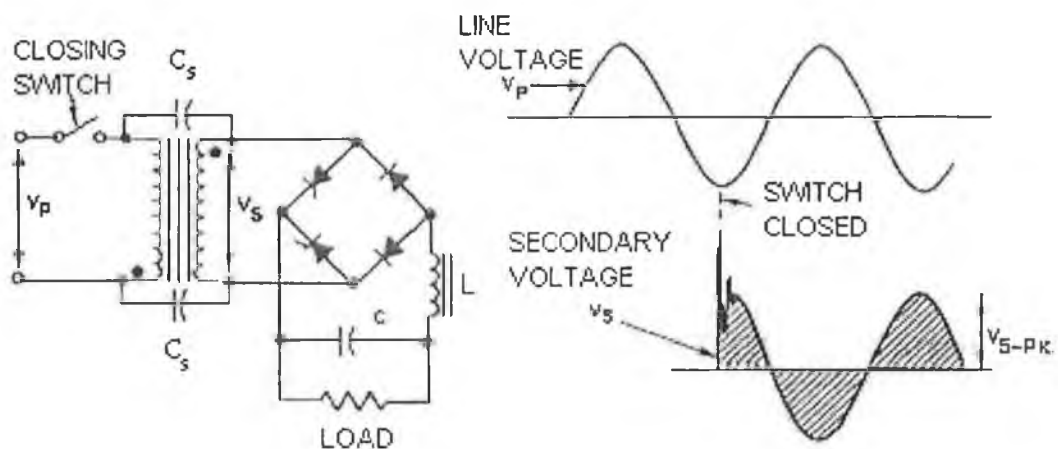


Figure 1.2 Voltage transient caused by energizing transformer primary

De-energizing the Transformer Primary

The opening of the primary circuit of a transformer generates extreme voltage transients⁹, especially if the transformer drives a high impedance load. Surges in excess of ten times normal voltage have been recorded across power semiconductors

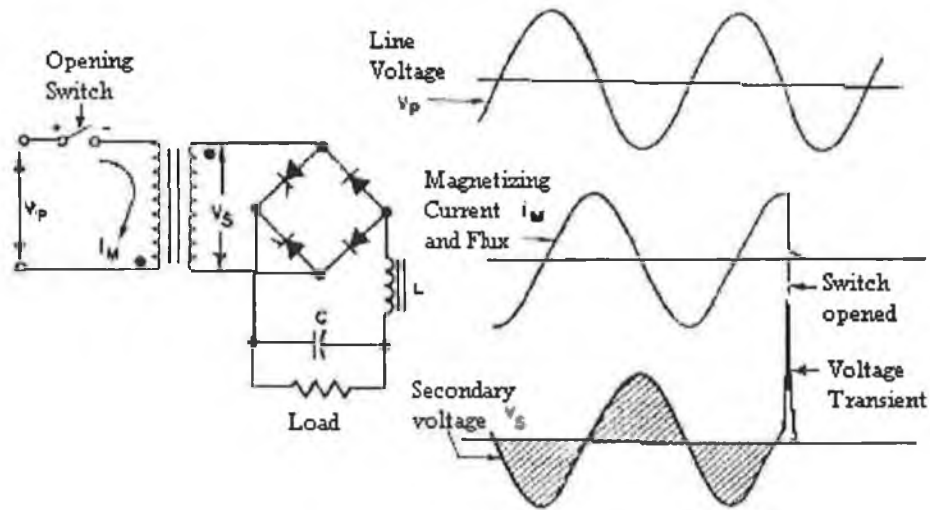


Figure 1.3 Voltage transient by interruption of transformer magnetizing current

when this type of switching occurs. Interrupting the transformer magnetizing current, and the resulting collapse of the magnetic flux in the core, couples a high voltage transient into the transformer secondary winding as shown in Fig 1.3.

Fault with Inductive Power Source

If a short develops on any power system, the fuse clears and devices parallel to the load may be adversely affected. When the fuse or circuit breaker opens, it interrupts the fault currents causing the slightly inductive power source to generate a high voltage and high energy transient across any parallel devices⁹ as shown in Figure 1.4. Sudden interruption of a high current load can have a similar effect.

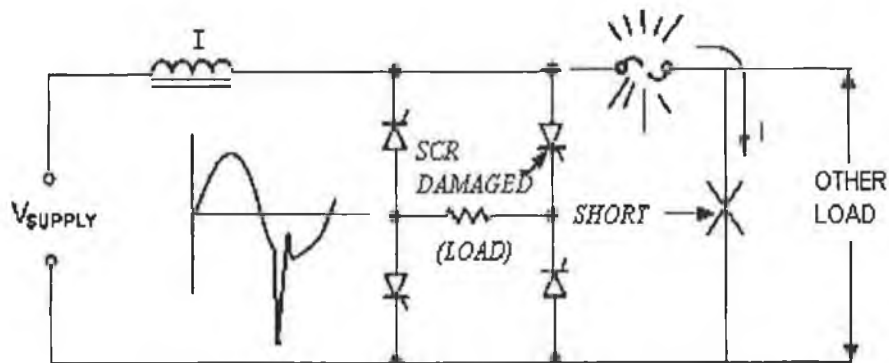


Figure 1.4 Voltage transient caused by fuse blowing during power fault

Switch Arcing

Switch arcing is another source of repeatable transients. When current in inductive circuits such as relay coils or filter reactors, is interrupted by any contactor, the

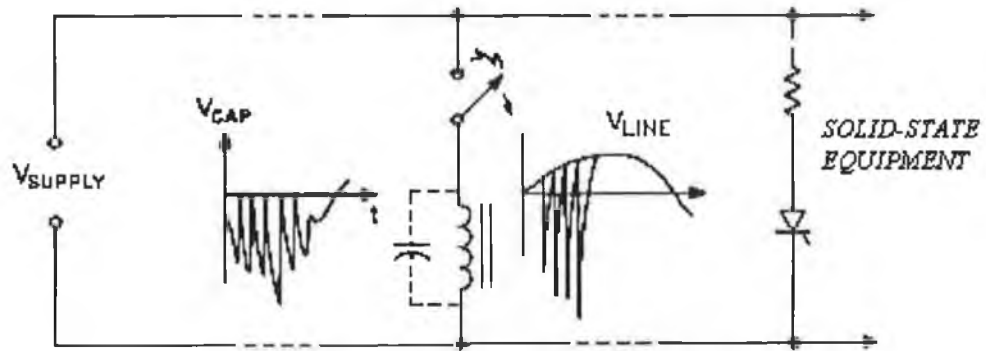


Figure 1.5 Voltage transients caused by switch arcing

inductance tries to maintain its current by charging the stray capacitance. The initial charging current will oscillate in the inductance and capacitance at a high frequency. Similar action can take place during a closing sequence if the contacts bounce open after the initial closing⁹ as shown in Figure 1.5.

Generally, a system should be examined for potential sources of overvoltages so that they can be eliminated. But if sources are too many compared to the susceptible components, it may be more practical then to apply suppression at the components.

1.2.2 RANDOM TRANSIENTS

This kind of transients may originate from a number of sources. The power source feeding the circuit can generate random transients which create the most problematic situation as it is difficult to define their amplitude, duration and energy content. These are generally caused by switching parallel loads on the same branch of a distribution system. Lightning is another prominent source of random transients. To deal with this kind of transients a deterministic approach is not realistic because of the

unpredictable nature of their characteristics such as amplitude, wave shape, energy content and frequency of occurrences. A statistical approach is usually adopted to deal with the random transients. Data collected from different sources provide the guidelines for estimating the nature of the overvoltage transients and designing the suppressors accordingly.

Transients on AC power lines

The amplitude of transient recordings covers the range from harmless values just above normal voltage to several kilovolts. For a 120 V AC lines, flashover of the typical wiring spacing produces an upper limit between 6 KV and 8 KV. Experience indicates that suppressor devices with less than 2 KV withstand capability will have poor service life in the unprotected residential environment. Prudent design will aim for 3 KV capability, although where safety is of utmost concern, designing for 6 KV can cope with the rare but possible occurrences⁹.

The amplitude of the transient depends more upon the amount of externally coupled energy and the system impedance than upon the system voltage. There is some uncertainty concerning the expected transient level found in the industrial practice of choosing semiconductor ratings. Most industrial users of power semiconductors choose semiconductor voltage ratings from 2.0 to 2.5 times the applied peak steady-state voltage in conjunction with rudimentary transient suppression, in order to ensure long-term reliability. But there are enough cases where this rule of thumb is insufficient and, therefore, a more exact approach is justified. The optimum situation is a combination of low cost transient protection combined with lower cost semiconductors having lower voltage ratings.

Telecommunication Line Transients

Transient overvoltages occurring in telephone lines can usually be traced to two main sources - lightning and 50 Hz or 60 Hz power lines. Lightning overvoltage is caused by a strike to the conductor of an open wire system or to the shield of a telephone

cable. Most modern telephone lines are contained in shielded cables. When lightning or other currents flow on the shield of a cable, voltages are induced between the internal conductors and the shield.

The close proximity of telephone cables and power distribution systems, often sharing right-of-way-poles and even ground wires, is a source of transient overvoltages for the telephone system. Overvoltages can arise from physical contact of falling wires, electromagnetic induction, and ground potential rise.

Automobile Transients

Four principal types of voltage transients are encountered in an automobile. These are 'load dump', alternator field decay, inductive switching and mutual coupling. In addition, service 'jump starts' with 24V batteries may occur.

The load dump transient is the most severe and it occurs when the alternator current loading is abruptly reduced. The case is often initiated by the disconnection of a partially discharged battery due to the defective terminal connections. Transient voltages have been reported over 100 V lasting up to 500 ms with a wide range of energy levels. Such a simulated sample pulse⁶ is shown in Figure 1.6.

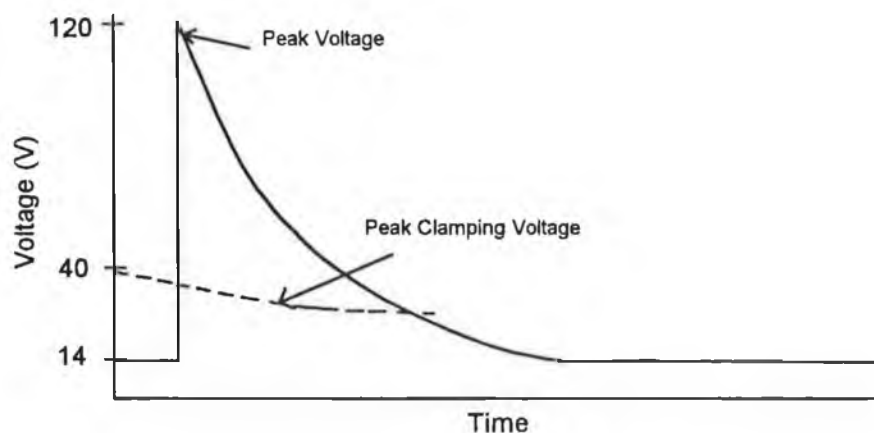


Figure 1.6 Overvoltage associated with the 'load dump'

Switching of inductive loads such as motors or solenoids, creates negative polarity transient voltages with a smaller positive excursion. Other unexplained transients have been recorded with peaks of 600 V upon engine shutdown.

1.3 TRANSIENT PROTECTION TECHNOLOGY

Several transient protection technologies are available. The two major categories of transient suppressors are; a) those that attenuate transients, thus preventing their propagation into the sensitive circuit; and b) those that divert transients away from sensitive loads and thus limit the residual voltages. Attenuating a transient is accomplished with filters inserted in series within a circuit. The filter, generally of the low pass type, attenuates the transient (high frequency) and allows the signal or power flow (low frequency) to continue undisturbed.

Diverting a transient can be accomplished with a voltage-clamping type device or with a 'crowbar' type device. The designs of these two types, as well as their operation and application, are different. A voltage-clamping device is a component having a variable impedance. Crowbar-type devices involve a switching action, either the breakdown of a gas between electrodes or the turn-on of a thyristor.

After switching on, the crowbar-type devices offer a very low impedance path which diverts the transient away from the parallel-connected load and short-circuits a high voltage to ground. This short-circuit continues until the current is brought to a low level reducing the line voltage. With a voltage clamping device, the circuit remains unaffected before and after the transient and the line voltage never reduces below its steady-state value as it does not contain any discontinuities in contrast to the crowbar device.

The voltage clamping action of a varistor results from the increased current drawn through the device as the voltage tends to rise. If this current increase is greater than the voltage rise, the impedance of the device is said to be non-linear, i.e. Ohm's law

($V=IR$) is applicable but the equation has a variable resistance, R . This feature⁹ is presented in Figure 1.7 demonstrating the I-V curve of a linear and non-linear resistor.

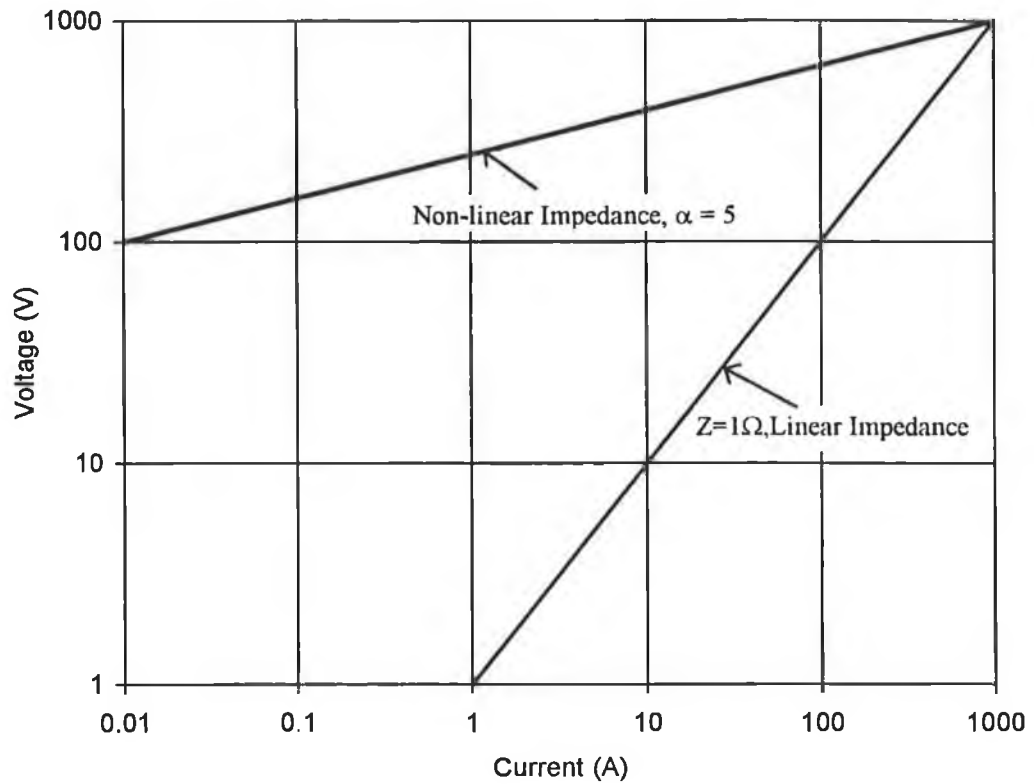


Figure 1.7 I-V characteristic for a linear and non-linear resistor (varistor)

Crowbar devices have two major limitations. The first is their higher delay time, typically microsecond, which leaves the load unprotected during the initial voltage rise. The second limitation is that a power current from the steady-state voltage source follows the surge discharge (called “follow-current” or “power-follow”).

1.3.1 VOLTAGE CLAMPING DEVICES

There are various voltage clamping devices. They all depend on their non-linear impedance in conjunction with the transient source impedance to perform the voltage limiting function. Basically three types of voltage-clamping devices are available.

These are reverse selenium rectifiers, avalanche (Zener) diodes and varistors. There are two categories of varistor - silicon carbide and zinc oxide.

Selenium Cells

Selenium transient suppressors apply the technology of selenium rectifiers in conjunction with a special process allowing reverse breakdown current at high energy levels without any damage to the polycrystalline structure. These cells, built by developing the rectifier elements on the surface of a metal plate substrate, have good heat dissipation performance. They, however, do not have the clamping ability of the modern metal-oxide varistors or avalanche diodes. As a consequence, their field of application is considerably diminishing.

Zener Diodes

These are very effective in clamping which comes closest to an ideal constant voltage clamp. Moreover, they are also available in low-voltage ratings. But since the diode maintains the avalanche voltage across a thin junction area during surge discharge, substantial heat is generated in a small volume. As a result of the localized heat generation, this type of device cannot handle much energy and hence faces a limitation in energy absorption capability.

Silicon Carbide Varistors

Until the advent of the ZnO varistors, the most common type of varistor was made from specially processed silicon carbide. But its protective level is too high for a device capable of withstanding line voltage. To produce an acceptable protective level, a series gap is required with SiC varistor to block the nominal voltage. In lower voltage electronic circuits, the use of silicon carbide varistors have not been widely acceptable. This is because of the need for using a series gap which reproduces some of the undesirable characteristics of gap in addition to the increased cost.

Metal Oxide Varistors

This family of transient voltage suppressors are made of sintered metal oxides, primarily zinc oxide with suitable additives. ZnO varistors have a non-linear coefficient considerably greater than those of silicon carbide. This high non-linearity along with some other excellent features of the metal-oxide varistor, has led to open completely new fields of applications.

1.3.2 COMPARATIVE SCENARIO OF DIFFERENT SUPPRESSORS

In figure 1.8 the I-V curve plotted for a number of common overvoltage suppressors⁸ compares the relative characteristics specially the non-linearity. But because of the diversity in characteristics it is not straight forward to compare the various transient suppressors. High non-linearity is very important and desirable for the clamping applications over a wide range of currents. However, it is also necessary to know the

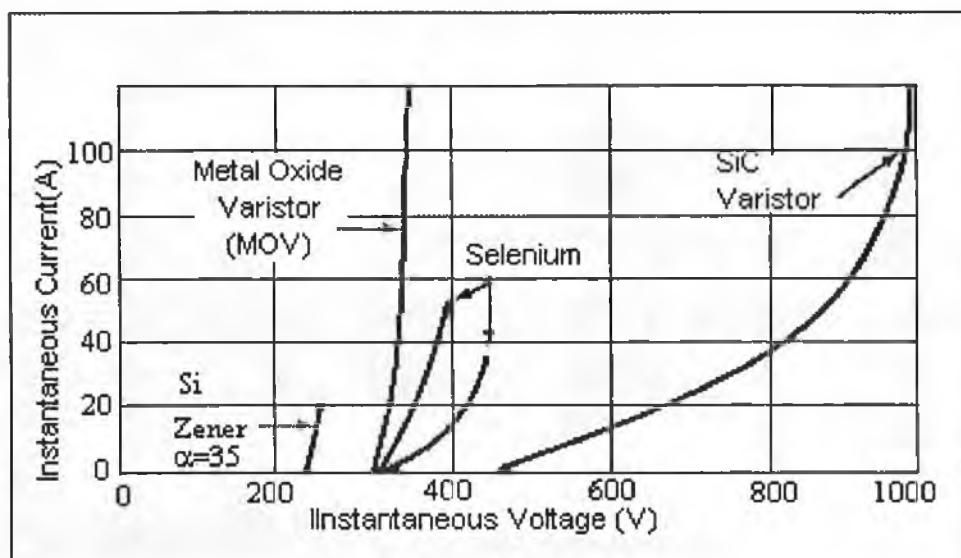


Figure 1.8 V-I Characteristics of Common Voltage Suppressors

device energy absorption and high current capability and other functional properties. In Table 1.1 a summary of the important parameters of commonly used suppressors⁹ is presented.

Table 1.1 I-V Characteristics and Other Features of Transient Voltage Suppressors

I-V characteristics	Device Type	Leakage	Follow on Cur	Clamp voltage	Energy capab.	Capacitance	Response	Cost
	Ideal Device	Zero To Low	No	Low	High	Low Or High	Fast	Low
	Zinc Oxide Varistor	Low	No	Moderate To Low	High	Moderate To High	Fast	Low
	Zener	Low	No	Low	Low	Low	Fast	High
	Crow-bar (Zener-SCR Combination)	Low	Yes (Latching Holding)	Low	Medium	Low	Fast	Moderate
	Spark Gap	Zero	Yes	High Ignition but low clamp	High	Low	Slow	Low To High
	Triggered Spark Gap	Zero	Yes	Lower Ignition but low clamp	High	Low	Moderate	High
	Selenium	Very High	No	Moderate To High	Moderate To High	High	Fast	High
	Silicon Carbide	High	No	High	High	High	Fast	Relatively low

In addition to the parameters mentioned in the table, other factors such as standby power, peak pulse power, ageing, failure modes etc. are functionally very important for a suppressor. Careful consideration is necessary to select the appropriate device because all the parameters are not strictly favourable with any particular category. Thus there may be some undesirable properties for specific applications, the ZnO varistor, in general, exhibits better overall performance characteristics.

1.4 BASIC PROPERTIES OF ZINC OXIDE VARISTOR

Zinc oxide varistors are basically electronic ceramic devices. They are known by various names such as non-linear resistors, variable resistors, surge suppressors, surge protectors and voltage limiters. Owing to some of their superior features compared to the competitors they are widely used for over-voltage protection. The opportunities for applications of the ZnO metal-oxide varistors have recently extended to a wide range of designs - from low power electronics to the largest utility-type surge arresters.

Unlike the resistor, varistors are designed to provide a threshold voltage below which practically very low or no current flows. This is to prevent interference with normal circuit operation in the absence of any transients. Once the transient voltage appears and surge current begins to flow through the varistor, the surge-developed voltage across the varistor becomes the key factor determining its ability to provide circuit protection. For all anticipated lightning stroke currents, this voltage must be held as low as possible.

The characteristics of voltage dependent, symmetrical clamping of ZnO varistor devices enable them to protect circuits against high voltage spikes (when properly selected) to meet the anticipated transients. When the protected equipment circuit encounters a high voltage spike, the varistor impedance changes from a very high standby value to a very low conducting value, thus clamping the transient voltage to a protective level. The excess energy of the incoming high voltage pulse is absorbed by the varistor, protecting voltage sensitive components against damage.

The protection afforded by the varistors not only guards the expensive and voltage sensitive equipment from physical damage, but also improves the functional reliability of the components that can encounter temporary upset due to transient voltages of lower amplitudes.

ZnO varistors are formed by mixing ZnO powder with the powder of other oxides such as those of Bi, Sb, Co, Mn, Ni, Cr, Si, etc. and subjecting the powder to conventional ceramic processing. After the sintering operation, the resultant product is a polycrystalline ceramic with a unique grain-boundary property that contributes to the well-known non-linear I -V characteristics of the device.

1.4.1 THE I-V CHARACTERISTICS

Zinc oxide varistor possesses a non-linear current (I) - voltage (V) characteristic with a symmetrical sharp breakdown, similar to that of a Zener diode. But unlike a diode, varistor can limit overvoltages equally in both polarities, thus giving rise to a I-V characteristic which is analogous to two back-to-back diodes. This has enabled it to provide excellent transient suppression performance. When exposed to a high voltage transient the varistor impedance changes many orders of magnitudes from a near open circuit to a highly conductive level, thus clamping the transient voltage to a safe level. The potentially destructive energy of the incoming transient pulse is absorbed by the varistor, thereby protecting the vulnerable circuit components.

The zinc oxide varistor is a high transient over-voltage suppressor. This is characterized by its excellent nonohmic properties¹⁰⁻¹⁶ in current-voltage relationship as shown in the I-V curve presented in Figure 1.9. It has a very large suppression capability, which is considered to be a combination of both the feature of silicon-zener diodes and silicon carbide varistor. The feature of zinc oxide varistor is a grain boundary phenomenon and this is an intrinsic property of this ceramic material. The non-ohmic relationship of zinc oxide varistor is expressed mathematically as follows

$$I = KV^{\alpha} \dots\dots\dots(1.1)$$

where I is the current density flowing through the material, V is the field (V/cm) across the varistor and K is the proportionality constant. The non-linear coefficient, α

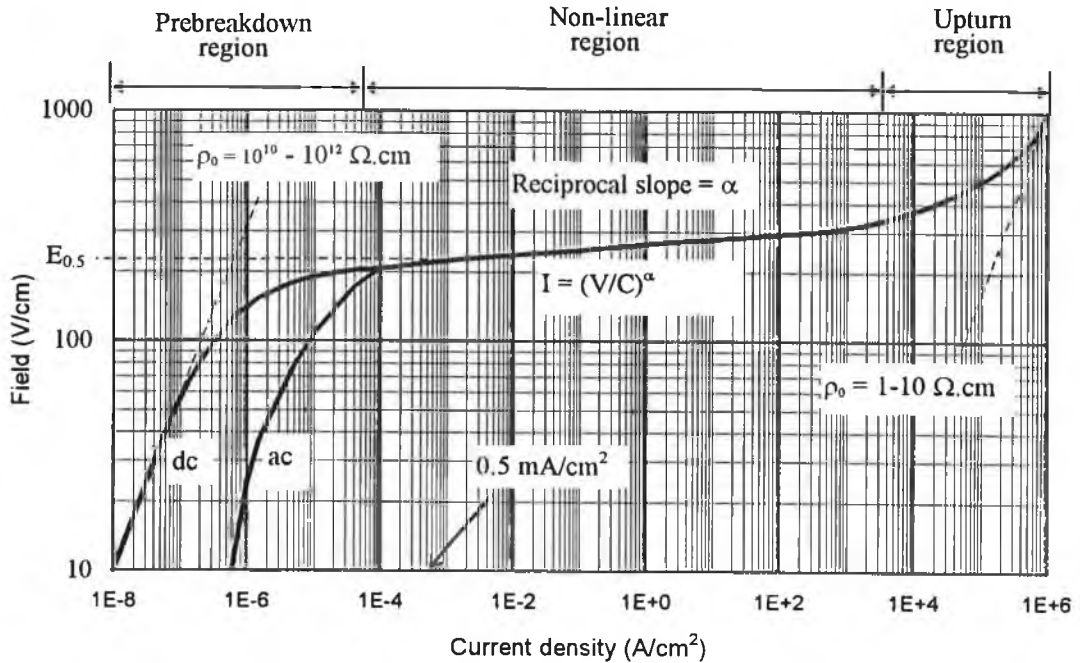


Figure 1.9 Typical current-voltage characteristics of ZnO varistor plotted

is a measure of non-linearity of the varistor resistance which can be expressed for a given range of current I_1 and I_2 with corresponding voltages V_1 and V_2 , as

$$\alpha = \frac{\ln\left(\frac{I_2}{I_1}\right)}{\ln\left(\frac{V_2}{V_1}\right)} \dots\dots\dots(1.2)$$

This relation is applicable for the non-linear region. The I-V relationship of a zinc oxide varistor has three distinct regions: a low current linear region (ohmic, $<10^{-4}$ A/cm²), an intermediate non-linear region (nonohmic) and a high current upturn region (ohmic, usually above 10^3 A/cm²). These three regions serve important functions in the design and operation of the surge protector.

Low Current Region

The I-V characteristic is ohmic in this region and is defined as the prebreakdown region. The alternating current is about two orders of magnitude higher than the direct current. The difference can be attributed to the contribution of the dielectric loss upon application of an alternating voltage. This region determines the leakage current and consequently the watt loss under normal steady state voltage. There is a need to balance the values of operating voltage and leakage current. On the one hand, the operating voltage should be as close to the onset of non-linearity ($E_{0.5}$, threshold voltage) as possible to maximize protective level and on the other hand, to keep the device safe from thermal runaway due to excessive heating. The voltage, $E_{0.5}$ is arbitrarily selected as a measure of breakdown voltage, recorded at 0.5 mA/cm^2 .

Intermediate Non-linear Region

The non-linear region of the intermediate current is the heart of the ZnO varistor, wherein the device conducts an increasingly large amount of current for a small increase in voltage. It is this large non-linearity over a wide range of current densities that makes the ZnO varistor distinctly different from any other non-linear resistor and thus makes it useful for a variety of applications.

The degree of non-linearity is determined by the flatness of the non-linear region, the flatter the I-V curve in this region, the better is the device. The controlling parameters for this important region are only qualitatively understood. The addition of Bi_2O_3 has been found to be essential for forming the nonohmic behaviour. Some oxide dopants are found to enhance the non-linearity.

High Current Upturn Region

In the high current region, the I-V characteristic is again linear, similar to that in the low-current region, the voltage rising faster with current than in the non-linear region.

This is also known as the upturn region. This region is controlled by the impedance of the grain in the ZnO microstructure.

To characterize a ZnO device, it is desirable to determine the I-V curve for all the three regions. However, due to the wide range of currents involved, different measurement techniques are adopted for different regions. Usually I-V characteristics below 100 mA/cm^2 are measured by direct current or 60 Hz alternating current and those above 1 A/cm^2 are measured by the impulse current.

1.4.2 MICROSTRUCTURE OF ZINC OXIDE VARISTOR

The property of metal-oxide varistor, fabricated from zinc oxide, is that the electrical characteristics are interestingly related to the bulk of the device. Each ZnO grain of the ceramic acts as if it has a semiconductor junction at the grain boundary. A cross-section⁹ of the varistor material is shown in Figure 1.10 which demonstrates the

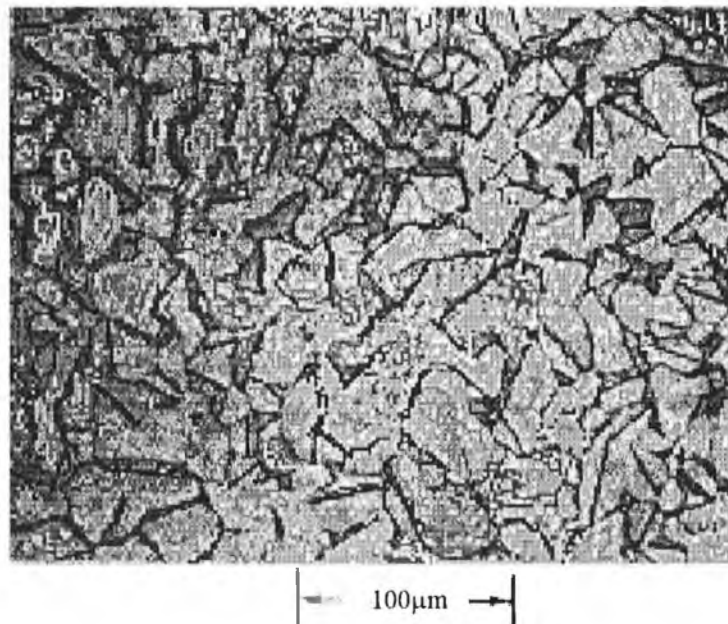


Figure 1.10 Photomicrograph of a polished and etched section of a ZnO varistor

ceramic microstructure. The ZnO grain boundaries can be distinctly identified. The grain size distribution plays a major role in the electrical behaviour. Since the non-

linear electrical characteristic occurs at the boundary of the semiconducting ZnO grain, the varistor may be considered a 'multi-junction' device composed of many series and parallel connections of grain boundaries. Thus the device behaviour can be analyzed with respect to the details of the ceramic microstructure.

The functional microstructure of ZnO varistor materials can be described as consisting of:

- (i) Doped semiconducting ZnO grains
- (ii) ZnO interfaces which provide the barriers to electrical conduction and which give rise to the non-linear current-voltage characteristics
- (iii) A continuous network of Bi-rich phases is located along the triple junctions of the ZnO grains. This network provides an alternative conduction path, that avoids the barriers that are associated with the ZnO interfaces, and can give a significant contribution to the conductivity in the prebreakdown region of the current-voltage characteristics.

The formation of the microstructure of the varistor is dependent on the sintering time, temperature and environment. Pure zinc oxide is a nonstoichiometric n-type semiconductor with a linear I-V characteristics. The addition of Bi_2O_3 is essential to form a non-linear region. However, multiple dopants¹⁷⁻²⁶ (additives) such as a combination of Bi_2O_3 , Sb_2O_3 , MnO_2 , SiO_2 , Cr_2O_3 and Co_3O_4 etc. are added to produce greater non-linearity than a single dopant.

The high current non-linearity can be enhanced by decreasing the grain boundary resistivity which is usually achieved by doping²⁷⁻²⁹ with aluminium or gallium oxide. Transition metal oxide Co_3O_4 and MnO_2 are used to improve the non-ohmic property and NiO, Cr_2O_3 , or a small amount of glass frit are included to improve the reliability

and peak pulse stability. The presence of different crystalline phases and their composition¹⁰ are diagrammatically presented in Figure 1.11.

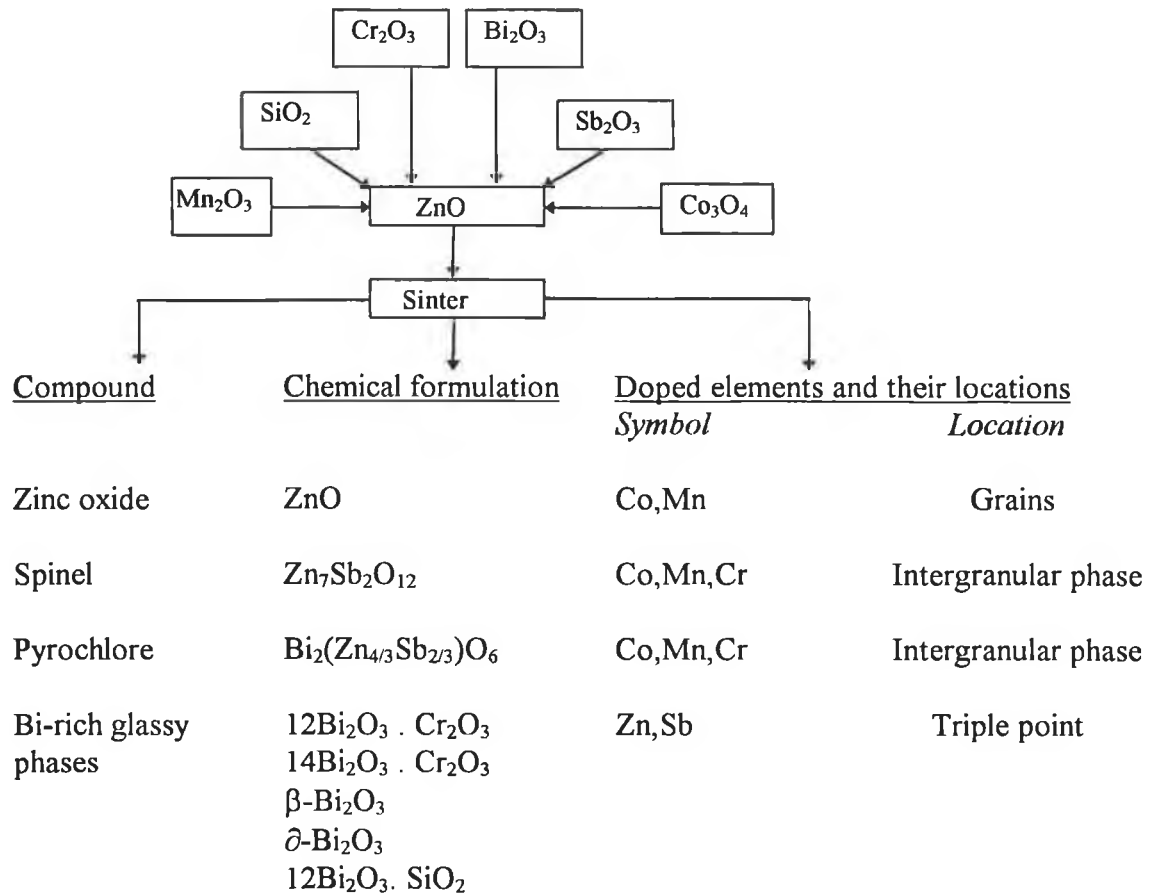


Figure 1.11 Microstructural components of ZnO varistor and their composition

Zinc oxide, spinel, pyrochlore, and several Bismuth rich phases are the four basic compounds³⁰⁻³² found in the microstructure. Zinc oxide and additives react with each other during the sintering process, forming intermediate compounds such as pyrochlore and spinel phases. Low temperature is favourable for the formation of pyrochlore phase, whereas, high temperature is for the spinel phase.

The increase of sintering time and temperature leads to an increase in grain size and results in fewer grain boundaries. The typical grain size^{9,10} of a commercial zinc oxide varistor is between 15-20 μm and the grains for this type of varistor composition show crystal twinning. A detailed physical structure of ZnO varistor grain⁶ is presented in Figure 1.12. with the location of various crystalline phases.

explaining metal-oxide varistor operation lies in understanding the electronic phenomena occurring near the grain boundaries, or junctions between the zinc oxide grains.

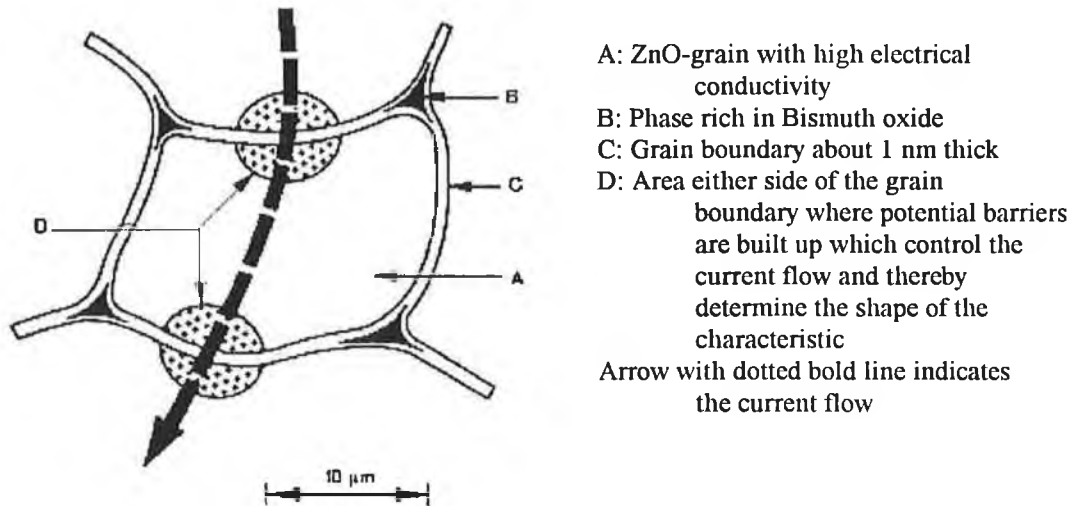


Figure 1.13 Schematic representation of the operating mode of varistor

While some of the earlier theories supposed that electronic tunnelling occurred through an insulating second phase layer at the grain boundaries, varistor operation is probably better described by a series-parallel arrangement of semiconducting diodes. In this model, the grain boundaries contain defect states which trap free electrons from the n-type semiconducting zinc oxide grains, thus forming a space charge depletion layer in the ZnO grains in the region adjacent to the grain boundaries. In Figure 1.13 a schematic representation of the mode of varistor operation is shown.

During sintering the nonstoichiometric nature of zinc oxide produces excess zinc ions. The excess ions are accommodated at the interstitial sites in the lattice and are “frozen in” at room temperature during cooling. Of the frozen interstitials some are trapped in the depletion layer^{9,33-35} which is 50-100 nm from the grain boundary to the grain. It has been determined that ZnO carrier concentration is about 2×10^{17} per cm^3 . The varistor action and stability are very much dependent on the charge characteristics of the depletion layer within the grains.

It is these depletion layer that block the free flow of carriers and are responsible for the low voltage insulating behaviour in the leakage region as depicted in Figure 1.14. The leakage current is due to the free flow of carriers across the field lowered barrier, and is thermally activated, at least above about 25 °C.

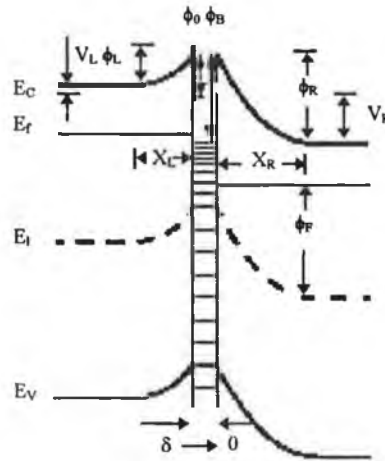


Figure 1.14 Energy band diagram of a ZnO-grain boundary-ZnO junction

The above figure shows an energy band diagram for a ZnO-grain boundary-ZnO junction. The left-hand grain is forward biased, V_L and the right side is reverse biased to V_R . The depletion layer widths are X_L and X_R , and the respective barrier heights are ϕ_L and ϕ_R . The zero biased barrier height is ϕ_0 . As the voltage bias is increased, ϕ_L is decreased and ϕ_R is increased, leading to a lowering of the barrier and an increase in conduction.

The barrier height ϕ_L , measured as a function of applied voltage and found to decrease rapidly at high voltage, represents the onset of the non-linear conduction. Transport mechanisms in the non-linear region are very complicated and still the subject of active research.

Various models have been developed to describe the conduction mechanism, life, and stability of zinc oxide varistors. These are: “Space charge-limited current” (Matsuoka)¹, “Hole-assisted tunnelling through Schottky barriers” (Mahan,

Levinson and Philipp)³⁶, “Tunneling through Schottky barriers” (Levine)³⁷, “Tunneling through Schottky barriers with heterojunctions” (Eda)³⁸, “Tunnelling through Schottky barriers” (Hower and Gupta)³⁹, “Hole-induced breakdown” (Pike)¹⁵. Of all barriers the Schottky barrier is considered to be the most likely barrier at the grain boundary of a zinc oxide varistor. A model of two back-to-back Schottky barriers at each interface can explain the non-ohmic properties, the temperature dependence of the I-V curve, effect of additives, dielectric properties and degradation phenomena.

But from the viewpoint of this study, theoretical models are not nearly as important as the understanding of the basic electrical properties as they are dependent on the processing parameters. The present investigation mainly concentrates on the evaluation of the effect of processing parameters on the final properties of the varistor, with a special emphasis on the energy absorption capability.

1.5 APPLICATION OF ZINC OXIDE VARISTOR

The state-of-the-art of the metal-oxide varistor is represented by a broad range of products manufactured to meet the need of the present day transient voltage suppression. The products cover arresters for power systems to the low power and low energy applications such as integrated circuits, automotive systems and other modern electrical and electronic circuits. To meet the continued demands of improved functional reliability of the systems and with the advent of new manufacturing technology, it is quite apparent that varistors with unique features will come into the marketplace.

The applications are usually classified according to the purpose. Among them varistors are used for the purpose of voltage stabilization or pulse suppression in TV sets, microwave ovens, and other consumer electronic equipment. Surge absorbers are used for protection from lightning and switching surges in many kind of applications such as consumer electronic equipment, industrial electronic equipment

and automotive use. The field of ZnO varistor applications³ is quite large, a schematic is shown in Figure 1.15.

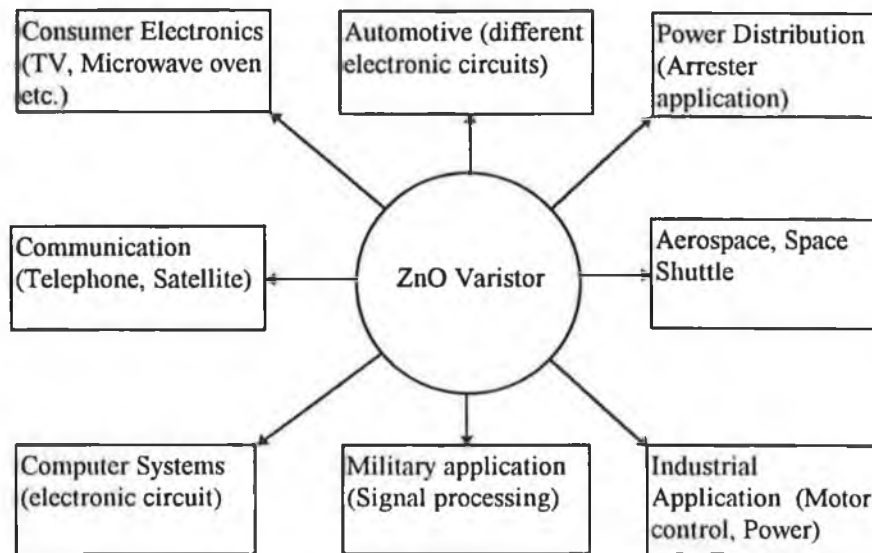


Figure 1.15 Important areas of zinc oxide varistor applications

Presently many kinds of metal-oxide varistors are available. The peak current carrying capability ranges start from a low value of 80 A to a high value of 100 KA and the rated energy absorption capability covers a range of 0.5 to 12000 Joules. They are known by different commercial names. The most traditional ZnO varistor is the high energy metal-oxide arrester block.

The high voltage application usually covers from KV to MV range for the protection of electric power distribution and transmission systems. Arresters are designed for the purpose of protecting the high-power distribution equipment from lightning and switching surges. Cylindrical discs are made to provide high-energy handling capability and long-term stability in stressful applications. These have been used successfully for more than a decade in power systems operated at all voltage levels².

Usually arrester discs assembled in the Porcelain Polymeric housing, “Under-oil” and Metal Clad Variety are applied for the lightning protection of electrical distribution

transformer and systems. An example of a surge arrester⁶ containing several ZnO discs connected in series is illustrated in Figure 1.16

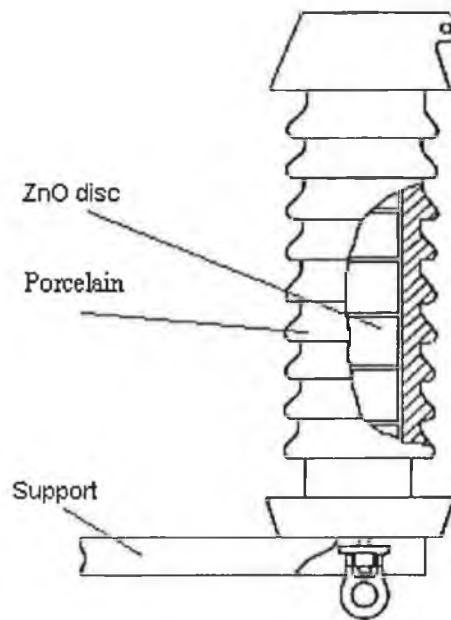


Figure 1.16 Surge arrester assembly by ZnO arrester discs

Multilayer is a recent development of varistor technology, mainly used in the automobile industry. The automotive multilayer (AUML) series of transient surge suppressers are specifically designed to protect the sensitive electronic equipment of an automobile, from destructive transient voltages. Almost all the electronic systems in the automobile, e.g. antilock brake systems, direct ignition systems, airbag control systems, wiper motors etc. are susceptible to damage from voltage transients. Multilayer suppressors are designed to fail short when overstressed and, thus protect the associated equipment. The devices are in the chip form, eliminating lead inductance and assuring the fastest speed of response to transient surges. Two main series of multilayer devices⁷ are available commercially.

Depending upon the purpose and application there are many developments⁹ in the ZnO varistor technology. The main of these are (i) Multilayer Surface Mount Transient Surge Suppressor (ii) Industrial High Energy Metal-Oxide Varistors (iii)

Radial Lead Metal-Oxide Varistors (iv) Industrial High Energy Metal-Oxide Disc Varistors (v) Surface Mount Metal-Oxide Varistors (vi) Connector Pin Metal-Oxide Varistors (vii) Radial Lead Metal-Oxide Varistors for Line Voltage Operation (viii) Axial Lead Metal-Oxide Varistors (ix) Industrial High Energy Metal-Oxide Square Varistors (x) Base Mount Metal-Oxide Varistors (xi) Low Profile Metal Oxide Varistors.

1.5.1 FUNCTIONAL PARAMETERS OF VARISTORS

The application of zinc oxide varistor is selected on the basis of some critical parameters such as non-linear coefficient, nominal voltage, leakage current, and energy absorption capability etc. The material and processing parameters like the density of the green and the fired body, homogeneity, grain size, porosity, varistor chemistry, and sintering parameters are identified to affect the energy absorption capability remarkably⁴⁰⁻⁴⁵. The life of varistors is largely dependent on the leakage current and energy absorption capability.

Varistor applications take the advantage of all the regions of the I-V curve. The low current region determines the watt loss and, hence, the operating voltage during the steady application of an external voltage. The non-linear region determines the clamping voltage upon application of a transient surge. The high current region presents the limiting condition for protection from high current surges such as those found in lightning. Devices where the upturn occurs at increasingly higher current density are, therefore, most desirable for applications involving high magnitudes of currents, since the voltage rise can be minimized with such devices.

There are several critical application parameters some of which are associated with various regions of the I-V curve. These parameters serve various functions in the design and operation of a surge protector. The most desirable device should have a high value of non-linear coefficient or low value of protective level, a low value of leakage current, a long varistor life and high energy absorption capability. The functional important parameters for a suppressor are in general assessed by the (a)

Standby Power (b) Peak Pulse Power (c) Clamping voltage (d) Speed of response (e) Leakage currents (f) Ageing (g) Failure mode (h) Capacitance.

Standby Power

The power consumed by the suppressor unit at normal line voltage is an important selection criterion. Peak standby current is one factor that determines the standby power of a suppressor. The standby power dissipation depends also on the alpha (non-linearity) characteristic of the device.

The amount of standby power that a circuit can tolerate may be the deciding factor in the choice of a suppressor. Though high-alpha devices have low standby power at the nominal design voltage, a small line-voltage rise would cause a dramatic increase in the standby voltage.

The gas discharge device may experience follow-on current when in use for protection of AC line surges. For this reason this type of device is useful for high current surges but is not effective in protecting low voltage, low impedance circuits.

Peak Pulse Power

Transient suppressors have to be capable to absorb large amount of power or energy in a very short time duration: nanoseconds, microseconds, or milliseconds in some rare instances. Electrical energy is transformed into heat and has to be distributed instantaneously throughout the device. For any material transient thermal impedance is much more critical than the steady state thermal impedance.

ZnO Varistors meet these requirements and are a reliable device with large overload capability. Zener diodes, on the other hand, transform electrical energy into heat in the depletion region: an extremely small area resulting in high temperature. With shorter pulses diode faces more difficulty.

Clamping Voltage

Clamping voltage is an important feature of a transient suppressor. Zener diode has lower clamping voltage than the ZnO varistor. Because all protective devices are connected in parallel with the system to be protected, a lower clamping voltage will apply less stress to the system.

Speed of Response

The response time of the suppressor to the transient current that a circuit can deliver is the appropriate characteristic to consider. ZnO varistor action depends on a conduction mechanism similar to that of other semiconductor devices and it occurs very rapidly with apparently no time lag even into the nanosecond range. However, for zener diode this time is claimed to be as low as 1 picosecond. In a conventional lead-mounted ZnO varistor, the inductance of the leads is responsible for masking the fast action of the varistor. The connector pin design of a ZnO varistor has eliminated the inductive lead effects.

Leakage Currents

The leakage current is an important factor in selecting the suppressor-the lower the leakage, the better is the device. Zener diode leakage is much higher than that for a varistor. At elevated temperatures, the comparison looks more favourable to the varistor.

Ageing

It is stated that the I-V characteristic of a varistor changes every time energy is absorbed due to a pulse. But this change due to the repeated pulse injection is not very remarkable. According to some manufacturer⁹ the term 'ageing' is a misnomer.

Failure mode

Varistors subjected to energy levels beyond specified ratings may be damaged. Varistors fail in short circuit mode. Subjected to high enough energy, however, they may physically rupture or explode, resulting in an open circuit condition. The latter kind of failures are quite rare but the possibility is there.

Zener diodes can fail either short or open. Designers must analyze which failure mode, open or short, is preferred for their circuits. A short is preferred when a device fails during a transient as it will provide a current path bypassing and will continue to protect the sensitive components.

Capacitance

Depending on the application, transient suppressor capacitance can be a very desirable or undesirable feature. Varistors in comparison to Zener diodes have a higher capacitance. For filter connectors varistor can perform dual functions of providing both filtering and transient suppression. But for high frequency digital or some analog circuits, capacitance is less desirable.

The structural characteristics of ZnO varistors unavoidably result in an appreciable capacitance between the device terminals, depending on the area, thickness and material processing. For the majority of power applications, this capacitance is not significant. In high-frequency applications, however, the effect must be taken into consideration in the overall system design.

1.6 SCOPE OF THE PRESENT STUDY

Processing parameters of varistors, though basically follow the conventional ceramic fabrication route, vary to a certain extent depending upon the configuration of the device. The present study was concerned with the cylindrical varistor discs applied for arrester application. Though compaction parameters were the main emphasis in

this study, other aspects of processing conditions were also investigated in terms of the critical performance characteristics of varistor.

Compaction is undoubtedly an important operation. The parameters considered in this processing step is the pressure, speed or rate of pressing and the dwell time. To conduct the study with pressing parameters a floating die was designed and fabricated. The analysis consisted of evaluating the effect on the green as well as on the fired properties of the varistor discs. Electrical characterization was also performed to assess the effects on the performance characteristics. These were the fundamental properties related to the I-V characteristics and energy absorption capability and high current performance.

Grinding or lapping of the flat faces is necessary for a number of reasons. The grindability of arrester discs is dependent on other processing conditions. A relationship was found between the sintering orientation and the grindability of arrester blocks. The evaluation was done by measuring the microhardness of the discs.

Sintering orientation of the discs affects several other physical properties of the sintered disc. The portion of the arrester disc remaining in contact with liner material was found to be mechanically weaker. The measured density gradient was also significantly high. As a consequence it was found that higher number of failure originated from the bottom part remaining in close contact with the liner. An alternative sintering orientation was attempted to get rid of these problems.

Arrester blocks are manufactured with circular cross-section. For the same volume of the disc increased heat transfer area is expected to enhance the stability of a varistor during the steady-state operating condition. This would eventually increase the life of a varistor by delaying the thermal runaway. Increased surface to volume ratio is possible by providing a hexagonal shape to the disc. An attempt was made to prepare hexagonal discs by grinding the side of the cylindrical discs. They were tested for determining the energy absorption capability and the I-V characteristics.

The electrode of an arrester disc is deposited on the circular face either with a margin at the periphery or without any margin i.e. covering the whole face. Both methods are practiced presently depending on the customer specifications. But the eventual impact specially on the energy absorption capability was not precisely known. In this study attempt was made to evaluate the effect of margin in electrode on the energy absorption capability.

Failure mode of arrester disc is dependent on the pulse duration. Short pulses usually cause crack or rupture of the discs. The fracture mechanism was analysed in the context of stress wave propagation during the injection of this kind of pulses. In this regard celerity (speed of propagation of a pulse) measured by a laser based device was correlated with the basic elastic properties of the arrester material.

Some microstructural analyses were also performed by Scanning Electron Microscopy (SEM) to correlate the microstructural results with the processing parameters.

In chapter 2, a brief literature survey has been incorporated on the processing parameters of ceramics with a special focus on electronic ceramics. Factors influencing the compaction phenomena were elaborated and the objectives were set for the study.

The experimental procedure and the equipment used have been briefly described. in chapter 3. The effects of the compaction parameters on the functional properties have been presented. The results are based on the experimental data obtained under specified experimental and testing condition.

In chapter 5, the mathematical models were developed on the basis of the design of experiments. In this regard the two-level factorial design and response surface methodology were adopted.

In the processing of ceramic the effects of sintering orientation of arrester was investigated and the influence was described in chapter 6. The adverse effect arising from the orientation was obvious in several physical properties as described in this chapter

To overcome the problems arising from the sintering configuration several alternative methods were proposed in chapter 7 with their relative merits and demerits. Moreover, the fracture mechanism in high current test was also investigated with subsequent presentation of the results in this chapter.

In chapter 8, the conclusions, thesis contribution and the recommendation for further work were briefly mentioned.

Chapter 2

LITERATURE SURVEY

2.1 INTRODUCTION

The application of metal-oxide varistor technology is very common now-a-days for voltage stabilization or transient surge suppression in electronic circuits and electrical power systems^{2-5,13}. Owing to the improvements of non-ohmic properties and functional reliability, the use of ZnO varistors is expanding rapidly. Moreover, with the advent of advanced manufacturing technology, varistors having new designs^{6,46,47} and configurations are expected to have wider application. In addition to some finishing operations, varistor manufacture basically follows the root of conventional ceramic processing.

2.2 BRIEF DESCRIPTION OF CERAMIC PROCESSING

Ceramic materials have been produced and used for centuries and have become very important in modern industrial and consumer technology. These are compounds of metallic and non-metallic elements often in the form of oxides, carbides and nitrides. A wide variety of ceramic materials with a large variation in their physical, mechanical, and electrical properties^{48,49} are produced by different elemental combinations and structural arrangements. Most of the ceramics have a crystal structure and strong ionic or covalent bonds. The unique properties of low electrical conductivity, refractoriness, hardness, wear resistance, high compressive strength are exhibited by ceramic materials because of the strong bonding and structural arrangements.

Depending upon the use and nature of the product, ceramics can be classified as traditional or advanced ceramics. Traditional ceramics refer to the common domestic

products. They can be fine (having particles under 0.2 mm) or coarse (particles as large as 8.0 mm) which in turn produce dense or porous fired bodies⁵⁰. The oldest ceramic product is pottery and it was originated from clay materials. Traditional approaches lack a clear methodology for controlling microstructural heterogeneity and uniformity of the product.

Advanced ceramics refer to the ceramic materials which exhibit superior mechanical properties, corrosion and oxidation resistance, or electrical, optical and magnetic properties⁵¹. Dielectric, semiconductors, insulators, transducers, lasers, emission control, sensors etc. are examples of advanced ceramics. The materials used to produce these products include monolithic ceramics as well as particulate whisker, fibre reinforced glass, glass ceramic and ceramic matrix composites. These materials should possess the necessary properties such as resistance to temperature, stress and environment.

Though the engineering implementation of advanced ceramic is still hindered by their poor formability and brittle nature, the processing technology has advanced in comparison to the traditional ceramic production techniques. Pressing grade advanced ceramic powders^{49,52} require a high degree of compositional and microstructural homogeneity, as well as high degree of purity and reliability.

Performance and reliability of electronic ceramic depends on the grain and the grain boundary phenomena^{3,10,49,53-55}. Hence in the development and production of more advanced ceramic materials, extra-ordinary control of the materials and processing parameters is a requisite to minimize microstructural defects. Compared to the long history of ceramic materials, the use of electronic ceramic as transient over-voltage suppression device is a recent development.

2.2.1 MANUFACTURING PROCESS OF ZINC OXIDE VARISTOR

Zinc Oxide varistors are basically ceramic materials, processed from a number of metal oxide powders. The ceramic body is primarily composed of zinc oxide with

small additions of bismuth, cobalt, manganese and other metal oxides^{3-4,18,21-22,56}. The structure of the body consists of a matrix of conductive zinc oxide grains separated by grain boundaries providing P-N junction semiconductor characteristics. These boundaries are responsible for blocking conduction at the steady-state low voltages and are the sources of the non-linear electrical conduction at higher voltages.

The basic material used to manufacture metal-oxide varistors are pulverized, very finely grained ZnO with particle sizes of about 1 μm , to which as many as 10 or more doping elements are added in the form of fine oxide powders. Its actual composition differs from manufacturer to manufacturer. The proportion by weight of all additives together is about 10 percent, with the share of the individual components ranging from ppm to percent. The purity and fineness of the metal-oxide powders and the homogeneity of the mixture are, therefore, of immense importance for the quality of the end product.

To achieve the required homogeneity the powder is treated in several processing steps, after which the mixture in the form of a slurry has to be spray-dried to obtain the dry granulates necessary for pressing. The resulting spheroidal granulates are about 50 μm in mean diameter with a wide distribution. Majority of the varistor devices are processed from this kind of powder except some category such as multilayer varistors which are made from a slurry paste.

Since the present study was undertaken to evaluate the properties of varistor disc the manufacturing process described here is based according to the procedure adopted in case of varistor disc or arrester fabrication. The major processing steps for the fabrication of zinc oxide arrester block is illustrated schematically in Figure 2.1.

The spray dried powder in the form of granulates are compressed into disc-shaped blocks with approximately 55 to 65 percent of their theoretical density. The pressing is performed by uniaxial double action compaction technique.

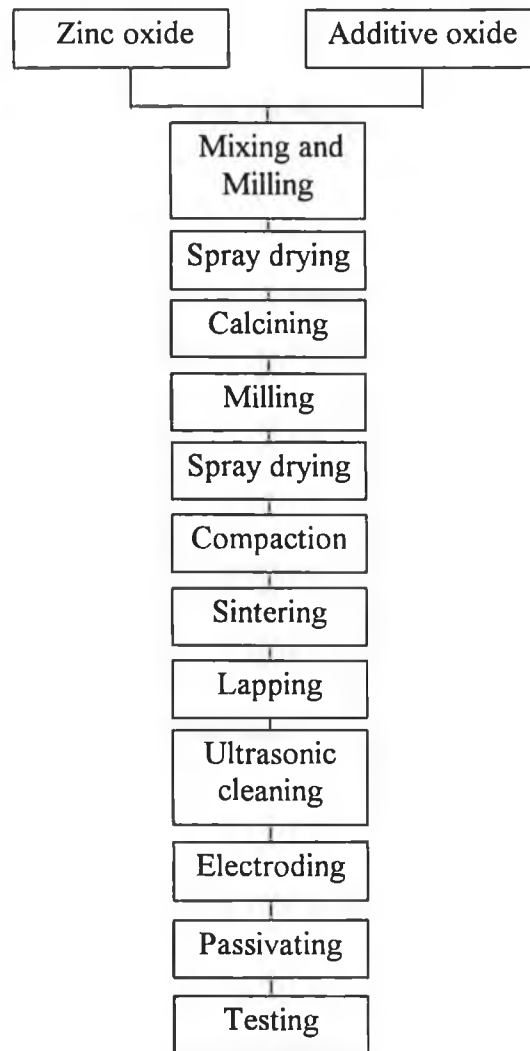


Figure 2.1 The fabrication procedure of the metal-oxide arrester block

The sintering of the discs is performed by a conventional sintering profile with a peak temperature of 1100 °C and a total sintering cycle time of about 70 hours. The sintered ceramic body takes the shape of a rigid cylinder with a theoretical density usually more than 95 percent. In the sintering process the adjacent powder particles are united by means of diffusion, and subsequently grow into large grains.

Zinc oxide varistors undergo a liquid phase sintering process. During this process the bismuth oxide melts to form the liquid phase which dissolves, at least in part, the other doping substances and promotes their uniform distribution. The liquid phase also favours the grain growth and dense sintering. The spinel precipitates, on the

other hand, inhibit grain growth and generates a uniform distribution of the ZnO grain size.

The researches in the varistor technology have been primarily aimed at improving the fundamental properties. In this regard much of the work is related to the investigation of material composition, microstructure, whilst grain and boundary phenomenon^{19-23,27-29,57-62} got the maximum attention. No such work investigating the effect of compaction parameters on ZnO varistor properties has been reported. Some attempt with HIP was made⁶³, but due to the lack in the development of grain boundaries the attempt was not very successful. Heat treatment at high temperature is necessary to facilitate grain growth.

Compaction is the process of applying pressure and simultaneously giving a desired shape on a powder material confined in a rigid die or in a flexible mould. The process depends on an external source of pressure for deforming the powders into a high density mass with required shape and dimensional accuracy. Powder feed is usually in the form of controlled granules containing pressing additives produced by spray drying.

The means of compaction, the mechanical constraints and the rate of pressurization are the significant process parameters which play a vital role in the resulting properties of the green body. Main concern with properties of the green as well as of the fired body dictates that high densities with minimum gradient be achieved following compaction operation. So compaction is undoubtedly a very important step in the manufacturing process of arrester discs. The main focus of this study in analyzing the effect of the compaction parameters on the eventual property of varistor disc.

2.2.2 GENERAL PHENOMENA OF COMPACTION PROCESS

Compaction process passes through different phases of material deformation. Three distinct stages can be identified in the compaction cycle⁶⁴. At the initial stage the

loose array of powder particles is compressed to a closer packing. Then the particle-to-particle point contact deforms as pressure increases. Finally the particles undergo extensive plastic deformation.

At the beginning of the compaction cycle, the powder has a density approximately equal to the apparent density. Voids are observed between particles and with vibration, the highest obtainable density at this stage is only the tap density. As pressure is applied, the first response is observed in the form of rearrangement of particles, giving a higher packing co-ordination. Large pores caused by particle bridging are initially filled by this rearrangement. This change process is aided by hard particle surfaces.

Increasing pressure results in better packing leading to a decrease in porosity⁶⁵. Initially, the number of contacts grows as particle rearrangement and sliding occur. High pressure increases the density by enlargement in contact area through plastic deformation. Thus pressure causes localised deformation at the contacts giving work (strain) hardening and allowing new contacts to form as distance between particles decreases. Interparticle contact zones take on a flattened appearance. However, for ceramic materials which are brittle little growth between junctions occurs.

Any further gains in green density demand more pressure which leads to considerable work hardening. This is especially applicable to metal powder. With brittle materials like ceramic, densification occurs by fragmentation. The compact surface area increases because of fragmentation, however, green strength shows little improvement. At very high compaction pressures, in excess of 1 GPa, massive deformation occurs, leaving fine pore sizes. Pressurization beyond this level⁶⁴ is of little benefit and the material response is similar to that of a dense solid. Moreover, too high a pressure leads to crack generation in the green body⁶⁶.

In contrast to the above three stages in the compaction process for metal powder Van Der Zwan and Siskens⁶⁷ proposed a four-stage phenomenon for ceramic. These are (i) filling of the holes between particles (ii) fragmentation and plastic deformation

of the granules (iii) filling of the holes between primary particles and (iv) fragmentation and plastic deformation of the primary particles. Their investigation was based on two different spray-dried ceramic powders, a wall-tile granulate, and a ferrite granulate.

Green and Fired strength

Bergman et al⁶⁸ investigated to correlate green and fired strength of Al_2O_3 with controlled defects. They observed the same fracture mode with higher variability in the strength of the sintered samples. Sintering has been identified as a critical step because this opens up voids and cracks. A new theory has been proposed by Kendall et al⁶⁹ on the elastic deformation and surface energy of smooth spheres which was verified by experiments on titania and alumina powders.

Pressure and Green Density

It is known that it is pressure which largely determines the ultimate green as well as fired properties. Aketa et al⁷⁰ have conducted a study on iron powder and deduced a theoretical formulation on density distribution on the basis of the assumption that the pressure-density characteristic can be expressed by a hyperbolic function. A similar study was conducted⁷¹⁻⁷³ and the theoretical density distribution has been compared with experimental data and found them fairly agreeable. Some excellent works⁷⁴⁻⁷⁶ have been carried out to simulate the compaction phenomena and various parameters of the compact.

The density gradient developed⁷⁷⁻⁷⁸ due to the die-wall and interparticle friction has been studied on different powder materials.

Compaction and Dimensional Accuracy

Green density is a key factor in keeping the dimensional accuracy of the ceramic discs after firing. It is apparent that lower green density of the compact will allow greater

shrinkage for the same composition of powder. Similarly higher green density will give less scope of shrinkage. Thus higher green density with less density gradient in the compact will reduce the scope of dimensional deviation in the fired body due to shrinkage.

2.2.3 FACTORS INFLUENCING COMPACTION

The compaction process is obviously influenced by a number of parameters. There are various sources of these influencing parameters. However, four distinct sources are clearly identifiable in the compaction process. These are (i) powder characteristics, (ii) organic systems, (iii) pressing technique and (iv) geometry of the compact body.

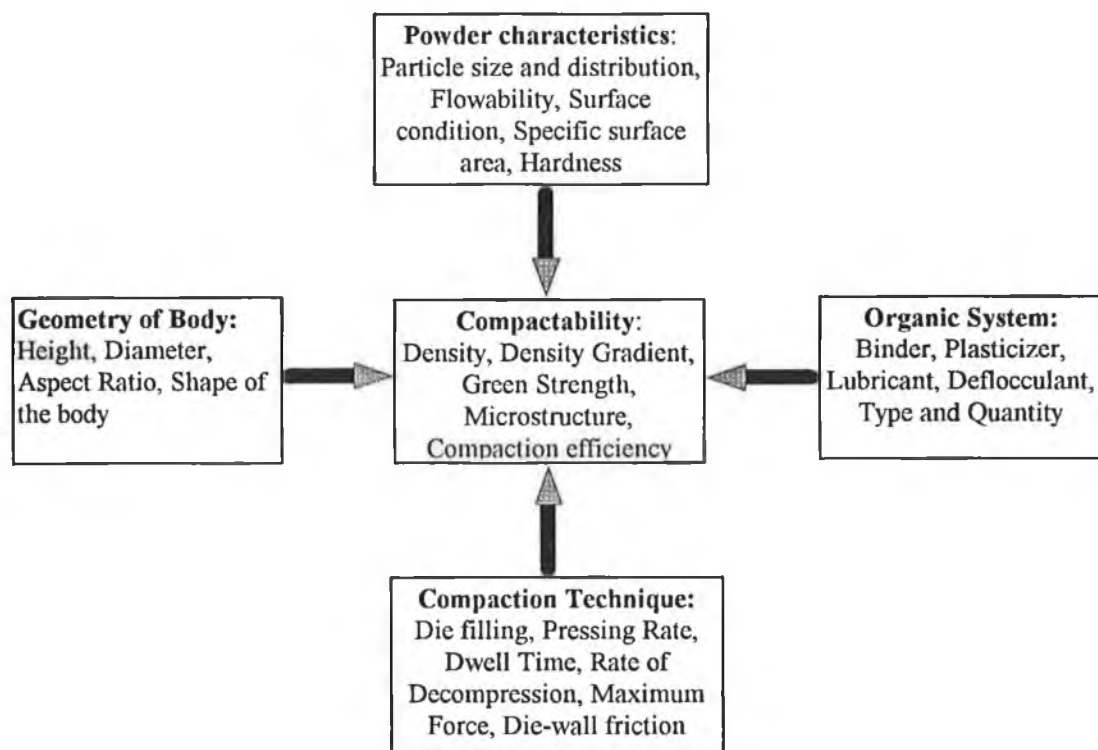


Figure 2.2. Factors affecting Compactability of powder

Compactability of powder is thus a resultant of complex interaction of the input parameters from these four sources. This feature is schematically demonstrated in Figure 2.2.

Powder Characteristics

There are inherent material properties which combine with crystallography, chemical bonding, friction etc. to determine the ease of compaction. Extrinsic powder parameters like the particle size and its distribution, shape, surface condition, flowability etc. can have an equally significant effect on compaction.

Systems used to prepare granulated pressing powders by spray-drying commonly contain a number of organic materials. These materials play a significant role in the process of compaction. The important powder characteristics which affect the compaction process are discussed.

Particle size and its distribution

Particle size and its distribution have been found to affect the compressibility of powder. Compression of non-metallic powders of equiaxed particles can be acceptably characterized by the Bal'shin relation and that the pressing modulus so defined is a simple exponential function of the particle size⁷⁹.

A fine particle size hinders compaction because of the higher interparticle friction⁶⁴. Dimilia and Reed⁸⁰ stated that higher densities might be attributable to the broader size distribution.

Shape of particles and agglomerates

Surface area and interparticle friction are dependent on the shape of the powder particles. In relation to friction the ideal situation is to have spherical shape particles. There is only one point of contact between two particles of spherical shape. Deviation from this shape will lead to more contact points between particles. So shape of particles greatly influences the flowability.

Specific surface area

Specific surface area (SSA) is one of the most important parameters used to characterise powders. This is actually dependent on other parameters like particle size, size distribution, shape and surface conditions. Surface area is often used as shape index. However, this parameter is not expected to directly affect the compressibility of powder. Higher specific surface indicates that the particle size is small and free surface energy is more. So it is quite clear that the SSA plays a significant role in case of sintering.

Flowability

Good powder flow is essential for reproducible volumetric filling, a uniform density of filling and rapid pressing rates. Dense, nearly spherical particles with smooth, nonsticky surfaces that are coarser than 40 μm have good flow behaviour and are preferred for pressing⁴⁹.

Moisture content

Water acts as a plasticizer for PVA. Just as with PEG, an increase in moisture content in the powder lowers T_g and the apparent yield point. Granulates with a relatively high moisture content (more than 8 percent) can be easily compressed with low compression pressure. At higher pressures, water fills all interstitial spaces and consequently no further densification can be obtained unless under very low speeds the water is allowed to escape.

Granulates which are too dry have little cohesion and insufficient lubrication to be adequately densified. Optimum moisture contents are in the range of 6-8 percent, which are comparable with industrial practice⁸¹. But for metal-oxide powder the moisture content is very low usually less than 1 percent.

Interparticle Friction

Powder flow and packing characteristics are the results of interparticle friction. As surface area increases, the extent of friction in the powder mass increases. Consequently, the friction between particles increases leading to less efficient flow and packing. This concerns automatic die filling in compaction⁶⁴.

Density and packing properties decrease because of poor flow past neighbouring particles. Apparent or bulk density is the density of loose powder without agitation, whereas tap density is measured with agitation usually giving a definite number of taps. The angle of repose (angle formed by pouring a powder into a pile) is another friction index.

Hardness and Ductility

The work hardening behaviour of a material and hardness are both expected to influence compaction⁶⁴. Cooper and Eaton⁸² conducted a study on compaction behaviour of four ceramic powders with different hardness and found that softer powders yielded a greater fractional compaction at a given test pressure. ZnO being a softer ceramic is expected to behave better in terms of compaction.

Organic System

Compressibility of a ceramic powder depends on the type and quantity of organics present. Various organic materials are added to prepare a slurry for spray-drying. These are added as deflocculent, binder, plasticizer, lubricant, wetting agent and defoamer.

Binder

Binder has the purpose of imparting green strength to the compact for ejection and subsequent handling prior to sintering. Binder content should be kept as low as

practicable to minimize both the higher binder cost and the amount of gas produced during binder burnout and its content is usually kept in the range of 2-12 volume percent⁴⁹. But for MOV powder it is even less than the lower limit.

Compaction is enhanced by factors tending to soften the binder system⁸³ such as increased humidity and temperature. Nyberg et al⁸⁴ has studied compaction behaviour of powder by testing 3 different binders and concluded that granules with latex exhibited better compaction properties and had the highest sintered densities. The experiment was carried out with Alumina powder.

Lubricant

Lubricant has the purpose of easing ejection, improve uniformity in density distribution in the compact and to reduce the die wear. Lubricating the die enhanced the stress transmission⁸⁵.

Pressing Technique

There are various techniques available for compaction of powder. However, each technique has its own advantages and limitations. Ultimate selection of a technique is dependent on the economic balance in terms of compact quality and the production rate. Capability of exerting pressure is an important criterion in the selection of pressing machine. Since the relationship between compacting pressure and the density is very vital and it is the pressure which largely controls the eventual attainment of density, strength and porosity in the green body more than any other factor¹². Moreover, improved green properties are likely to impart better sintered properties.

Classification of compaction techniques

There are various approaches in which compaction techniques can be classified. However, depending on the scale of use they can be broadly categorized into two major groups (a) conventional compaction and (b) alternative compaction.

Conventional Compaction Technique

There are two common techniques under conventional compaction. These are (i) uniaxial or single stroke static compaction and (ii) isostatic compaction. Uniaxial compaction can again be subdivided into two forms - single action and double action while isostatic compaction can be cold isostatic pressing (CIP) and hot isostatic pressing (HIP).

Most conventional presses can again be classified as either mechanical or hydraulic. Mechanical presses typically have a higher production rate. These can be (i) single stroke press (ii) rotary press (iii) toggle press with pressing capacities usually up to 100 tons. But toggle presses are available with up to 800 tons capacity. Hydraulic presses can be very large and can exert as much as 5000 tons of load⁸⁶. But the hydraulic presses have a much lower cycle rate than mechanical presses.

Recently there are some compaction machines in which a new feature of 'Ejection Position Constant (EPC)' has been incorporated. This eliminates adjustment of ejection stroke.

Uniaxial compaction

Uniaxial compaction involves the pressing of powder into a rigid die by applying pressure along a single axial direction through a rigid punch. For evaluation of the compressibility of powder single action is carried out while for green and fired strength of the green compact and the electrical properties of the varistor double action method is used for compaction operation. It has been noticed that compaction cycle and the design of die are very important parameters.

Compaction Cycle

The compaction cycle is very important to obtain a good quality compact. Usually a compaction cycle with a characteristic of long pressing time ensures good powder

compaction. However, in the context of productivity, a shorter pressing cycle is preferable.

Die Design

To reduce external powder friction the die-wall must be ground in the axial direction. Application of a wall lubricant is most effective if the particles are small and the lubricant thickness is large⁸⁷. Lubricant thickness should be much larger than particle size.

Cold Isostatic Pressing

Isostatic pressing or compaction involves application of pressure equally to the powder from all sides. This technique remarkably reduces the problems of nonuniformity due to die-wall and interparticle friction and thus permits uniform compaction of a larger volume of powder. Thus this technique can conveniently press compact of high aspect ratio and of complex geometry. However, it is well-known that isostatic compaction cannot compete on a production line basis with die compaction⁸⁸.

CIP on precompact body

This is actually a combination of uniaxial and isostatic compaction. G. Andersson⁸⁹ conducted creep experiment on precompacted tungsten carbide powder specimen. Less strain change was observed on precompacted (20 MPa) specimens compared to loose powder compaction.

Alternative Compaction Technique

Alternative compaction techniques are not widely used methods. But they have some interesting features which may be advantageous compared to their limitations. There may be a number of alternative compaction technique, however, only three will be

mentioned here. These are (i) compaction with ultrasonic vibration (ii) cyclic compaction and (iii) dynamic compaction.

Compaction with Ultrasonic Vibration

In this process the pressing tool is mounted at a motion node and is excited by means of magnetostrictive ultrasonic transducer. The powder is located at a motion anti-node of the acoustic vibration system and is thus subjected to high accelerations. E. Lehfeltd⁹⁰ conducted experiment using this technique. For a metal powder (iron) it has been found that a significant increase in green density can be attained with ultrasonic vibration, particularly in the initial stages of the pressing process.

Regarding the green strength it has been found that strength of the compact made using the ultrasonic vibration is not higher than that of the test-pieces of the same density pressed without ultrasonic vibration. This indicates that for specimens of the same green density, no increase in strength can be achieved with ultrasonic vibration.

Springback effect is minimum when ultrasonic vibration is used providing greater dimensional stability. Experiment was carried out on tin test-pieces. This feature is attributable to the fact that the enclosed air in the powder can leak away more easily during vibrations. This is specially important when high pressing speeds are used.

E. Emeruwa et al⁹¹ investigated the compaction behaviour of ceramic powders by ultrasounds. They found that compact density would increase with ultrasonic parameters such as amplitude and time of application. Other effects such as improved porosity and microstructure were also observed.

Thus ultrasonics can offer considerable advantages in the compaction process. This can be used to lower the flow boundary of the material. In addition the working temperature required to attain a given density can be lowered.

Cyclic Compaction

Kim and Son⁹² proposed this type of compaction technique. It has been found that cyclic compaction is more efficient than the conventional uniaxial technique. A densification equation, based on the Cooper and Eaton compaction equation has been proposed to describe the cycle dependent pressure-volume fraction relation for ceramic powder compaction. This has been found to be well represented for the alumina powder. The experimental results also suggest that the cyclic compaction with zero bias pressure is more efficient.

Dynamic Compaction

In this process the powder metallurgy and explosive forming methods have been combined. The purpose was to make parts from nonequilibrium powders which were either hard to compact or which might lose their unique properties in the high temperature sintering operation⁹³.

Dynamic processing enhances locked-in elastic strains and lattice defects, often resulting in a stronger material. Because dynamic high-pressure state is transient, lasting only nanoseconds, the whole compacting process is completed before thermodynamically immiscible components of the particles have time to separate. Thus dynamic compaction can lead to non-equilibrium materials with unique mechanical, electromagnetic, or chemical properties.

Geometry of Compact Body

Arrester discs are cylindrical in shape. So the geometry of the compact body is simple. However, the aspect ratio (height to diameter ratio) is very important for uniform properties of the green body. Generally, when this ratio exceeds five, die compaction is unsuccessful⁶⁴. Better pressing results are observed with smaller aspect ratio.

2.3 OBJECTIVE OF THE STUDY

The objective of the study was mainly based on the efforts to secure the improvement on the energy absorption capability of ZnO varistor disc for arrester application. Much of the work was related to investigate the effects of the compacting parameters on the physical and electrical characteristics of varistors. Some other relevant processing aspects were also studied to identify the contributing factors in enhancing the performance. Though the energy absorption capability was considered to be the main parameter, some other critical characteristics were also evaluated.

The objectives of the study were as follows:

- To correlate the physical and functional parameters of varistor in terms of the compacting pressure and speed
- To evaluate the effect of dwell time in the pressing cycle on the energy absorption capability, high current performance
- To evaluate the effect of sintering orientation on the fired disc e.g. density gradient, hardness, mechanical strength and microstructures
- To verify and propose alternative approaches in the light of better performance, improved process capability etc.
- To investigate the fracture mechanism in high current pulse and suggest appropriate measures to enhance the behaviour
- To identify the possible areas of future work for further improvement.

Chapter 3

EXPERIMENTAL PROCEDURE AND EQUIPMENT

3.1 INTRODUCTION

Zinc oxide varistors are produced in different shape and size to meet the specific requirements of application. Though there is a broad range of varistor products available to combat a wide range of possible transient voltage suppression conditions, the experiments during the course of the study was carried out only on arrester blocks and discs. These test specimens were cylindrical in shape but different in size - the small discs and the standard production line arrester blocks. The smaller samples were pressed by using a 17 mm floating die, designed and fabricated exclusively for the purpose of evaluating the effect of compaction parameters and the measurement of compressibility of powders.

The controlled load and speed were applied on the upper punch through the anvil of an Instron machine to form the green compact. Standard discs were pressed in a hydraulic compacting machine by changing the pressing cycle parameters mainly the dwells. Metal-oxide varistor powder with standard formulation was used for making all the test samples. After the pressing operation, the usual procedure of sintering, passivation, grinding, electroding was performed to prepare the samples for testing.

The functional reliability of a zinc oxide varistor is determined by a number of critical parameters. In this context the I-V characteristics, the energy absorption capability and the high current performance are very important. The grain size and the grain boundary of the ceramic largely influence the I-V characteristics whereas the homogeneity, integrity of the varistor material are vital for the energy handling capability and the high current performance. The level of perfection in the various finishing operations is certainly of significant importance in this regard. So each of the processing operations - starting from the powder preparation to the electroding,

is of great importance in terms of the functional reliability of the varistor. A minor flaw in the earlier processing stage could adversely affect the ultimate electrical property. Sufficient green strength of the compacted disc is necessary for handling them prior to sintering while post sintered mechanical properties are vital for further processing results and the eventual field performance.

There are some apparently uncontrollable defects generated in the ceramic during sintering such as pinhole, void, crack etc. These defects may affect the uniformity of the material and result in earlier failure of the discs. This kind of flaws or defects may originate from other sources as well. It is envisaged that not only the higher degree of homogeneity of the ceramic material but also the quality of passivation and electrode can be responsible. Suitable passivating material with optimum thickness and proper electrode of the varistor are conducive to achieve a high level of energy absorption capability and enhanced high current performance.

Mechanical characteristics such as the hardness, density gradient, strength etc. are the indicators of the quality of the ceramic material. So in the course of the study the important mechanical and electrical parameters were investigated adopting the standard methodology for possible correlation. A brief description of the critical testing parameters, the procedure adopted and the equipment used in preparation and testing of the samples is presented in the following sections.

3.2 PREPARATION OF SAMPLES

The study substantially focused on the effect of the compaction parameters. The samples were pressed adopting the uniaxial double action compaction technique either with the floating die applying load through an Instron machine or with a hydraulic compacting press available in the production line. However, to study the additional functional parameters production line 'as produced' discs were used. Microhardness was measured on standard discs to correlate with their grindability.

3.2.1 SMALL SIZE ARRESTER DISC

Standard metal-oxide varistor powder was pressed to prepare the cylindrical discs with a nominal green diameter of 17 mm using a uniaxial double action floating die applying controlled load with the help of a precision Instron machine. The discs were then sintered followed by the finishing operations such as the glassing or passivation, grinding and electroding.

Compaction Procedure

A target amount of standard MOV powder was weighed and poured manually into the die cavity. The load was applied on the upper punch of the die-set through the anvil of the cross-head of the Instron machine. With the lowering of the upper punch the powder was progressively compressed with the increase in load. At a certain level of increasing pressure the floating die started to go downward as a result of the load transmitted through the die-wall. The powder was also pressed from the other side through the lower punch. The pressing parameters were the peak load and the speed of cross-head. The peak load and the cross-head speed were set digitally with the electronic control console of the Instron. The pressing operation was conducted by the uniaxial double action compaction technique.

Sintering and finishing operation

Considering the smaller size of the discs the sintering of the 17 mm samples was performed by a slightly modified temperature profile from the conventional one. A shorter soak duration at peak temperature was selected with a total sintering cycle time of about 65 hours. Sintering operation was carried out in a pot kiln with the temperature profile demonstrated in Figure 3.1. The sintered discs were passivated by the standard procedure. This includes preheating of the discs up to a temperature of 120 °C followed by the spraying of glass in the form slurry on the side or C-face of the disc. The purpose of preheating is to facilitate sticking of the glass slurry on the surface. The samples were then passed through the glassing oven for firing at a

maximum temperature of about 800 °C. The flat faces of the cylindrical discs were ground using a polishing machine on the grinding paper of grit size 240. They were then washed with deionized water in an ultrasonic cleaner, Hilsonic. A thin layer of silver was painted by brush on the ground and clean face of disc to act as electrode.

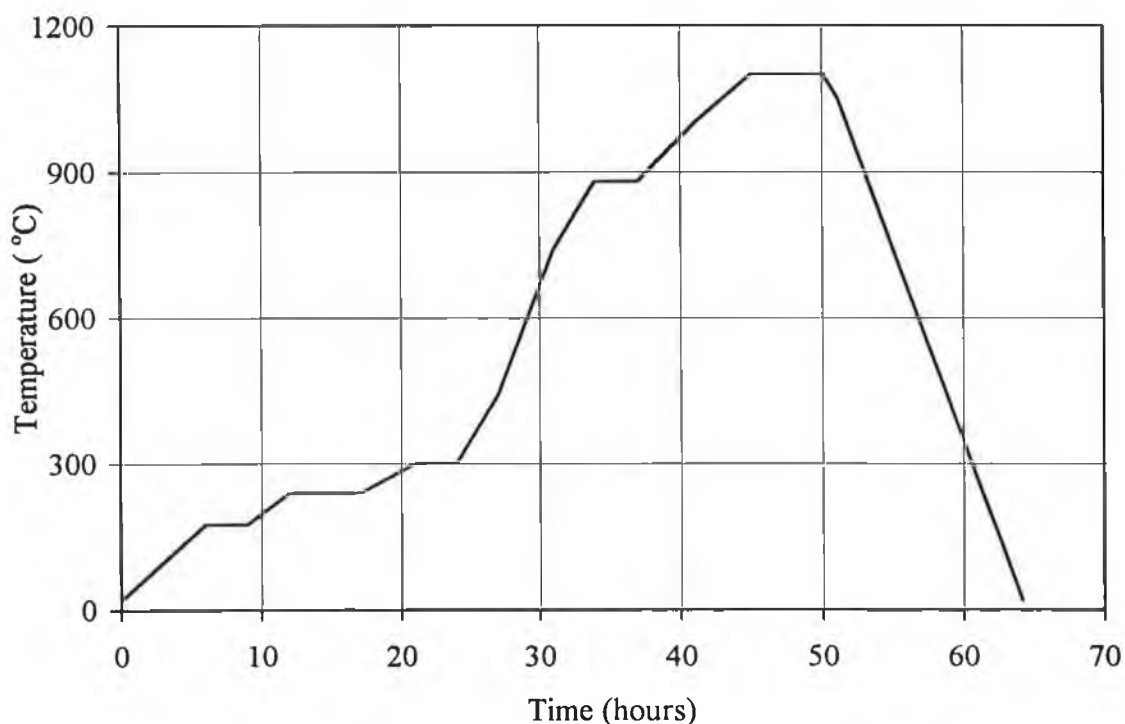


Figure 3.1: Temperature profile for the sintering of small size samples

The dried silver electrode was cured by passing the samples through a glassing oven to secure perfect adhesion with the ceramic.

3.2.2 STANDARD ARRESTER BLOCK

Most of the investigation was conducted using standard arrester blocks as samples. These were 32 mm and 42 mm in diameter of the fired disc with nominal voltages of 3 KV and 5 KV respectively. They were used for both the mechanical and electrical characterization. To evaluate the effect of dwell time in the pressing cycle, an experiment with two level factorial design was performed using the standard production line arrester discs. Investigation with sintering orientation, stress wave

propagation, performance of hexagonal disc in energy absorption capability was also conducted with the standard samples.

Compaction Procedure

Standard arrester blocks were compacted in a hydraulically operated production line compaction machine. In addition to the possible adjustment in the peak load, the pressing cycle is composed of a number of functional steps such as jog, dwell times. The filling of the die with powder was facilitated by a number of jogs and pressing with a number of holding times at different phases of loading. The blocks were pressed by the uniaxial double action compaction method. However, except for the experiment with dwell time, other investigations were conducted with the discs pressed under standard pressing cycle.

The compacting machine, Hydramet (Model HC 75 EC) used for pressing the arrester blocks is equipped with special features having precise and reliable controls. The pressing cycle consists of three main steps - filling, pressing and ejecting. Filling of the die with powder is facilitated by 8 jogs. After reaching a low pressing load (approximately 10 tons for three compacts of 49 mm in diameter, equivalent to about 18 MPa), a pre-press dwell time of 0.5 second is maintained followed by a higher load of 60-70 tons (equivalent to 108-126 MPa) at which the compacts are held for 2.5 second as press dwell. On releasing the load but keeping the disc inside the die an ejection delay for 2.0 seconds is provided. The compact is ejected by the lower punch but keeping it in contact with the upper punch. A delay of one second is adopted to detach the upper punch from the compact. Thus the operation is completed by a total cycle time of 28-30 seconds. A target green density is maintained within a range of 3.30 - 3.50 gm/cc.

Sintering and other finishing operation

The sintering of the larger size samples was performed in the production line large capacity kiln. The temperature profile was similar to that mentioned earlier except a

longer soak duration at the peak temperature of 1120 °C with a total sintering cycle time of 70 hours. However, it is known that there are temperature differences from location to location inside the overhead large capacity (16,000-20,000 discs in a single charge) kiln. Therefore, a particular zone in the kiln was chosen to sinter the discs so that the variation arising due to the deviation in temperature over the whole cycle could be neglected.

3.3 ELECTRICAL CHARACTERIZATION

The small arrester discs were tested for evaluating the effects of the compacting parameters on the physical, mechanical and electrical properties. Thus the green and fired density, axial, radial and overall volume shrinkage, diametral depression were computed by using standard digital measuring instruments. Important electrical parameters concerning the I-V characteristics and the energy absorption capability were evaluated. The procedure of measurement and evaluation of these critical parameters is briefly described in the following sections.

3.3.1 CURRENT-VOLTAGE CHARACTERIZATION

Zinc oxide varistors are characterized by the I-V curve in the low, medium, and high current regions. These three regions are popularly known as the pre-breakdown, breakdown and upturn regions associated with the I-V characteristics. They serve various functions in the design and operation of varistor under the steady-state condition as well as under the transient overvoltage surges. The most desirable varistor should have a low clamping ratio (the ideal value is unity) and a leakage current, a higher value of non-linear co-efficient and energy absorption capability with a longer operating life.

Prebreakdown region

The prebreakdown region determines the steady state joule heating and the nominal voltage of the varistors. The current voltage relationship is ohmic in this region and is

controlled by the resistivity of the grain boundary. High Voltage Test System was used for smaller size samples to measure the values of current at preset voltages and the values of voltages at the preset current. The data obtained from the piece by piece measurement are stored in the computer memory and are obtained as computer printout at the completion of the test. The current-voltage values were normalized to compare the effects of the input parameters.

Measurement of the voltages and currents at the prebreakdown region for bigger samples (arrester blocks) was performed in a Watt loss tester. The necessary data on voltage were obtained by adjusting manually the powerstat knob to set the target current. The tester generates sinusoidal pulses and the peak voltages for a set of specified currents were recorded.

Breakdown or Non-linear Region

This region is termed as the heart of varistor, wherein the device conducts a large amount of current for a small increase of voltage. The degree of non-linearity is determined by the flatness of the region. For the small arrester discs the voltages at a current of 100 A and 1 KA were measured by the Classifier and the High Current Tester respectively. The pulses were of $8 \times 20 \mu\text{s}$ wave shape. The same equipment was used for characterizing the standard arrester block with the same wave shape.

Upturn Region

This is the high current region where the I-V characteristics are again linear and the voltage rises faster with the current. For the cross-section of the small arrester discs the 10 KA current was in this region and the test for this current was performed in the Impulse Current Test System with the pulse of $8 \times 20 \mu\text{s}$ wave shape. However, for the arrester blocks the 100 KA corresponds to the current of the upturn region. These blocks were characterized with a pulse of $4 \times 10 \mu\text{s}$ wave shape using the same equipment.

3.3.2 ENERGY ABSORPTION CAPABILITY

The energy absorption capability of a varistor is determined by the maximum energy density injected into the ceramic body up to which it can sustain for a cycle of three shots. The energy absorbed by a disc is evaluated by dividing the total energy injected into the varistor body with its volume. Thus this important parameter actually indicates the maximum energy density of varistor expressed in terms of Joule.cm^{-3} .

To measure this parameter the varistor disc is subjected to a cycle of three pulses injecting energy of approximately equal quantity in each pulse. Unlike the measurement of mechanical strength, this test for the energy absorption cannot be performed in a single step. The temperature rises in the ceramic body due to the application of a pulse. Hot disc, already under stress due to the high temperature, if subjected without cooling to the next cycle of pulses with increasing energy level may fail too early. To avoid this problem, after each cycle of shots, the varistor is cooled down to the room temperature before being subjected to the next cycle. The test is initiated with a lower charging voltage, sufficient to inject energy in the lower range of $125 - 150 \text{ J.cm}^{-3}$.

Selection of the lower range of energy is attempted to keep the probability of failure at the first cycle to a minimum level. Since higher charging voltage leads to higher energy injection, for every subsequent cycle of pulses the charging voltage is increased marginally so that the energy injection level goes up by not more than five to ten percent. This process of testing by the discrete increment of charging voltage is undertaken for the whole lot of the samples. Defective discs start to fail early and the better discs sustain higher energy levels. Thus the sample size reduces progressively as the disc fails step by step with the increment of charging voltage. The testing procedure was continued until all the discs failed at a certain stage.

The energy density of a disc calculated on the basis of the clamping voltage and the peak current from the cycle of shots preceding to which the disc failed is considered to be the energy absorption capability. It is clear that the resolution of measurement

is dependent on the value of increment of the charging voltage. Thus for higher accuracy lower value of increment in charging voltage is necessary leading to a greater number of cycles to complete the test.

Rectangular Impulse

The definition of the rectangular impulse for a current is derived from the Figure 3.2. This millisecond duration pulse is conventionally termed as long wave and is experienced in switching surges. The pulse duration is actually the time measured from the instant of 90 percent of the peak current during rise to the same level during the fall as indicated by $T_{90\%}$. For a typical test pulse this duration is 2 milliseconds. The impulse is not perfectly rectangular in shape and the duration from 10 percent of the peak between the rise and fall, $T_{10\%}$ is more than $T_{90\%}$ and is typically 2.6 milliseconds.

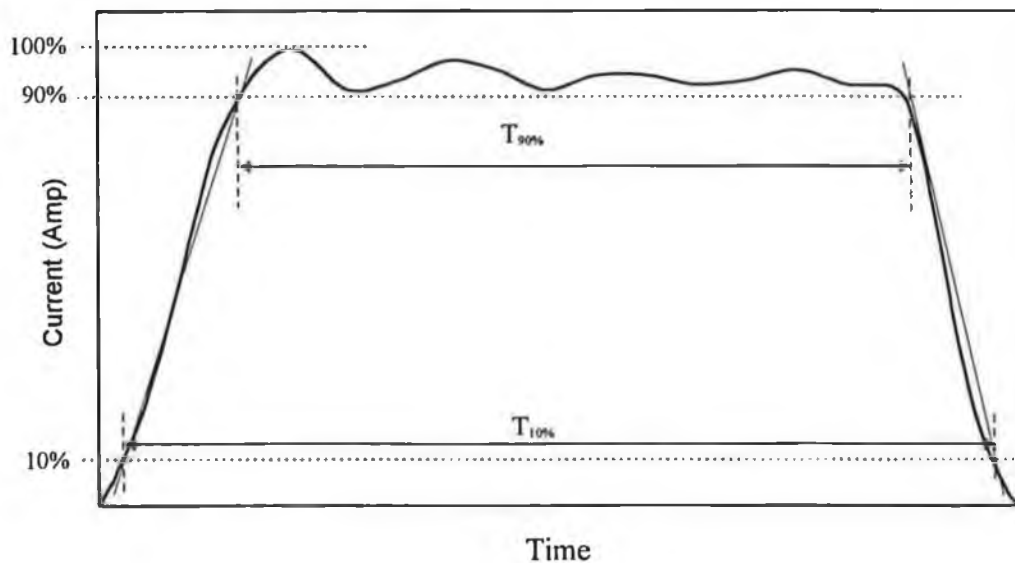


Figure 3.2 Definition of the long wave for measuring energy absorption capability

Calculation of Injected Energy

The energy injected in a pulse is the integrated value of the product of the instantaneous voltage and current over the pulse duration. So the amount of energy can be expressed mathematically with the following relationship:

$$Energy = \int_0^t vidt \dots\dots\dots(3.1)$$

However, the instantaneous values of the voltage, v and current, i are not regular functions of time. Moreover, their instantaneous values are not practically recorded to evaluate the integrated energy. In practice the peak values of the clamping voltage of the arrester block and peak current passing through it are recorded for computation of the energy. For a pulse of quasi-rectangular shape, the relationship can be expressed in terms V_{pk} = peak voltage, KV and I_{pk} = peak current, A for a duration of time T in millisecond as follows:

$$Energy = \int_0^t vidt = KV_{pk} I_{pk} T \dots\dots\dots(3.2)$$

where K = constant, which depends on the wave-shape. For a quasi-rectangular pulse as shown in Figure 3.2, $K=1.14$, a value computed from the wave geometry. Thus the total injected energy by such a pulse of 2 milliseconds is estimated as

$$Energy = 2.28 V_{pk} I_{pk} \text{ Joules} \dots\dots\dots(3.3)$$

The energy absorption capability is evaluated by dividing the quantity of energy computed from the above equation with the volume of the varistor disc.

3.3.3 HIGH CURRENT PERFORMANCE

The short duration pulses are in the range of microseconds' duration but with high amplitude. This is a simulated pulse of the actual lightning stroke. Typical short pulses used for testing the varistor is $4 \times 10 \mu s$ or $8 \times 20 \mu s$ where the first value (virtual front time) indicates the rise time from 10 percent to 90 percent of the peak current and the second value (virtual time to half value) is the duration up to 50 percent of the peak during falling.

Typical clamp voltage and current of short pulses exhibited by a 42 mm diameter disc with a nominal voltage of 5 KV are shown respectively in Figures 3.3 and 3.4. The 8x20 μs pulse is used for classification of the varistor while 4x10 μs pulse is applied to verify the high current capability by the high current short duration (HASD) shot. In practice the HASD pulse is not applied to all the discs of the lot, rather an acceptance sampling plan is adopted to pass a lot by testing a small number of samples.

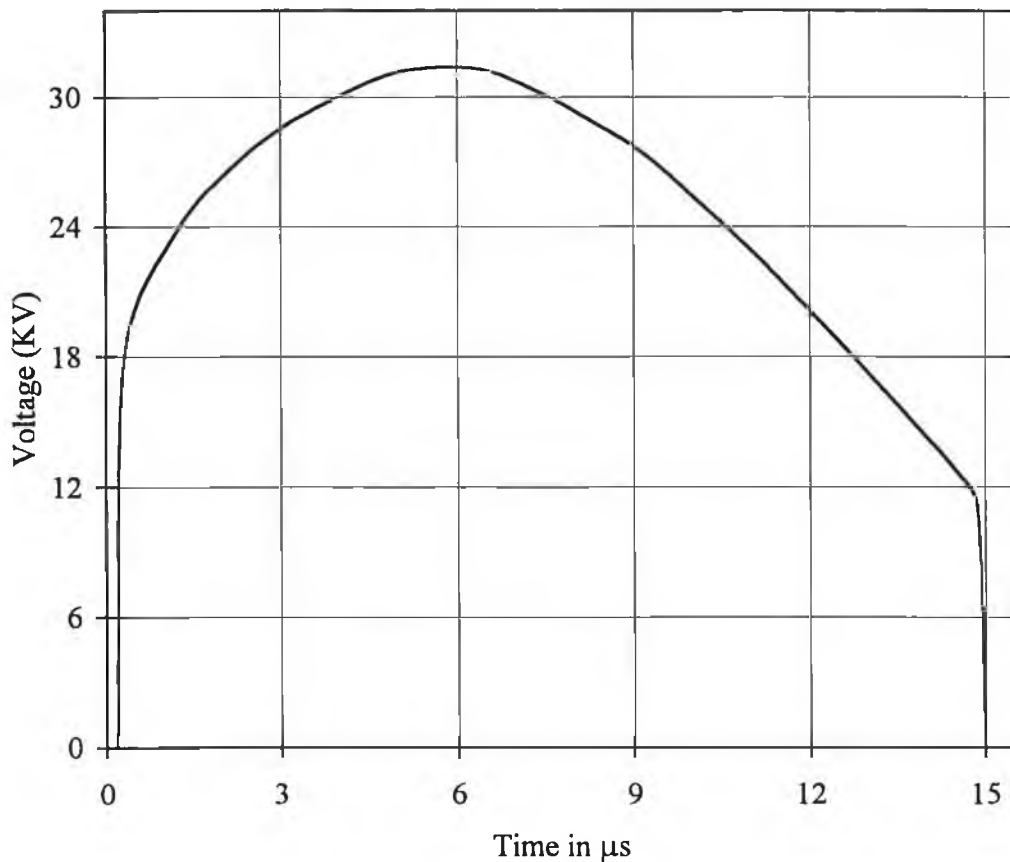


Figure 3.3 Typical clamping voltage for a high amplitude short duration pulse test

Unlike the test for the energy absorption capability only one shot is applied at a time for the high current capability. The energy injection, though strictly dependent on the clamping voltage as well as the current, is usually more than 350 j/cc per shot for

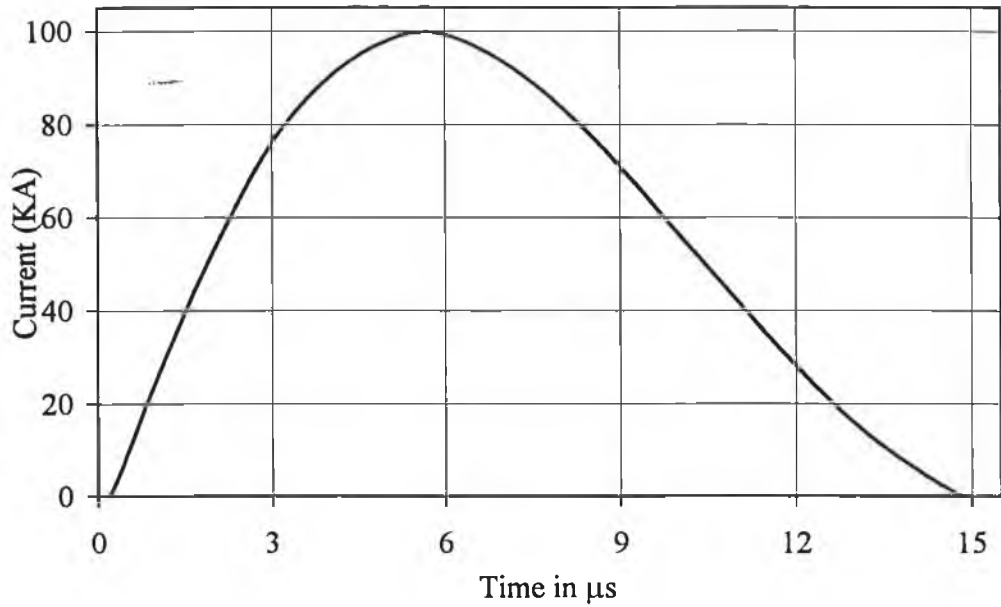


Figure 3.4 Typical current pulse in HASD test

a current density of about 7.5 KA/cm^2 . A typical energy injection curve is plotted in Figure 3.5 with the values computed numerically from the voltage and current pulses

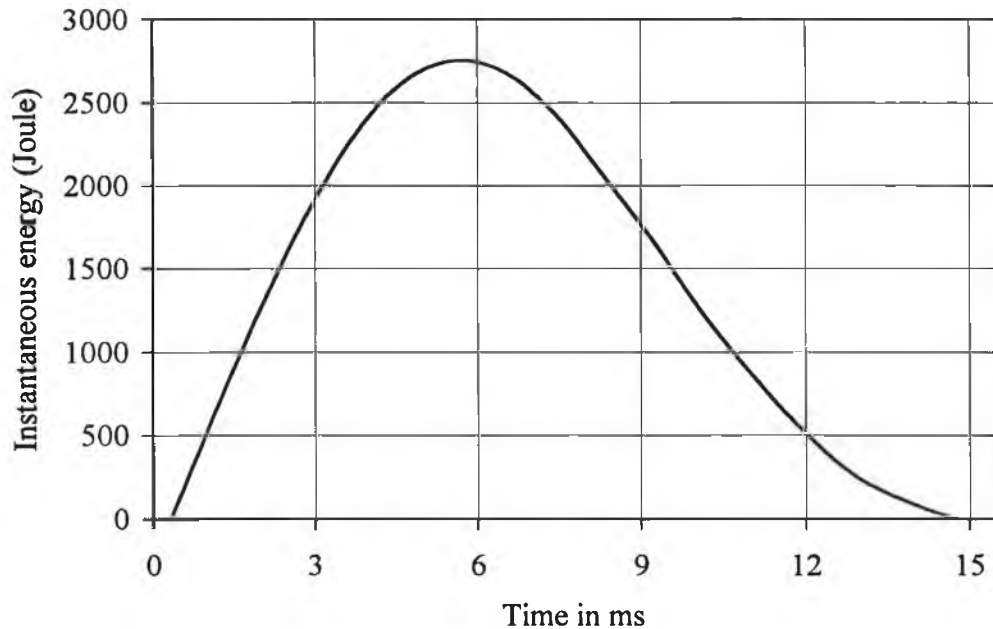


Figure 3.5 Instantaneous energy injection in HASD pulse

shown respectively in Figures 3.3 and 3.4. The purpose of this test is different from that of the long pulse. The failure mode in this test is predominated by cracking rather

than by the thermal runaway or puncture as observed in the case of long pulse test. The severity of the short pulse is dependent on the steepness of the wave front. In this respect usually the shape of the current pulse is considered ignoring the variation in the clamping voltage. But in practice the clamping voltage does not remain constant over the pulse duration. This leads to the instantaneous energy injection curve which appears to have a distinctly steeper wave front than that of the current pulse. So the severity is obviously more than what is normally thought.

The generated clean fracture surface due to the high amplitude short duration pulse cannot always be explained in terms of the stress developed due to temperature gradient alone. Usually high voltage part (with the same geometry but having smaller grains) is more susceptible to failure in the high current. This may be attributable to the effect of higher energy injection arising from the higher clamping voltage but with the same current.

The I-V characteristics, the energy absorption capability and the high current performance are the general investigating parameters. However, main attention was focused on the energy absorption capability throughout the study with a view to optimizing the input variables.

3.4 MECHANICAL CHARACTERIZATION

The number of influencing physical and mechanical parameters of varistor are quite large. Some are important in the processing operation while the other are vital for reliable varistor function. Thus the surface hardness significantly affects the grinding performance while the mechanical strength appears to be important for the energy absorption capability and the high current performance.

In addition to that some correlation was found between the mechanical strength and the sintering orientation of the discs. Significant density gradient was also observed. Archimedes' principle was adopted to measure the density gradient while Vicker's hardness method was adopted to evaluate the microhardness. The mechanical

strength was evaluated by diametral compression test and the three point bending method.

3.4.1 DENSITY GRADIENT

In failure mode analysis it has been observed that sintering orientation of the disc plays a significant role. The face in contact with the liner material was found to be vulnerable in the context of failure initiation. This behaviour of the disc was verified by observing the variation in fired density of the disc from point to point. Segments cut from different grid points were investigated for the density. Archimedes' principle was adopted to measure the density.

Parallelepiped shaped specimens cut from different grid points of the disc were wrapped by masking tape with proper care so that no air could be trapped. This method was adopted so that water could be prevented from entering into the open pores of the samples. Constant density lines were drawn from the measured apparent density of the segments

3.4.2 MICROHARDNESS

The hardness was identified to be responsible for unsatisfactory grinding performance of the fired disc. Distribution of the hardness was found to be dependent on the sintering orientation of the disc and the liner material used. The hardness was measured by the Vicker's hardness method using a microhardness tester, a brief description of which is given in the subsequent section.

3.4.3 DIAMETRAL COMPRESSION TEST

This is a very simple and convenient method for evaluating the mechanical strength of arrester discs since these are readily available in cylindrical shape. This test, also known as the Brazilian disk test, is widely used to measure the tensile strength of the

brittle materials. The orientation of the arrester disc and the application of force is shown in Figure 3.6.

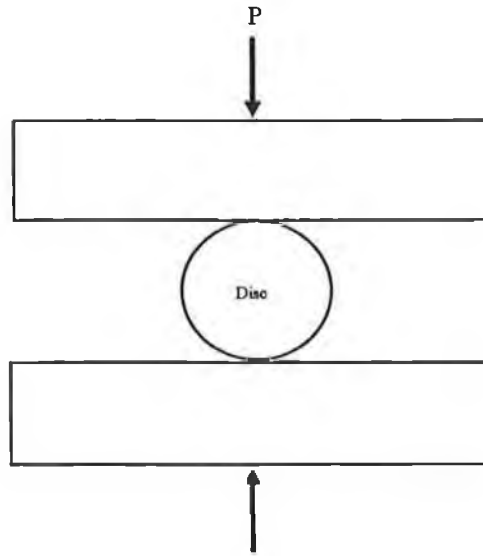


Figure 3.6 Arrangement of test specimen in diametral compression test

3.4.4 MICROSTRUCTURAL ANALYSIS

The general microstructures were imaged by scanning electron microscope (SEM). The microstructure developed during sintering plays an important role in the electrical performance of a ZnO varistor. Few microstructural analyses were performed by using Jeol JSM-840A instrument. The samples were prepared from cut-pieces which were polished with diamond paste having a grain size of $0.25\ \mu\text{m}$ as a final step.

SEM is a popular method for the direct observation of surfaces because they offer better resolution and depth of field than optical microscope. The process principally involves the generation of a primary beam of electrons from an emission source which are then accelerated by a voltage of between 1-30 KeV and directed down the centre of an electron optical column consisting of two or more magnetic lenses. These lenses cause a fine electron beam to be focused onto the specimen surface. Scanning coils made to pass through the corresponding deflection coils of a CRT so

as to produce a similar but larger raster on the viewing screen in a synchronous fashion.

There are various modes of SEM operation. Improved contrast between the microstructural constituents were obtained by using back scattered electron imaging which made use of differences in average atomic number in the various phases. The sizes of ZnO grains were determined by linear intercept measurements.

3.5 ELECTRICAL EQUIPMENT

To carry out the I-V characteristics, the energy absorption capability and the high current performance, various types of electrical equipment was used. High Voltage Test System and Watt loss High Temperature Tester were used to measure the pre-breakdown region of the I-V curve respectively for the small and the standard samples. For the measurement of non-linear and upturn region a classifier and HASD tester were used. Energy absorption capability was measured by a rectangular pulse generator.

3.5.1 HIGH VOLTAGE TEST SYSTEM

This equipment was used to measure the current and voltage of the prebreakdown region of I-V curve for the small arrester samples. High Voltage Test System consists of two main parts: (i) Kepco power supply unit (model BOP 1000M) and (ii) Keithly data measurement unit (model 237 SMU). The power supply unit can be operated in dc mode within the range of 0-5000 volt and 0-5 mA current.

The system is capable of measuring the leakage current at preset voltage, the rated voltage V_r at 10 μA , ΔV at 50 μA , and the nominal voltage at 1 mA. Varistor was placed one by one in the sample holder and the lid was closed to switch on the system for measuring the preset values. The data measured automatically were stored in the computer memory. On completion of the test with all the samples, the stored data were retrieved in the printed form.

3.5.2 WATT LOSS HIGH TEMPERATURE TESTER

This equipment (model LC-1201B) is composed of (i) High voltage control panel and (ii) Ambient test/Select panel. Unlike the High Voltage Test System this machine is operated in the ac mode and the current-voltage characteristics up to 10 mA can be measured. Of the available modes a set point of 10 mA at the ambient temperature was selected to measure the I-V characteristics at pre-breakdown region for arresters. By placing the individual test sample in the holder, powerstat knob in the control panel was adjusted clockwise until the desired current level was attained. The voltages for a set of currents were recorded and the procedure was continued for all the test pieces.

3.5.3. CLASSIFIER

With the help of this equipment the voltage in the non-linear region was measured at a current of 100 A and 5 or 10 KA with the peak of the 8X20 μ s pulse wave-shape. This is Haefely impulse generator (model no WO 4433-34) with the capacity of 30 KV charging voltage and 4KJ/27KJ energy. The main components of the machine are (i) impulse current generator (ii) impulse peak voltage and (iii) trigatron.

There are two parts of the impulse current generator test circuit consisting of inductance, capacitance and resistance. The values of them are different for 100 A and 5 or 10 KA test. Impulse peak voltmeter measures and stores the peak values of impulse voltage and current. The trigatron is used for automatic control of impulse generator which performs the following functions:

- (i) regulates the charging of the impulse generator with digitally adjustable charging time and voltage.
- (ii) automatic stabilization of charging voltage at preset value.
- (iii) automatic adjustment of the 'sphere gap' of the generator in accordance with the selected charging voltage

3.5.4 ELECTRICAL STRENGTH TESTER

This equipment used to measure the energy absorption capability which is also known as 'strength test to destruction' tester. This is a very accurate and reliable impulse test system. The machine is composed of a number of functional units such as:

- (i) rectangular impulse current generator
- (ii) triggering system
- (iii) impulse peak voltmeter and
- (iv) control units.

The system is equipped with a highly sophisticated electronic control and triggering facility 'Trigatron type 94' which is an automatic digitally adjustable triggering unit with remarkable accuracy and reliability in spite of the strong electromagnetic fields and overvoltages. These features are achieved by incorporating special screening, filters and overvoltage protection circuits.

Rectangular Impulse Current Generator

The generator is capable of producing rectangular current impulse of 2 ms duration with a maximum charging voltage of 50 KV up to an energy level of 45 kilojoule.

Charging Voltage and Time

The charging voltage and the charging time are selected manually or by the program controller. Proper adjustment of the spark gap according to a non-linear characteristic is automatically derived from the preselected charging voltage value. The charging sequence of the impulse generator is controlled by the Trigatron through the solid state controller. The transient current peaks are suppressed and the generator is charged with an approximately constant current level. The charging voltage rises linearly to 95 percent of the preselected value. From this point on, the

charging voltage curve continues with 20 percent of the previous steepness so that the top stages of multiple-stage generators can also be fully charged. This feature is demonstrated in Figure 3.7.

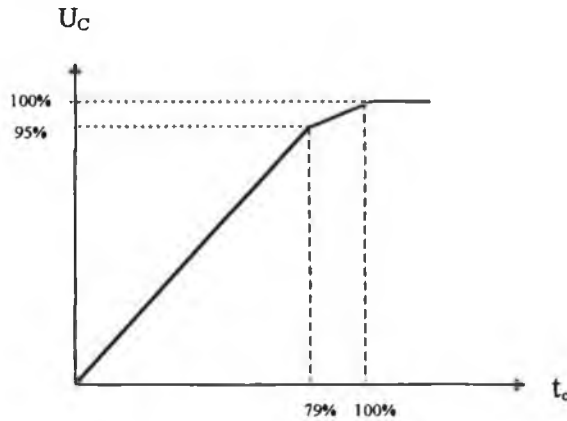


Figure 3.7 Charging voltage and time for long pulse

Triggering

Once the pre-selected charging voltage has been attained, the impulse generator is triggered directly or with an optional 2 second delay preceded by a warning signal. Time 0 is defined by the trigger reference signal which triggers the generator and starts the oscilloscope recorder through two independently adjustable delay circuits. All the trigger impulses can be digitally adjusted from 0 to 999.9 μs with an accuracy of 0.1 μs .

3.5.5 HIGH CURRENT TESTER

The high current performance and the voltage at the upturn region of the I-V curve is measured by an impulse current test system (model WO 4924). The generator is capable of maximum charging voltage of 100 KV with peak energy of 62.5 KJ. The main functional components of the equipment are (i) the impulse current generator (ii) the charging rectifier (iii) the control unit (iv) the resistive impulse voltage divider (v) digital impulse analysis system.

The charging voltage is capable of adjusting with the range of 0-99.9 KV with stability of 0.5 percent. The resolution is 100 V and the charging time selector range is 10-99 seconds with resolution of one second. The impulse generator is capable of measuring the high amplitude pulses of different duration.

3.6 MECHANICAL TOOLS AND EQUIPMENT

Various mechanical fixtures, tools and equipment have been used to investigate the different mechanical properties of varistors. A brief description of important equipment are given.

3.6.1 UNIAXIAL FLOATING DIE

The floating die was designed and fabricated for multiple purposes. The primary objective was to press the discs of 17 mm in green diameter and measure the

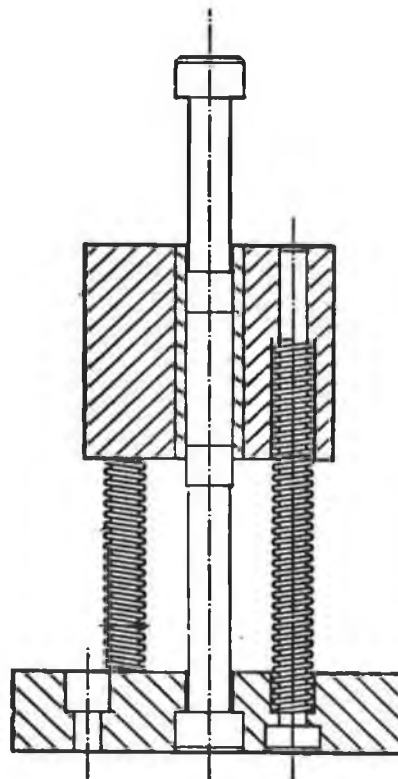


Figure 3.8 Uniaxial double action floating die set

compressibility of powders. The assembly drawing of the die is shown in Figure 3.8. Three guide pins placed at 120 ° apart will secure the motion of the floating die in the perpendicular plane arresting any oblique movement.

The base plate of the die set when fixed with the Instron sample holder is expected to clamp it firmly during pressing with the high speed. The die is also equipped with the single action block to arrest the movement of the floating die, specially needed for measuring the compressibility of powder. The shape of the ejection tool was made such that the coaxial load is imparted on the floating die during ejection of the pressed disc minimizing the scope of any possible damage due to oblique application of ejection load. Detailed drawing of the floating die set is attached in Appendix A.

3.6.2 MICROHARDNESS TESTER

The microhardness tester, (Leitz Miniload 2) was used to measure the hardness. Though Vicker's hardness method was adopted to measure the hardness of varistor, the equipment was suitable to evaluate the Knoop and Scratch hardness. The Vicker's hardness test, also known as the diamond pyramid hardness test, uses a pyramid shaped diamond indenter. The two diagonals of the square shape indentation were measured in μm and their average were taken to compute the hardness.

3.6.3 INSTRON MACHINE

The Instron machine used for pressing the sample discs is capable of a peak load of 50 KN. The force rating is 500 mm/min up to 25 KN up to and 100 mm/min up to 50 KN. The cross-head speed accuracy of ± 0.2 percent over 100 mm. The machine is equipped with a plotting facility.

3.6.4 HYDRAMET COMPACTING PRESS

The Hydramet press (model HC-75 EC) though is equipped with the same basic compaction features of FILL - PRESS - EJECT. The machine is programmed by a

combination of electrical, hydraulic, and mechanical controls and motions. The pressing force is adjustable from a minimum of 75 KN to a maximum of 750 KN. The fill depth is adjustable up to a maximum of 178 mm. The maximum achievable speed of both the upper and the lower ram is 6250 mm/min at no load condition and 884 mm/min while applying load. The stroke length of 127 mm is equal for both the upper and lower rams.

The press is facilitated with the standard pressing and filling motions. The filling mechanism is facilitated with the feed shoe jogs which can be varied from 0 - 40 for each cycle. The pressing cycle rate (cycle per minute) is completely adjustable from a minimum of one to a maximum of thirty. Each motion speed and dwell time adjustment is totally independent of any other adjustment. There are two individual speed adjustments for each of the upper and lower ram and the feed shuttle cylinder. Different dwell times in the pressing cycle can be adjusted within 0-10 seconds.

Chapter 4

COMPACTION PARAMETERS - STRESS, SPEED AND DURATION OF DWELL

4.1 INTRODUCTION

A homogenous compact body having higher green density with less density gradient is commonly expected to yield an improved sintered body. Better physical and mechanical properties of a sintered varistor device should similarly secure superior functional characteristics. In this context, the parameters in compaction operation are very important, for they can greatly influence the green properties and consequently the fired properties. The apparent purpose of compaction is to provide a desired geometrical shape and to impart sufficient strength to the green body for the purpose of handling prior to sintering. The shape and size of the ZnO varistor discs are important in the context of mounting and functioning for the protection of specified surge voltage and current. However, the effect of compacting parameters on the functional characteristics of ZnO varistors is not well known. This study was aimed at investigating and correlating the compacting parameters and their effect on the properties of the varistor.

The objective of the experiment was to observe the effect of compaction parameters on (i) the physical properties (ii) the I-V characteristics (iii) the energy absorption capability and (iv) the high current performance of ZnO varistors. The parameters were the peak compacting stress applied, the speed and the duration of different dwells in the pressing cycle.

Three separate experiments were conducted to evaluate the effects of the compacting parameters. The first and second experiments were carried out with the stress and speed or rate of compression to evaluate respectively the effect on the physical and electrical properties. The third experiment was performed to study the effect of dwell

time on the physical as well as on the electrical properties of arrester blocks. The study with stress and speed was performed on 17 mm (green diameter) discs while the experiment with dwell time was conducted on 49 mm (green diameter) standard production line arrester blocks.

4.2 STRESS AND SPEED - EFFECT ON PHYSICAL PROPERTY

The experimental condition with compacting stress and speed was varied at three levels. Two variables with three levels constituted nine sets of pressing conditions and at every set condition five discs were pressed to consider the statistical variation.

Sample Preparation

Powder with a target weight of 13.5 gm, was weighed in a laboratory type balance and poured manually into a 17 mm floating die and pressed in an Instron machine to form the green disc. The pressing condition with the identification of the corresponding cells of discs is summarized in Table 4.1.

Table 4.1 Experimental condition for pressing the samples

Expt Sequence	Experimental Condition		Sample Size	Cell Identity
	Stress (MPa)	Speed(mm/min)		
1	66	5	5	I
2	110	5	5	II
3	154	5	5	III
4	66	8	5	IV
5	110	8	5	V
6	154	8	5	VI
7	66	11	5	VII
8	110	11	5	VIII
9	154	11	5	IX

To avoid the effect of uncontrollable variation, the sintering operation was performed in a single run using a pot kiln. A conventional sintering profile was adopted with a peak temperature of 1100 °C and a total sintering cycle time of 65 hours.

4.2.1 BRIEF DESCRIPTION OF THE PHYSICAL PARAMETERS

The physical properties evaluated are the green and fired density, shrinkage and the diametral depression or distortion. Definition and method of calculation of these parameters are briefly described.

Green density

In calculating the green density, the weight of disc was measured by a laboratory type balance while the volume was evaluated from the geometrical relationship. Compacted green discs assume a regular cylindrical shape - the diameter (d_g) and height (h_g) are sufficient to calculate the volume (V_g) from the simple geometrical relationship (4.1).

$$V_g = \frac{\pi d_g^2}{4} h_g \dots\dots\dots(4.1)$$

Fired density

The sintered disc does not assume a regular cylindrical shape. During die pressing, density gradients⁸⁵ occur due to the frictional forces at the powder and die-wall interfaces and at particle to particle contacts. As a result the disc does not remain perfectly cylindrical after sintering and a depression is observed at the middle height. Moreover, during shrinkage the bottom face of the disc slides with the supporting powder or the liner material and ends up with a bigger diameter assuming a shape popularly termed as 'elephant foot'. So the volume of a fired disc, if calculated on the assumption of regular cylinder, will be inaccurate. To make a better approximation the fired volume (V_f) was calculated by considering the disc as a combination of the bottom parts of two cones. The following relationship was derived and used for computing the fired volume of the disc.

$$V_f = \frac{\pi}{24} h_f [(d_b + d_m)^2 + (d_m + d_t)^2 - d_m(d_b + d_t)] \dots\dots\dots(4.2)$$

where h_f , d_b , d_m and d_t indicate respectively the dimensions of the height, the diameter at the bottom, middle and top of the fired disc.

Shrinkage

The theoretical density of ZnO material⁴⁹ is 5.68 gm/cc. Since more than 90 percent of the constituent materials of a varistor is zinc oxide, this value can be conveniently considered to be the theoretical density of varistor material. The green compact density commonly lies between 55 - 65 percent of the theoretical density and the sintered density of the varistor is usually more than 95 percent. Since during sintering the loss in weight is very small-only about 2 percent, it is easily conceivable that a significant level of volume shrinkage occurs during this process. The overall volume shrinkage has been evaluated from equation (4.3) as the ratio of the change in volume to the original green disc volume.

$$\text{Volume Shrinkage} = \frac{V_g - V_f}{V_g} \dots\dots\dots(4.3)$$

A green disc shrinks both axially and radially during the sintering process. Green properties of the disc such as density and its gradient play a major role in this regard. The radial shrinkage was calculated using the following equation:

$$\text{Radial shrinkage} = \frac{d_g - d_f}{d_g} \dots\dots\dots(4.4)$$

where d_f is taken as the average of the three diameters of the fired disc at the bottom, middle and top. The axial shrinkage was evaluated as the ratio of the reduction in height to the green height as given by,

$$\text{Axial Shrinkage} = \frac{h_g - h_f}{h_g} \dots\dots\dots(4.5)$$

Diametral depression

The diametral depression can be treated as an indicator of the shape distortion of the fired disc. It is preferable to keep this undesirable parameter to a minimum level. The value of this depression was calculated as the difference between the average of the top and bottom diameters, and the diameter at the middle height. The mathematical relationship is presented by,

$$\text{Diametral depression} = \frac{d_b + d_t}{2} - d_m \dots\dots\dots(4.6)$$

4. 2.2 OBSERVATION AND ANALYSIS OF THE EFFECTS

It has been found that the effect of the compacting stress on the green density is quite significant and consistent - the higher the stress the higher is the density. The influence of stress is shown in Figure 4.1.

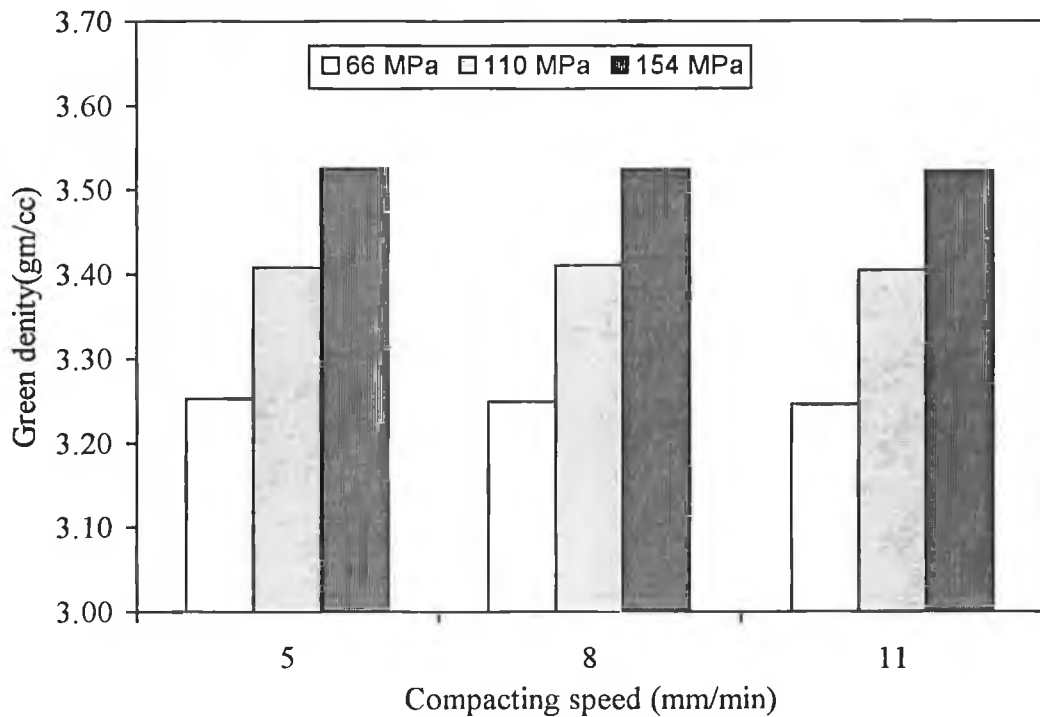


Figure 4.1 Effect of compacting stress on green density

The pressing speed slightly influences the green density. With lower speed the powder material under pressure gets more time to remove the trapped air leading to a slightly higher green density as demonstrated in Figure 4.2. This effect, however, appears to diminish in the higher range of stress.

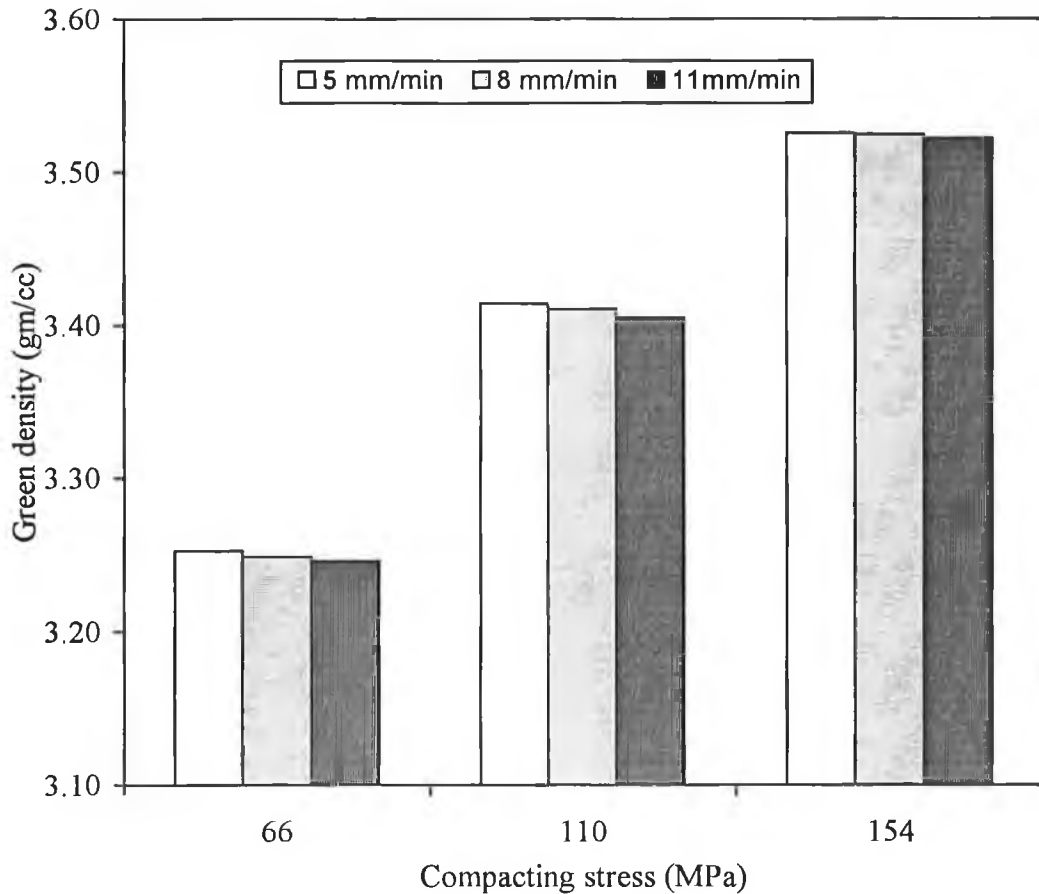


Figure 4.2. Effect of compacting speed on green density

In general, the peak pressure or stress applied during compaction largely determines the green property of the compact body. This feature is very much observed for the varistor material. The compaction stress significantly affects the green as well as the fired density of the ZnO varistor disc. Increasing the stress leads to the increase in density in both the green and the fired state as illustrated in Figures 4.1 and 4.3. But the extent of the effect of stress on the fired density is not as prominent as that on the green density.

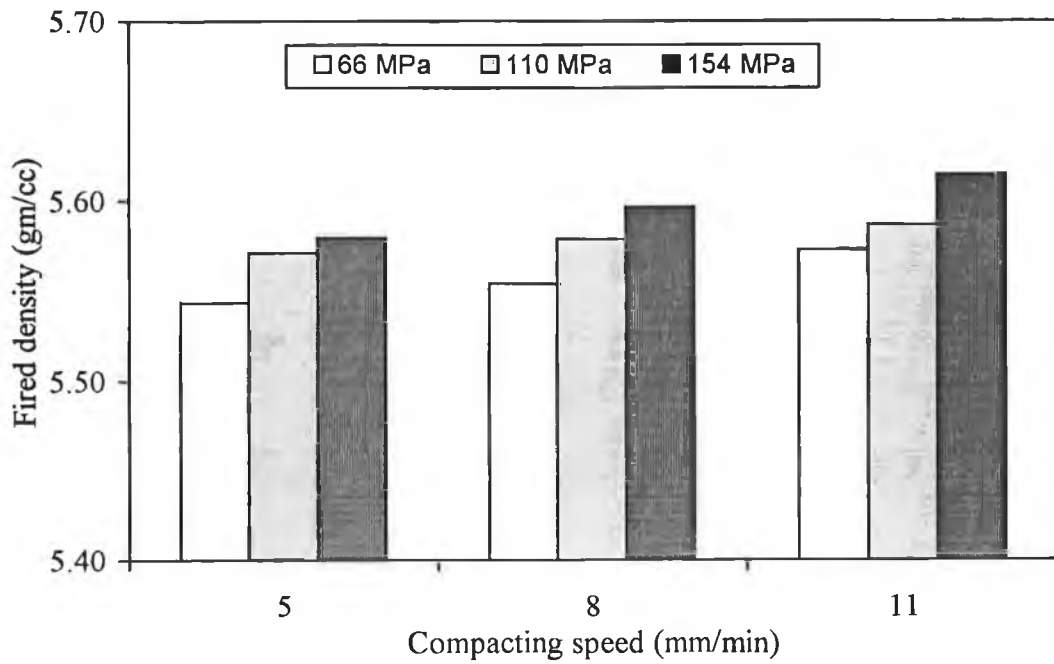


Figure 4.3 Effect of compacting stress on the fired density

Regarding the effect of the pressing speed, the differential increase in the green density due to the lower speed does not eventually ensure higher fired density of the varistor material. Rather, the effect of the pressing speed is found to be opposite in the case of the fired density as shown in Figure 4.4.

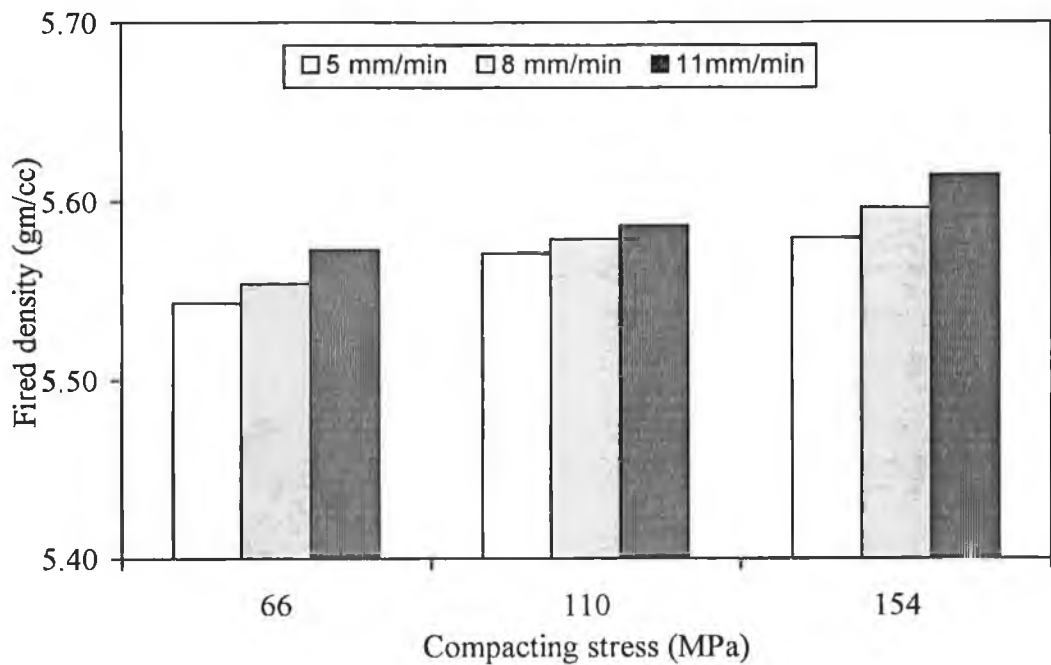


Figure 4.4 Effect of compacting speed on fired density

The effect of pressing speed on the green and the fired state of the ZnO varistor material is demonstrated in Figure 4.5. The error bar indicating the standard deviation from the mean fired density facilitates comparison among the level of change due to the pressing speed.

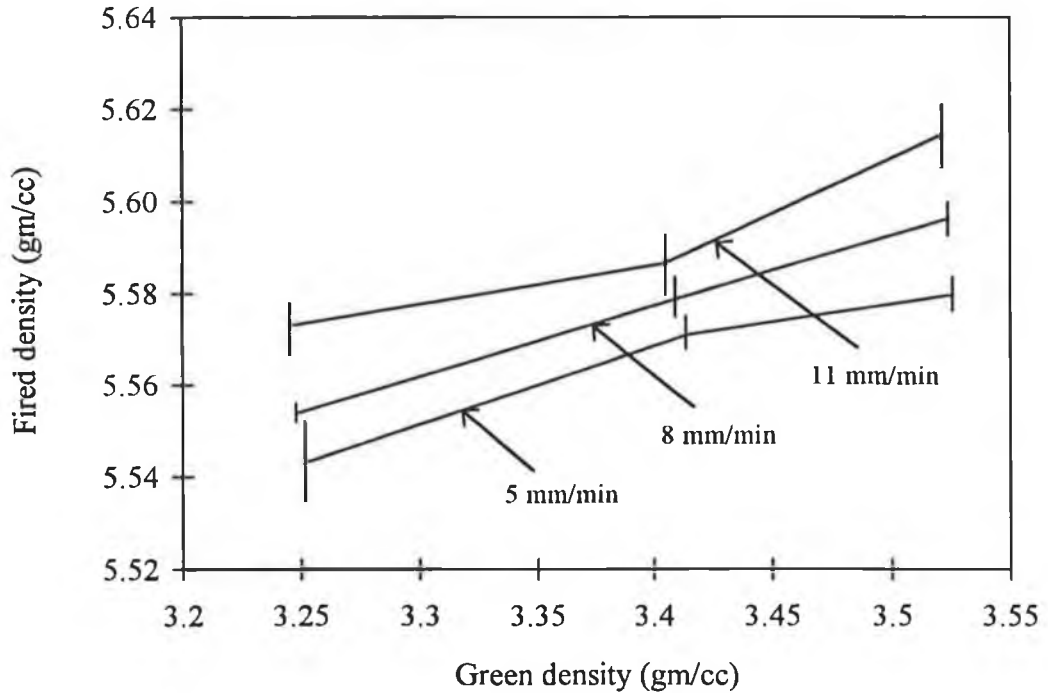


Figure 4.5 Effect of pressing speed on the green and the fired density

Shrinkage

Shrinkage is an indicator of volume reduction in the sintering operation. It is obvious that the discs with higher green density will experience less shrinkage. Moreover, it is claimed that the higher the green density, the better is the overall sinterability, and more effective the control of final microstructure⁹⁴. It is also evident that a higher green density can help reduce the sintering time if rate controlled sintering (RCS) is adopted. In the case of using a sintering profile with a specific optimized rate of shrinkage, a disc with higher green density should require less time to complete the total amount of shrinkage. This will eventually reduce the total sintering cycle time.

For the experimental conditions under study, the range of the overall volume shrinkage was found to be within 38.08 - 42.84 percent. Naturally the discs with higher green density due to higher compacting stress underwent less shrinkage. So the overall shrinkage of the ZnO varistor material can be seen as a function of compacting parameters. This feature shown in Figure 4.6 is just opposite to what was observed in the case of fired density. A higher compacting stress leads to the higher green density leaving less scope of shrinkage in sintering.

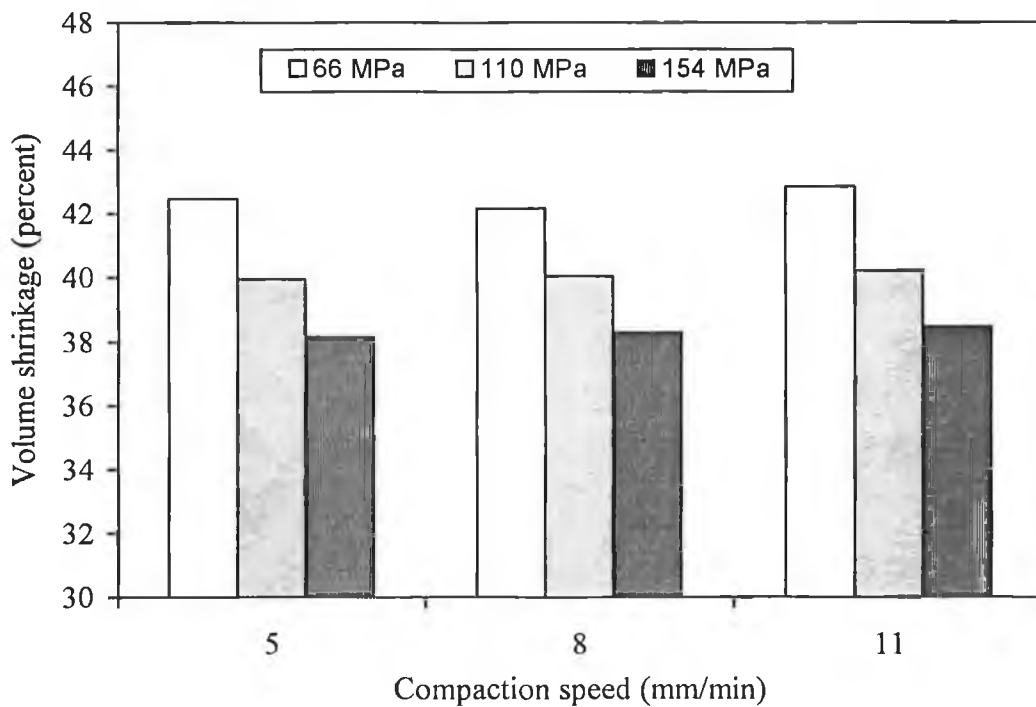


Figure 4.6 Overall volume shrinkage as a function of compaction stress

A variation in shrinkage was observed between the axial and the radial direction of a disc. Shrinkage in radial direction was found to be within the range of 15.12 - 17.20 percent while that in the axial direction was within the range of 13.87 - 16.46 percent. On the average the extent of radial shrinkage was found to be higher. This is attributed to the effect of uniaxial pressing on the rearrangement of materials. Under die compaction the spheroidal shaped spray dried particles move much closer in the axial direction than in the radial direction. Thus the disc shrinks more in the radial direction during sintering because of the higher average interparticle gap in that direction.

The effect of pressing speed is found to be marginal in this regard. A higher pressing speed leads to more shrinkage.

Diametral depression

The diametral depression can be treated as a measure of distortion of the sintered body. This parameter at the mid region is not same for all the cells. Discs pressed with the lower speed were found to exhibit more depression as depicted in the analysis of factorial design in Table 4.2.

Fired diameter

The variation in green diameter due to the pressing parameters is not very remarkable. Though pressed in the same die, a small difference in the green diameter of the compact is expected as a result of variation in stress relaxation. Thus with the highest compacting stress the diameter of the green discs was bigger by 0.02 mm compared to that of those presses with the lowest stress. But after sintering a significant difference in diameter was observed. The diameter of those pressed with the highest pressure was 0.37 mm higher than that of those pressed with the lowest pressure.

The variation in diameter leads to the difference in cross-section of the varistor. This affects the performance of the varistor as current carrying capacity of a device is directly related to its cross-sectional area. It can be inferred from this observation that a tighter control of pressing load with closer tolerance will be helpful in minimizing the process variation.

Two Level Factorial design

Factorial design has been performed by considering the lowest and highest level of the two input variables. Responses in the form of main and interactive effects for the

green density, fired density, the shrinkage, the diameter at middle height and the diametral depression are presented in Table 4. 2.

Table 4.2. Main and interactive effects of compacting stress and speed

Effects	Responses						
	Green density (gm/cc)	Fired density (gm/cc)	Overall shrinkage (percent)	Axial shrinkage (percent)	Radial shrinkage (percent)	Fired diameter (mm)	Diametral depression
Stress	0.2743	0.0124	-4.3750	-2.29	-1.935	0.347	2.5
Speed	-0.0054	0.0058	0.3850	0.30	0.145	-0.011	-19.5
Interaction	0.0015	-0.0239	0.0050	0.06	-0.035	0.007	-3.5

Ejection Force

Higher ejection force is undesirable in compaction operation. Some of the green defects such as capping and lamination are thought to be caused by the higher ejection force. Higher compacting stress results in the higher green density but at the same time necessitates higher ejection force to remove the compact from the die. The trend in the increase of ejection force with the compacting stress is evident in Figure 4.7. Though no defect was found in the green body within the experimental range, further increase in compacting load may lead to generate defects.

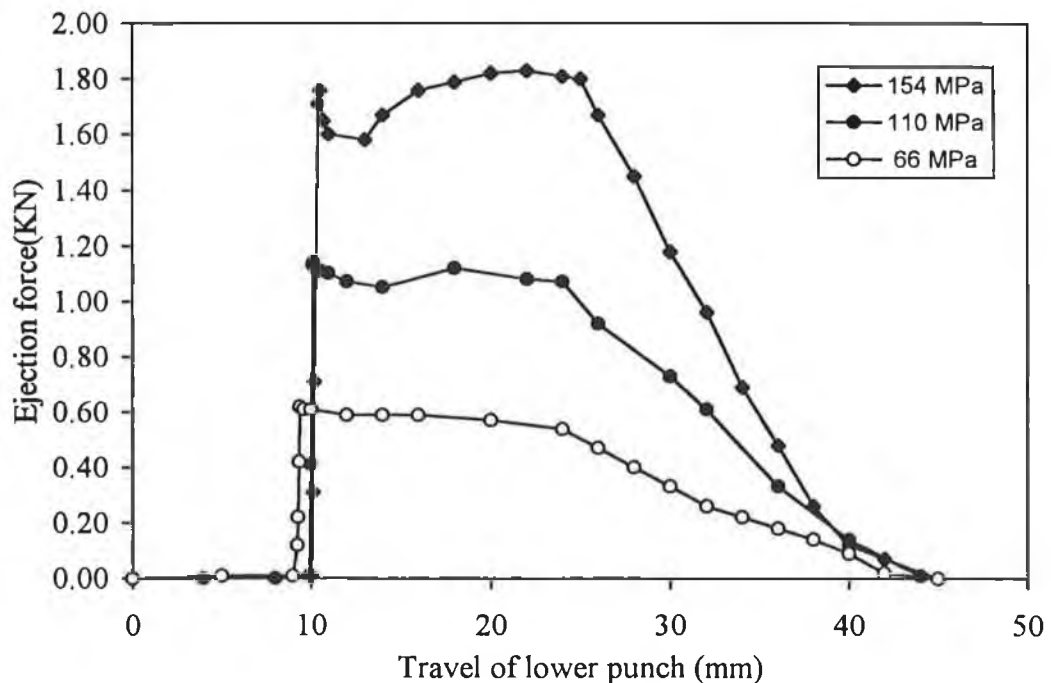


Figure 4.7 Ejection force as a function of compacting stress

4.2.3 SUMMARY OF THE EFFECTS ON PHYSICAL PROPERTIES

In the processing of conventional ceramic, the pressing speed is usually maintained at low level to secure a higher green density with intended ultimate attainment of the higher fired density. However, the present study on the ZnO varistor powder reveals that the differential increase in green density due to lower pressing speed does not eventually lead to the higher fired density. This phenomenon may be attributed to the effect of high temperature reaction due to the more trapped oxygen/air in the compact during the liquid phase sintering.

A higher pressing speed leads to higher fired density in contrast to its reverse effect on the green density. This also reduces the diametral depression and can ensure better dimensional stability of the disc after sintering. The pressing or compacting stress remarkably affects the green density and, to a considerable extent, the fired density. This also influences the fired diameter and thereby the cross-section of the fired disc - higher stress leading to higher cross-sectional area. So in the context of process control it is important to keep the variation of pressing load to a minimum level for securing better dimensional control.

The performance of a ZnO varistor mainly depends on the electrical characteristics, energy handling capability etc. So it will be more worthwhile to assess the effect of the compaction parameters on the basis of the I-V characteristic, energy absorption capability etc. Since the pressing speed range adopted in this study was very narrow, further work is necessary with a wider range of speed.

In the context of ejection force higher green density achieved through higher compacting pressure may not be a good approach. Compacts pressed with high load require higher ejection force to remove from the die and thus become vulnerable to a risk of creating defects in the body. Moreover, application of too high a load will be detrimental to the tool life and will consume more energy.

4.3 COMPACTING STRESS AND SPEED - EFFECT ON THE ELECTRICAL PROPERTIES

The study concerning the effect of the compacting stress and speed on the electrical characteristics of the ZnO varistor discs was carried out with a wider range of pressing speed. The stress was changed in three levels. Both the minimum and the maximum load limits were smaller than what had been selected in the case of the study on physical property. Selection of the input parameters was made to cover the range commonly adopted in the industry. Moreover, the parameters were varied following some experimental design so that a functional relationship could be developed. The important electrical properties of varistor such as the non-linear exponent, the clamp ratio, nominal voltage, watt loss and the energy absorption capability were evaluated. All of these parameters are functionally very significant as they determine different important aspects of varistor performance.

Sample Preparation

The three selected peak loads of 9, 15 and 25 KN were equivalent to the compacting stresses of 40, 66 and 110 MPa for the 17 mm die set. The pressing speeds were maintained at 5, 10, 20, 40, 60, 80 and 160 mm/min. A precision Instron machine was used for the pressing operation. With three levels of compacting stress and seven levels of compacting speed there were 21 set conditions.

Five discs were pressed under each condition to take into account the statistical variation. However, additional 20 discs were pressed at the central point of the experimental condition (at a stress of 66 MPa and at speed of 40 mm/min), the data on which were used in the analysis of variance for estimating the reliability of the developed model. The disc cells compacted at various set conditions were identified according to the letters presented in the Table 4.3. Pressing of the samples was performed in the 17 mm floating die with a same target weight of 13.50 gm of standard metal-oxide varistor powder.

Table 4.3 Pressing condition and corresponding identification of the arrester discs

Pressure (MPa)	Speed of pressing (mm/min)						
	5	10	20	40	60	80	160
40	A	B	C	D	E	F	G
66	H	I	J	K	L	M	N
110	O	P	Q	R	S	T	U

Sintering was also conducted with the same temperature profile as before. The whole lot of discs was passivated through standard line process - glass slurry was sprayed on the side (C-face) of the disc to achieve a desired thickness of passivation after curing. The flat faces of the discs were then manually ground in a grinding machine using a grinding paper (grit size 240). Electroding was also performed by painting silver manually on the whole face. The wet silver was dried by passing the samples through an electric dryer followed by a curing operation in an oven at a peak temperature of about 800 °C. The purpose of this operation is to secure proper adhesion of the electrode with the ceramic.

Electrical Characterization

The prebreakdown region of the I-V characteristics was measured with direct current in a high voltage test system (model BOP 1000M). The non-linear coefficient was calculated with the data at 50 μ A and 1 mA current. The nominal voltage was measured at 1 mA current corresponding to a current density of about 0.6 mA/cm². The watt loss was measured in a watt loss tester with sinusoidal pulse at 80 percent of the voltage at a current density of 0.4 mA/cm².

Voltages and currents at the nonlinear or upturn region of the I-V curve were measured by pulses. To evaluate the clamping efficiency, the clamp ratio was computed as V_{100A}/V_{1mA} . The energy absorption capability was evaluated in a rectangular wave generator (Haefely). Each disc was subjected to a cycle of three 2ms quasi-rectangular impulses at a particular charging voltage. The process was continued by discretely increasing the charging voltage until the disc failed. However,

after injecting the energy into the disc body in a cycle of 3 impulses, they were allowed to cool down to room temperature before being subjected to the next cycle.

4.3.1 INVESTIGATED ELECTRICAL CHARACTERISTICS

The parameters investigated as a function of compacting stress and speed are the nonlinear exponent, clamp ratio, watt loss, nominal voltage, energy absorption capability. Origin of failure was found to be influenced by the disc position during sintering. So the role of sintering orientation and the frequency of failure origin is also discussed. A few microstructural analyses are incorporated to investigate the effect of compacting stress on the grain size which influences the electrical property.

Nonlinear exponent

This is a very important parameter for a varistor. The higher value of the exponent is preferable as it improves the varistor performance. The average of the five values of the exponent for different pressing conditions are summarized in Table 4.4. The variation is not very significant. However, a trend of declining exponent values is observed with higher compacting stress. Neither too high nor too low speed appears to be favourable in this case.

Table 4.4 Nonlinear Exponent as a function of stress and speed

Pressure (MPa)	Speed of pressing (mm/min)						
	5	10	20	40	60	80	160
40	32.80	33.40	33.71	35.07	35.85	32.84	32.42
66	30.18	31.20	35.07	31.96	34.42	31.20	30.16
110	30.77	31.02	29.89	32.30	32.01	28.02	29.56

Clamping Ratio

The protective level of a varistor is determined by the clamp ratio. A varistor device should have a protective level as low as achievable, an ideal value is unity. So the

closer the clamp ratio to unity, the better is the device performance. This parameter was evaluated as the ratio of the voltage at 100 A (V_{100A}) to the voltage at 1 mA (V_{1mA}) and the values are presented in Table 4.5. Effect of stress and speed is not very significant - a trend of lower clamping ratio is observed with higher stress.

Table 4.5 Effect of Compaction parameters on the Clamp ratio

Pressure (MPa)	Speed of pressing (mm/min)						
	5	10	20	40	60	80	160
40	1.367	1.408	1.368	1.372	1.372	1.366	1.369
66	1.361	1.362	1.357	1.364	1.362	1.361	1.362
110	1.345	1.352	1.354	1.355	1.357	1.360	1.360

Watt Loss

Watt loss is an undesirable parameter in transient protection. But this is unavoidable for a zinc oxide varistor and is, therefore, preferable to keep this parameter to a minimum possible level. The lower watt loss enhances the varistor stability. Higher watt loss generates more heat in the disc body under the steady-state condition and reduces the varistor life as it fails prematurely through thermal runaway. The data on the watt loss ($w.cm^{-3}$) as the effect of compaction stress and speed are presented in Table 4.6.

Table 4.6 Variation in watt loss due to compacting stress and speed

Pressure (MPa)	Speed of pressing (mm/min)						
	5	10	20	40	60	80	160
40	0.00291	0.00233	0.00240	0.00149	0.00157	0.00199	0.00259
66	0.00343	0.00343	0.00268	0.00294	0.00227	0.00318	0.00310
110	0.00379	0.00345	0.00370	0.00354	0.00362	0.00413	0.00379

It is seen from the data that higher compacting stress leads to a higher watt loss. The effect of speed is also prominent for watt loss. The middle range of compaction speed is found to be suitable for this parameter. Too low or too high a speed of pressing leads to the increase of the watt loss values.

Nominal Voltage

The nominal voltage (V/cm) of a ZnO varistor indicates the steady-state operational voltage corresponding to a current density at the knee level of the I-V curve. The following values presented in Table 4.7 indicate the nominal voltage for various cells corresponding to a current density of 0.6 mA/cm².

Table 4.7 Average nominal voltage for discs under different pressing condition

Pressure (MPa)	Speed of pressing (mm/min)						
	5	10	20	40	60	80	160
40	2550	2532	2505	2549	2507	2497	2498
66	2494	2482	2511	2489	2489	2474	2467
110	2480	2490	2465	2523	2460	2467	2469

Higher nominal voltage of a varistor allows to reduce the height or thickness of the device and, therefore, can be advantageous in terms of material use. Though there is a trend of higher nominal voltage with lower pressure, the influence in general is not very great. The effect on the nominal voltage may be explained in terms of the grain growth. Lower compacting stress does not compress the spray dried granules as close as that is done by the application of higher pressure. So the grain growth in the less compacted discs during sintering cannot be as effective as that in case of highly compacted discs. The lower stress eventually leads to smaller average grains in the ceramic body leading to a higher nominal voltage.

A variation of nominal voltage is found among the discs belonging to the same cell. In Figure 4.8 the nominal voltage is shown with error bar for the cells A, H, O - all of which were pressed at a speed of 5 mm/min. The error bar indicates the range computed by adding and subtracting the standard deviation from the mean value. The I-V curve for these cells are presented in Figure 4.9. It is seen that the small difference in the prebreakdown and breakdown region due to the compacting stress diminishes in the upturn region.

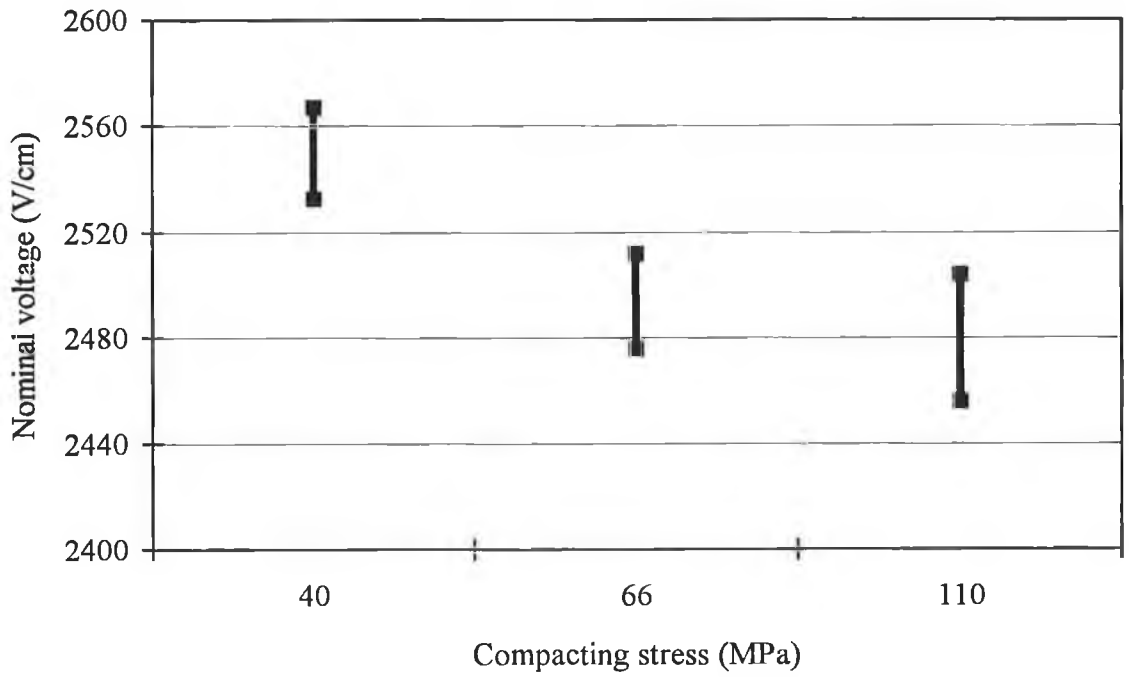


Figure 4.8 Effect of compacting stress on nominal voltage (for a speed 5 mm/min)

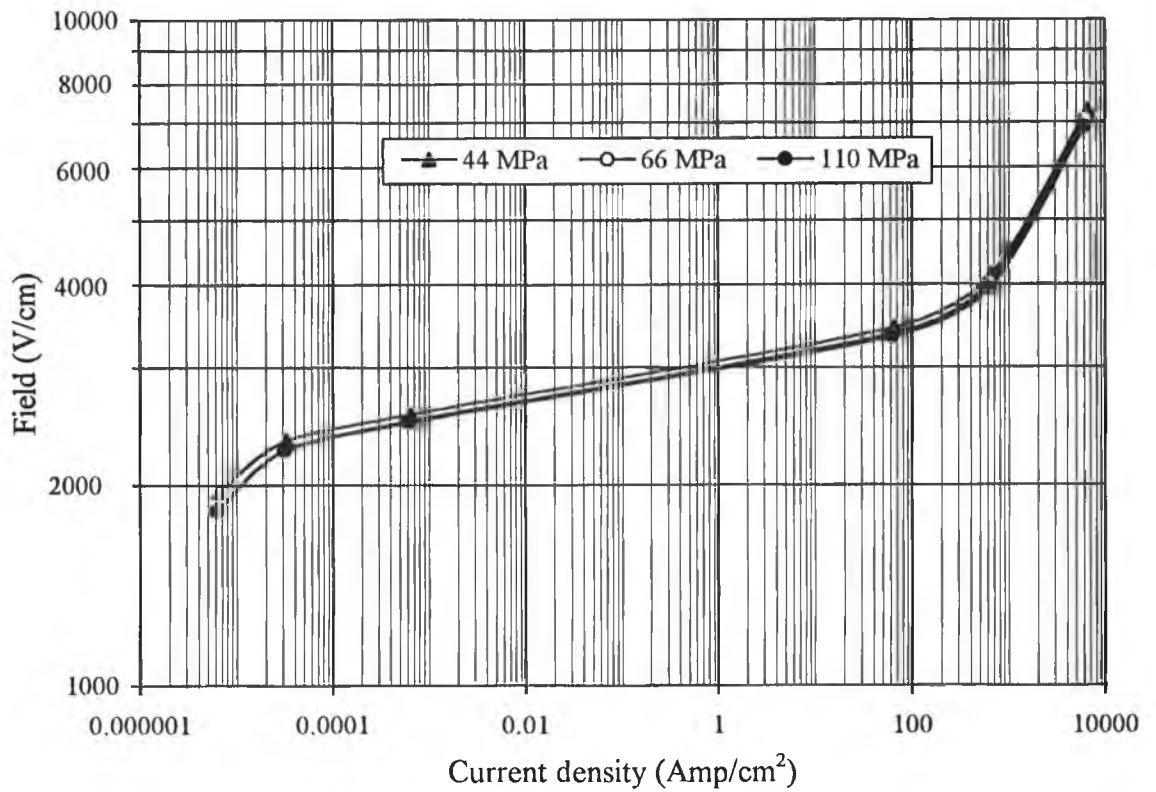


Figure 4.9 Current-voltage curve showing the effect of compacting pressure (For a constant speed of pressing of 5 mm/min)

4.3.2 ENERGY ABSORPTION CAPABILITY

This is a very important property for a varistor. A higher value of energy absorption capability can allow a reduction in the volume of the disc or the same disc can be used for more demanding applications. The average energy absorption capability of present day varistors¹⁰ should be more than 400 J.cm⁻³. The commercially available varistors have rated energy absorption capability of about 200-250 J.cm⁻³. These values are conservatively selected specially because of the possibility of some rare occurrences of earlier failures.

The values presented in Table 4.7 indicate the average of the five values of energy absorption capability for the cells pressed under different pressing conditions. The variation in compacting stress and speed does not show any remarkable influence on the energy absorption capability of the arrester discs.

Table 4.8 Effect of stress and speed on the energy absorption capability
(mean and standard deviation)

Pressure (MPa)	Speed of pressing (mm/min)						
	5	10	20	40	60	80	160
40	459 (41)	438 (90)	541 (52)	494 (71)	544 (37)	404 (92)	419 (77)
66	357 (74)	537 (141)	526 (170)	451 (115)	488 (121)	564 (73)	457 (69)
110	421 (93)	502 (144)	488 (83)	527 (97)	525 (117)	445 (63)	418 (61)

The plot in Figure 4.10 shows the mean values of green density, fired density and the median energy of the discs pressed under different loads. Within the experimental limit the physical property such as the green and fired density of varistor discs do not affect the energy absorption capability very significantly. The interactive effect of speed has been neglected to plot the figure. The higher fired density due to more compacting stress has led to a higher energy but the level of increase is not at all significant. In Figure 4.11 the plot of the cumulative percent failure of discs is shown. This indicates the relative trend of failure with the increase in energy along with the

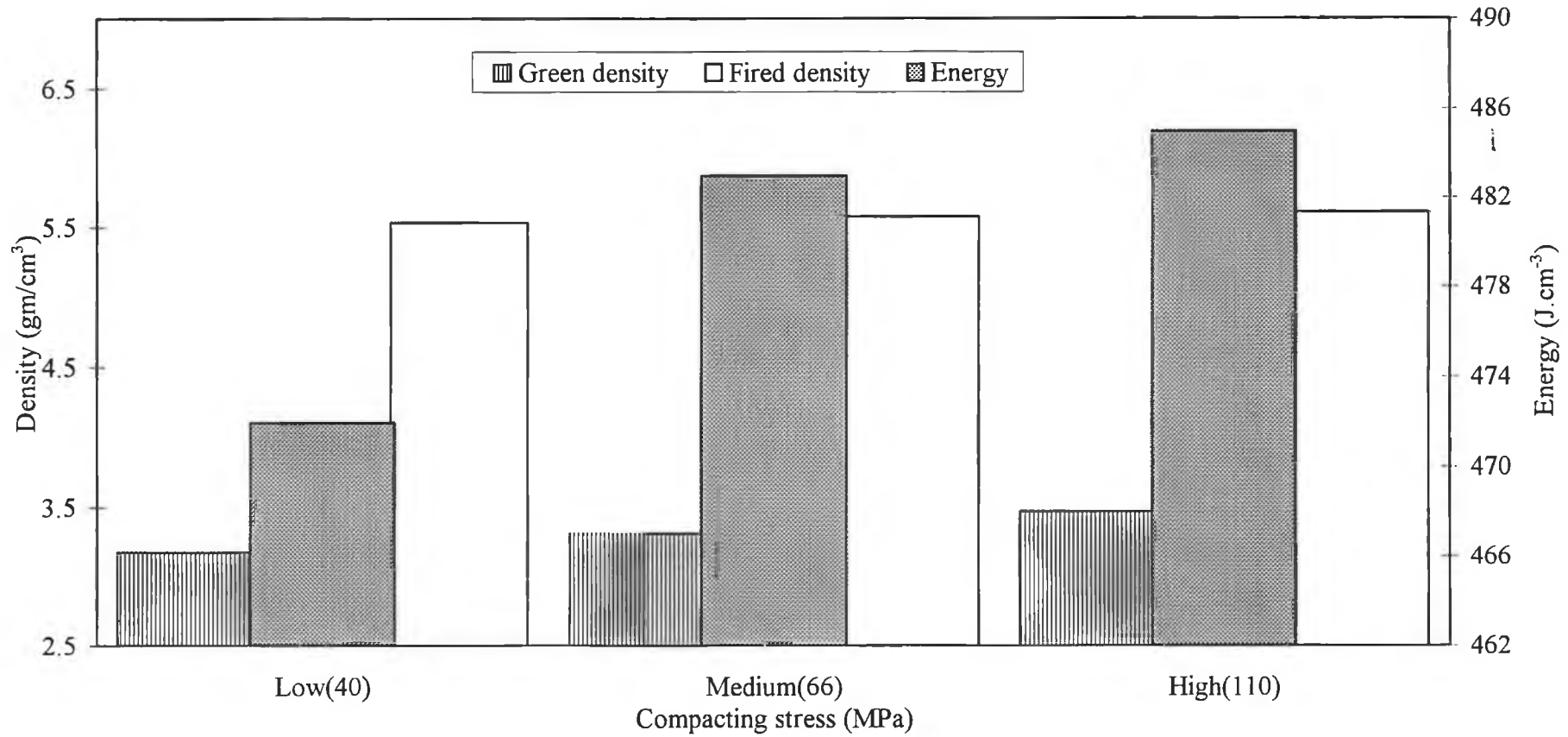


Figure 4.10 Green and fired density, energy absorption capability as function of compacting stress

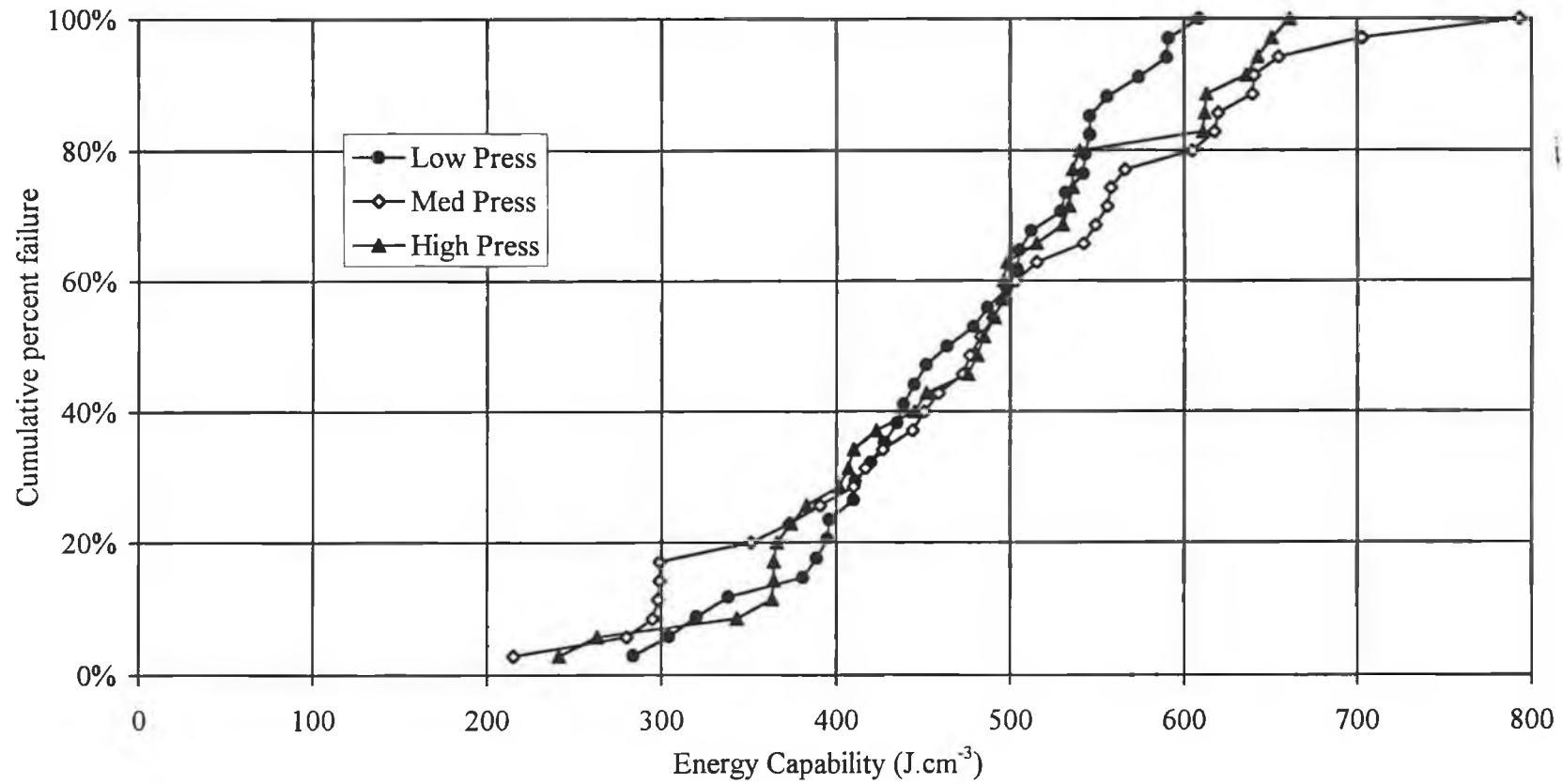


Figure 4.11 Effect of Compacting Stress on the energy absorption capability of varistor

initial failure and the sustaining capability at higher energy levels. Discs pressed with lower compacting stress look poor in the context of withstanding capability in the higher level of energy. The discs pressed with maximum load also did not show the best results whereas those pressed with medium pressure exhibited best performance.

The effect of compacting speed on energy is shown in Figure 4.12 with the error diagram. It appears that neither too low nor too high speed is conducive to the

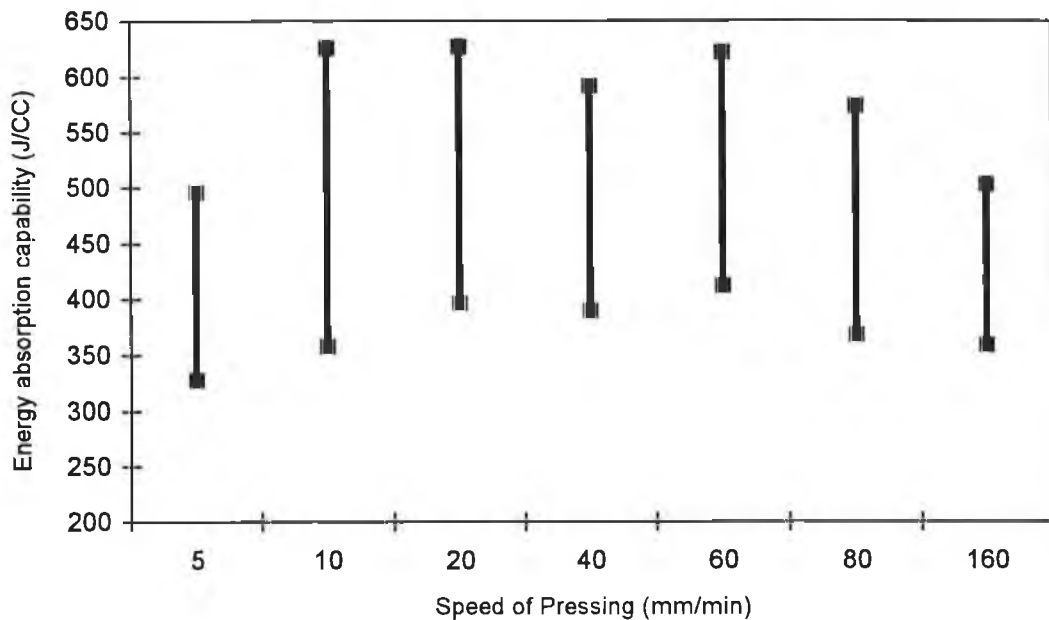


Figure 4.12 Effect of pressing speed on the energy absorption capability

energy absorption capability. In this case also the interactive effects of compacting stress has been neglected.

Sintering Orientation and Origin of Failure

The orientation of the cylindrical arrester discs or blocks during sintering is shown in Figure 4.13. The face of the disc remaining in contact with the liner material (bottom face) is not physically as good as the top face. As a result this face needs more material to be ground off. from this face. But even with the removal of more material, this face does not become functionally as good as the top face. In this experiment the

origin of failure has been tracked. It was found that the distribution of failure origin is not same for both the faces. A higher number of failures originated from the bottom

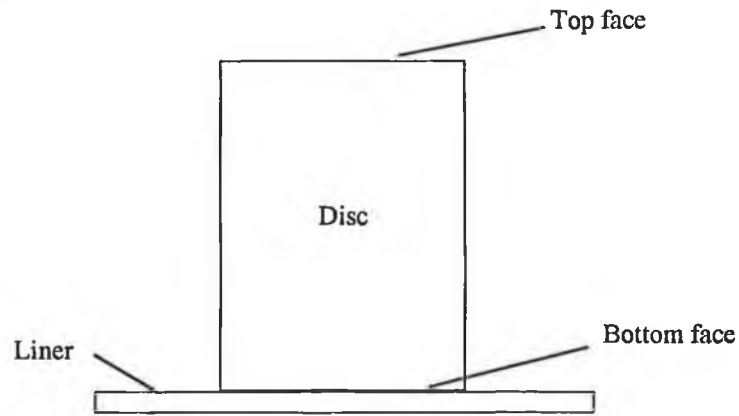


Figure 4.13 Sintering orientation of arrester disc

face during the test for the energy absorption capability. More than two-thirds of the failures originated from the bottom face, the percentage is shown by the pie chart in the Figure 4.14.

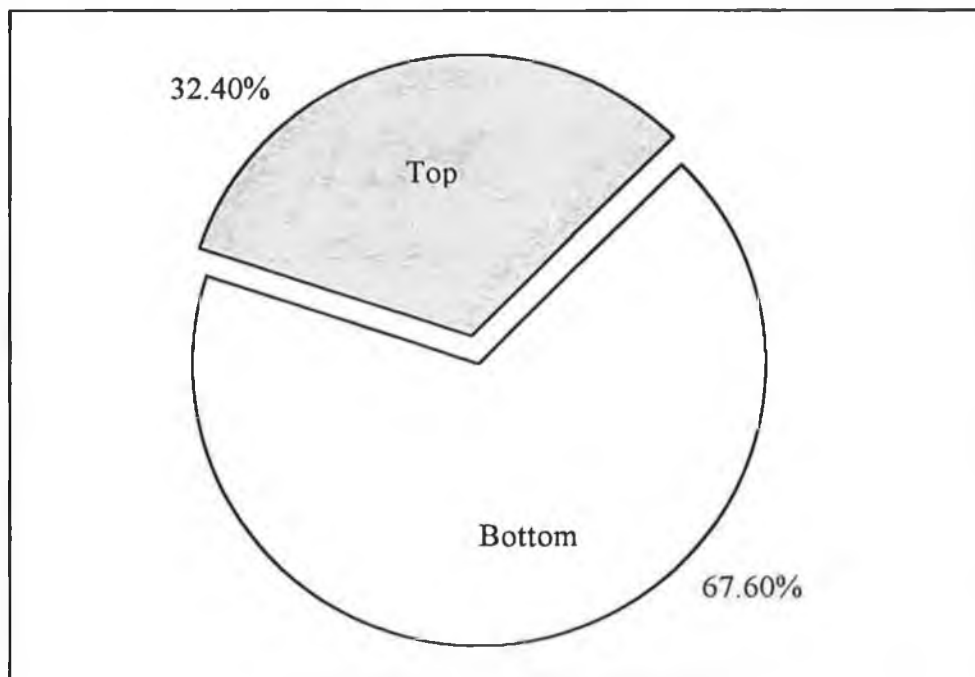


Figure 4.14 Frequency of failure origin as observed in energy test

4.4 MICROSTRUCTURAL ANALYSIS

The micrographs have been developed for a few samples to reveal the effect of compacting stress on the microstructure of the varistor disc. The sample specimens were cut from three discs pressed with different pressures from a relatively same location. The compacting stress applied on the three discs were respectively 40, 66 and 110 MPa. But speed of pressing was same for all of them and was 60 mm/min.

Micrographs were taken with two different magnifications using Scanning Electron Microscope. The lower magnification was 250 and the higher one was 1000. The lower one was intended to cover a wide area so that a representative view can be obtained whereas the higher magnification was necessary for the topography of the microstructure. Moreover, from the micrographs with higher magnification the grain size distribution was measured.

The microstructure was taken by the secondary emission image (SEI). The Figures 4.15, 4.17 and 4.19 indicate respectively the microstructures of the discs pressed with compacting pressures of 40, 66 and 110 MPa. The magnification was 250 for these three micrographs. In Figures 4.16, 4.18 and 4.20 the micrographs represent the same sequence of samples but with a magnification of one thousand.

The samples were prepared from cut pieces, following the conventional sequence of polishing order. The surface for microstructure was polished on grinding paper with increasing finer grains. As the final step liquid containing 0.25 μm diamond particles was used at of polishing operation. The specimen was then dipped into nitric acid for 10 seconds to clean the face to be scanned.

It may be mentioned here that the specimens were taken from the top part in respect of the sintering configuration. The specimens were cut by a diamond cutter from a relatively same position of the disc. Such a selection was made to ignore the influence due to position in sintering operation on the fired properties..

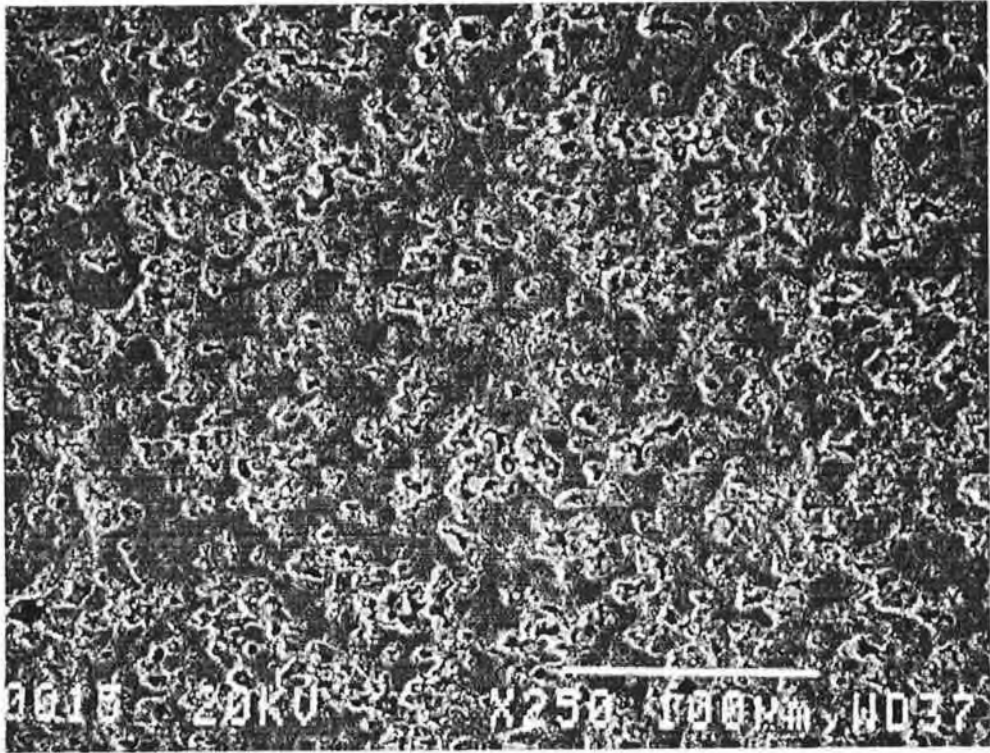


Figure 4.15 Micrograph for a disc pressed with 40 MPa (X250)

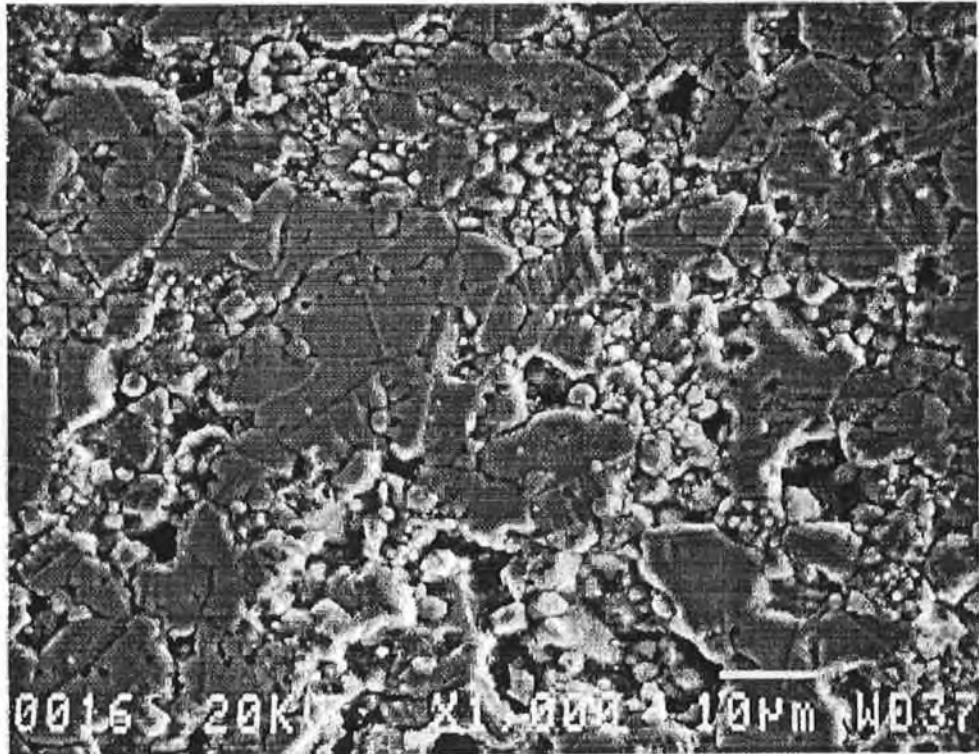


Figure 4.16 Micrograph for a disc pressed with 40 MPa (X1000)

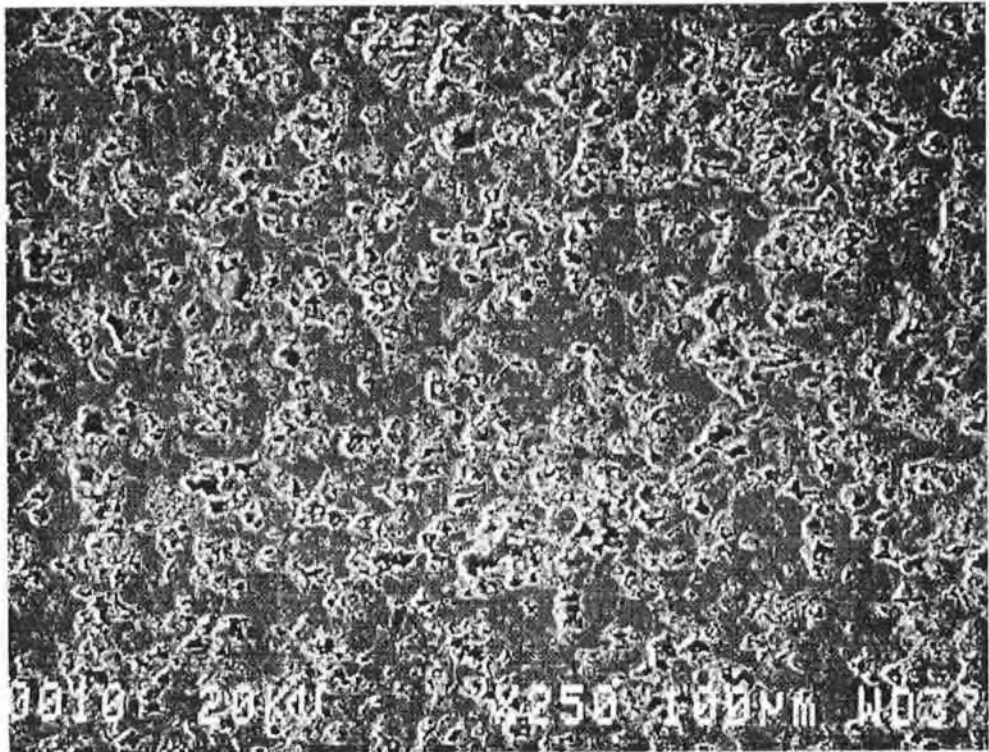


Figure 4.17 Micrograph for a disc pressed with 66 MPa (X250)

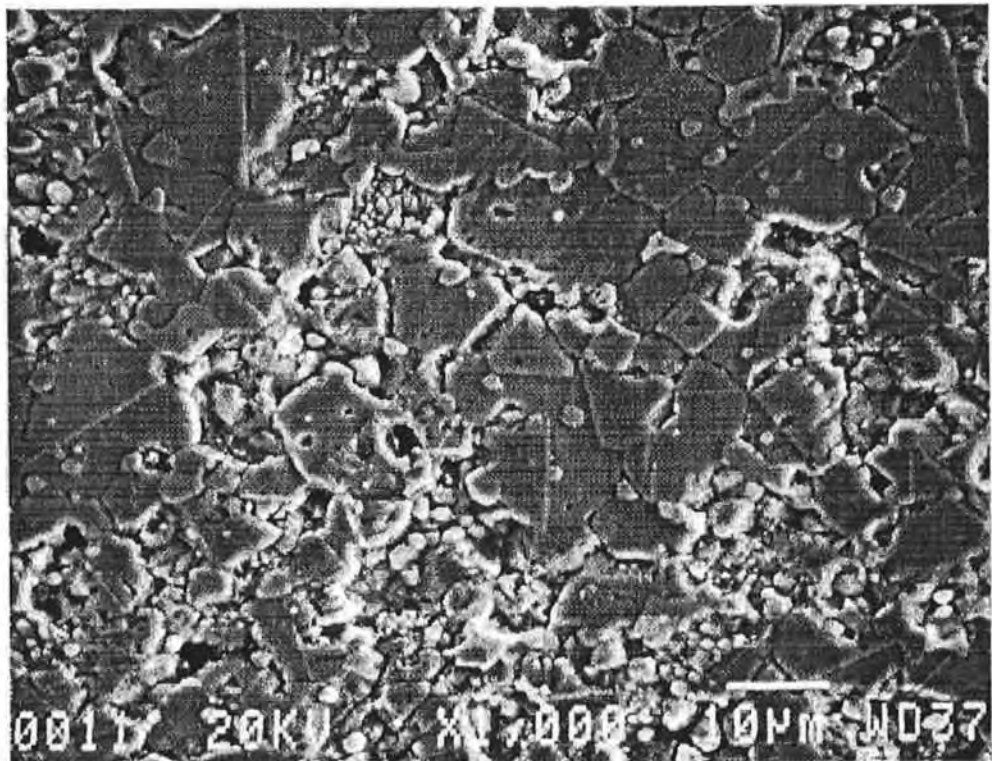


Figure 4.18 Micrograph for a disc pressed with 66 MPa (X1000)

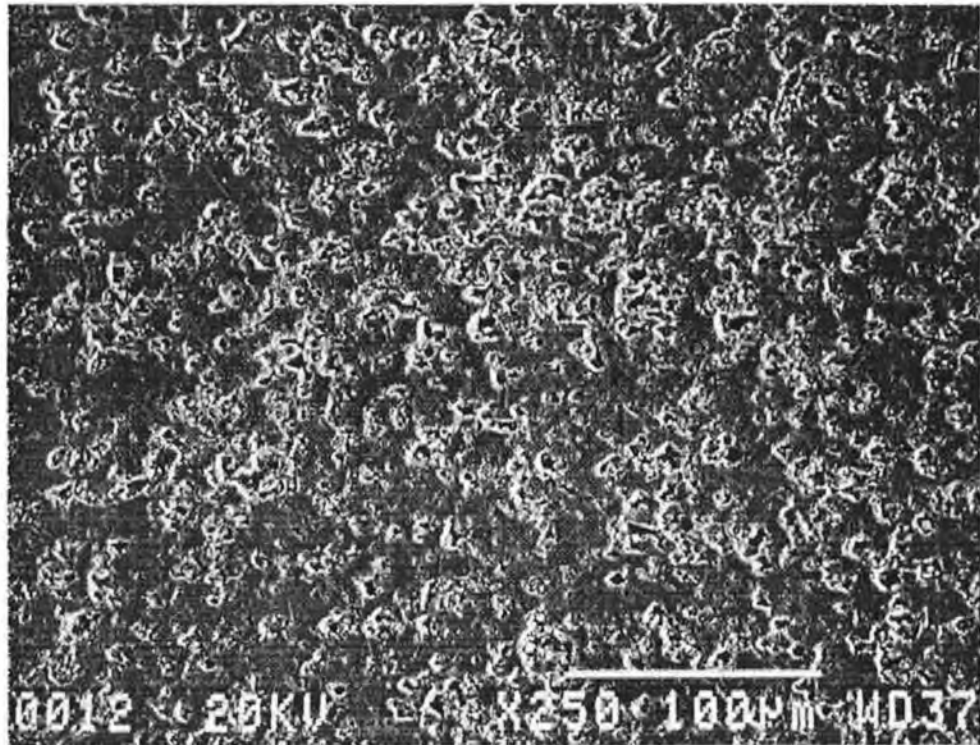


Figure 4.19 Micrograph for a disc pressed with 110 MPa (X250)

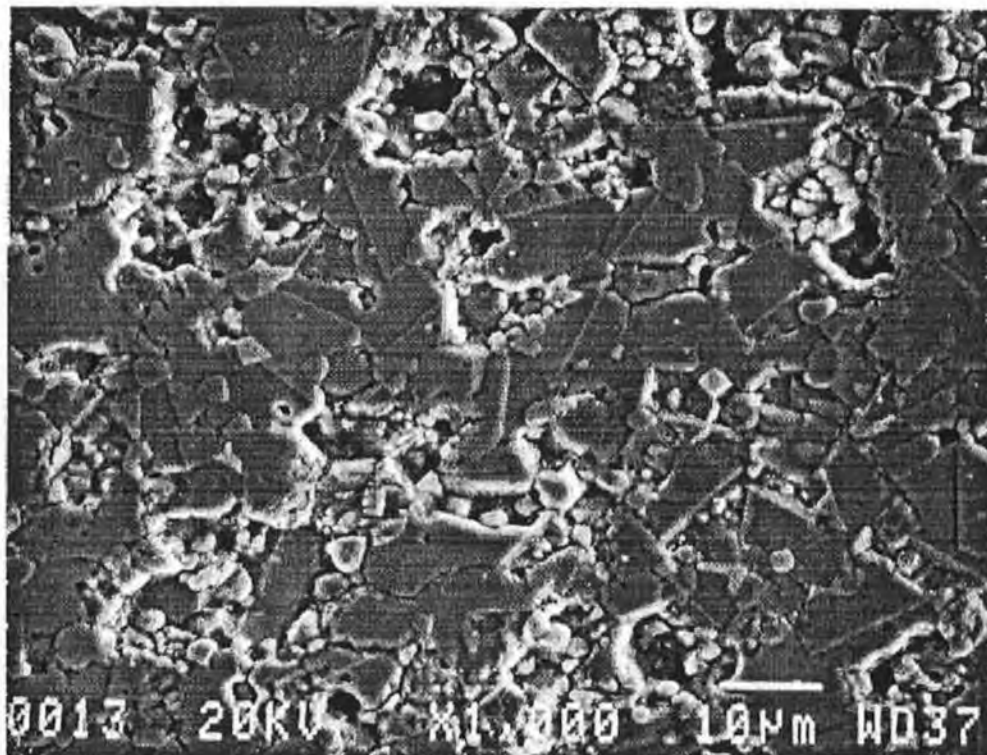


Figure 4.20 Micrograph for a disc pressed with 110 MPa (X1000)

General features of a ZnO varistor microstructure such as the grain boundaries, the twinning, the porosity etc. are equally apparent in the three categories of micrographs. The porosity appears to be more in the microstructure of the disc pressed with the lowest pressure. The grain size in the microstructure of the disc pressed with the highest pressure is slightly bigger. The average diameter of the grains, D_{av} has been calculated according to the following equation.

$$D_{av} = 1.56\bar{L} \dots\dots\dots 4.7$$

where L is the measured intercept of grains along a line on the micrograph. The intercepts were measured along a line drawn diagonally on the micrograph. The distribution of grain size is presented in the Table 4.8

Table 4.8 ZnO grain size of the discs pressed with different pressure

Parameter	Specimen taken from disc pressed at a stress of		
	40 MPa	66 MPa	110 MPa
Mean size	14.95 μm	15.16 μm	15.34 μm
Std deviation	3.17 μm	3.80 μm	2.89 μm

Mechanical Strength

The mechanical strength was measured by diametral compression method. The arrangement of the test specimen in the test has been discussed in section 3.3.2. The breaking strength was calculated using the following formula.

$$\sigma = \frac{2P}{\pi dh} \dots\dots\dots (4.8)$$

where σ = tensile strength, MPa
 P = breaking load, N
 d = diameter of disc, mm
 h = height of disc, mm

The test was conducted in an Instron machine with a cross-head speed of 1 mm/min. The aim was to observe the eventual effect of the compacting stress on the mechanical strength of the varistor discs. There were ten samples from each of the three categories in terms of the compacting pressure. The results are presented in Table 4.9.

Table 4.9 Effect of compacting stress on the tensile strength of the varistor disc

Tensile strength (MPa)	Discs pressed at a compacting stress of		
	40 MPa	66 MPa	110 MPa
Mean	16.72	15.29	18.22
Std deviation	5.55	2.07	3.97
Coeff. of variance	0.3319	0.1354	0.2179

Though the varistor discs pressed under the highest pressure have the highest strength, it is evident from the results that there is no significant difference. However, discs pressed with the lowest pressure exhibited a very inconsistent result as shown by the deviation in strength data. In this regard the medium pressure looks superior as indicated by the lowest value of the coefficient of variance.

4.5 DWELL IN PRESSING CYCLE

The pressing cycle usually adopted for compacting zinc oxide varistor discs is similar to that followed in the case of conventional ceramic processing. The approach consists of applying force through punches on the powder filled in the die and a number of holding or dwell times in different phases of loading. Depending on the frictional surface area and the volume of the disc the duration of total holding or dwell can be about 20-30 percent of the pressing cycle. There are some specific purposes of these dwells in obtaining the desired quality of the ceramic green body. The resultant effect on the sintered physical and electrical property of the varistor is not reported. The present study was conducted to investigate the influence of dwell. Three input variables - pre-press, press dwell and ejection delay were varied at two levels to undertake a factorial design for evaluating the main and interactive effects of these parameters. It was observed that dwell times have considerable influences on

the physical as well as on the electrical properties of the arrester blocks leaving scope of optimization.

Pressing Cycle

The pressing cycle consists of a number of steps beginning from filling the die with powder and ending with the ejection of the green body. Rise of pressure during compaction follows the pattern of a typical compressibility curve. The pressure increases at a lower rate in the initial stage and then with a rapidly higher rate in the final stage. The hydraulic compacting machine used in this experiment was equipped with the facility of pressing three discs at a time. The complete pressing cycle for the compaction of three arrester blocks with $V_{nom} = 5 \text{ KV}$ takes about 30 seconds. By taking the indicated data on load and estimating the ejection force in terms of the peak pressure a pressing cycle has been simulated. In Figure 4.21 the schematic diagram of the simulated pressing cycle with the dwell is presented. The flat regions represent a standard cycle with the duration of dwell at pre-press, press and ejection delay respectively.

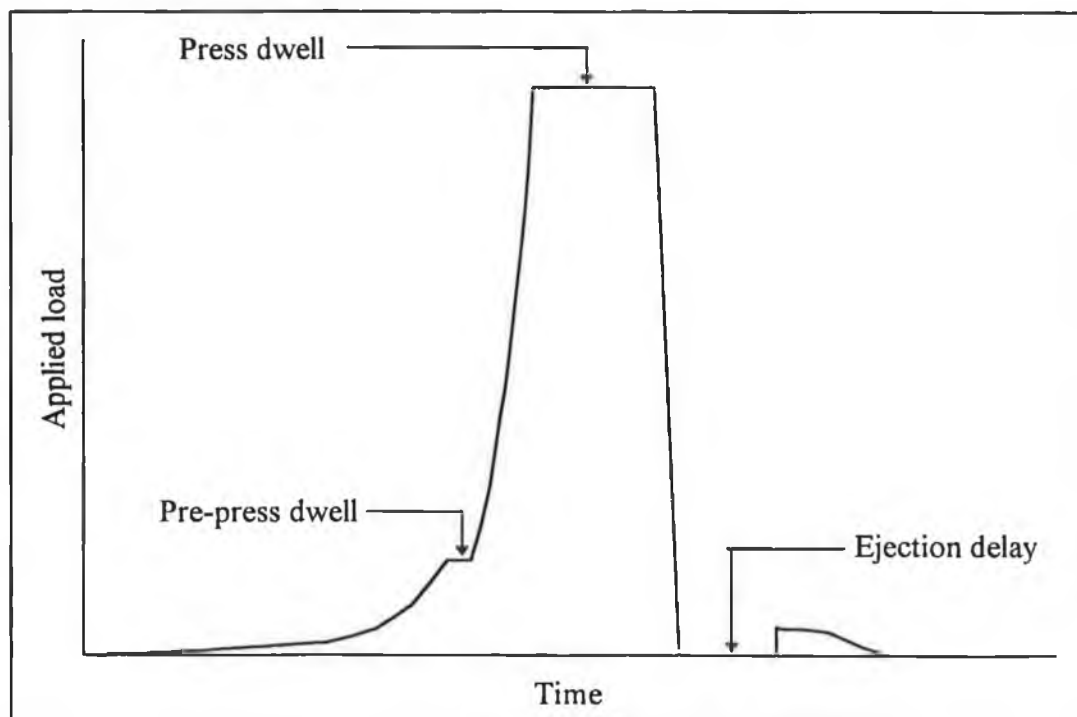


Figure 4.21 Schematic diagram of Pressing Cycle with different dwells

A two level full factorial design was made to evaluate systematically the effect of dwell time. Three variables with two levels constituted eight sets of experimental conditions. This approach is more economical compared to the one-factor-at-a-time design⁹⁵. The identification of various cells pressed with the specified duration of the dwell is presented in Table 4.9.

Table 4.9 Two level factorial design of experiment to analyze the effect of dwell

Cell Identity	Pre-press dwell (second)	Press dwell (second)	Ejection delay (second)
A	(-) 0	(-) 0	(-) 0
B	(-) 0	(-) 0	(+) 4
C	(-) 0	(+) 4	(-) 0
D	(-) 0	(+) 4	(+) 4
E	(+) 2	(-) 0	(-) 0
F	(+) 2	(-) 0	(+) 4
G	(+) 2	(+) 4	(-) 0
H	(+) 2	(+) 4	(+) 4

Preparation of samples

Standard metal-oxide varistor powder was pressed to fabricate the disc with nominal green dimensions of 49 mm in diameter and 51.2 mm in height with a target green density of 3.35 gm/cc. The pressing operation was performed in a double action fixed die using a hydraulic compacting machine. Thirty discs were pressed under each set condition stated in Table 4.9. The green discs were sintered in a kiln using a conventional sintering profile with a peak temperature of 1100 °C and a total sintering cycle time of about 70 hours. The locations of the discs in the sagger were randomized so that the variation due to the sintering position could be ignored. The sintered discs were passivated through a standard method with the rated amount of glass. The flat faces of the discs were ground, followed by washing using deionized water. Electroding was performed by conventional electric arc spray method

depositing a typical thickness of aluminium on both the flat faces leaving a small margin at the periphery.

4.5.1 INVESTIGATED PHYSICAL AND ELECTRICAL PROPERTIES

Apparent fired density was evaluated by Archimedes' principle of immersing the discs in water covering their whole surface with water-tight wrapping paper so that the open pores were not filled up with water. The diameter of disc at middle height was measured by a standard instrument.

Fired density

Ceramic density is commonly considered to be an important property which is usually less than the theoretical value. This parameter also indicates the level of porosity of the material. The effect of dwells on the fired density is very small. Three discs from each cell were measured by Archimedes' principle to determine the fired density. To prevent the open porosity from being filled up by water, the discs were carefully wrapped with water-proof wrapping paper. The mean fired density for different cells is presented in Table 4.10.

Table 4.10 Fired density (gm.cm^{-3}) of arrester blocks belonging to different cells

A	B	C	D	E	F	G	H	Con
5.5938	5.5907	5.5959	5.6003	5.5942	5.5902	5.6030	5.5978	5.5979

The variation in fired density due to the dwell is very small. The effects were evaluated by the two level factorial design.

Fired diameter

The variation in the green body diameter due to the dwell was not very remarkable. But a small but consistent trend in variation of the fired diameter was observed. The effect on the diameter of different cells is presented in the Figure 4.22 with the error

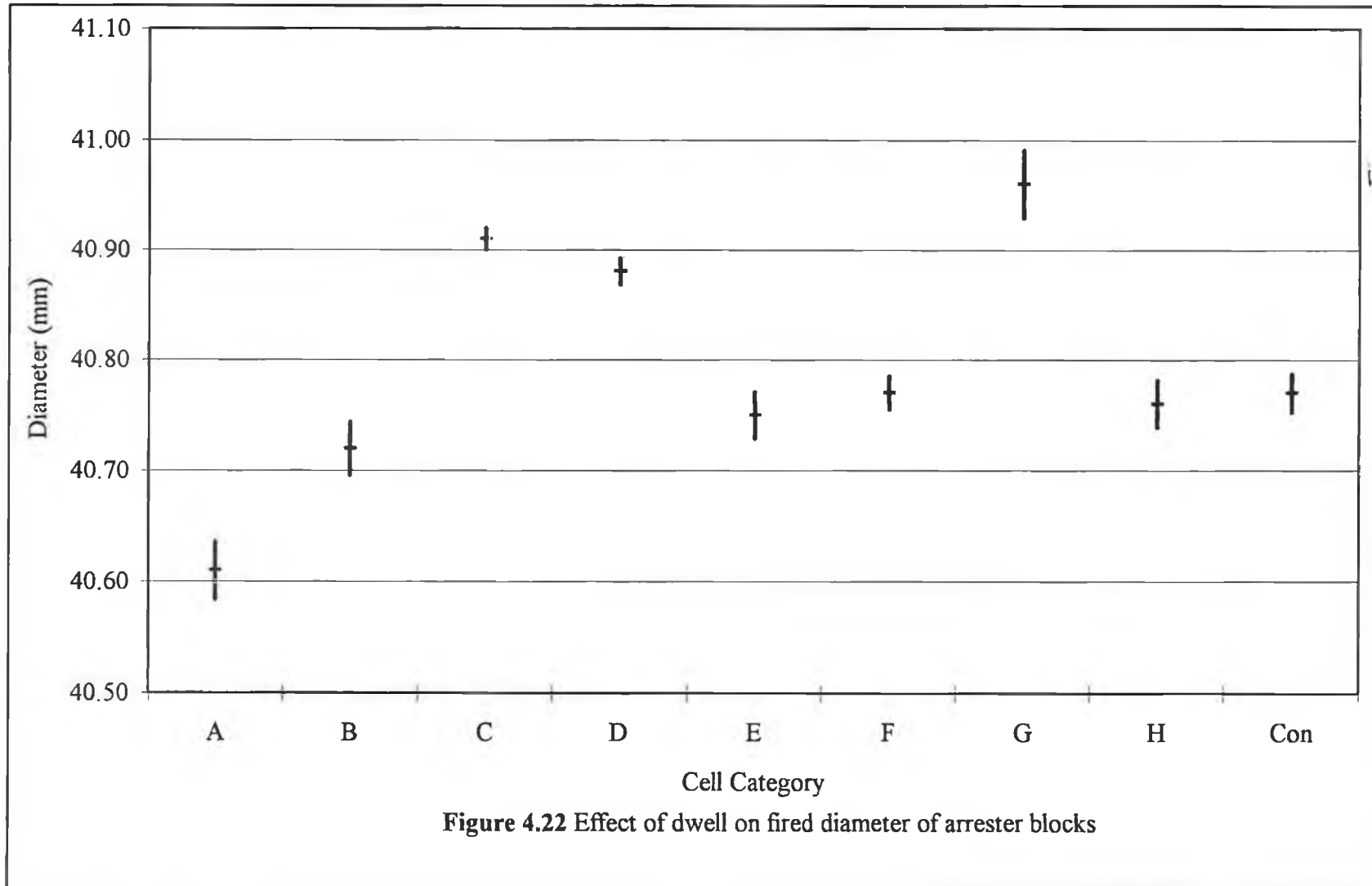


Figure 4.22 Effect of dwell on fired diameter of arrester blocks

bar. The discs belonging to the cell A exhibited the smallest diameter while the discs of cell G were the largest in diameter. Cell A was pressed without any form of dwell and therefore, the material in the compact did not get enough time during compaction to rearrange by springback neither in radial nor in the axial direction. Cell G was not allowed any ejection delay time and therefore compact material could not relax due to springback in the axial direction. As a result the diameter of cell G, on the average, was higher.

4.5.2 INVESTIGATED I-V CHARACTERISTICS

To investigate the effect of dwell times, the I-V characteristics have been evaluated. These include the nominal voltage, I-V curve, nonlinear co-efficient or exponent, clamp ratio and watt loss.

The nominal voltage was recorded at 5mA current which is equivalent to a current density of about 0.38 mA/cm^2 . The variation of the current density due to the small difference in the cross-sectional area among the different cells of arrester blocks was neglected. The I-V characterization was carried out by alternating current with sinusoidal wave at pre-breakdown region. Impulses with $8 \times 20 \mu\text{s}$ and $4 \times 10 \mu\text{s}$ wave shapes were applied for the high current measurement at the nonlinear and at the upturn region. The clamp ratio was evaluated as the ratio of voltage at 100 A and the voltage at 5 mA. The watt loss was measured at 80% of the nominal voltage.

Nominal voltage

The effect of dwell times on the nominal voltage of arrester blocks is shown in Figure 4.23. Nominal voltage is basically dependent on the grain size for a fixed composition of the ceramic material. The discs pressed without any dwell (cell A) exhibited a higher average value of the nominal voltage. This indicates that the ceramic material contains smaller grain size. The less packing of material and more trapped air/gas in the pressed body due to the absence of dwell may be attributed to inhibit grain growth.

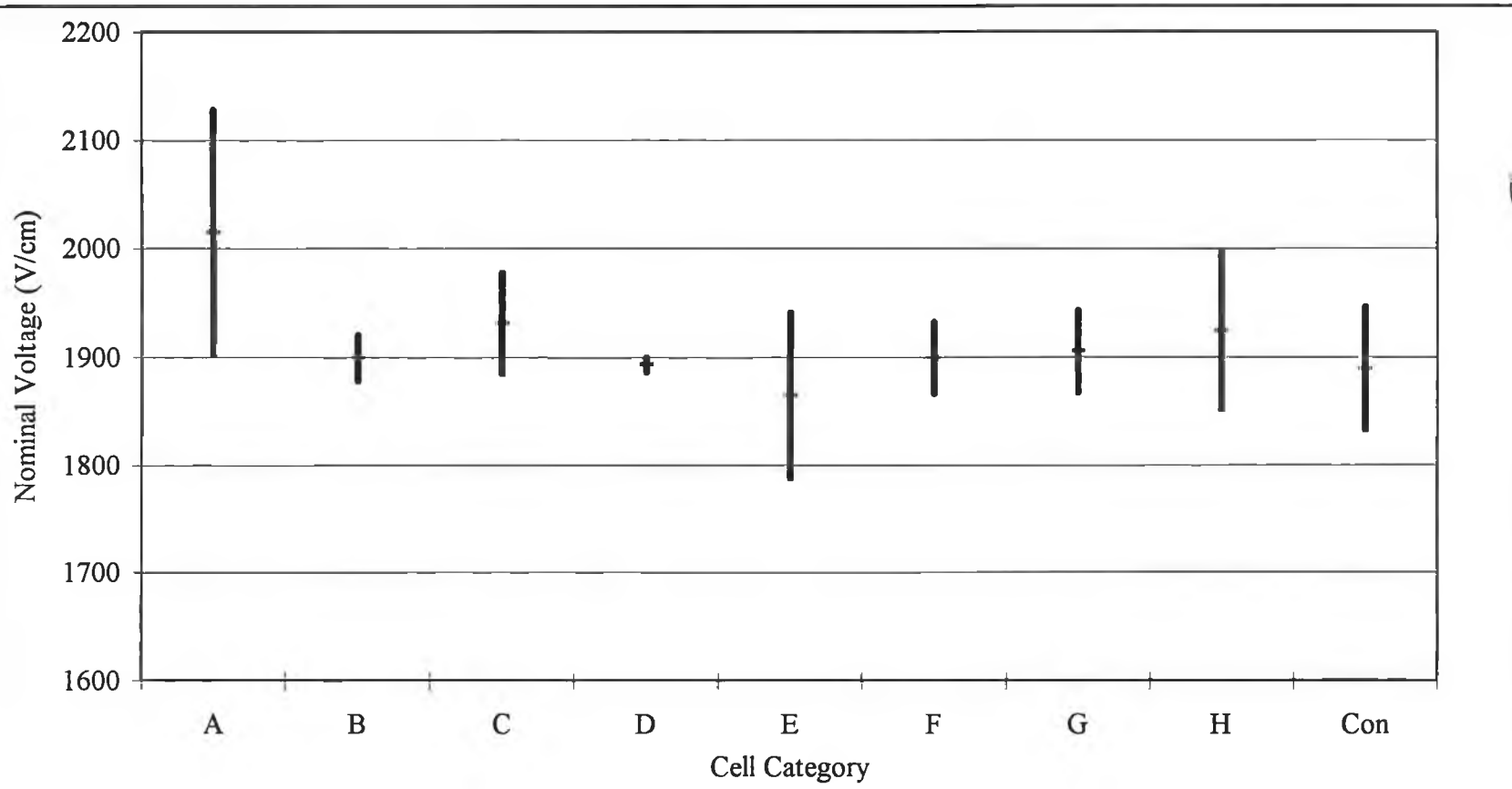


Figure 4.23 Effect of dwell on nominal voltage of different categories of arrester blocks

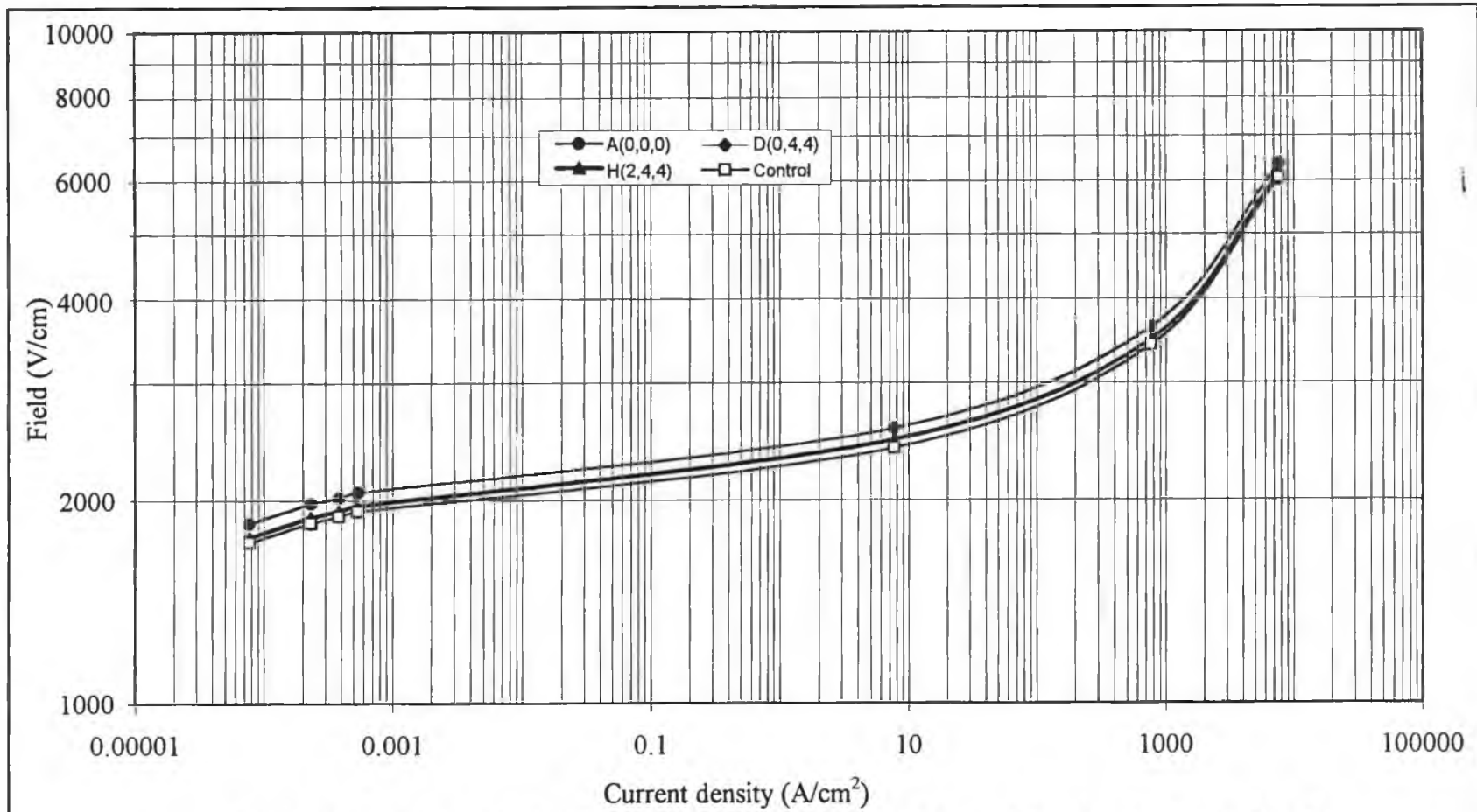


Figure 4.24 I-V curves of discs belonging to cells A, D, H and Control showing the effect of dwell

I-V curve

The I-V curves of a selected number of cells are presented in Figure 4.24. It is seen from this plot that the relative position in the current-voltage characteristics is similar to that observed in the case of the nominal voltage. The apparent parallel curves in the I-V plot for different cells indicate that the dwell time does not affect protective level or the clamp ratio significantly.

Nonlinear Coefficient

Non-linear coefficients (α) or exponents at the pre-breakdown and breakdown regions are shown in Figure 4.25. The exponents were calculated according to the equation (1.2) given in section 1.4.1. In this case the current and voltage values were taken corresponding to the current density of 0.23 and 0.54 mA/cm² for pre-breakdown region while to 0.54 mA/cm² and 7.68 A/cm² for breakdown region. A small variation of the exponents is observed among the different cells.

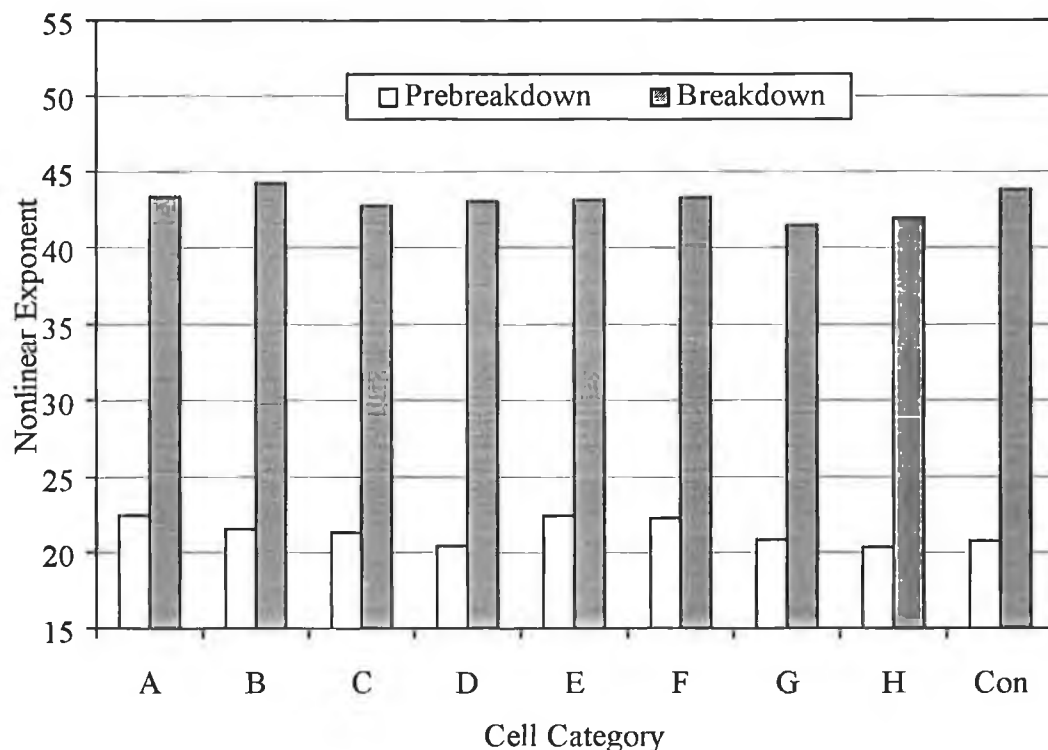


Figure 4.25 Nonlinear exponent at the pre-breakdown and breakdown region

Clamp ratio

This is a very important parameter for determining the clamping capability of arrester blocks. Variation in dwell in pressing cycle does not show any remarkable influence on this parameter. The data on clamp ratio corresponding to the computed values of V_{100}/V_{5mA} for different category of discs are presented in Table 4.11.

Table 4.11 Clamp ratios (V_{100}/V_{5mA}) for various cells of arrester blocks

Cell	A	B	C	D	E	F	G	H	Con
Clamp ratio	1.272	1.266	1.276	1.269	1.267	1.267	1.278	1.281	1.268

Watt loss

Watt loss was recorded at the initial stage without applying any high current pulse. Following the application of a 100 KA pulse the watt loss was measured on both the polarity of the discs. Recorded initial values of watt loss and those on the forward and reverse polarity after the high current shot are presented in Figure 4.26. The values for watt loss indicate the mean of five measurements for each cell and they were not normalized as the disc volumes were practically the same.

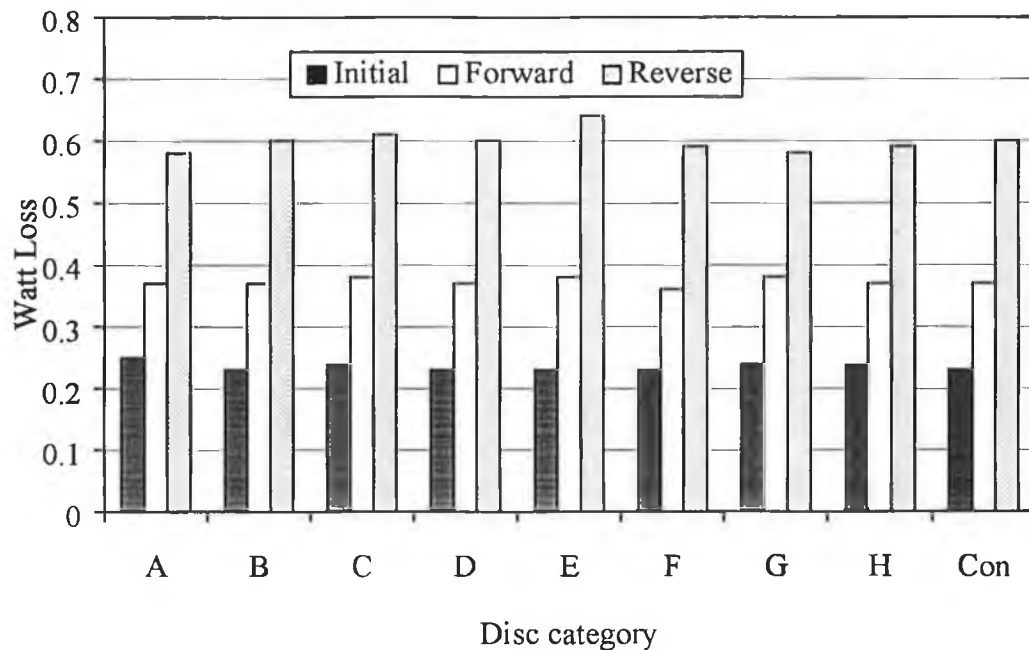


Figure 4.26. Watt loss behaviour with the initial value and after HASD shot

Two level factorial design

Two level factorial design was performed to analyse the effects of the variables on various important characteristics. Table 4.12 presents the consolidated results as the responses on the cross-section, fired density, nominal voltage, non-linear exponent at pre-breakdown and breakdown region. The sample size for calculating the responses was not the same. Diameter of thirty discs for each cell was measured to calculate the cross-section. Three discs from each cell were investigated to measure the fired density while five were characterised for the nominal voltage, exponents at pre-breakdown and breakdown regions. Mean of all the observed data were used to determine the main and interactive effects on the respective responses.

Table 4.12 Calculated effects and standard errors for 2³ factorial design with the pre-press, press dwell and ejection delay time

Main and interactive effects	Responses (estimate ± Standard error)				
	Cross-section (mm ²)	Fired density (gm/cc)×10 ³	Nominal volt (V/cm)	Exponent (Pre-breakdown)	Exponent (Breakdown)
Pre-press dwell (1)	1.78±0.18	1.13±3.58	-36.5±21.3	0.050±0.49	-0.883±0.38
Press dwell (2)	10.46±0.18	7.03±3.58	-6.0±21.3	-1.433±0.49	-1.188±0.38
Ejection delay (3)	-1.81±0.18	-1.98±3.58	-25.0±21.3	-0.627±0.49	0.463±0.38
Interaction (12)	-4.30±0.18	1.18±3.58	39.0±21.3	-0.313±0.49	-0.318±0.38
Interaction (13)	-4.01±0.18	-2.63±3.58	52.0±21.3	0.273±0.49	-0.118±0.38
Interaction (23)	-5.55±0.18	1.58±3.58	15.5±21.3	-0.078±0.49	-0.073±0.38
Interaction(123)	-1.25±0.18	-2.18±3.58	-23.5±21.3	-0.078±0.49	0.238±0.38
Average	1307±0.09	5595±1.79	1916±10.7	21.50±0.24	42.93±0.19

Discussion on I-V characteristics

The data on effects are presented with the standard error so that the significance of influence can be justified. The main and interactive effects are evident on the fired diameter or cross-section of the disc. Press dwell increases the fired diameter with significant effect. Pre-press dwell also acts positively but at lower extent. Apart from the data in Table 4.11, the effect of ejection delay can be visualized from Figure 4.22 when the diameters of the cell G and H are compared. In the former cell there was no

ejection delay and therefore, the material could not rearrange from the radial to axial direction. As a consequence, the discs ended up with higher fired diameter.

The fired density is found to be mainly influenced by the press dwell. At the peak load the holding time allows the trapped air/gas to escape from the compact due to the maximum pressure gradients resulting in higher fired density.

Nominal voltage is influenced negatively by the pre-press and ejection delay but there are interactive positive effects too. The cell A for which all the dwells had been kept at zero level exhibited the maximum nominal voltage as shown in Figure 4.23. The same trend is maintained all over the I-V curve as presented in Figure 4.24. So the arrester blocks pressed with no dwell time may leave a scope of minimizing the thickness due to the increased nominal voltage. But the deviation in the voltage for cell A was quite high posing a risk of higher rejection in classification test. In this context cell D exhibited a superior performance with consistent result.

Non-linear coefficient or exponent (α) is also found to be slightly influenced by the holding time. Discs belonging to cell A, E and F exhibited the higher values as illustrated in Figure 4.25. It is evident from the two level factorial analysis that the press dwell inversely affects the exponent both at the pre-breakdown and breakdown region. Ejection delay has the opposite influence. This reduces the exponent at pre-breakdown while enhances at breakdown. Pre-press dwell appears to be significant at breakdown region with a negative effect.

The watt loss behaviour of the discs is also found to be slightly changed with the variation in holding times as shown in Figure 4.26. Though the initial watt loss was slightly higher for cell A, subsequent results following HASD (high amplitude short duration) test indicated that Cell A got better stability with less degradation. This trend may be attributed to the influence of trapped oxygen in the compact during sintering. Influence of oxygen on the varistor properties is identified in other cases and reported in the literature. ZnO varistors become stable when they are annealed¹⁰ in any oxygen atmosphere.

With the observation on the I-V characteristics, it may be concluded that the influence of dwell time in pressing cycle is not confined within the domain of green properties of arrester blocks. But the effect of these parameters is considerably noticeable on the varistor performance characteristics. The properties such as the nominal voltage, the watt loss and the non-linear coefficient are found to change with the variation in the holding time. But there is no strictly particular combination of pre-press, press dwell and ejection delay time which can ensure best values for all of the performance characteristic parameters. It will, therefore, be necessary to make a compromise to set the optimum dwell time in the pressing cycle depending upon the effect on the critical properties.

Arrester blocks compacted with longer press dwell and ejection delay, exhibited a highly consistent nominal voltage. Though in this case there is a scope of slight reduction in non-linear coefficient, this selection of dwell time could allow to specify close tolerances for the nominal voltage.

4.5.3 ENERGY ABSORPTION CAPABILITY

The investigation concerning the energy absorption capability was carried out by injecting electrical energy in the form of a long duration pulse. Apart from the I-V characteristics the energy absorption capability is vital for reliable operation of varistor. The advantage of a varistor with higher energy absorption capability is that the device size can be proportionally reduced. Alternatively the same size could be upgraded for more demanding applications. This study with two level factorial design was aimed at evaluating the effect of dwell on the energy absorption capability.

Testing Procedure for Energy

The test for energy absorption capability was conducted in a rectangular wave generator (Haefely) having a capacity of charging voltage of 50 KV and an energy level of up to 45 KJ. Each disc was subjected to a cycle of three 2 ms impulses at a particular charging voltage. Three discs were placed for testing at a time, and

impulses were applied in sequence with a charging time of 8 seconds. So for a particular disc there was an interval of 24 seconds between two consecutive shots. Starting charging voltage was set at 24 KV which led to an energy injection in the range of 140-150 J.cm⁻³. The charging voltage was increased discretely by 1.2 KV for every subsequent cycle, resulting in an increase in the total amount of energy injection by about 5-10 percent.

The test pulse used for measuring the energy absorption capability has been briefly described in section 3.2.2. The arrester blocks were subjected to the test until they failed. Due to the uncontrollable variation in the manufacturing process every parameter of varistor is found to differ from disc to disc, even among those belonging to the same cell. To take into account this statistical variation a considerably large sample size was taken for carrying out the test. Sixteen samples from each cell were tested to estimate the energy absorption capability.

Due to the injection of energy by the electrical pulse, the arrester blocks became hot and they were allowed to cool down to room temperature before being subjected to the next cycle. The test had been continued with increasingly higher charging voltage until a an energy level was reached at which the disc could not sustain and subsequently failed in any mode of failure.

Computational Procedure for Energy

The energy injected into the varistor body by a pulse is the integrated value of the product of the instantaneous clamping voltage and current over the pulse duration. The basic equation used for computing the injected energy is given in section 3.1. The peak values of the clamping voltage of the arrester block and the maximum current passing through it, were recorded and used for computing the energy. The relationship expressed in terms of peak voltage, V_{pk} and peak current, I_{pk} for a duration of time, T is as follows:

$$Energy = KV_{pk}I_{pk}T.....(4.9)$$

where $K =$ constant depending on the wave-shape. For a 2 ms quasi-rectangular shape pulse as shown in Figure 3.2, $K=1.14$, which can be evaluated from the geometry of the wave shape. Thus the total injected energy for a pulse duration of 2 ms is estimated from the following formula:

$$Energy = 2.28 V_{pk} I_{pk} \dots\dots\dots(4.10)$$

The total injected energy by a pulse was estimated by the equation (4.10). The recorded values of V_{pk} and I_{pk} , corresponding to the first shot of the cycle up to which the disc sustained without failing, were used for computation. Energy absorption capability, defined as the energy density was evaluated by dividing the total injected energy with the volume of the disc.

Failure mode

The most common failure modes observed in the test for energy absorption capability are flashover, puncture or pinhole (thermal runaway). However, among them the pinhole accompanied by flashover occurs very frequently. The pinhole or puncture is developed due to the flow of excessive electrical current through any of the preferential paths. It is to be noted that the pinholes were mainly located at the periphery of the disc face. But a few failures by cracking were also observed which usually occurred at the very high level of energy.

Observed Behaviour of Different Cells in Terms of Energy Absorption

The energy absorption capability indicates the highest level of energy density up to which a disc survives. The cumulative percentage of discs with ascending order in terms of the energy absorption capability is plotted. Since there are eight cells, the curves are presented in three figures to avoid superimposition. Figures 4.27, 4.28 and 4.29 demonstrate results from Cells A, B, C, Con, Cells D, E, F, Con and Cells G, H, Con respectively.

The curve for control cell (Con), has been kept common in all the figures to facilitate comparison between the various cumulative distributions. It may be mentioned here

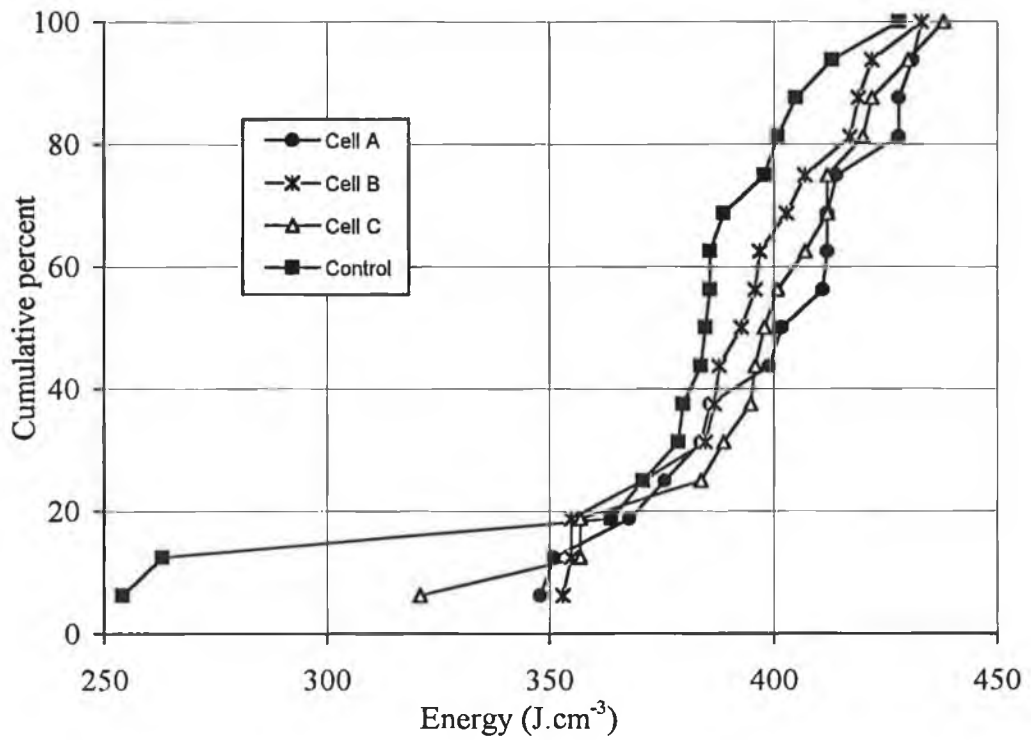


Figure 4.27 Energy absorption capability of cells A, B, C and Control

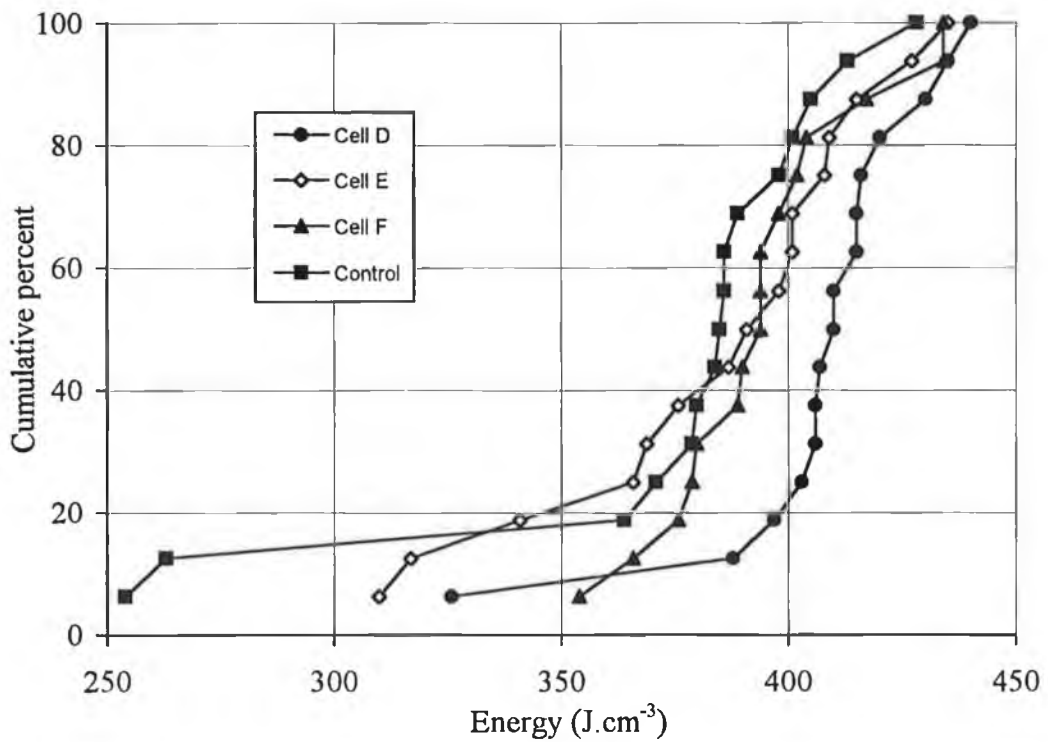


Figure 4.28 Energy absorption capability for cells D, E, F and Control

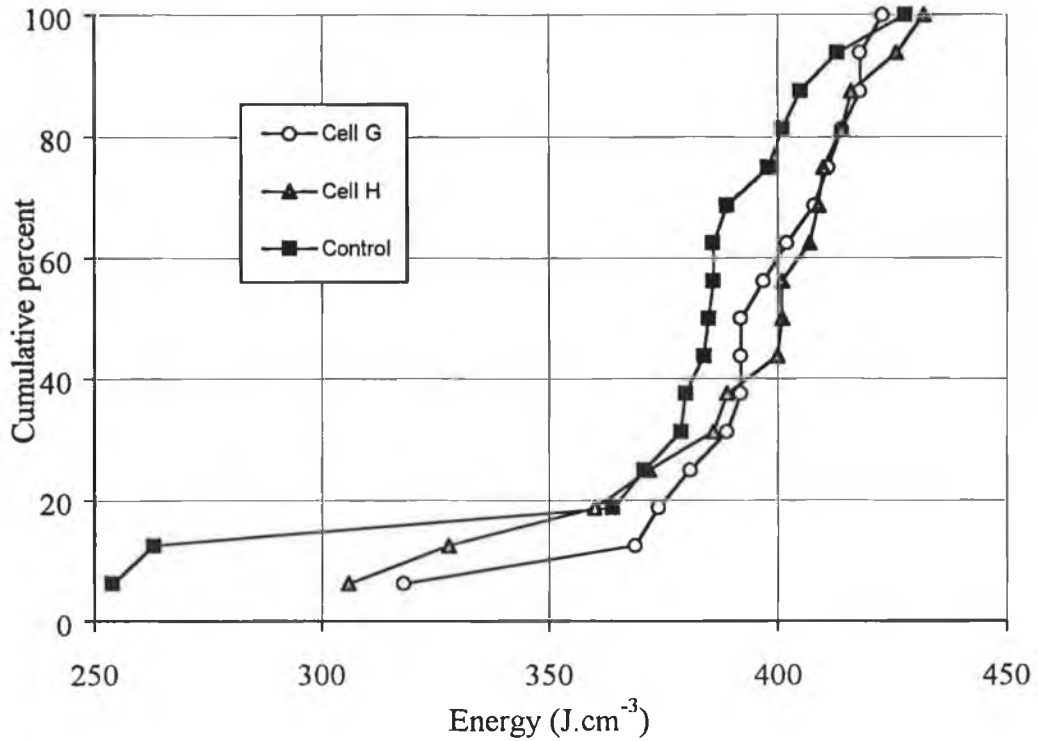


Figure 4.29. Energy absorption capability for cells G, H and Control

that the control cell was pressed with the standard dwell for the specified arrester blocks. The holding time maintained for this category of arrester blocks is within the range of time specified in the design of experiment (pre-press dwell-0.5 second, press dwell-2.5 seconds and ejection delay-2 seconds).

The overall relative performance is illustrated in Figure 4.30. The error bar represents the mean \pm standard deviation of energy absorption capability of individual cells. The bar indicates the measure of central tendency as well as the scattering of distribution. As shown in the Figures 4.27 - 4.29, the highest levels of energy attained by all of the cells almost coincide, except for cells B and G. In this context these two cells appear to be less capable.

Although the highest level of energy indicates the possible maximum achievable target, commercial arrester blocks are rated conservatively based upon the initial failure. So the lowest value of energy absorption capability for a distribution under a particular treatment is very critical. But the extreme values are not generally treated

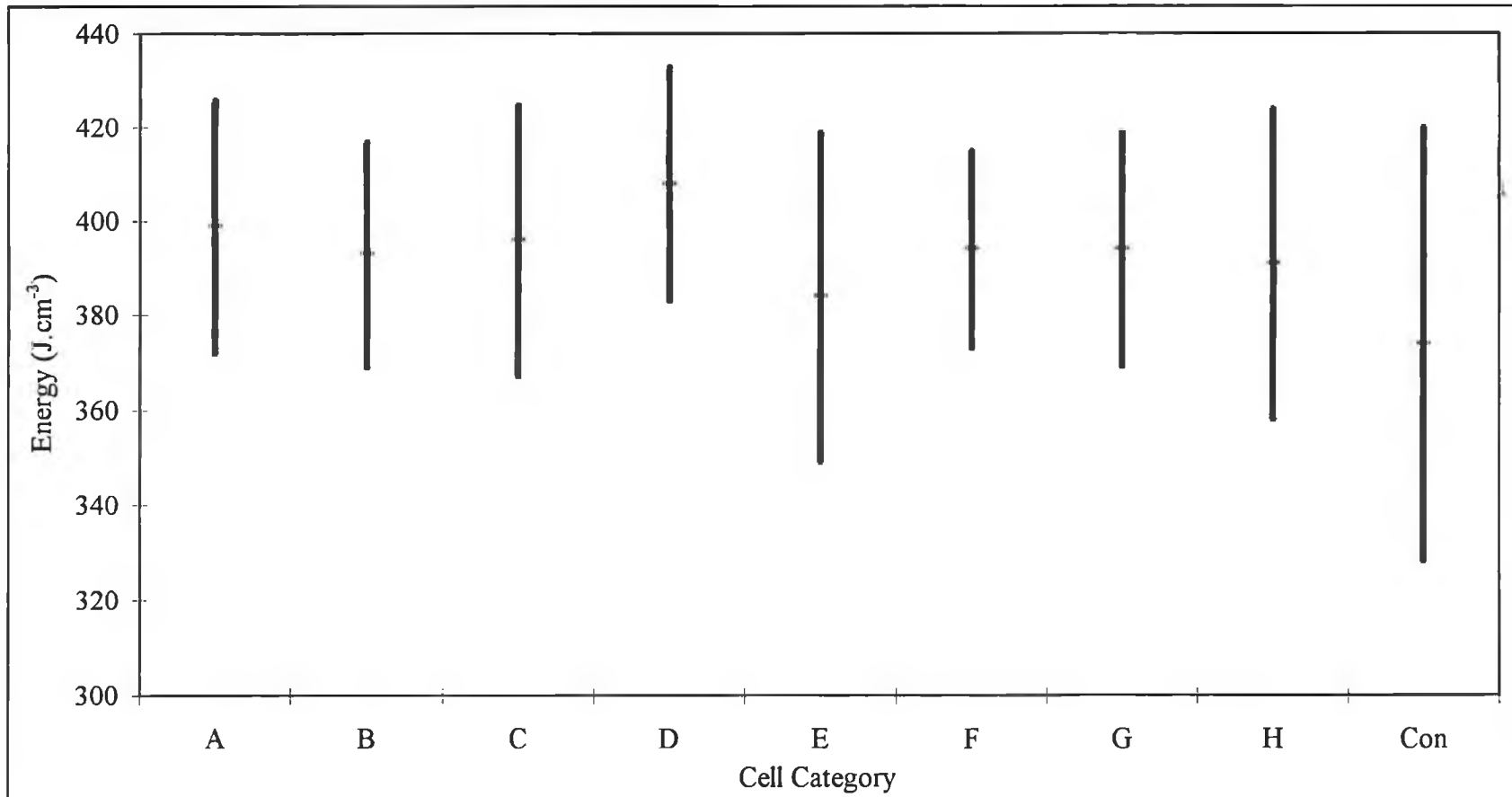


Figure 4.30 Relative energy absorption capability of all the cells by error bar

as valid parameters in statistics⁹⁶. This is because of the fact that inference on the basis of an extreme value in a distribution - either the lowest or the highest - is very often unreliable for any conclusion. In the present study different cells were, therefore, compared on the basis of their mean and median energy - the measures of central tendency for a distribution.

It is evident from the Figure 4.30 that among all, the cell D has attained the highest mean value of energy absorption capability with low scattering. So the dwell adopted in pressing the discs of this cell should be considered as the optimum in terms of the energy absorption capability.

It is worthy of note that a random setting of dwells may not necessarily improve the varistor characteristics. Discs from cell A for example, which were subjected to no dwell, performed better than some of the other cells as evident in Figure 4.27.

4.5.4 HIGH CURRENT PERFORMANCE

The high current performance is important to evaluate the withstanding capability of transient pulses with a very high amplitude. These pulses last for a very short time but are characterized by a very high amplitude. So the behaviour of arrester blocks in this case cannot be predicted from the performance in the energy test.

High current performance was evaluated by a short duration pulse. During this test current passes through the disc for a very short time, but with high amplitude. The electrical impulse is a simulation of an actual lightning stroke. The average duration of a stroke⁸ is considered to be approximately 30 microseconds. A typical short pulse adopted for testing the arrester block is usually of shorter duration, and defined⁹ as the $4 \times 10 \mu\text{s}$ wave as shown in Figure 3.4. Injection of a large amount of energy into the disc within a very short time results in a fracture mechanism which is usually different from that observed with long pulses. The failure mode⁴⁴ in this test is predominantly by cracking or rupture rather than the thermal runaway or puncture observed in the case of long pulse test.

The HASD test was performed in an Impulse Current Test System (Haefely). The impulse generator is capable of a maximum charging voltage of 100 KV, and maximum energy of 62.5 kilojoule. The arrester blocks were tested individually, one pulse being applied at a time. Subsequent pulses were applied at an increasingly higher charging voltage, with the target test currents of 98, 101, 104, 107 and 110 KA. Similar to the test with long pulse, the discs were allowed to cool down before being subjected to the subsequent shot of the higher rated current.

In a high current test the failure mechanism is different from what is observed in case of test for energy absorption. In this case the injection of huge energy within a very short time leads to cracking in the longitudinal direction. However, a very small percentage of failures may occur by pinholes and flashover.

Observation on High Current Performance

Five samples from each cell were tested to evaluate the high current performance. The short duration impulses with increasing magnitude of rated peak current have been applied and the corresponding number of survivor discs is recorded. The performance is summarized in Table 4.13.

Table 4.13. Number of survivor discs at different rated peak currents of HASD pulse

Cell ID	Shot number (Rated Current)				
	1 (98KA)	2 (101KA)	3 (104KA)	4 (107KA)	5 (110KA)
A	5	5	3	3	0
B	5	5	3	3	1
C	5	5	4	2	0
D	5	5	5	5	2
E	5	5	5	3	1
F	5	5	4	3	0
G	5	5	4	2	0
H	5	5	5	1	0
Con	5	5	2	1	0

A parameter to express the high current performance of a particular cell can be defined mathematically in the following form:

$$\text{High Current Performance}(\%) = \frac{\sum n_i x_i}{\sum NX_i} \cdot 100 \dots\dots\dots(4.11)$$

where N = sample size of discs to be tested
 X_i = rated peak current at the ith pulse
 n_i = number of discs successfully passing the ith pulse and
 x_i = actual peak current in the ith pulse

The plot in Figure 4.31 delineates the high current performance computed according to the parameter according to the equation (4.9). Out of a maximum achievable score of 100%, the higher the value of the parameter, the better is the device. As apparent in the Figure 4.31, cell D is found to exhibit the highest level indicating the best performance in high current tests. The performance of control cell is very poor. The relative position of this cell is even worse than what was observed in the case of energy absorption capability.

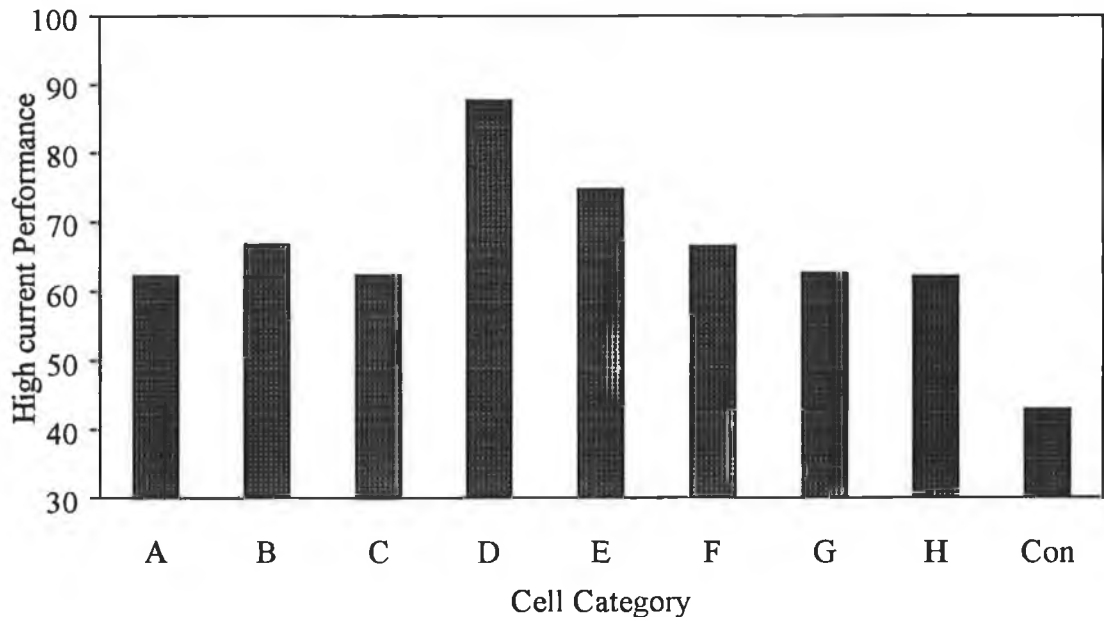


Figure 4.31. High current performance of different cells pressed with different dwell

Dwell or holding time during different phases of the pressing cycle has considerable influence on the eventual property of the varistor disc. However, incorporation of longer dwell in the pressing cycle does not necessarily lead to the better performance. Rather discs pressed with randomly selected combination of dwells may perform worse than those pressed without any dwell time at all.

Among the various cells, the discs belonging to that compacted with the longer press dwell and ejection delay but with no pre-press dwell time exhibited better trends in energy absorption capability. Moreover, the same processing condition was found to yield superior high current performance. So there is a scope of adjusting the dwell time in pressing operation to optimize the varistor performance. However, since the duration of dwell is usually on the basis of the volume of powder to be compressed. So the combination and the duration of dwell optimized for the arrester blocks with $V_{nom} = 5$ KV, may not be appropriate for all other sizes of varistor discs. It is, therefore, recommended that dwell in pressing cycle should be selected depending upon the individual size, shape and volume of varistor discs.

4.5.5 REPLICATE EXPERIMENT WITH DWELL TIME

The influence of dwell initially observed on the energy absorption capability of arrester blocks was verified by replication of the experiment on two cells - cell A and cell D as specified in the earlier design of experiment. Following the previous experiment the arrester blocks belonging to the cell A were pressed without any dwell whereas those belonging to cell D were pressed with longer level of pre-press dwell and ejection delay. Standard powder was pressed to produce discs of the same nominal dimensions as with the previous experiment. The observation of the replicated experiment is presented in Figure 4.32 with cumulative percentage of failures.

It is quite apparent from the above figure that there is a distinct difference between the two cells and arrester blocks belonging to cell D (according to Table 4.9) were

found to exhibit superior performance than those belonging to cell A. A similar trend in energy absorption capability was noticed in the previous experiment. So the results

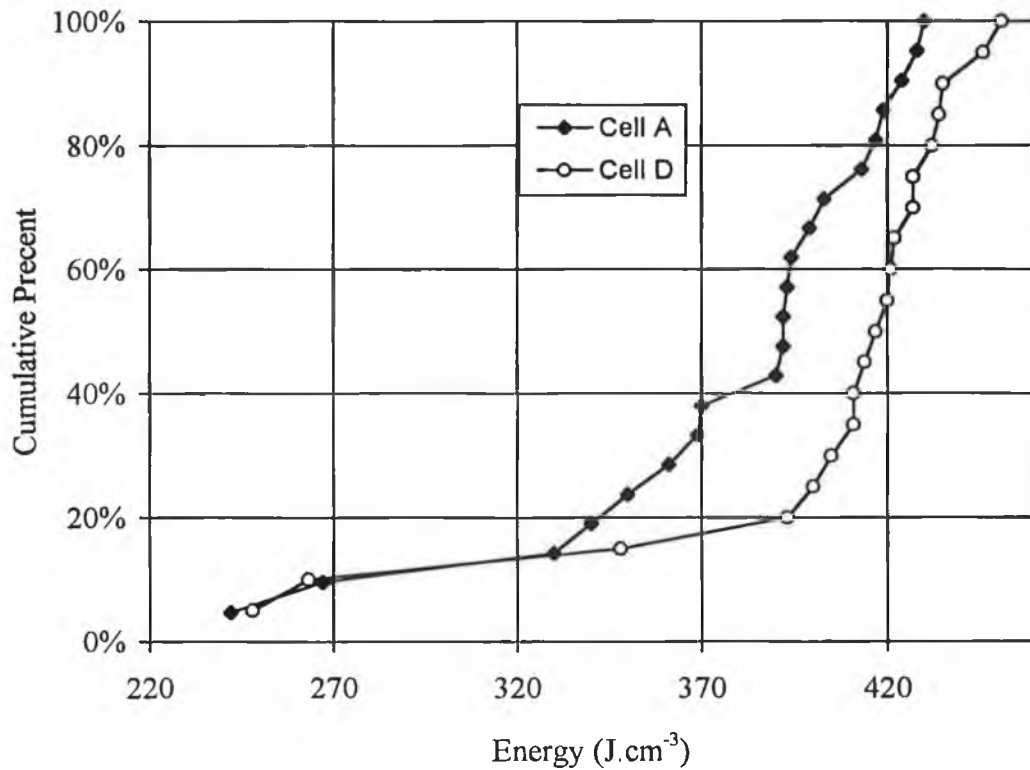


Figure 4.32 Energy absorption capability in replicated run

experiment. So the results of this investigation confirm that the influence of dwell in pressing cycle is reproducible.

It should be mentioned here that the origin of failure location was recorded in this experiment to identify whether the disc failed due to the flaw or weakness on the top or on the bottom face of the disc. The number of failures from the top face was zero for cell D whereas for cell A there were nine failures from the top face of the disc in the sample size of 19 discs. Due to the better compacting condition arresters belonging to cell D were able to prevent failures from the top. The comparative weakness of the bottom face is attributed to be the adverse effect of contact during sintering. Thus it can be inferred from this difference in failure origin from the top face that better consolidation of ceramic is possible by optimum selection of dwells and their duration in the pressing cycle.

Chapter 5

FORMULATION OF A MATHEMATICAL MODEL

5.1 INTRODUCTION

Mathematical formulation of the responses in terms of the input parameters is based on the design of experiment. Due to normal variation in the processing operations, data on different physical and functional parameters of varistor are found to deviate within a very narrow to a considerably wide range. In such cases statistical methods are very often considered to be useful tools to analyze the results. These methods are easy and simple but very effective to evaluate the data and also to quantify their reliability on the responses which are influenced by multiple input parameters. In this regard factorial design and response surface methodology are very common.

5.1.1 FACTORIAL DESIGN

Factorial designs are widely used in the experiments to estimate the main and interacting effects of several independent variables on the response^{95,97}. There are various special cases of factorial design. The two-level factorial design is particularly very important in the early stage of the experimental work. The experimental method with two-level factorial design is helpful in conducting investigations effectively by saving time and in presenting results in an explicit form. This is necessary to avoid misleading conclusions especially when interactions may be present. Moreover, this approach is economical compared to one-factor-at-a-time design.

The two-level factorial design is denoted by 2^k where k is the number of factors or variables. In this case only two levels are considered for each of the k factors and it is assumed that the response is linear over the range of the chosen level. The variables are denoted as “-” and “+” or “-1” and “+1”. This is entirely arbitrary but very effective for analyzing the results. The 2^k factorial design allows independent estimates of k (where k is called the dimension of the design) main effects, kC_2 two-

factor interactions, kC_3 three-factor interactions, so on and one k-factor interaction. That is, for a 2^k design the complete analysis will contain $2^k - 1$ effects.

It is often true that the main effects are larger than the two-factor interactions, which in turn tends to be higher than the three-factor interactions and so on. The “effect” of a factor or a variable means the change in response due to the movement from the lower level to the higher level and the average of the “effect” is called the “main effect” for a particular variable. All of the variables in an experiment do not behave additively and are, therefore, said to “interact”. Usually the higher order interactions tend to become negligible and can be disregarded.

5.1.2 RESPONSE SURFACE METHODOLOGY

Response surface methodology (RSM) is a collection of mathematical and statistical techniques used in the empirical study of the relationships between the measured responses and a number of input variables. The ultimate goal of the use of RSM is to optimize the response.

The RSM method is widely used because of some attractive features such as (i) it is a sequential approach, the result at each stage guiding the experimentation to be conducted at the next (ii) it casts the experimental problem in readily understandable geometric terms and (iii) it is applicable for any number of variables. The independent variables are denoted by $x_1, x_2, x_3, \dots, x_k$ and are assumed to be continuous and controllable by the experimenter, whereas, response, y , is assumed to be a random variable in response surface methodology.

As the relationship between the response and the independent variables is unknown, the first step in RSM is to fix a true functional relationship between y and the set of independent variables. Usually a low order polynomial is considered for the first-order model and a higher-order polynomial is assumed for the second order model. In the first order model, $(y = \beta_0 + \sum \beta x_i + \epsilon)$, orthogonal first order designs are adopted which includes the 2^k factorial. The k factors are coded to the standardized

levels ± 1 . But the 2^k design does not afford an estimate of the experimental error, until some runs are replicated. Hence, a centre point is considered and replicated. The addition of the centre point does not influence $\{\beta_i\}$ for $i \geq 1$, but the estimate of β_0 becomes the grand average of all observations. Furthermore, the addition of the centre point does not alter the orthogonal property.

5.2 MATHEMATICAL MODELING

The mathematical model developed from the data on the important physical and electrical parameters of varistor discs will be helpful in various aspects. The derived model from the two-level factorial design will reveal the individual and interactive effects of the variables. The RSM will provide functional relationships which will indicate the trend of the response for a change of input variables.

5.2.1 FACTORIAL DESIGN WITH DURATION OF DWELL

A two level full factorial design was adopted to evaluate the effect of dwell time on the performance of arrester blocks. The results have been presented in the previous chapter. The three input variables - pre-press, press dwells and ejection delay varied at two levels constituted eight sets of experimental conditions.

Table 5.1. 2^3 factorial design and the corresponding data on various responses

Type of Dwell			Responses				
Pre-press	Press	Eject	Energy (J.cm ⁻³)	Vnom (V/cm)	Exponent	Diameter (mm)	Density (gm.cm ⁻³)
(-)	(-)	(-)	407	2015	22.42	40.59	5.5938
(-)	(-)	(+)	395	1899	21.52	40.69	5.5907
(-)	(+)	(-)	400	1931	21.30	40.92	5.5959
(-)	(+)	(+)	410	1893	20.40	40.89	5.6003
(+)	(-)	(-)	395	1864	22.43	40.74	5.5942
(+)	(-)	(+)	394	1899	22.23	40.72	5.5902
(+)	(+)	(-)	395	1905	20.84	40.99	5.6030
(+)	(+)	(+)	401	1924	20.33	40.70	5.5978

Table 5.1 contains the 2^3 factorial design along with the corresponding mean or median values of different responses on the electrical and physical properties of the arrester blocks. These data will be used to develop the mathematical formulation.

The quantitative parameter, Y to be investigated is called the response. It is determined as a polynomial function of possible influencing factors. Considering all the effects either main or interactive of the factors the response, Y can be represented in the following general form:

$$Y = a_0 + \sum_i a_i x_i + \sum_{ij} a_{ij} x_i x_j + \sum_{ijk} a_{ijk} x_i x_j x_k \dots\dots\dots(5.1)$$

where the coefficients a_i , a_{ij} and a_{ijk} represent respectively the main, two-factor and three-factor interactions among the parameters x_i , x_j and x_k . The constant, a_0 is evaluated as the average of the responses. In the present work all the main and interactive effects were evaluated. There were three variables making a total of seven coefficients with three main effects, three two-factor interactions and one three-factor interaction.

The calculated value of the coefficients using the median values of energy absorption capability of the arrester blocks are

$$a_1 = -6.75, \quad a_2 = 3.75, \quad a_3 = 0.75, \quad a_{12} = -0.25, \quad a_{13} = 1.75, \quad a_{23} = 7.25, \quad a_{123} = -3.75$$

and the constant $a_0 = 399.6$.

Neglecting the small coefficients and substituting the value of the significant ones in equation (5.1) yield the following relationship:

$$\text{Energy} = 399.625 - 6.75x_1 + 3.75x_2 + 1.75x_1x_3 + 7.25x_2x_3 - 3.75x_1x_2x_3 \dots\dots\dots(5.2)$$

The energy absorption capability is expressed as a function of three dwells x_1 , x_2 , x_3 respectively for pre-press, press and ejection delay. It may be noted that in the above

equation the independent dwell time will assume a value of either zero for the lower level or unity for the higher level of the input variables.

Similarly, other functional parameters of arrester block can also be expressed in terms of the significant effects. In this case the coefficients comparable to the standard error have been considered. Thus the relationship for the nominal voltage corresponding to a current density of 0.4 mA/cm² is represented by the equation (5.3)

$$\text{Nominal voltage} = 1916 - 36.5x_1 - 25x_3 + 39x_1x_2 + 52x_1x_3 - 23.5x_1x_2x_3 \dots\dots(5.3)$$

The non-linear exponent (α) for the prebreakdown region is calculated on the basis of the currents of 0.23 and 0.54 mA/cm² and the corresponding voltages.

$$\alpha = 21.43 - 1.43x_2 - 0.63x_3 - 0.31x_1x_2 + 0.27x_1x_3 \dots\dots\dots(5.4)$$

Dimensional change such as fired diameter of the arrester blocks is also observed due to the variation of dwell to a very small amount but in consistent manner. The dimension (mm) of diameter at middle height is given by

$$\text{Diameter} = 40.78 + 0.19x_2 - 0.06x_3 - 0.075x_1x_2 - 0.095x_1x_3 - 0.1x_2x_3 \dots\dots\dots (5.5)$$

It is evident from this relationship that the main and interactive effects of ejection delay is negative. This is because of this reason that the fired diameter of arrester increases when there is no ejection delay in the pressing cycle.

Fired density (gm.cm⁻³) of the arrester block is also slightly affected by the dwell, the relationship is given by the following expression.

$$\text{Density} = 10^{-3}(5595.74 + 7.02x_2 - 1.98x_3 - 2.63x_1x_3 + 1.57x_2x_3 - 2.17x_1x_2x_3) \dots(5.6)$$

The coefficients in the above equations (5.2 -5.6) indicate the effects, the sign of which indicates whether the influence is positive or negative. Thus it is evident from

the equation (5.2) that the pre-press dwell time negatively affects the energy. Even the term with the higher co-efficient having interaction with x_i is also found to have a negative influence. So the level of the pre-press dwell time can be conveniently kept at low level to maximize the energy absorption capability. This implies that pre-press dwell should be eliminated from pressing cycle particularly for energy. Among the eight experimental conditions, the dwells set for cell D appear to be most suitable. Inference derived from the equation is found to be in good agreement with the results presented in Figure 4.30 in chapter 4.

Similarly, for other variables the influence of the pre-press, press dwell and ejection delay can be estimated from the functional relationships.

5.2.2 RSM WITH COMPACTING STRESS AND SPEED

Response Surface Methodology (RSM) is a useful tool to develop a relationship for the dependent variable (response) as a function of the independent variables⁹⁷ (input parameters). This method is widely used⁹⁸ to develop useful mathematical model. The compacting pressure and the speed were considered as the input parameters. The responses on the operational properties such as the energy absorption capability, nominal voltage, clamp ratio, watt loss and the physical characteristics such as the fired diameter and density were evaluated. The general mathematical relationship of a response in terms of input variables can be written as

$$R = f(p,s) \dots\dots\dots(5.7)$$

where R is the response, p is the compacting stress and s is the speed.

The above functional relationship between the response and the investigated independent variables can be represented by the following equation:

$$R = C p^l s^m \dots\dots\dots(5.8)$$

where R is one of the six output variables while C , l and m are the model parameters to be estimated by the use of the experimental data. Equation (5.8) can be written in the following logarithmic form

$$\ln R = \ln C + l \ln p + m \ln s \dots\dots\dots(5.9)$$

A linear form of the equation (5.9) can be expressed as follows

$$\hat{y} = y - \varepsilon = b_0 x_0 + b_1 x_1 + b_2 x_2 \dots\dots\dots(5.10)$$

where \hat{y} is the estimated response of the parameter and y is the measured value on a logarithmic scale, ε is the experimental error, $x_0 = 1$ (a dummy variable) and x_1 , x_2 are respectively the coded values of compacting stress and speed with logarithmic transformation. The constants b 's are the estimated model parameters. The basic formula of b is given as

$$b = (X^T X)^{-1} X^T y \dots\dots\dots(5.11)$$

where $b = b_0$, b_1 and b_2 is the matrix parameter estimates, X is the calculation matrix, X^T is the transpose of X , XX^T is the variance matrix, $(XX^T)^{-1}$ is the covariance matrix and y is the matrix of the measured response on the logarithmic scale. The calculation procedure is presented in Appendix B.

Experimental Design and Condition

In order to estimate the parameters of the model, a first-order orthogonal design was adopted as depicted in Figure 5.1. The design consisted of nine experiments of which four, representing a 2^2 factorial design, were located at the corner of the square while the rest five were replicated at the centre points to estimate the pure error.

This experiment was conducted on the 17 mm (green diameter) discs. Except the four replicated experiments at the centre of the orthogonal design, data presented in

section 4.3 of the previous chapter were used corresponding to the corner and one at the centre. The limits of the variables were selected to cover a wide range. The pressure was changed from a lower limit of 40 MPa to a higher limit of 110 MPa while speed limits were 10 and 160 mm/min. The mid-point comprised of 66 MPa pressure and 40 mm/min speed.

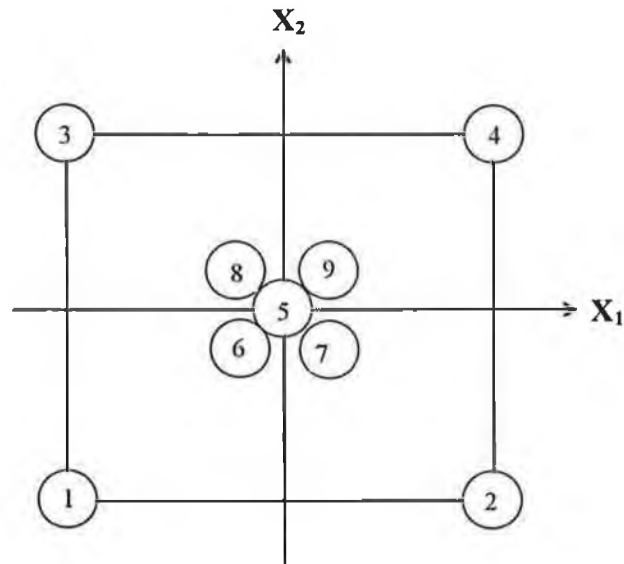


Figure 5.1. First-order orthogonal design for 2 factors

The values of the coded variables along with the actual values of the variables adopted for this analysis are presented in Table 5.2. The independent coded variables can be expressed in the following manner:

$$x_1 = \frac{(\ln p - \ln 66)}{(\ln 110 - \ln 66)} \dots\dots\dots(5.12)$$

and

$$x_2 = \frac{(\ln s - \ln 40)}{(\ln 160 - \ln 40)} \dots\dots\dots(5.13)$$

Five discs under each of the processing conditions were characterized. The analysis is based on the mean values of the measurable responses. The experimental data along with the test conditions are presented in the following Table 5.3.

Table 5.2. Levels of the independent variables with the coding

Variables	Levels		
	-1 (Low)	0 (Centre)	1 (High)
Coding			
Pressure (MPa)	40	66	110
Speed (mm/min)	10	40	160

The first-order model for the energy absorption capability, nominal voltage, clamp ratio, watt loss, fired diameter and density was developed using the least square method. The estimated parameters of the model were evaluated using equation (5.10)

Table 5.3. Experimental data on different input and output parameters

Trial No	Input variables				Responses					
	Stress MPa	Speed mm/min	Coding		Energy J.cm ⁻³	V _{nom} V.cm ⁻¹	Clamp ratio	Watt- loss w.cm ⁻³	Dia- meter (mm)	Den- sity g.cm ⁻³
			X ₁	X ₂						
1	40	10	-1	-1	438	2532	1.408	0.00233	13.968	5.528
2	110	10	1	-1	502	2490	1.352	0.00345	14.292	5.600
3	40	160	-1	1	419	2498	1.369	0.00259	13.974	5.556
4	110	160	1	1	418	2469	1.360	0.00379	14.338	5.612
5	66	40	0	0	451	2489	1.364	0.00294	14.090	5.584
6	66	40	0	0	472	2490	1.357	0.00292	14.110	5.575
7	66	40	0	0	460	2486	1.362	0.00301	14.078	5.581
8	66	40	0	0	436	2488	1.355	0.00287	14.081	5.577
9	66	40	0	0	425	2497	1.371	0.00304	14.120	5.589

Thus, the model for the six important electrical and physical parameters such as the energy absorption capability, nominal voltage (V_{nom}), clamp ratio, watt loss, fired

diameter and density can be developed in terms of the compacting stress and speed by substituting the model parameters as:

$$\hat{y}(\text{energy}) = 6.13877 + 0.033498 x_1 - 0.056867 x_2 \dots\dots\dots(5.14)$$

$$\hat{y}(V_{nom}) = 7.8213 - 0.0071 x_1 - 0.0055 x_2 \dots\dots\dots(5.15)$$

$$\hat{y}(\text{clamp ratio}) = 0.31215 - 0.011795 x_1 - 0.005547 x_2 \dots\dots\dots(5.16)$$

$$\hat{y}(\text{watt loss}) = -5.82038 + 0.193304 x_1 + 0.049945 x_2 \dots\dots\dots(5.17)$$

$$\hat{y}(\text{diameter}) = 2.64707 + 0.012161 x_1 + 0.000911 x_2 \dots\dots\dots(5.18)$$

and

$$\hat{y}(\text{density}) = 1.71882 + 0.00572 x_1 + 0.001798 x_2 \dots\dots\dots(5.19)$$

The above equations are transformed by replacing the values of x_1 and x_2 from the equations (5.12) and (5.13) in the form of general functions containing the independent pressing variables as

$$\text{Energy} = 409.668p^{0.06558}s^{-0.04102} \dots\dots\dots(5.20)$$

$$V_{nom} = 2681.6p^{-0.01390}s^{-0.00397} \dots\dots\dots(5.21)$$

$$\text{Clamp ratio} = 1.52778p^{-0.02313}s^{-0.00399} \dots\dots\dots(5.22)$$

$$\text{Watt-loss} = 0.00050306p^{0.37907}s^{0.03601} \dots\dots\dots(5.23)$$

$$\text{Diameter} = 12.7398p^{0.02385}s^{0.00066} \dots\dots\dots(5.24)$$

$$\text{Density} = 5.2965p^{0.01122}s^{0.00130} \dots\dots\dots(5.25)$$

The sign of the exponents on the independent variables of the above equations indicates whether the effect leads to the increase or decrease of the response. The magnitude of exponent is indicative of the significance of influence on the resultant parameters. The above models are valid within the limits of experimental conditions.

The energy absorption capability is considered to be a very important parameter for a varistor. The influence of the compaction parameters on this parameter is evident from equation (5.20). In Figure 5.2 the constant energy lines are shown.

Higher pressure enhances the energy while a higher speed has a deteriorating effect. But the extent of enhancement in energy is not very great. However, within the experimental limits it is apparent that higher compacting pressure is necessary for the sake of improvement in energy absorption capability.

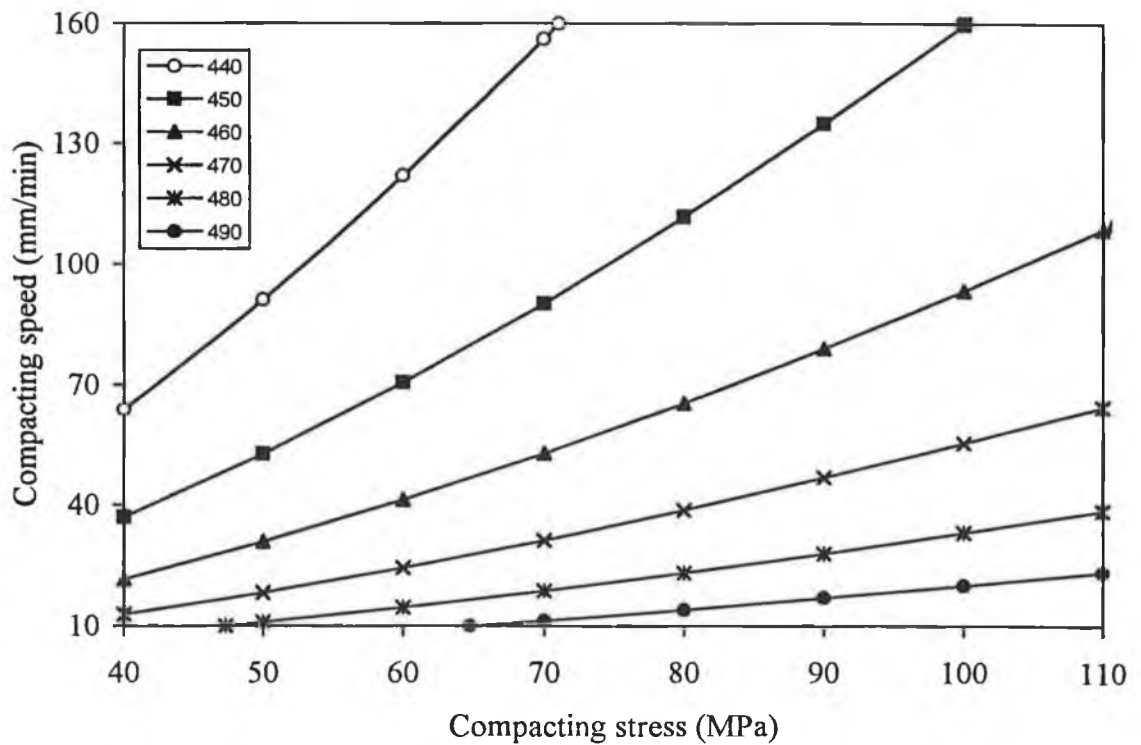


Figure 5.2. Constant energy absorption lines developed from the model

The nominal voltage is reduced with the increase in both the pressure and the speed and the constant nominal voltage lines are shown in Figure 5.3.

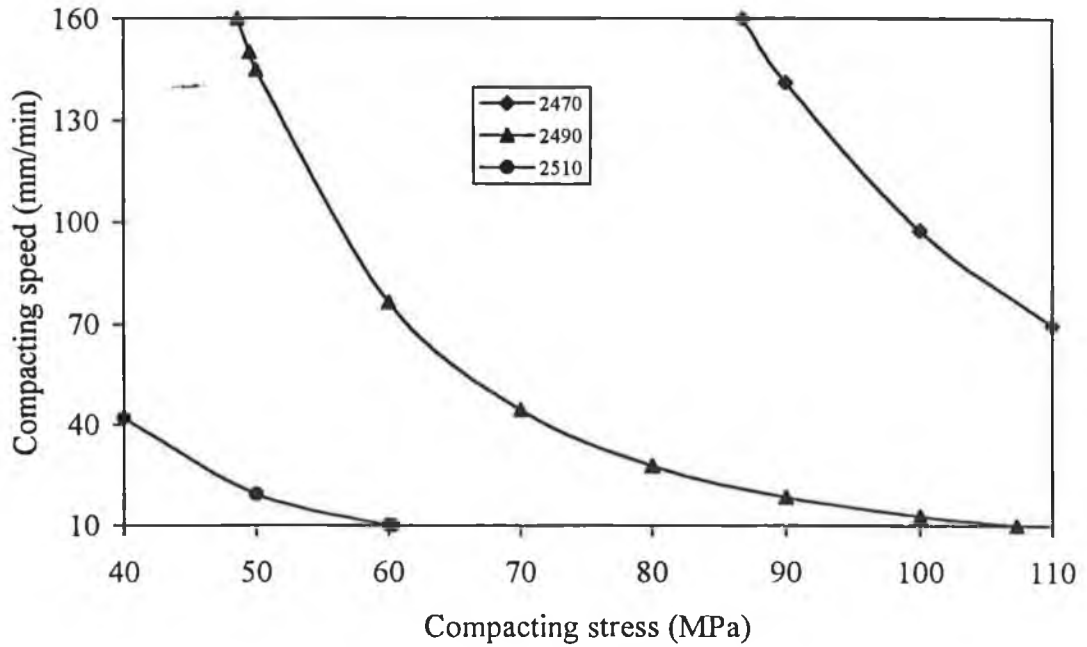


Figure 5.3 Constant nominal voltage lines as function of compacting parameters

The varistor with a lower clamp ratio and a lower watt loss is functionally a better device. As shown in Figures 5.4 and 5.5 the effect of the pressure and speed on these two parameters are opposite.

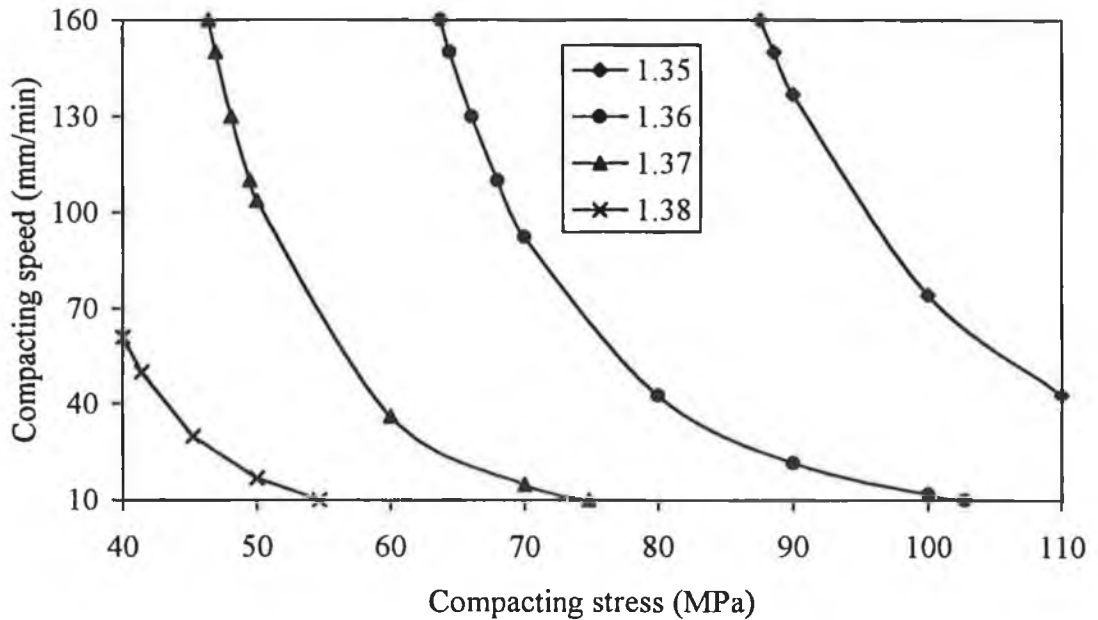


Figure 5.4 Contour lines for clamp ratio as function of compacting parameters

Increased values of pressure and speed lead to reduced clamp ratio but raise the watt loss. So the advantage obtained in the clamp ratio cannot be entirely exploited

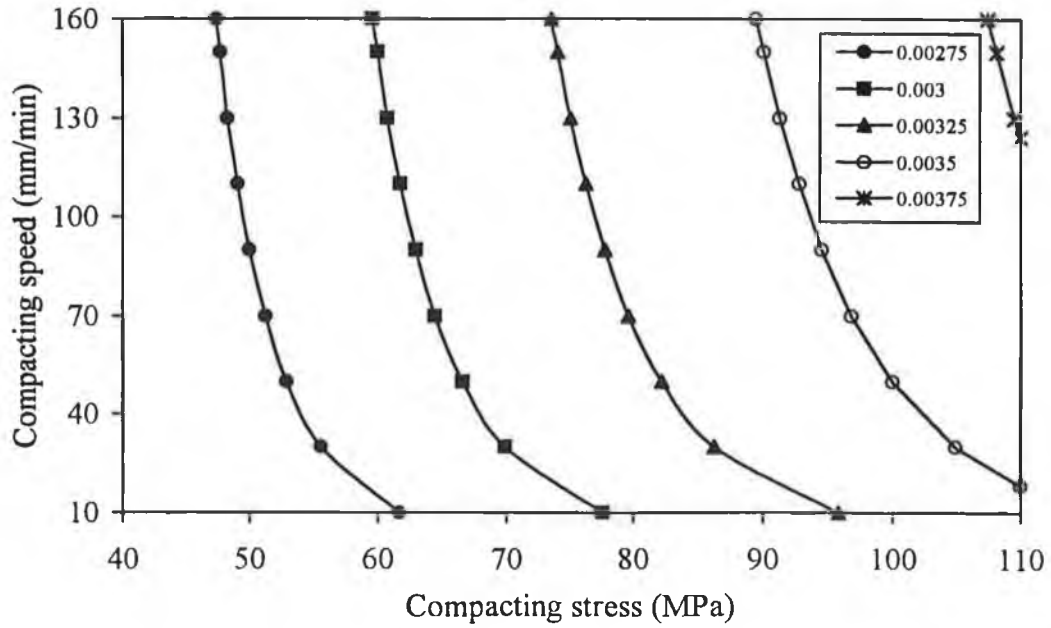


Figure 5.5 Constant watt loss as function of compacting parameters

due to the increase in watt loss. In both the cases the influence of pressure is higher than that of the speed. Physical parameters are demonstrated in Figure 5.6 and 5.7.

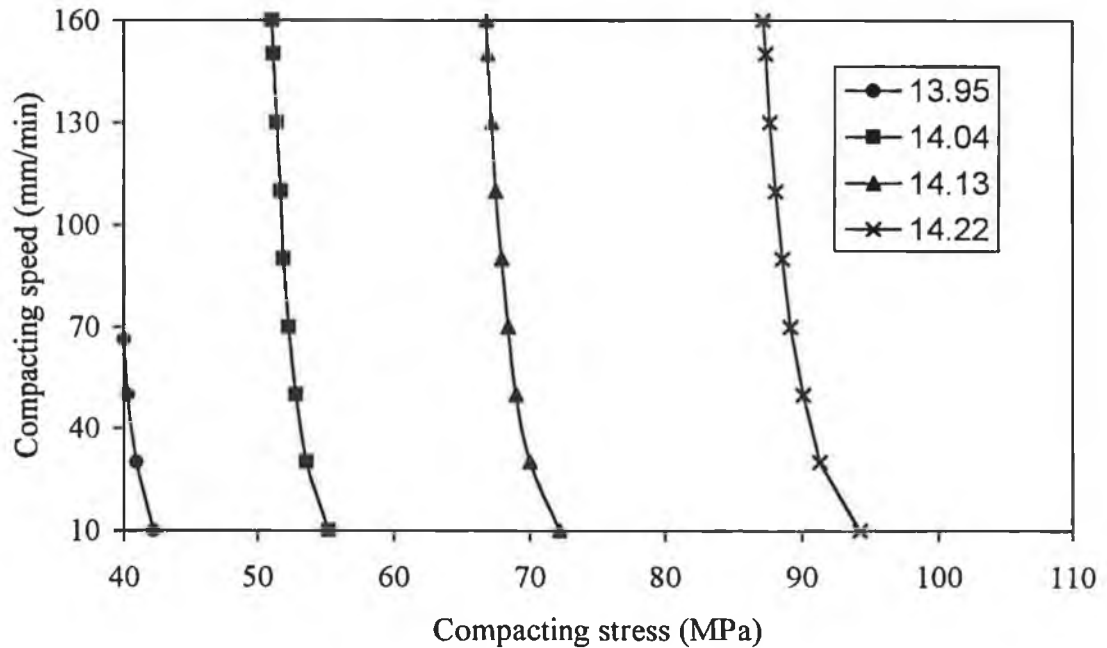


Figure 5.6 Contour lines for the fired diameter as compacting parameters

Fired diameter is highly influenced by the compacting pressure, independent of compacting speed. The stress is undoubtedly dominate the fired density but there is some influence compacting speed.

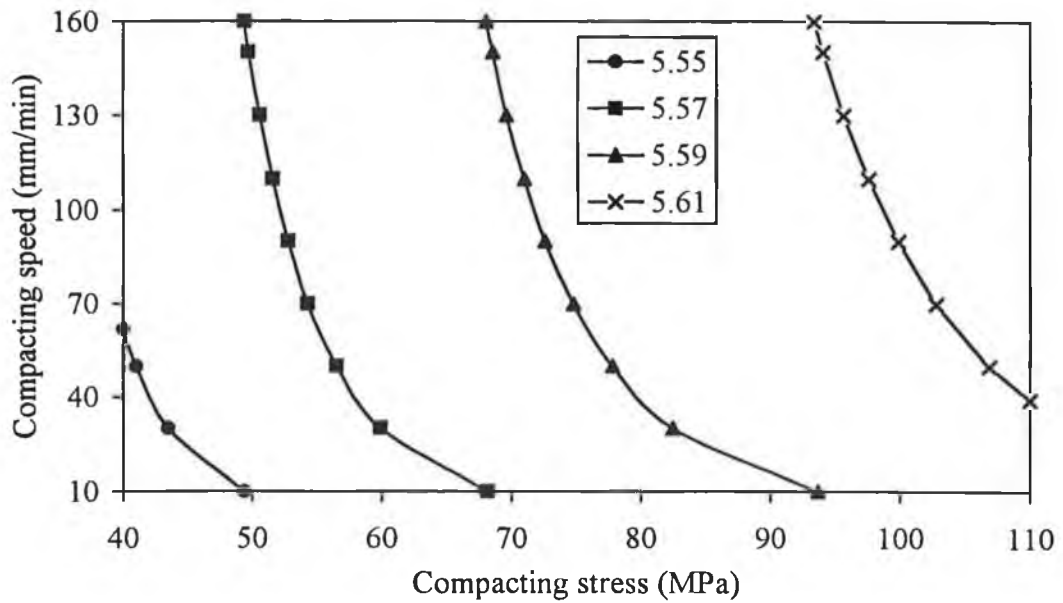


Figure 5.7 Contour lines for fired density as function of compacting stress and speed

Adequacy of the predictive model

The adequacy of the model can be verified by the analysis of variance. Such an analysis for the energy absorption capability is presented in Table 5.4. The calculated F value for the lack of fit and pure error is 2.96 and the tabulated value for 5% significance level with degrees of freedom 2 and 4 is 6.94. Since the calculated F value is lower than the tabulated one, the model appears to be adequate.

Table 5.4. Analysis of variance for energy absorption capability model

Source	Sums Square	DF	Mean Square	F _{cal}	F _{tab}	Remarks
Zero-order terms	334.9336239	1	334.93362390			
First-order terms	0.0174237	2	0.00871185			
Lack of fit	0.0051526	2	0.00257630	1.477	6.94	adequate
Pure error	0.0069756	4	0.00174390			
Total	334.9631758	9				

Similar calculations for other output parameters also suggest that the model developed is adequate. The calculated F values for the nominal voltage, watt loss and fired density are 4.39, 0.179 and 2.94 respectively. Each of them is less than the tabulated F value of 6.94 indicating the adequacy of the model. However for clamp ratio and fired diameter the calculated F values are respectively 9.68 and 7.52. They are adequate at 99 percent confidence interval as the tabulated value is 18.00.

Considerable influence of the compacting pressure and speed are observed on the physical and electrical characteristics of varistor. But unfortunately the effects are not favourable for all the critical parameters. Out of the two input variables the pressure is a more dominant factor than the speed. Marginally better clamping efficiency is achievable by increasing the pressure as well as the speed. However, this condition will lead to the undesirable increase in the watt loss. A trend of higher energy absorption capability is observed with the increase in the compacting pressure. According to the first-order linear model a higher speed has a negative effect on energy. At a lower level of pressure the reduction in the nominal voltage is more prominent than for higher levels of pressure.

Chapter 6

SINTERING CONFIGURATION AND THE PROPERTIES OF ARRESTER DISCS

6.1 INTRODUCTION

The sintering process of the zinc oxide arrester blocks or discs is commonly carried out in the electric kilns with controlled temperature profile. Like all other ceramic products, this operation requires the green compact bodies of varistor to be placed upon some sort of supports or saggars. To prevent the contamination from the direct contact of the repeatedly used sagger material the discs are kept physically separated from them by a liner material either in the form of a fine powder or a solid plate. The liner material needs also to be changed after a few cycles of use as it becomes contaminated due to the exposure of high temperature reaction. But even with this practice the adverse effects arising from the contact face of the disc cannot be eliminated completely.

Processing of the ZnO arrester discs is frequently encountered with the undesirable results at the bottom face specially in the case of grinding operation. It is a common practice to remove more material from this face by grinding. Investigation of the poor grinding performance revealed a number of features concerning the face remaining in contact with the liner material. Extensive measurement of the hardness enabled a correlation of the grinding performance with the value of microhardness.

A follow up study on the role of the bottom face of the arrester discs in the electrical testing exposed the fact that even after the removal of more material by grinding the bottom face was not functionally as good as the top face. The frequency of failure originated from the bottom zone is substantially higher. The measured mechanical strength, the density gradient and the microstructural analysis have confirmed the inherent weakness of the bottom face.

6.1.1 SINTERING CONFIGURATION

As already mentioned the zinc oxide varistor discs are conventionally sintered in a vertical position resting on a liner material in the form of ZnO powder or ceramic flat plate as shown in Figure 6.1. It is known that a varistor disc undergoes a process of

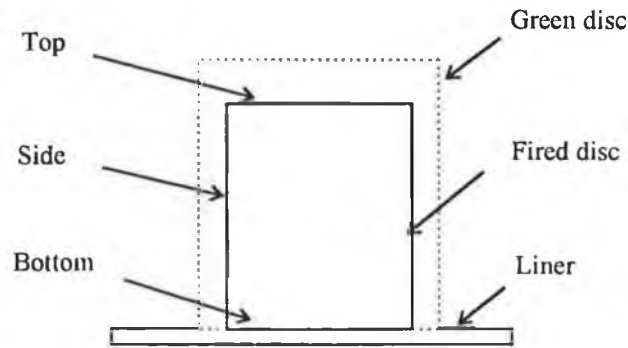


Figure 6.1 Sintering orientation of arrester block

considerable shrinkage during sintering. However, due to the density gradient in the green compact the fired diameter at the middle height of the disc is found to be the lowest. Apart from the scope of contamination, the bottom part of the disc passes a phase of sliding against the supporting liner material during shrinking. The frictional effects due to sliding with the liner material cause the diameter at the bottom face to become greater than that at the top.

6.2 MICROHARDNESS AND GRINDABILITY

The processing of sintered ZnO arrester discs requires grinding on their flat faces to achieve primarily the appropriate surface finish to be favourable for proper adhesion of the electrode and perfect parallelism of faces with good edge quality within acceptable dimension. But there is a perceived unpredictability in the way that a lot will behave during this operation. Rate of chipping, edge flaking etc. differ from lot to lot and even disc to disc belonging to the same lot. This problem is mostly encountered with the bottom face which remain in contact with the liner material during sintering.

Poor grinding performance often necessitates regrinding of more than 50 percent of the lot with eventual rejection levels of 10-15 percent. This high level of rework and rejection led to a study on the phenomenon by measuring the microhardness of varistor discs at different locations of their surface and correlating them with the grinding performance. Samples from lots yielding good as well as bad edge quality have been studied. Discs belonging to the bad lot were found to be significantly harder on the bottom face.

The primary cause of contamination of the bottom face leading to the higher hardness could be the effect of interaction of a number of sintering and material parameters. But it is understood that the increased hardness and brittleness of the bottom part primarily owing to the sintering orientation of the disc and the form of the liner material on which it is placed lead to the poor edge quality following grinding operation. Sintering of ZnO varistor disc is performed by a temperature profile with a peak of 1100-1200 °C. This is followed by a number of finishing operations such as grinding, passivating and electroding.

6.2.1 NEED FOR GRINDING OPERATION

Grinding or lapping operation is very important in the fabrication process of ZnO varistor blocks and the necessity of this operation is felt for a number of purposes. There is a natural variation in the height of the sintered disc due to the uncontrolled deviation in the amount of powder filled in the die during compaction. Maintenance of perfect parallelism of faces is essential in preventing excessive current flow through any preferential zone leading to an uneven stressing of the disc. In addition the surface of faces are found to be defective, especially the bottom one due to the high temperature reaction of material during sintering and the shrinking phenomenon of the ceramic. So the grinding or lapping operation is performed with the following objectives:

- (i) to achieve the required dimensional accuracy within tolerance limits,
- (ii) to generate parallel faces of the varistor discs with good edge quality,

- (iii) to remove the contaminated surface as skin effect and also
- (iv) to provide proper surface roughness for adequate adhesion of electrode.

Factors Influencing the grinding operation

The grinding or lapping operation is not dependent solely on the property of the workpiece material. Rather the performance quality, in general, is the interactive effect of a number of variables emerged from three distinct sources - grinding wheel, grinding machine and the workpiece. Chatter is particularly critical in grinding as it adversely affects the surface finish and the wheel performance⁴⁸. However, for the zinc oxide arrester blocks grindability can be described as a result of interaction of

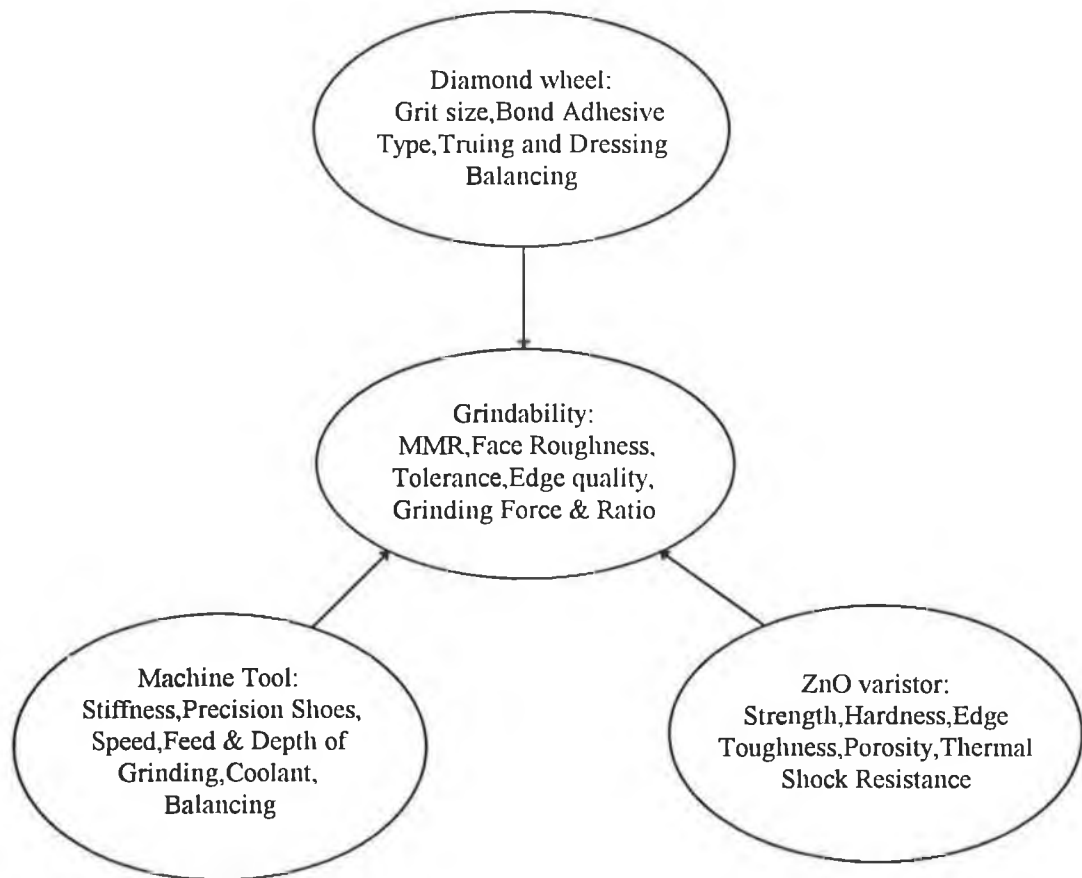


Figure 6.2 Factors affecting grindability of ZnO varistor disc

a number of factors such as the material removal rate (MRR), power or grinding force required, face roughness, dimensional tolerance, edge quality and grinding ratio etc. This feature is schematically presented in Figure 6.2, adapted from reference⁹⁹. The uneven grain in the face of the wheel is likely to impart impact loading which could cause 'chipping' or 'flaking' of the edges. The ability of a material to resist the edge damage has been termed as 'edge toughness'. This parameter defined by McCormick and Almond¹⁰⁰ as a function of load applied on the indenter and the distance from the edge is expected to provide a picture of the integrity of the material at the edges or corner.

In this study the same grinding machine and the diamond wheel had been used for the grinding of varistor discs at the same operating conditions. So the considerable variation in grindability was obviously assumed to be originating from the varistor material. Consequently effort was made to investigate the variation of the mechanical properties of the ceramic. In this context the hardness of the arrester disc was the primary factor and, therefore, was extensively measured by the Vicker's hardness method for possible correlation.

Vickers Hardness Method

There are various techniques to measure the hardness of a material using different indenter material and geometry. Though it has been found that the hardness, usually defined as the resistance to indentation, depends on the shape of the indenter and the load applied, this measurement is widely accepted as one of the common tests for assessing the mechanical properties of materials.

The Vickers hardness test, also known as the diamond pyramid hardness test, uses a pyramid shaped diamond indenter. The indenter has a square base and the angle between the opposite faces of the pyramid is 136° . This results in the depth of penetration, h , being one-seventh of the indentation size, d , measured on the diagonal. The Vickers hardness number (H_V) is obtained by dividing the applied force

P with the surface area of the pyramidal depression. This yields to the following general formula:

$$H_v = \frac{2P}{d^2} \sin \frac{\theta}{2} \dots\dots\dots(6.1)$$

where d is in mm and P in Kg. A wide range of standard forces usually between 1 and 120 Kg are used. However, a load range of 5 gm to 2000 gm is suggested for measuring microhardness⁴⁸. But irrespective of the load range, this technique is considered to be suitable for testing materials with a wide range of hardness including very hard steels and ceramics.

Measurement Procedure

The Micro Hardness Tester¹⁰¹ (Leitz Miniload 2) used to study the hardness was capable of measuring the Vickers, Knoop and Scratch hardness with an accuracy level of $\pm 0.2 \mu\text{m}$ to measure the indentation diagonal. The test was initially conducted to identify the distribution of hardness at different locations of the varistor disc with the intention of correlating them with the grinding performance. The positions of indentation selected primarily were the faces and side of the discs. On circular faces indentation was made radially from centre to near of the periphery while along the side this was started from near of the bottom to a height close to the top. The line of measurement was selected randomly.

Sample preparation

Initial experiment was conducted with four sets of arrester discs having five in each, selected from a lot yielding unsatisfactory edge quality following grinding operation. Discs belonging to the four sets (A, B, C, and D), though taken from the same lot, differed in terms of subsequent cutting and passivating operation. Discs belonging to the group E and F were later taken from a lot yielding good edge quality with a view to comparing them with those from the bad lot.

Moreover, the initial observation of declining trend of hardness with depth of grinding was verified by measuring the hardness of these discs. Out of ten glass coated arrester discs five belonging to the group E were ground off by 1, 2, 3, 4, 5 mm respectively from their original top face while the discs from group F were similarly cut from the bottom face. The identification of the samples with salient features in preparation is summarized in Table 6.1.

Table 6.1 General information on the samples prepared for measuring hardness

Disc ID	Sample size	Nominal dia. (mm)	Height (mm)	Glassed or unglassed	Face ground (mm)	Liner material used
A	5	32	34	Glassed	0	powder
B	5	32	32	Glassed	1	powder
C	5	32	32	Unglassed	1	powder
D	5	32	27	Glassed	3.5	powder
E	5	42	38-43	Glassed	1-5	flat plate
F	5	42	38-43	Glassed	1-5	flat plate

Location of indentation

Hardness was measured by the indentation made on the face and the side of the arrester discs. The number of indentation made on each face was the same for all the discs. Six hardness values were calculated for each face starting from the centre to

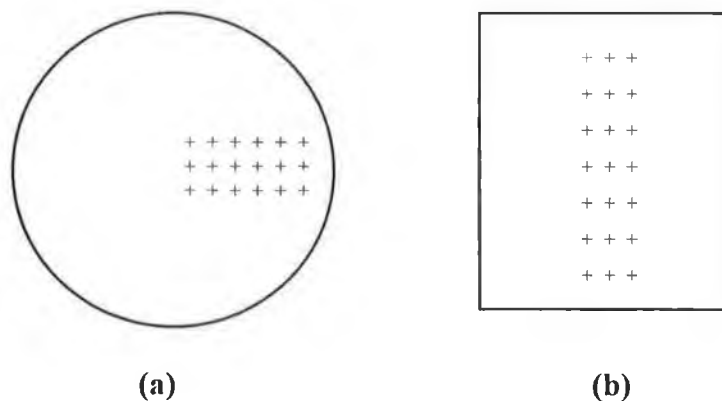


Figure 6.3 Location of indentation (a) face (b) side

near of the periphery at equal interval. But for each measurement there were three indentations - one was along a radial line while the other two were across the point by 300 μm away as shown in Figure 6.3. So there were eighteen indentations on each face and hardness at a particular radial distance was actually an average of the three indentations. This approach was adopted to avoid the localized influence of the material characteristics. Hardness along the side was measured for the uncoated disc i.e for the 'C' type discs with similar manner, making altogether twenty-one indentations.

Measurement of Hardness

Since the instrument had been equipped with load designated in gram and the diagonal of the indentation measured in μm, the Vickers hardness number (H_v) was calculated from the following formula:

$$H_v = 18.544 \frac{P}{d^2} \dots\dots\dots(6.2)$$

where the multiplying factor was worked out to keep the unit in GPa for the specific angle of opposite pyramidal faces of the indenter, $\theta = 136^\circ$.

It is commonly recommended that hardness tests should be carried out with the highest possible test forces tolerated by the sample to be investigated. This is due to the fact that with hardness tests involving high forces the error occurring with the results is at its smallest. So the test force of 500 gm, the maximum load available with the equipment was used.

The H_v number was calculated for each indentation using the equation (6.2) taking the load $P = 500$ gm and the mean of the two diagonals 'd' in μm. Moreover, since there is an effect of the period of descent and dwelling of the load on the results, the same duration was maintained for making all the indentations.

6.2.2 RESULTS

The hardness results on different faces are presented by the mean values. To show the dispersion in the hardness the standard deviation has been used. Thus the distribution of hardness on the two faces and the side of the discs for the bad quality lot is presented in Figure 6.4. It is evident that the bottom face is clearly harder than

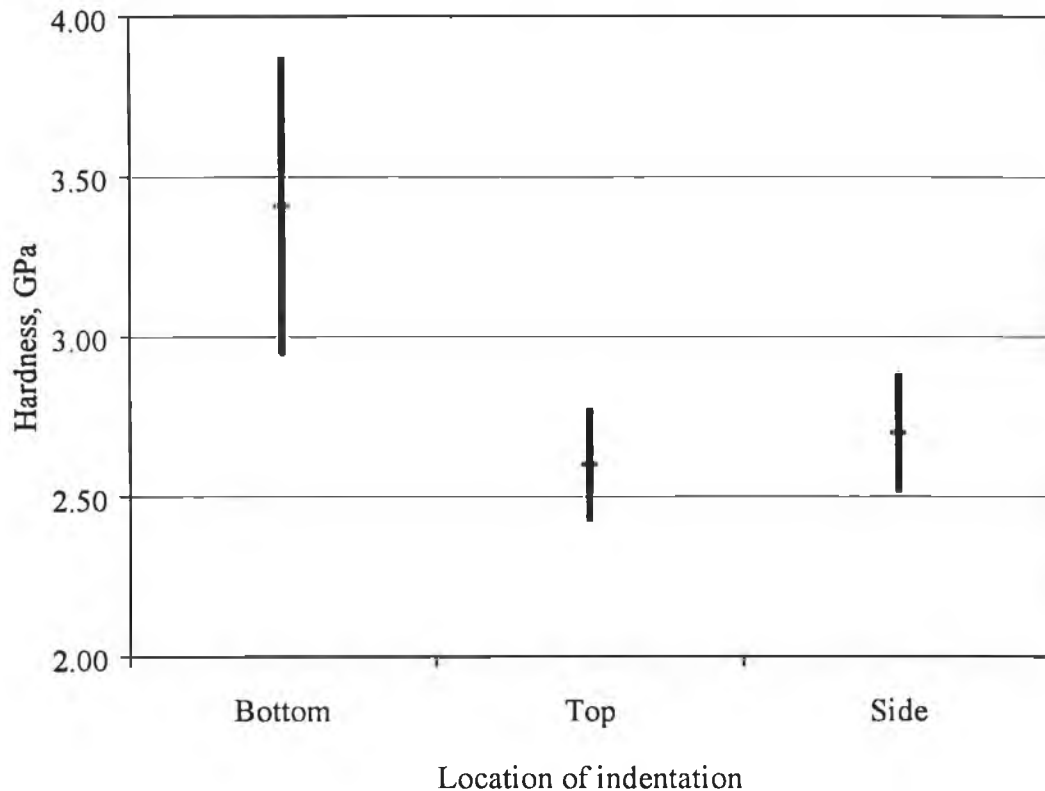


Figure 6.4. Hardness on bottom, top and side of arrester disc (bad lot)

the top and the side. The plot is based on the data measured on the top and bottom face for disc category 'A' and on the side for 'C'. The plot for the hardness for each of the surfaces is based on a large number of indentations - 90 for both the top and bottom faces and 105 data points for the side. The dispersion in general is quite large, however, in the bottom this is the maximum as evident from the error bar represented by the standard deviation. Average hardness at different radial locations is shown in Figure 6.5. In all the radial locations hardness observed in the bottom face was found to be higher than what was found on the top face.

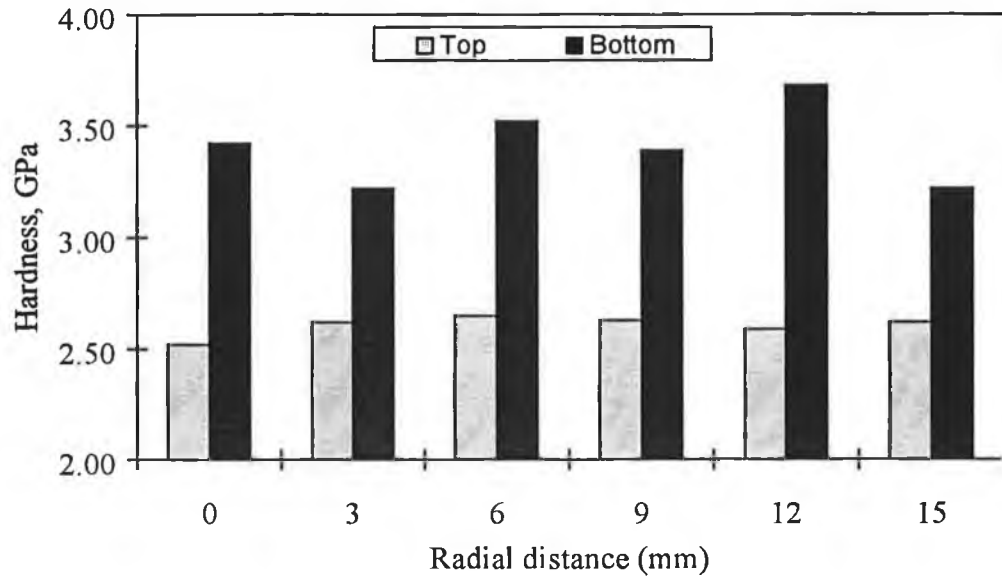


Figure 6.5 Mean hardness on face at various radial locations of disc (bad lot)

It is apparent that there is no increasing or decreasing trend of hardness observed along the radial direction neither for the bottom nor for the top face. This reveals the fact that there is no clear correlation of hardness with the density gradient generated in the green body due to the frictional effects in uniaxial pressing. For the ease of comparison in Figure 6.6 the density gradient⁶⁴ generally observed in the green body due to uniaxial die compaction is shown.

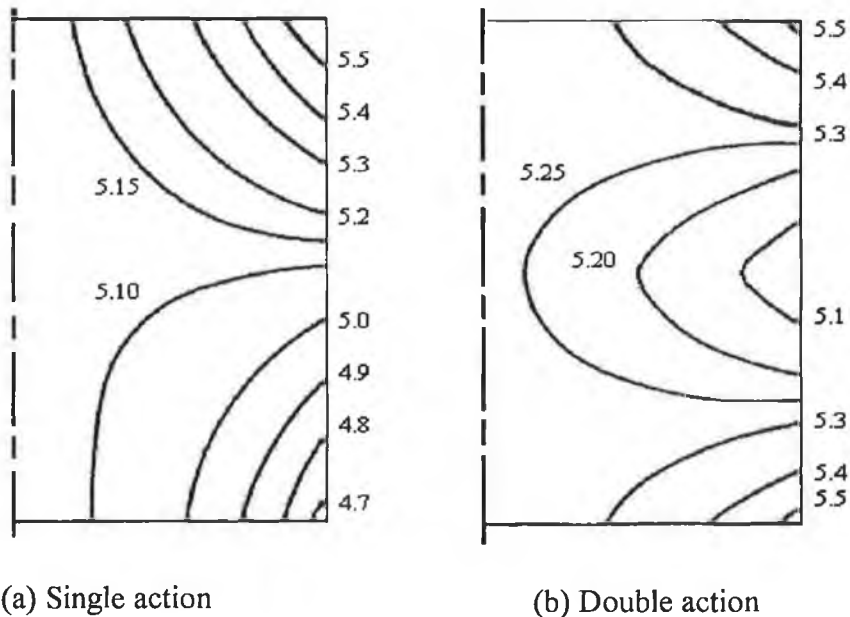


Figure 6.6 The density gradient in the green compact for copper powder

Hardness on the side (or C-face) along the height is presented in Figure 6.7. A very high value of hardness is observed on the side surface but near the bottom region which sharply decreases upto a near middle height and then increases gradually. Difficulty in grinding is encountered mainly with the bottom face. It can be inferred that higher hardness of the bottom is responsible as one of the causes for the poor

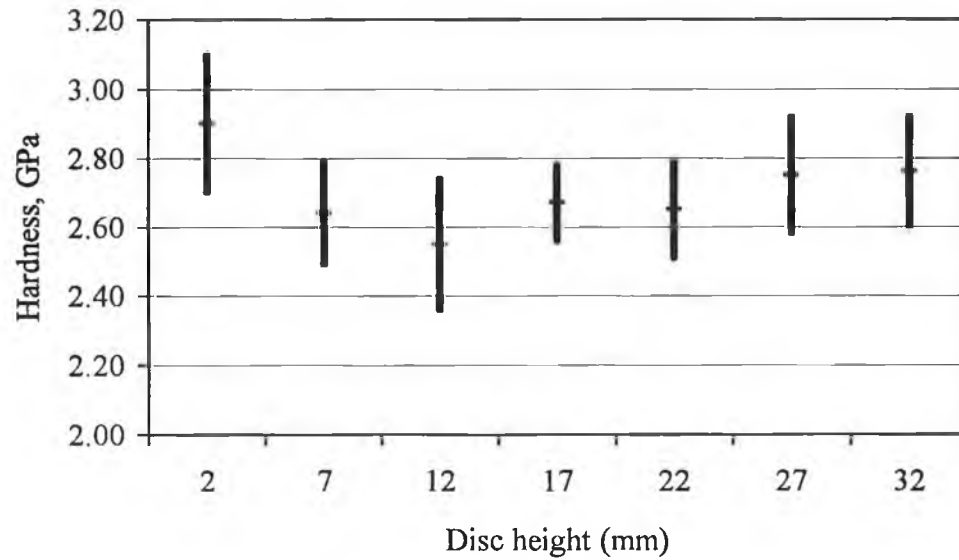


Figure 6.7 Variation of hardness along the vertical height of disc

performance in grinding operation. This can be further verified by the remarkably harder bottom face for the lot with unsatisfactory results as illustrated in Figure 6.8.

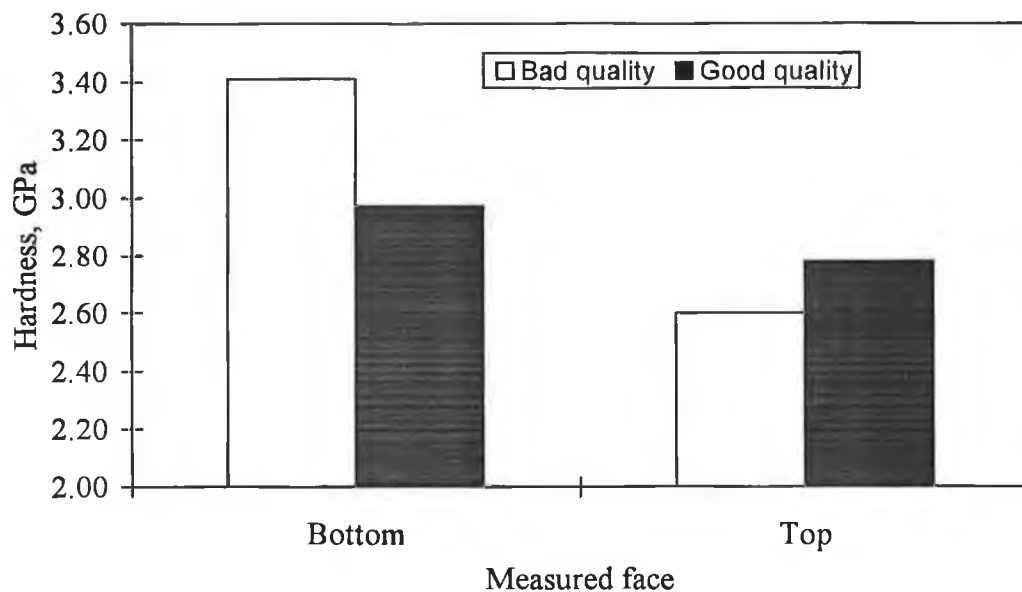


Figure 6.8 Comparison between the good and bad lot

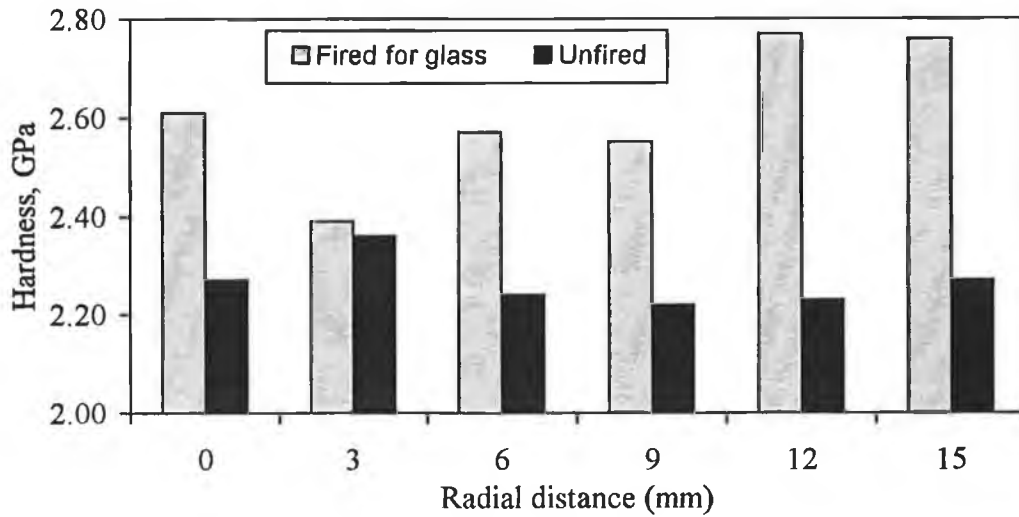


Figure 6.9. Effect of firing for glassing on the hardness

The effect of exposure of the discs to a high temperature for firing of glass is shown in Figure 6.9. This represents the data on the top face. Disc type 'B' differing from 'C' only in terms of glassing exhibits higher hardness. This is actually true for both the top and the bottom face and at all radial locations. The fact that the hardness decreases as the material is removed from the initial face is demonstrated in Figure 6.10. These data are based on the hardness on the disc category E and F. It appears that there is a skin effect. After removing one millimetre from the initial face hardness

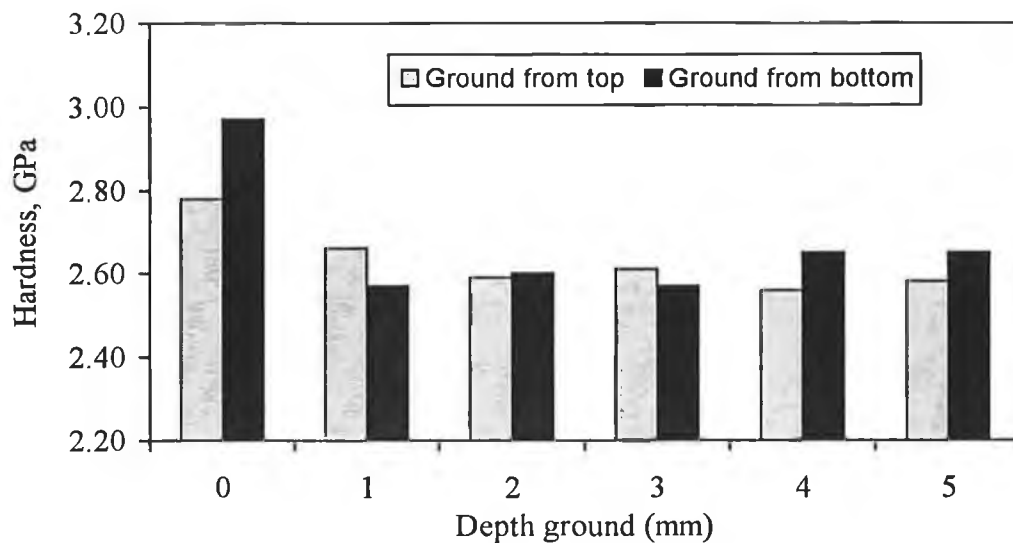


Figure 6.10. Variation of hardness with depth ground from the face

does not reduce further with depth ground. Similar trend in hardness is reported¹⁰² for a copper slider as an effect of work hardening. Hardness decreases exponentially with depth from initial surface up to a fraction of a millimetre. But the dispersion or scattering of hardness does not appear to change as delineated in Figure 6.11 as the

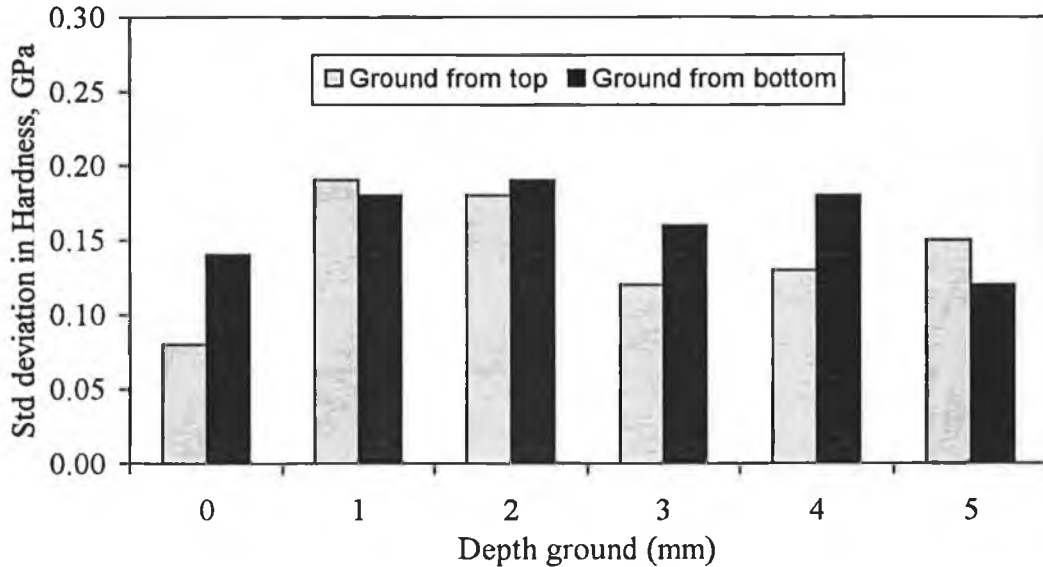


Figure 6.11. Standard deviation of hardness on faces with increasing depth

standard deviation of hardness at different faces generated with increasing depth of grinding. This implies that the degree of homogeneity of material property remains at the same level as we go deeper from the initial surface. This scattering in hardness is

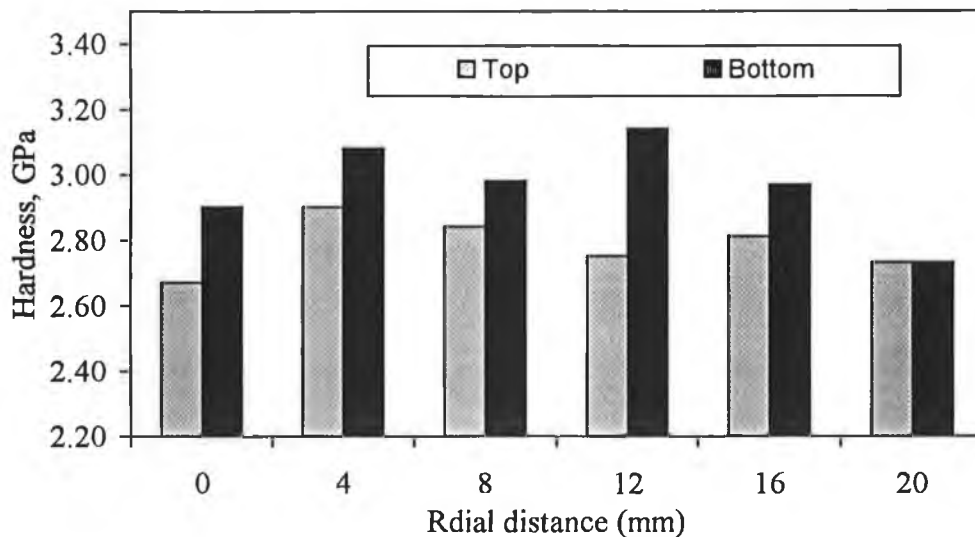


Figure 6.12. Variation of hardness on the unground top and bottom face (good lot)

not unusual for ZnO varistor material. Comparable deviations in hardness are observed for other materials. Hardness measured by nanoindentation technique on nanocrystalline ZnO shows a similar trend of deviation as reported by Mayo¹⁰³. As shown in Figure 6.12 the unground bottom face is found to be harder than the top face at all radial positions, though the extent is lower compared to the difference observed among the faces of the discs of the bad quality lot shown in Figure 6.5.

6.2.3 DISCUSSION

The measured hardness on the top and bottom face and on the side of the discs indicates that there is a considerable variation of hardness on different surfaces. Discs belonging to the lot of poor grinding performance have been found to be very hard at the bottom face. Though the same trend is observed for the discs of the good quality lot, the difference in hardness between the two faces is not as large as that were found in the case of the bad lot. Apart from the fact that the bottom face remains at a higher temperature for longer time during cooling due to the contact with the liner, the shrinking process makes the edge more brittle presumably because of the work hardening effect and less tough due to the presence of pores.

Faces with different depth of grinding from the initial face exhibited clearly a declining trend of hardness. However, the same level of scattering or dispersion in hardness values indicates an equal degree of homogeneity in property as we go deeper from the initial face. But compared to the pure metal or a particular ceramic material the observation of higher scattering in hardness for ZnO varistor is attributable, to a certain extent, to the presence of various additive materials.

Complete elimination of the causes of higher hardness leading to unsatisfactory edge quality may not be possible. However, the change of the sintering orientation of the discs as well as the use of other suitable liner material may have some positive effect and endeavour to improve the grinding condition could be beneficial. In this regard soft-grade wheels, frequent dressing of wheel, reduction in MMR, and a more rigid support of the discs could be advantageous.

6.3 SINTERING ORIENTATION AND TENSILE STRENGTH

The influence of sintering orientation on the mechanical strength of the arrester blocks was evaluated by the diametral compression test. Measurement was conducted on five arrester blocks having a nominal diameter of 32 mm and a height of 34 mm. They were sectioned perpendicular to the axis by a diamond cutter into three equal disc shaped pieces. Load was applied on the disc specimen by an Instron machine with a cross-head speed of 1 mm/min. The breaking load was recorded. Equation (4.8) was adopted to calculate the tensile strength of the specimens. In Figure 6.13 the tensile strength for the three sections is plotted.

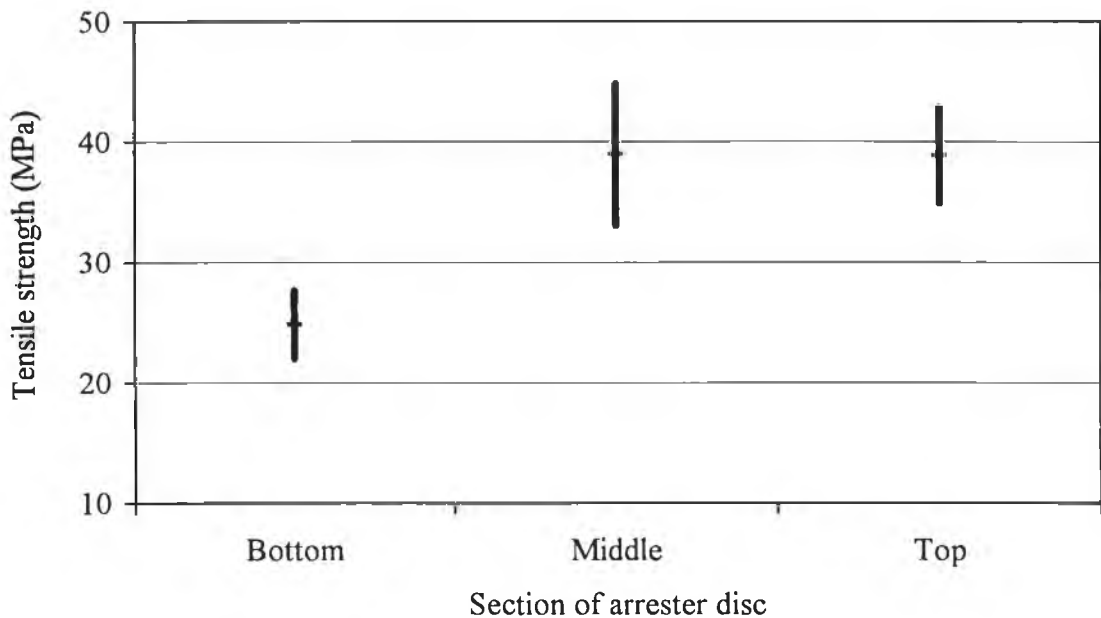


Figure 6.13 Variation in tensile strength due to sintering orientation

It is clear that the bottom section, one face of which remains in contact with the liner material during sintering is relatively weaker. The strength of this section is about 40 percent less than that observed in case of the middle or the top section. The top and the middle sections appear to have similar strength. It is clear that at least up to two-thirds of the height of the 34 mm tall disc is not affected by the contact with the liner material. Though it may not be possible from this investigation to quantify how far

the effect of contact reaches, it is definite that the bottom section is weaker. This lower mechanical strength of the bottom part of the disc can only be attributed to the influence of sintering orientation..

6.4 SINTERING ORIENTATION AND DENSITY GRADIENT

To further investigate the effect of the sintering orientation, the density gradient of a fired disc was evaluated. A central piece cut from an arrester block with a diameter of 42 mm and the same height has been sectioned as shown in Figure 6. 14.

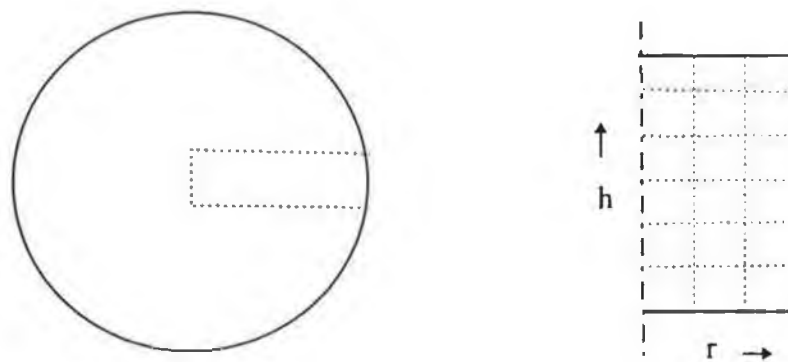


Figure 6.14 Sample preparation for measuring the density gradient

The small specimens taken from the eighteen grid points were measured for density. Each parallelepiped shape specimen was polished with the fine grinding paper to make the surface sufficiently smooth. They were then washed in deionized water using ultrasonic washing bath so that all the loose debris was removed from the specimens. They were then dried in an oven at 125 °C for more than one hour to expel completely the trapped water or moisture content from the open pores. Weighing was performed in a high precision laboratory type balance by adopting Archimedes' principle.

It should be mentioned here that the specimens were wrapped with water-tight masking tape to prevent water from being entered into the open pores during weighing. Care was taken so that there was no air bubble could be trapped inside the

wrapping. The density was evaluated by using the worked out value of the masking tape density, the immersed weight of the individual specimen, its weight in air and the ambient temperature which might affect the density of water. In Table 6.3 the density of the specimens are given according to the grid points in terms of radius and height.

Table 6.2 Density (gm/cc) of varistor material at different grid points

Radial grid(r)	Grid number along the height (h)					
	1	2	3	4	5	6
1	5.36	5.55	5.49	5.55	5.57	5.53
2	5.56	5.52	5.57	5.56	5.58	5.61
3	5.59	5.59	5.58	5.62	5.59	5.59

With the grid point densities the contour lines indicating the constant-density lines are drawn in Figure 6.15.

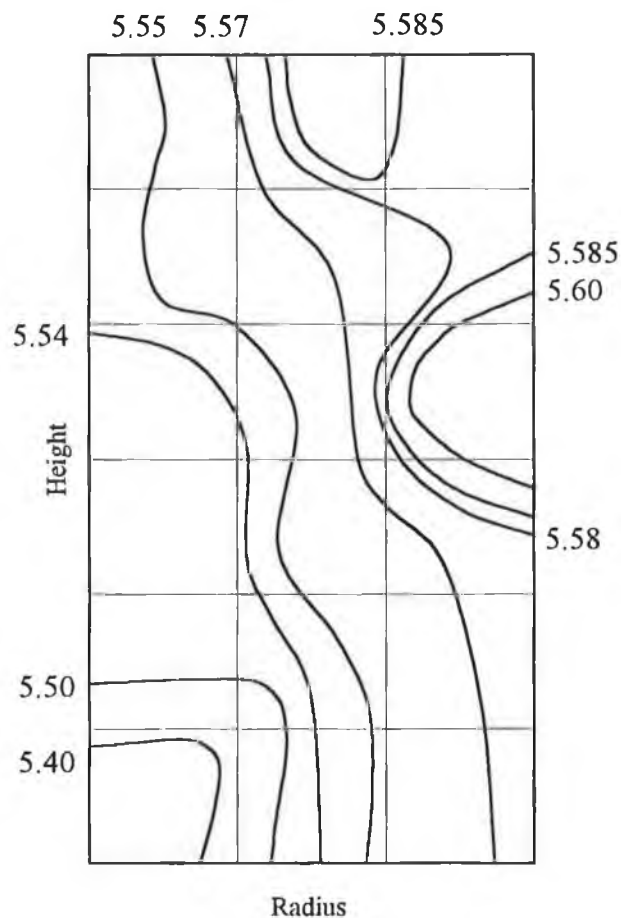


Figure 6.15 Density gradient as a function of sintering orientation

Comparison of the fired density gradients with the density gradients for a green compact shown in Figure 6.6 indicates that there is no evidence of correlation. ZnO varistor material undergoes a liquid phase sintering process. The capillary force developed during this kind of sintering within the ceramic body is very significant and plays a dominant role in densification¹⁰³. Due to the low green density at the middle height of the disc the diameter at that location comes out to be minimum after sintering.

6.5 MICROSTRUCTURAL ANALYSIS

The microstructures were taken for the specimens having a variation in fired density. Three specimens having the lowest, the highest and a medium density were selected. These were belonging to the grid points (1,1), (1,3) and (3,4) where the first and second co-ordinate numbers indicate respectively along the radial direction from the central axis and the height of the cylindrical disc. Density of the three specimens were respectively 5.36, 5.49 and 5.62 gm.cm⁻³. For each of the specimens both secondary

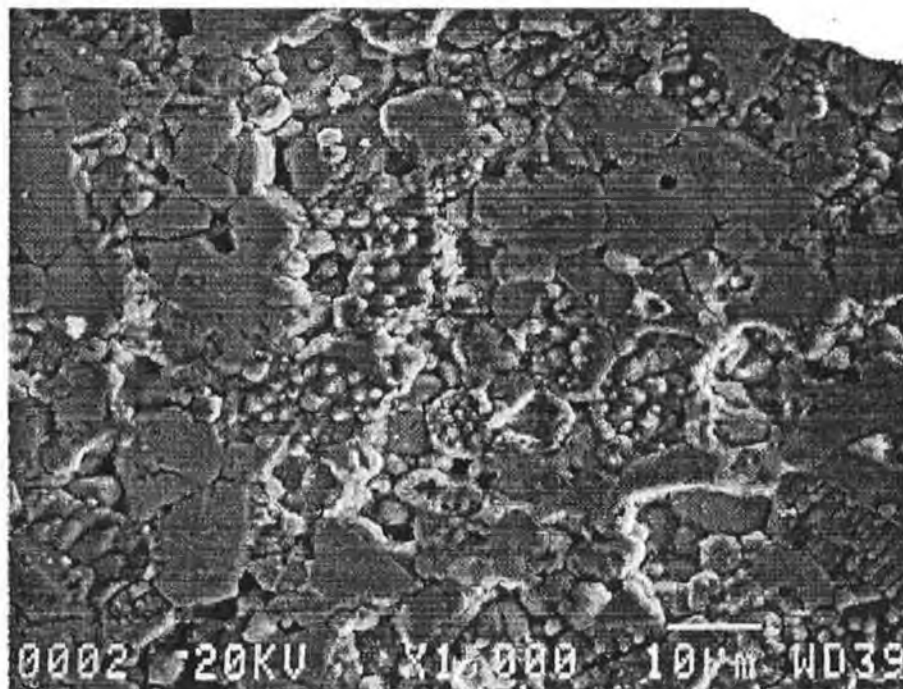


Figure 6.16 SEI for the low density specimen

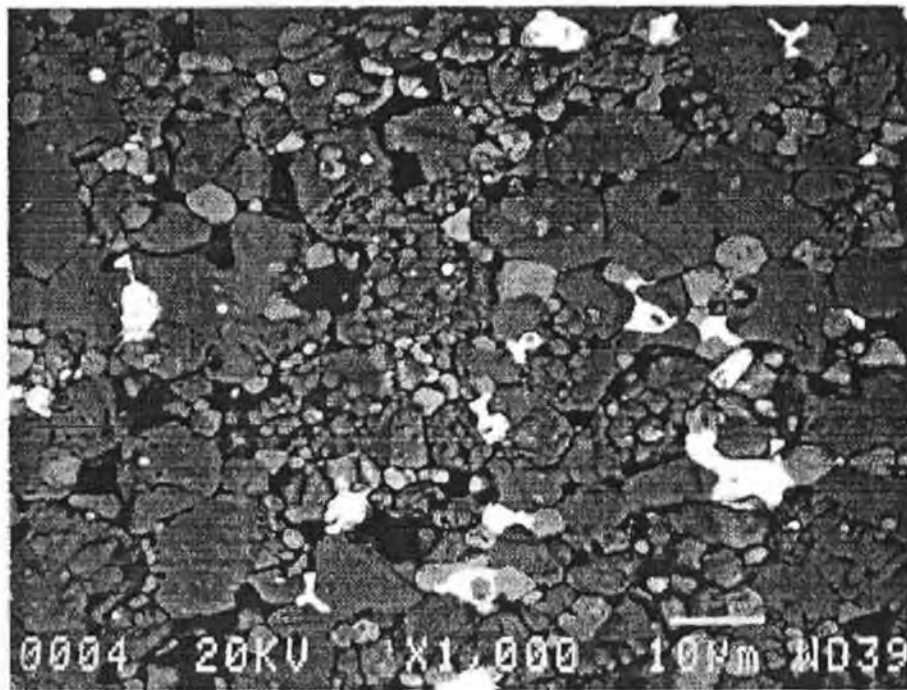


Figure 6.17 BSEI for the low density specimen

emission image (SEI) and the back-scattered emission image (BSEI) were taken. The micrographs are presented in Figures 6.16 to 6.21. Comparison of microstructures

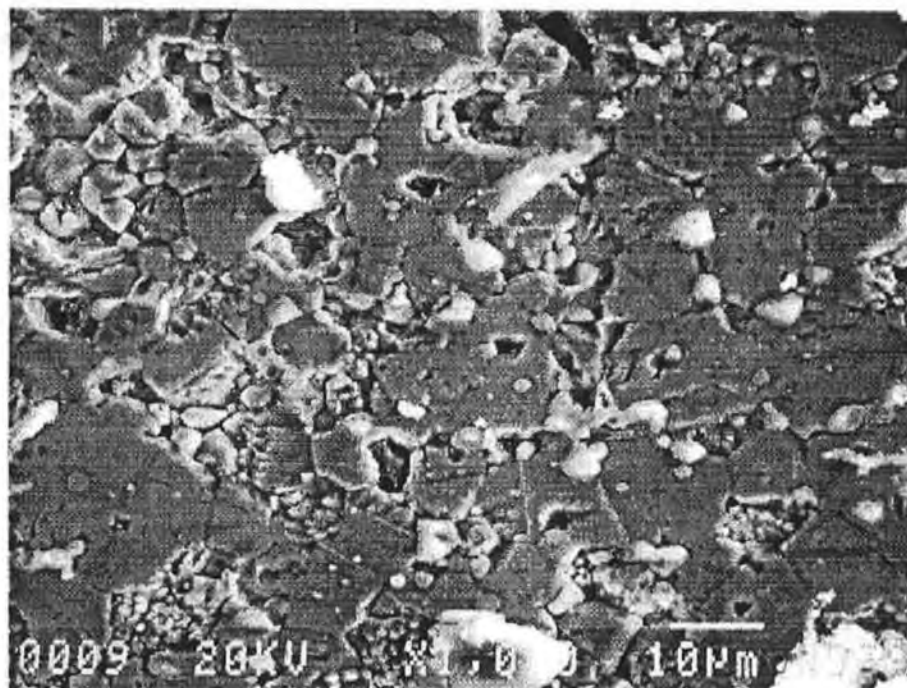


Figure 6.18 SEI for the medium density specimen

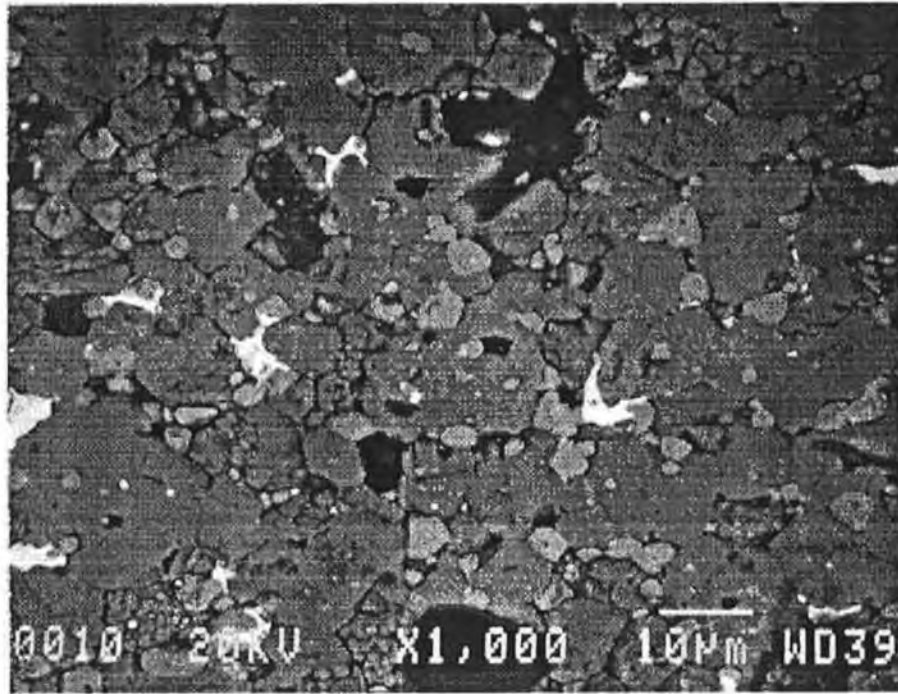


Figure 6.19 BSEI for the medium density specimen

reveal the differences in grain size and porosity among the three specimens prepared from the same disc. The difference in the grain size is not very significant as presented in Table 6.3.

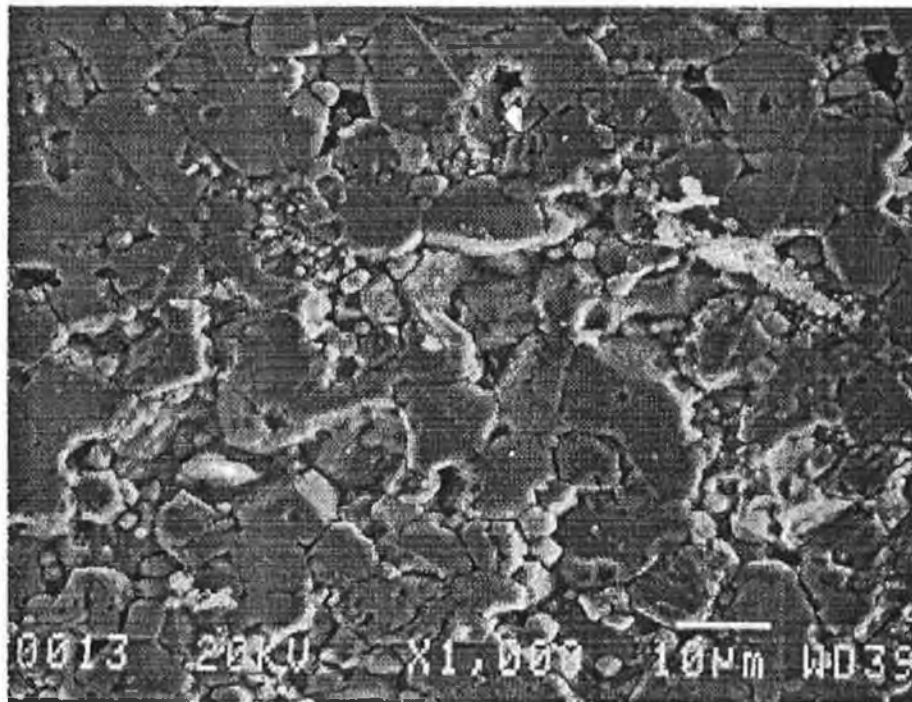


Figure 6.20 SEI for the high density specimen

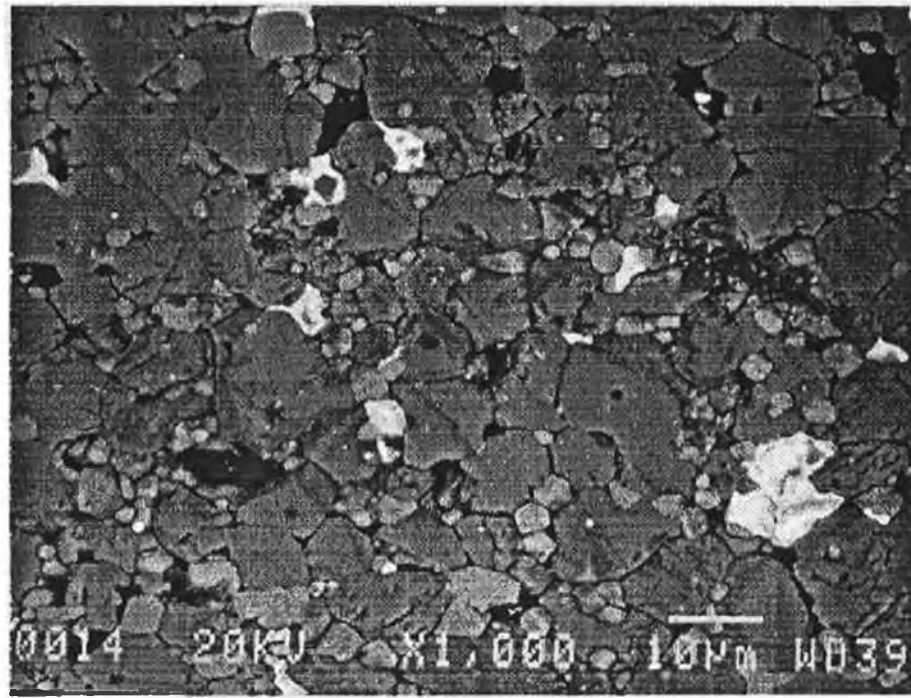


Figure 6.21 BSEI for the high density specimen

Table 6.3. Grain size of different specimens as located in a standard arrester

Parameters	Specimens having		
	Low density	Med density	High density
Av intercept	9.15µm	10.35µm	9.60µm
Av grain size	14.27µm	16.15µm	14.98µm
Std deviation	3.29µm	2.75µm	2.26µm

The specimen with the medium density was taken from the core of the disc. During sintering operation this region of the disc remains at higher temperature for a longer time. So it is quite likely that grain growth of this region will be more compared to the other regions of the disc.

It appears from the back scattered electron (BSE) images presented in Figures 6.17, 19 and 21 that the porosity levels also vary among the specimens. The specimen with the lowest density exhibits naturally the highest porosity while the specimen having the highest density shows lowest level of porosity. The porosity level for the specimen with the medium density looks to lie in between the two extreme levels.

Chapter 7

ALTERNATIVE SINTERING CONFIGURATION, DESIGN AND ANALYSIS OF FRACTURE

7.1 INTRODUCTION

It is clear from the observation presented in the previous chapter that the contact zone of a disc remaining in the vicinity of the liner material during the sintering process is more susceptible to failure. Even after deeper grinding most of the failures originate from this zone during the testing. But sintering a disc without keeping in contact with some form of support is practically impossible. However to minimize this undesirable effect, a number of alternative configurations have been attempted by changing the sintering orientation i.e. placing the disc on different kinds of support.

The investigation is mainly based on the effect on the energy absorption capability and high current performance. In some cases the influence on processing operation such as the performance in grinding was also studied. The analysis was performed by appropriate statistical indicator for the process capability to view the different methods in the context of their functional outcome. Compared to the control (processed under standard condition), some of the arrangements demonstrated a promising result.

Arrester blocks are electroded by covering the whole face or keeping a margin at the periphery. Both methods are industrially practiced to meet the specifications of different customers. The margin on electrode appears to be helpful in preventing current from flowing through the vulnerable peripheral zone and thus reduce the number of failures in a lot. But in this method there is an undesirable effect too. A margin on the electrode obviously reduces the current carrying area of a disc and consequently lowers the effective volume for absorbing the energy injected by a pulse. This method can, therefore, have an adverse effect on the energy absorption capability of a disc. So it is not straight forward to conclude about the total effect

from the two opposing factors. An experiment was undertaken to investigate the influence of margin incorporated in the electrode by making three categories of discs.

The geometry of a disc can play an important role on the performance. The failure mechanism is generally influenced by a number of factors. Apart from the basic material properties the heat transfer mechanism can be a critical factor for steady state operation. In this respect the geometry of a disc is very important. Commercial arrester blocks are available in cylindrical shape. An alternative design approach was attempted by providing a hexagonal shape to the arrester blocks.

The fracture mechanism of an arrester disc in short pulses with high amplitude of current is different from what is observed with long pulses in the energy test. Rupture or cracking is the main mode of this fracture. A theoretical study was conducted to correlate this fracture mechanism in the light of the theory on the propagation of stress wave. The fracture surfaces and the result of the experiment conducted by two different kinds of supporting metal block having different characteristic impedance were also found to be supportive of the theoretical predictions. Moreover, the speed of the longitudinal stress wave calculated on the basis of the elastic parameters of ZnO ceramic material was found to match closely with the measured celerity by a LASER assisted technique.

7.2 ALTERNATIVE SINTERING CONFIGURATION

This investigation includes (i) the scope of alternative sintering configuration (ii) the influence of the margin on electrode. The evaluation is based on the data (i) the influence on the frequency of regrinding (ii) the energy absorption capability, and (iii) the high current performance.

The objective of this study was to evaluate the feasibility of alternative liner support and sintering orientation of arrester blocks. The sintered discs were characterized to evaluate the effect of the new method. In addition, to enhance the process capability in terms of the performance the foreseeable advantages are (i) reducing the problem

arising from regrinding (ii) minimizing the level of bismuth contamination from the liner material due to contact (iii) increasing the scope of repetitive use of the liner material (iv) lowering the allowance of block height for grinding and (v) better geometry of the disc.

The experiment was completed in two phases. The first phase was performed with the objectives already mentioned above. The second phase was carried out as a follow up attempt with a more ambitious target of processing the arrester blocks skipping the grinding operation. To study this possibility two types of liner powder have been tried and their effects were analyzed and compared.

7.2.1 EXPERIMENTAL PROCEDURE

The orientation of a varistor disc in conventional sintering operation has already been shown in Figure 6.1. The modified arrangement for this experiment is presented in Figures 7.1. and 7.2. It should be mentioned here that for the horizontal sintering, the

The spinel is known to have an inhibiting effect on the grain growth and its selection was attributed to keep the dimensional elongation along the contact to a minimum.

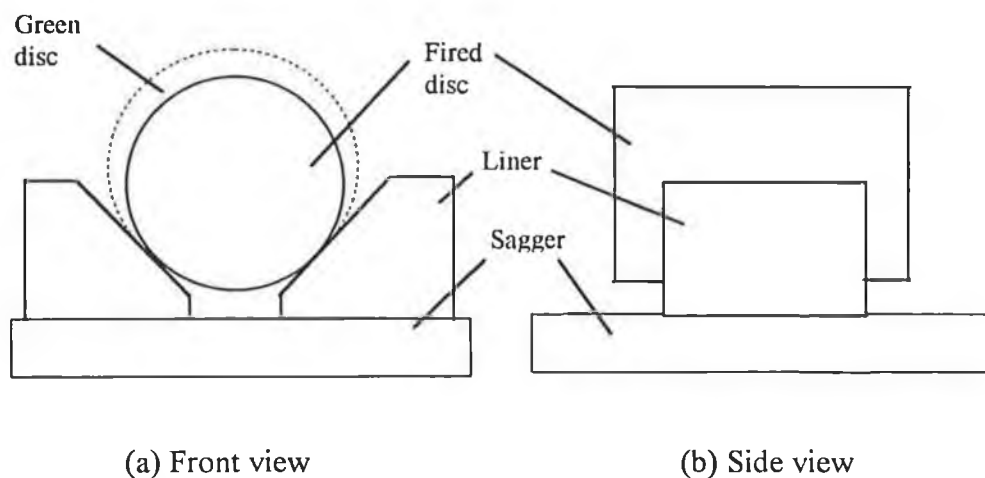


Figure 7.1 Simplified horizontal or Vee-groove sintering orientation

Vee-groove supports were made from the fired arrester discs. To prevent sticking of the discs during the sintering operation the supports were covered by spreading spinel powder. But the dry powder poured on the surface did not stick to it due to the inclination of the surface. To ensure proper adhesion of the dry liner power with the inclined surface, it was necessary to lightly wet the supports by spraying water.

These three orientations were selected for different purposes. The Vee-groove support can facilitate to keep the edges free from any physical contact during the sintering process. Thus improved faces with uniform edges were possible to achieve.

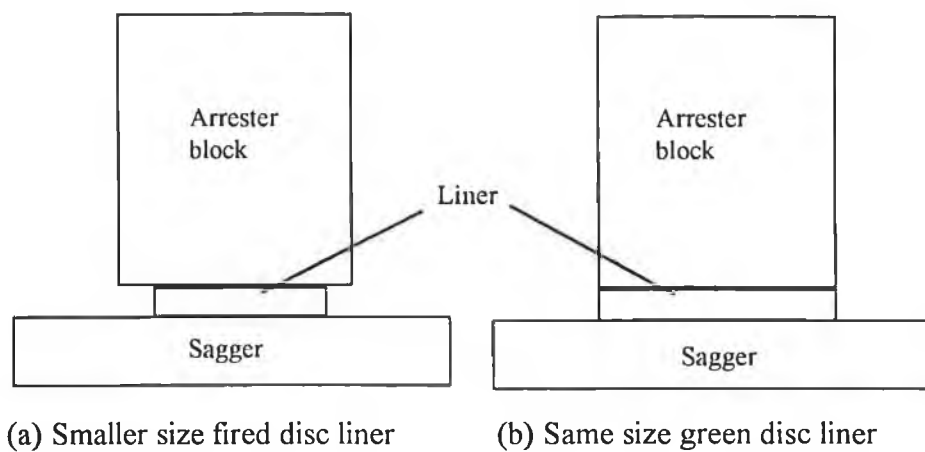


Figure 7.2 Circular disc liners to improve the bottom face quality

The fired smaller support system (Figure 7.2 (a)) was chosen to keep the edges free from the liner material to ensure good edge quality. The green support of the same diameter made from the standard varistor material (Figure 7.2 (b)) was expected to yield the bottom edges unaffected from the adverse effects of sliding with the sintered liner material during the shrinking process. Like the conventional sintering process the green discs in these two arrangements were kept separated from the direct contact of the supporting liner by sparsely spreading the ZnO powder.

Identification of different cells

The discs were categorized according to the description given in Table 7.1. For convenience the following coded names will be referred in the subsequent sections.

Table 7.1 Test condition and the identification of various cells

Cell ID	Brief Description of the support system
CSS	Control Support System (Fired ZnO flat liner and spreaded ZnO powder)
VSS	Vee-groove Support System (Spinel powder layer in between contact)
SSS	Smaller Sintered support System (Keeping bottom edge free of contact)
TGS	Total Green support System (Allowing the bottom undisturbed shrinkage)

7.2.2.PERFORMANCE IN GRINDING OPERATION

The need for the grinding operation has been described earlier. Regrinding a face is felt necessary when defects are observed by the physical inspection following the first grinding operation. Two types of defects such as the pinhole on the face and the chipping of edges are usually detected. However, the size of a defect is important - a very small chip usually under some specified dimension is neglected. If the chip is big enough the arrester disc may be rejected without any further grinding depending on whether it will satisfy the minimum target height. For any visible pinhole regrinding is recommended as its depth cannot be easily ascertained through physical inspection.

Regrinding is always an undesirable operation in the context of associated costs - material, labour, equipment and productivity. It is always preferable to have a process that can keep the figure of regrinding to a minimum. In this experiment a considerable

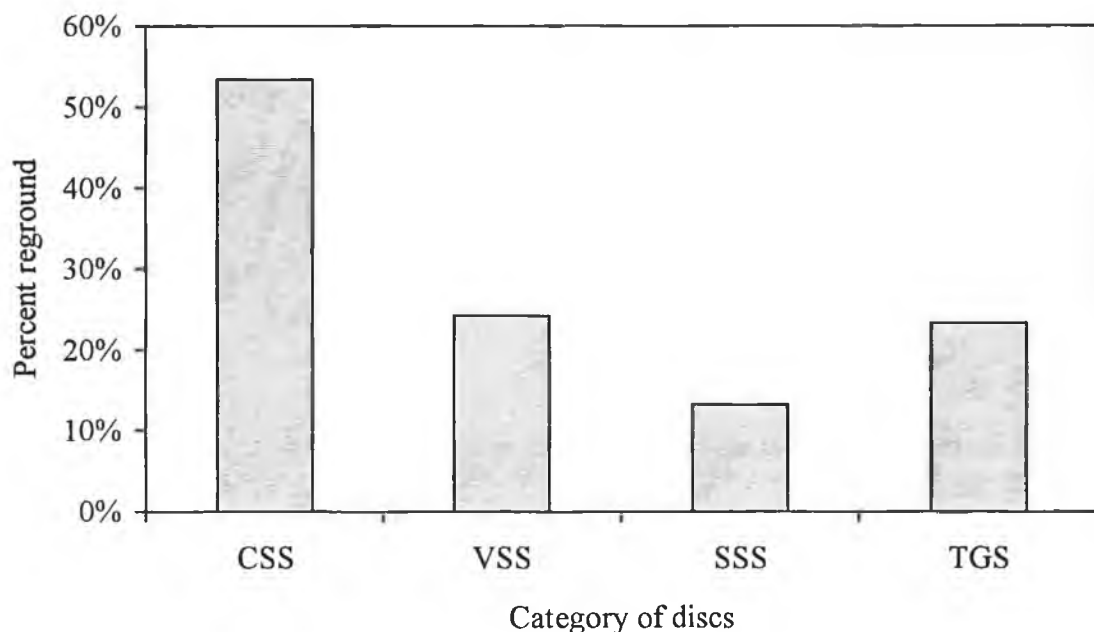


Figure 7.3 Percent of regrinding necessary for different cells

variation was observed among the four cells indicating the significance of sintering configuration . In Figure 7.3 the graph shows the percentage of discs required for each cell to be reground. It is evident that the control is the worst in terms of the grinding operation. Discs sintered on the smaller liners (SSS) keeping the edge free of any contact are found to be the best. The VSS cell and TGS have exhibited considerably improved performance compared to the control.

This regrinding frequency is not uniformly distributed over the top and the bottom faces of the sintered arrester discs. A considerable difference was observed in the percentage share of regrinding among the two faces. Since there is no scope of identifying the bottom or top for the discs sintered horizontally, this classification on the cell VSS is not applicable. The observation was therefore made for the rest of the cells. It has been found that for the three cells-CSS, SSS and TGS, the bottom faces were highly susceptible to defects which led to regrinding. The relative percentage of of regrinding is shown in Figure 7.4. It is noticeable that for the three cells there is no marked difference in the percentage share.

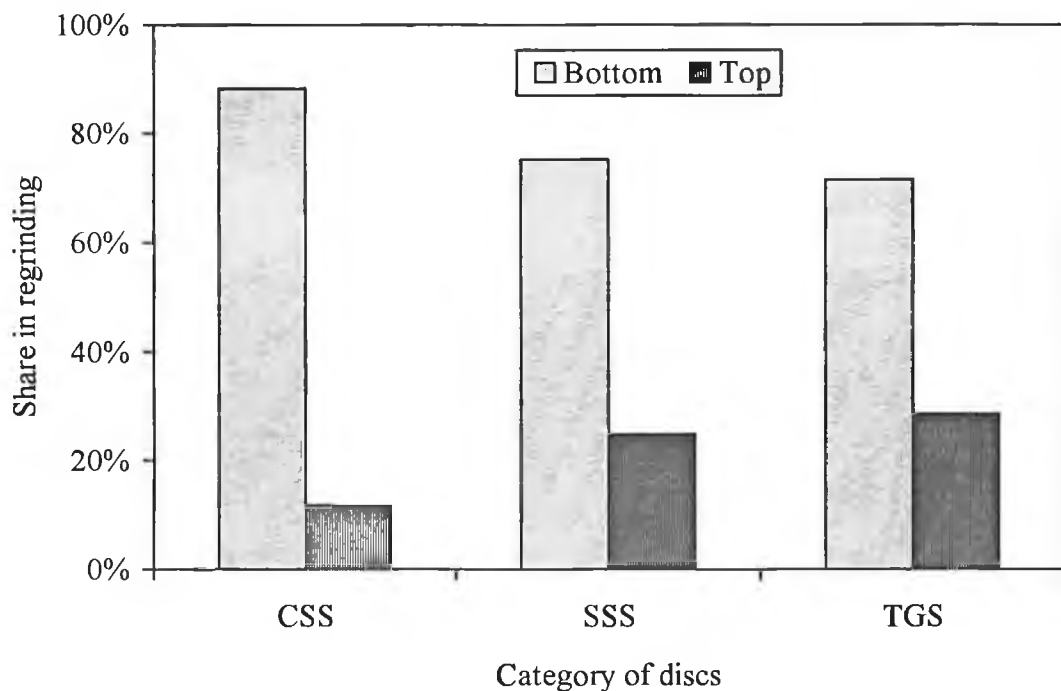


Figure 7.4 Percentage share of face reground on the top and the bottom

The contact during sintering is certainly responsible to generate defects at the bottom face. Any alternative process or liner material which can reduce the level of this contamination will be helpful in reducing the frequency of regrinding. It is envisaged that the process should also be helpful in enhancing the varistor properties specially in terms of the energy absorption capability and the high current performance.

7.2.3 ENERGY ABSORPTION CAPABILITY

The energy absorption capability is a vital indicator for the arrester performance. The test procedure is already described in section 3.3.2. To minimize the effect of the process variation the necessary operation was conducted in a single run under the same set condition. Thus the same pressing cycle was adopted for compacting the discs. Except the variation in the sintering orientation according to the design of experiment all the discs were fired in a single run. The same principle was applied for other finishing operations.

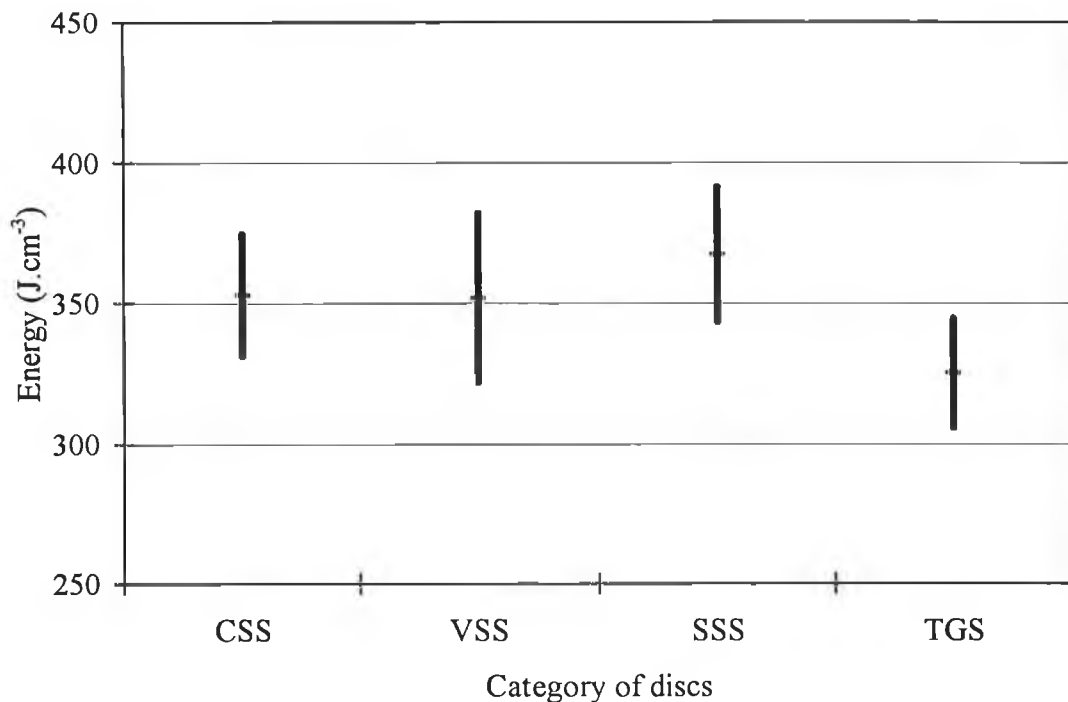


Figure 7.5 Variation in energy absorption capability of various categories

It may be mentioned here that the sample size for this experiment was not the same for all the cells. The test for energy also known as the 'strength test to destruction' is

usually conducted with the discs having apparently good physical condition. However, a reasonably large sample size was selected. Number of arrester blocks tested for this test were 10, 12, 14 and 16 respectively for the CSS, VSS, SSS and TGS cells. The results are plotted in Figure 7.5 with the error bar.

In terms of the energy absorption capability there is no significant difference among the first three cells. However, the mean value of energy for the discs sintered on the same size green support (cell TGS) is about 10 percent less compared to the other cells. It may be mentioned here that the discs sintered horizontally on the Vee-groove support had a contact mark on the side. But after passivation with glass these impressions were no longer visible.

Frequency of failure - top and bottom face

For the three cells the percentage share of failure from the bottom and the top are presented in Figure 7.6. In cell SSS the percentage of failure from the bottom has

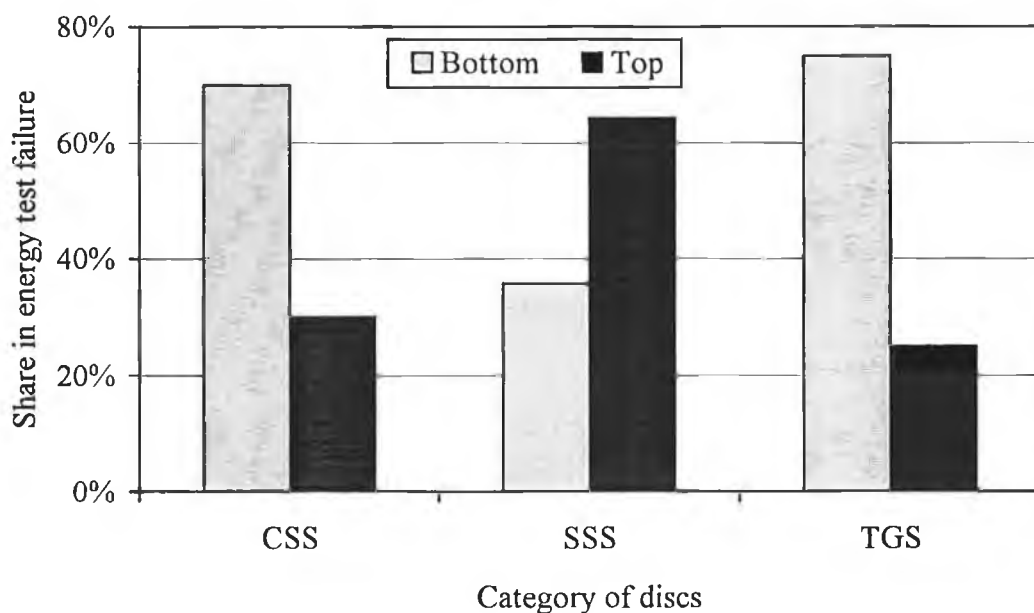


Figure 7.6 Percentage share of failures from top and bottom in energy test

decreased tremendously compared to the other two cells. The edges of arrester bottom faces were free of contact during sintering and therefore defects could not

generate along the lower peripheral zone. As a result the percentage of failures arising from the top and the bottom were close. It may be mentioned here that in the test for energy absorption capability, most of the failures are found to originate from the periphery. In the Table 7.2 the failure mode and the location of the failure mark are given. It is quite apparent that failure occurs mostly from the periphery of the face

Table 7.2 Statistics on the failures with the location, type and effects

Cell ID	Sample size	Failure mode		Location of failure mark				After effect	
		Flashover	Pinhole	Top	Bottom	Periphery	Centre	Small Split	C-face spot
CSS	10	4	10	4	6	10	0	5	8
SSS	14	2	14	9	5	14	0	8	10
TGS	16	3	16	4	12	16	0	6	8

either on the top or on the bottom. Out of the forty discs none failed from the central part of the disc. According to the observed fired density gradient presented in Figure 6.13, the bottom centre should be the most vulnerable location for failure. But usually this does not initiate from the centre. Peripheral locations are found to be very prone to originate the failure. It may be explained in terms of the deposition of larger quantity of energy. Current needs to change its direction maximum at the peripheral

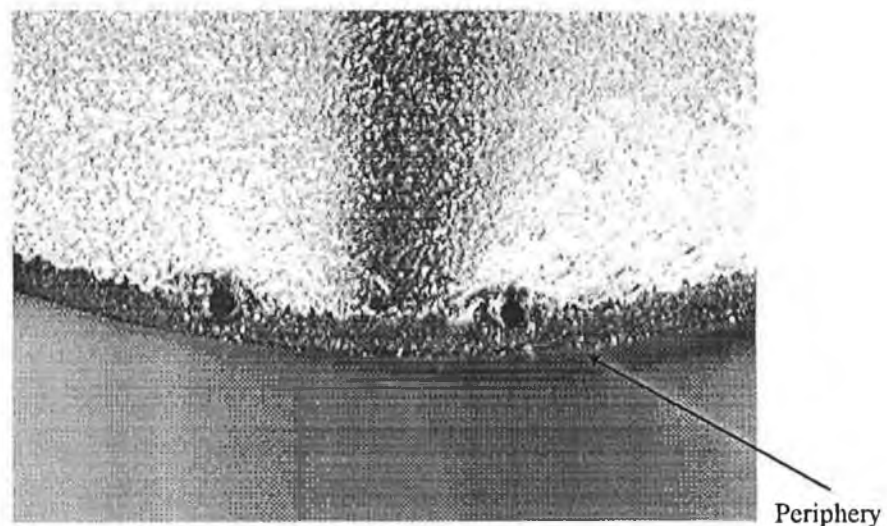


Figure 7.7 A typical failure in the test for energy absorption capability (X3.5)

zone of the arrester face resulting in higher inductance. Thus due to the greatest impedance higher energy is likely to be deposited at the periphery. In Figure 7.7 a typical failure by pinhole is shown. In this experiment almost all the failures were accompanied by this kind of failure mark at the periphery.

7.2.4.HIGH CURRENT PERFORMANCE

Multiple number of arrester discs from each of the cells were tested for the high current performance. The rated current was selected with an increment of 5 KA for every subsequent shot for every disc. The starting current was 100 KA and there were no survivor after 115 KA shot. The test results are presented in Table 7.3.

Table 7.3 Number of survivor discs in HASD test at increasing rated current

Cell Identity	Shot number (Rated current)			
	1 (100 KA)	2 (105 KA)	3 (110 KA)	4 (115 KA)
CSS	10/10	10/10	3/10	0/10
VSS	15/15	15/15	7/15	0/15
SSS	5/5	5/5	3/5	0/5
TSS	5/5	5/5	4/5	0/5

The relative performance is shown graphically in Figure 7.8 by the values of high current performance parameter described in equation (4.9)

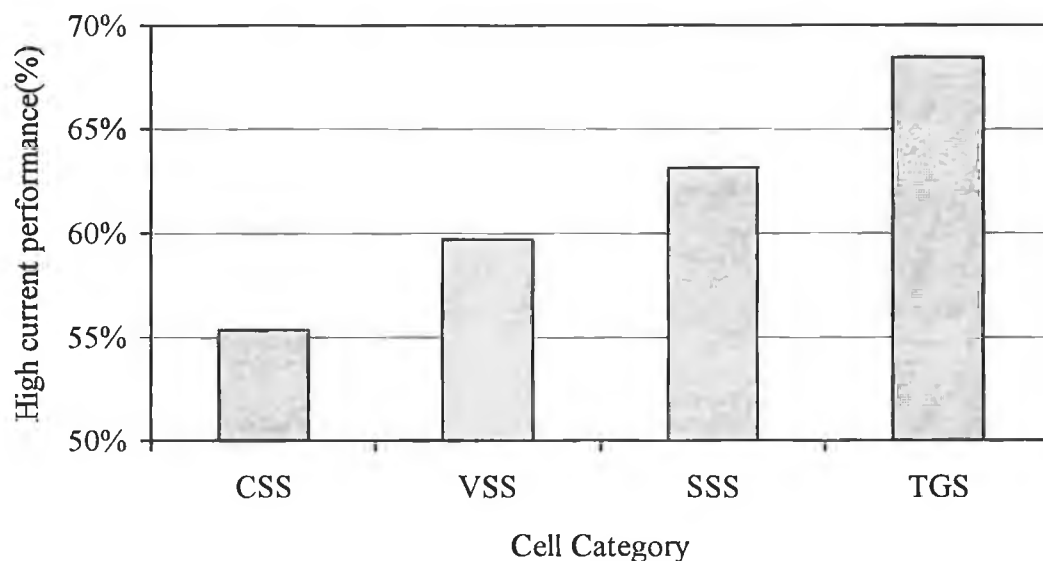


Figure 7.8 High current performance as affected by sintering orientation

The high current performance was not found to have any significant correlation with the results obtained in the test for energy absorption capability. Comparison of Figure 7.5 and 7.8 shows that the discs sintered on same size green liner (TGS) was the worst in energy but exhibited best high current performance. Considering the overall performance both in energy and HASD, the cell SSS looks promising. So this sintering orientation is expected to yield superior performance.

But there is a problem in placing the discs properly on the smaller circular liner and handling them prior to sintering. The unstable equilibrium in the sagger can be solved by appropriate design of the sagger with suitable support from the side.

7.3 ASSESSMENT OF UNGROUND FACE AND LINER MATERIAL

This study was undertaken to investigate to the scope of processing arrester discs by skipping the grinding operation as well as to assess the effects of two liner materials. By adopting the horizontal sintering process it was possible to maintain a good surface finish of the faces with proper geometry. So the feasibility of processing arrester discs without grinding the faces was studied using the Vee-groove support system. A control cell was also processed in parallel under normal route to compare the results. The evaluation is based on the data on the energy absorption capability. Table 7.4 summarizes the condition and the identification of the corresponding cells for subsequent references.

Table 7.4 Processing condition and identification of various cells

Cell ID	Brief description of the processing condition
CON	CON trol (Fired on ZnO flat liner and sparsely spreaded powder)
HSG	H orizontally sintered on S pinel powder and discs were G round
HSU	H orizontally sintered on S pinel powder and discs were U nground
HZG	H orizontally sintered on Z inc oxide powder and discs were G round
HZU	H orizontally sintered on Z inc oxide powder and discs were U nground

The liner powders used to cover the inclined surface of the groove were the spinel and ZnO powder. As referred in the Table 7.4 the horizontally sintered discs were processed differently in terms of grinding. Some of the discs from each category in the context of liner powder uses were not ground on their faces. So there were four cells - HSG, HSU, HZG and HZU from the horizontally sintered discs, the processing condition has been described above for each of them. The control (CON) cell was processed under standard condition with both the faces ground as usual. The discs of the whole lot were electroded keeping a margin on the periphery of the face. Other processing operations were also common.

7.3.1 ENERGY ABSORPTION CAPABILITY

The test for evaluating the energy absorption capability was conducted following the procedure described in section 3.3.2. The performance of various cells in terms of the energy absorption is plotted in Figure 7.9 against cumulative percentage failure.

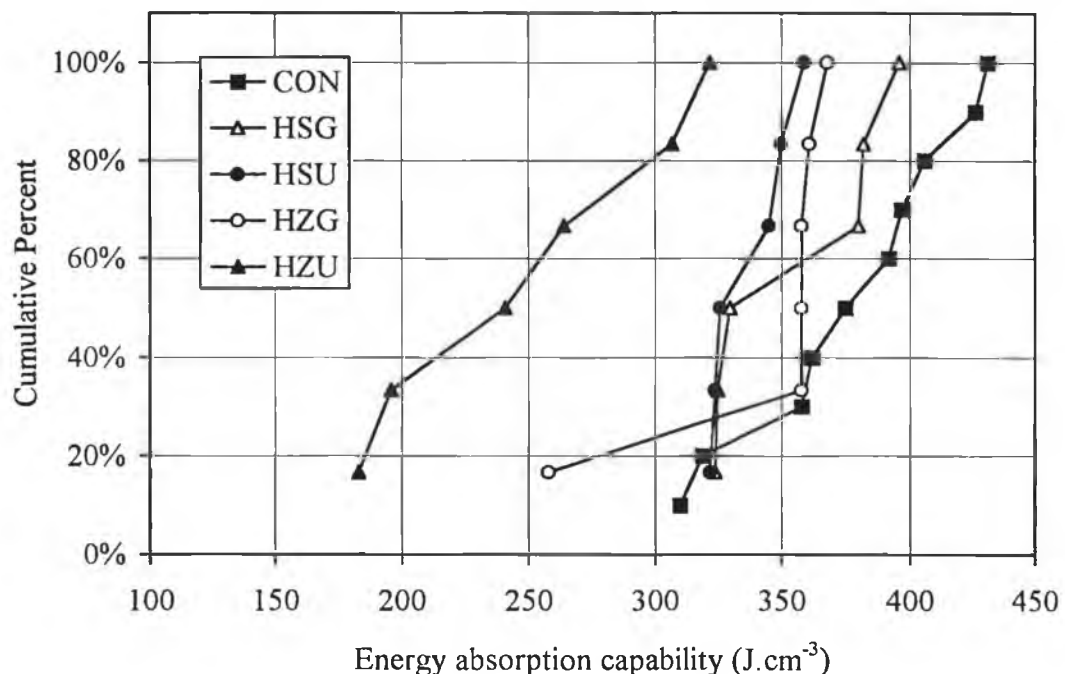


Figure 7.9 Effect of liner material and grinding operation on the energy

It is obvious from the relative performance presented above that the influence of grinding is highly sensitive to the type of liner material used. The horizontally sintered

discs using ZnO liner powder exhibited significantly improved performance when processed with the grinding operation (when cell HZG and HZU are compared). But there is a negligible difference at the median values due to the incorporation of grinding operation when the spinel powder was used as the liner material.

7.3.2 OBSERVATION AND DISCUSSION

The effect of the liner material on the energy absorption capability is not obviously understood. But the observed difference may be explained in terms of the grain growth facilitated due to the presence of a particular type of liner material. Spinel powder is recognized as having an inhibiting influence on the grain growth while pure ZnO powder is conducive to this growth.

The larger grains developed along the contact zone due to the presence of ZnO powder may create a preferential path for current flow through the bismuth rich layer. Consequently the discs fail at an earlier stage of energy. But when the faces are ground the bismuth layer is disconnected from the face. In this regard investigation on the conductivity of bismuth layer may be helpful to justify the explanation. However, the location of failures observed in the test on the disc surface also supports the proposition. The data in column 5 and 6 of Table 7.5 indicate the number of failures occurring through or near the contact zone in sinter. Discs processed using ZnO liner powder are more susceptible to failure around this zone.

Table 7.5 Statistics of failure mode, location and after effects

Cell ID	Sample size	Flash over	Pinhole	Location of damage at				Small split	C-face spot
				Within zone	Outside zone	Periphery of face	Centre of face		
HSG	6	2	6	3	3	4	2	1	2
HSU	6	3	6	1	5	6	0	2	4
HZG	6	2	4	5	1	3	1	1	3
HZU	6	1	6	5	1	5	1	4	5

It is apparent from the results of the study that spinel powder is a better option as liner materials for horizontal sintering. It may also be noted here that with spinel the impression created on the contact zone was also less prominent and better dimensional accuracy of the arrester block was possible to attain. Moreover, no sticking problem with the Vee-groove support was encountered in contrast to that when ZnO powder was used.

It is observed from the relative position of different cells in Figure 7.9 that except HZU all other cells are comparable in terms of energy. However, the mean and the deviation are two important parameters for the assessment of a process. Figure 7.10 demonstrates the energy absorption capability of different cells with error bars indicating the mean and standard deviation. There is a difference among the mean values and standard deviations for different cells. A parameter to evaluate the process

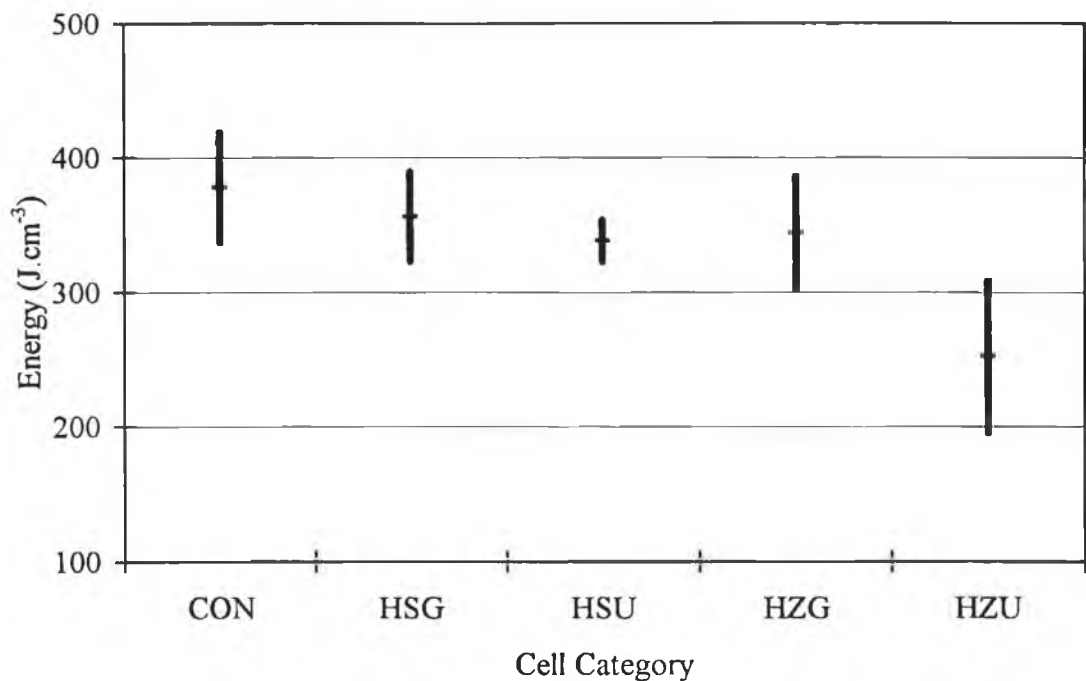


Figure 7.10 Variation of energy as the effect of liner material and grinding of face

capability¹⁰⁵ called C_{pk} is defined in terms of the sample mean value and standard deviation and the control limit. The parameter, C_{pk} is expressed mathematically as follows:

$$C_{pk} = \frac{\bar{x} - E_L}{S} \dots\dots\dots(7.1)$$

where \bar{x} = sample mean
 E_L = Lower limit of energy
 S = Sample standard deviation

The worked out C_{pk} for different processes is presented in Table 7.6. The lower limit of energy absorption capability was assumed to be 200 J.cm⁻³ (target of the BRITE project).

Table 7.6 Process capability index for different cells

Cell ID	CON	HSG	HSU	HZG	HZU
C_{pk}	4.3	4.7	9.3	3.41	0.915

A C_{pk} value less than 1.33 implies the inadequacy of a process. The higher the value of the index, the better is the process. In this context the processing of varistor discs on the Vee-groove support using spinel powder looks very promising with the highest value of the index.

7.4 EFFECT OF MARGIN ON ELECTRODE

The margin on electrode looks to be advantageous in one respect but harmful in other. This experiment was undertaken to identify the effect of margin on the energy absorption capability.

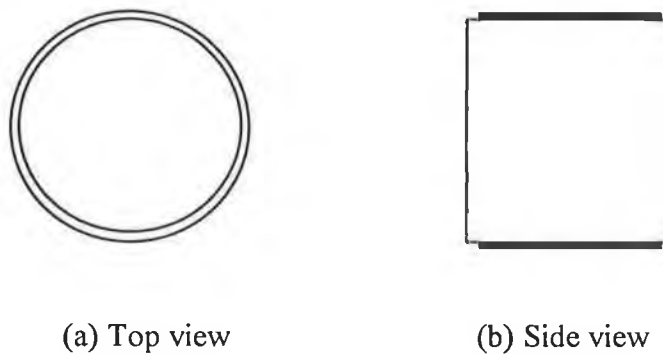


Figure 7.11 Electrode with margin as shown on the face of an arrester disc

This experiment was conducted to evaluate the effect of margin left with the covering of the top and bottom face of an arrester block. Three options were selected (i) control leaving a margin on electrode on both the face (ii) one face electroded with margin and the other face fully electroded i.e. no margin and (iii) both the faces were fully electroded leaving no margin. The three categories of arrester discs were identified by CONT, OFFE and BFFE respectively.

The arrester discs were pressed under the same pressing condition. The target green density was 3.46 gm/cc with a nominal diameter of 49 mm and a height of 51.2 mm. The nominal fired height after grinding was 42 mm having a rated nominal voltage of 5 KV (r.m.s. value) at 5mA.

7.4.1 ENERGY ABSORPTION CAPABILITY

The energy absorption capability was evaluated by the testing procedure described in section 33.2. The performance of the three cells is demonstrated in Figure 7.12.

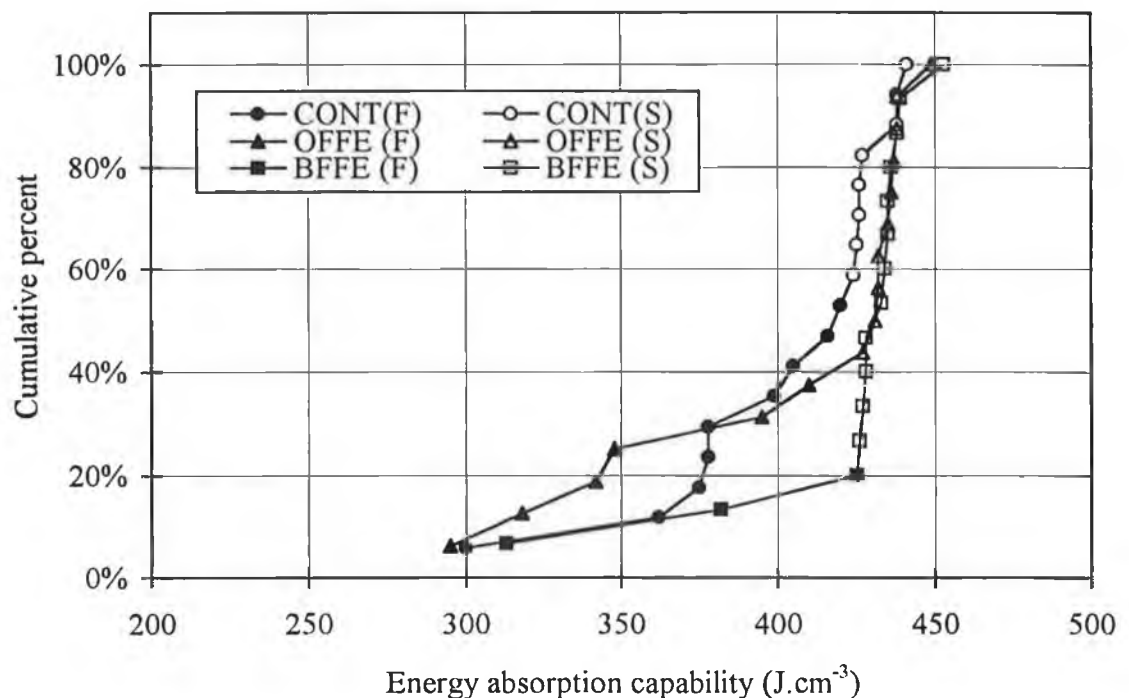


Figure 7.12 Effect of margin on electrode on the Energy absorption capability

The sample size was 17, 16 and 15 respectively for CONT, OFFE and BFFE. It should be mentioned here that the test for energy was initiated with a charging voltage of 24 KV which was equivalent to a level of 140 J.cm^{-3} . With the increment of 1.2 KV for every subsequent cycle testing was continued up to 49.9 KV, the maximum limit of the generator. But it was unusual that even at that stage out of 48 discs only 18 failed while the rest 30 discs survived. Energy absorption capability of the survivor discs was computed on the basis of the data obtained at the last cycle of test at the charging voltage of 49.9 KV of the generator. In the legend the letters 'F' and 'S' in parenthesis stand respectively for the failed and survived disc. Among the survivor discs, it is evident that the discs of BFFE and OFFE cells absorbed more energy than those of the CONT. This is attributable to the effect of full face electrode leading to more current carrying cross-sectional area. However, in this regard there is no difference observed between the BFFE and OFFE.

Since it is not very clear from the above Figure about the influence of electrode on the energy absorption capability, the percentage of discs survived after the maximum possible energy injection for the three cells is plotted in Figure 7.13. It is apparent from the consistent trend of higher survival rate that the full face electrode is conducive to energy absorption capability. Some unsatisfactory results with full face electrode are not unlikely when the quality of passivation and its thickness are not properly maintained.

7.4.2 SPIN-OFF OBSERVATION ON BISMUTH CONTAMINATION

The manufacturing process of metal-oxide varistor undergoes a liquid phase sintering. The additive Bi_2O_3 is transformed into liquid at the high temperature and sometimes a portion of the disc base remains under the accumulated liquid. This happens when the sintered liner plate is not perfectly flat and possesses a little curved shape - a favourable condition to store a liquid. This naturally occurs with the bottom face. In most of the cases the traces of bismuth contamination are removed due to the greater depth of grinding at the bottom face. But still there are some of the discs which bear the marks of this effect.

In this experiment there were 18 discs having the traces of bismuth contamination which were distributed almost evenly among the three cells. These discs, though

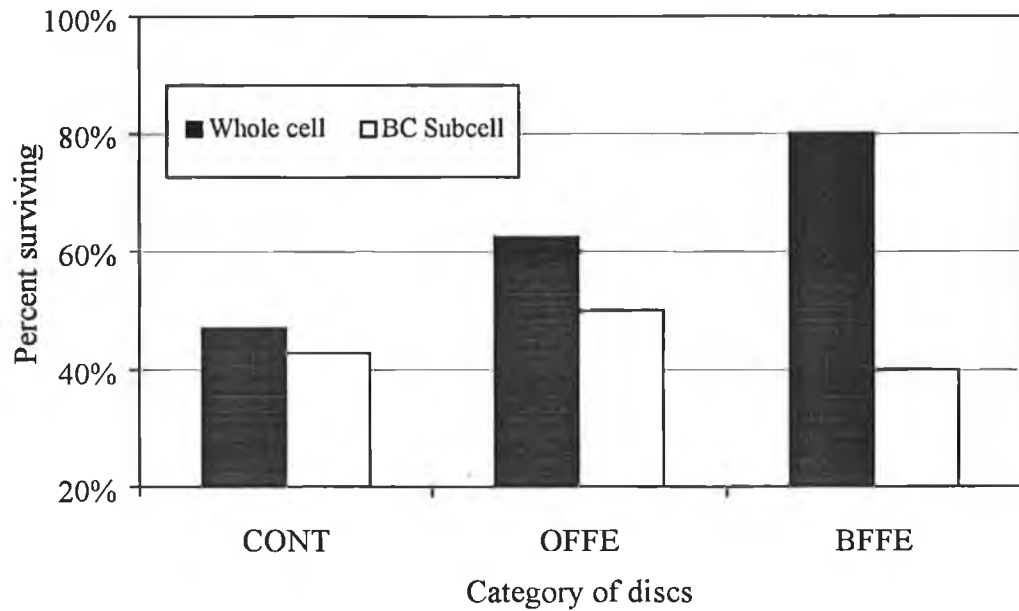


Figure 7.13 Percentage survived of individual cell and bismuth contaminated sub-cell

passed through the normal inspection as bismuth contamination is not considered to be a defect, exhibited a poor performance. When compared with percentage survivor of each cell, the survivor from this subgroup was found to be remarkably low as in Figure 7.13.

It is clear from the above observation that contamination arising from the bottom part submerged in the liquid bismuth should not be overlooked. There should be some reject criteria regarding the bismuth contamination.

It has been noticed further that the level of contamination is directly related to failure. In the associated experiment the arrester discs were categorized depending on the affected area as slightly, moderately and highly contaminated. After the test failure

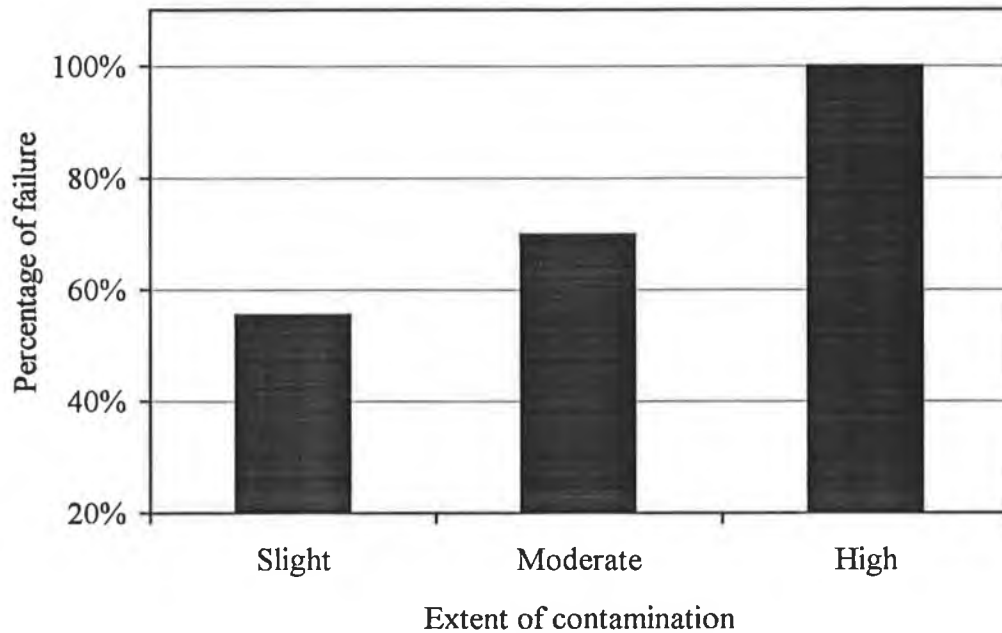


Figure 7.14 Trend of failure with the level of bismuth contamination

rate was found to be different for these three subgroups as shown in Figure 7.14. It appears that there is a good correlation between the level of contamination and the performance. Horizontal sintering procedure will be very helpful in this regard. The liquid bismuth will not be able to be accumulated on the inclined supporting surface. As a result there will be no scope of contamination from the liquid bismuth.

7.5 HEXAGONAL DISCS - EFFECT OF MODIFIED GEOMETRY

In the test for evaluating the energy absorption capability of an arrester the energy is injected into the body by electrical impulse. The injected energy is transformed into heat and is dissipated through the surface area of the disc body. The aim of this study was to observe the effect of higher surface to volume (S/V) ratio on the energy absorption capability. The charging time of the generator was set at 8 seconds. Since there were three discs to be tested in sequence, the time between two pulses was 24 seconds for a particular disc. The heat transfer process for a 2 ms duration square wave can be considered to be adiabatic. But the time between two pulses on a disc is

considerable and higher S/V ratio of hexagonal disc should be conducive to heat dissipation.

7.5.1.SAMPLE PREPARATION AND EVALUATION OF ENERGY

The cylindrical discs were ground by diamond wheel on the side at an angle of every 60 degree with a worked out depth of cut as shown in Figure 7.15. All other processing operations were same except electrode. Because of its noncircular cross-section it was not possible to deposit electrode on the hexagonal discs through the normal production line process. The flat faces of the hexagonal arrester discs as well as those of control were painted by silver and cured at 800 °C.

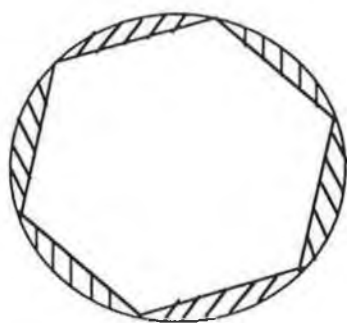


Figure 7.15. Cross-section of cylindrical disc ground to hexagonal shape

The disc with the hexagonal cross-section assumed an S/V ratio of 1.1265 cm^{-1} . In calculating this ratio only the side surface was considered as the heat dissipating area. Similarly the S/V ratio for the original cylindrical disc having a diameter of 4.1 cm was 0.976 cm^{-1} . Thus there was an increase of more than 15 per cent in the S/V ratio for the hexagonal discs.

Effect of this enhanced S/V ratio is evident on the energy absorption capability as presented in Figure 7.16. The average energy absorption capability for the hexagonal discs was 416 J.cm^{-3} whereas that value for cylindrical discs (control) was 358 J.cm^{-3} .

This significant enhancement of energy may be attributed to the combined effect of increased S/V ratio and the removal of the bismuth rich skin. The influence of the

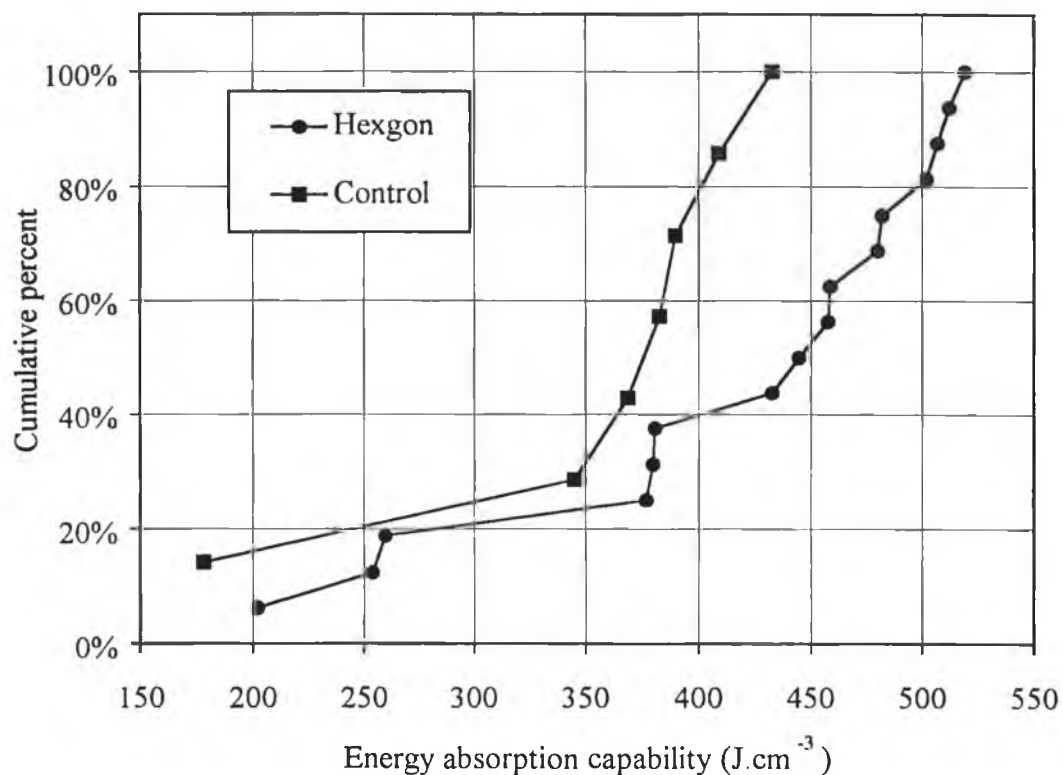


Figure 7.16 Enhancement of performance due to the change in geometry

skin can be visualized from the location of failure marks as summarized in Table 7.7. The number of failures occurring from the periphery appears to be lower than what is normally observed in case of cylindrical discs [Table 7.2]. Most of peripheral originated from the corners of the hexagon where least or no material was removed by grinding. The percentage share of failure originated from the top and the bottom face is similar to that observed in earlier cases - about 70 percent from the bottom face.

Table 7.7 Data on the post-failure marks and their location

Disc ID	Sample size	Location of failure mark				After-effect	
		Centre	Periphery	Bottom	Top	P/H	F/O
Hexagon	16	8	8	10	6	15	12
Cylinder	7	3	4	6	1	6	5

However, irrespective of this observed benefit, higher S/V ratio can play an important role in a steady state operating condition and enhance the varistor life.

7.5.2 EFFECT OF HIGHER S/V RATIO ON VARISTOR LIFE

If there is no mechanical or electrical failures, the life of a ZnO varistor is dependent on the magnitude of I_R (leakage current) and its increase in temperature¹⁰. As the magnitude of I_R increases, so does the amount of heat which, if not allowed to dissipate, can rapidly raise the temperature of the device. Consequently, the device after maintaining an initial steady state condition, will eventually run away thermally and end its life.

A quantitative approach was adopted by Gupta⁹⁸ for predicting the 'life' of a varistor. A varistor is considered to be 'technically dead' when it reaches a limiting power density (P_L) defined as the point where power generated (P_G) exceeds power dissipated (P_D) or

$$P_G > P_D \dots\dots\dots(7.2)$$

and

$$P_G = \frac{1}{2} Ah(xE_{0.5})I_R \dots\dots\dots(7.3)$$

$$P_D = \lambda S(T - T_S) \dots\dots\dots(7.4)$$

where $xE_{0.5} = V_{SS}$ is the steady-state voltage (with $x < 1$) in KV.cm⁻¹, I_R is the resistive component of the leakage current, A and h are the area (cm²) and thickness (cm) of the device, λ is the composite heat dissipation coefficient in W.cm⁻².°C⁻¹, S is the total surface area of the device and T and T_S are the disk and outside ambient temperatures ($T > T_S$). P_G and P_D are both measured in watts, with P_G having an exponential, and P_D a linear dependence on temperature.

Now for a normal operation P_G has to be smaller than P_D - the greater the difference the more will be the stability. So for a constant power generation, any situation at

which the heat dissipation rate from a varistor can be enhanced, will be helpful for varistor life. The condition can be expressed in the mathematical fashion as follows:

$$P_G < P_D \dots\dots\dots(7.5)$$

By replacing them with the right hand side of equations (7.3) and (7.4) we can write

$$\frac{1}{2} Ah(xE_{0.5})I_R \leq \lambda S(T - T_s) \dots\dots\dots(7.6)$$

where Ah is nothing but the current carrying volume (V) of the disc. Now division of both sides of the above equation by the volume V yields

$$\frac{1}{2} (xE_{0.5})I_R \leq \lambda \left(\frac{S}{V}\right)(T - T_s) \dots\dots\dots(7.7)$$

During the steady-state operation, the faces of a varistor disc in the arrester assembly remain in contact with other discs or metal support. Therefore, heat dissipated through the faces may be negligible and the effective surface area should consist of the side of a varistor. Now for an increased S/V ratio, the right hand term of (7.7) will be greater and thus the difference between P_G and P_D will also increase resulting in an enhanced stability of a varistor disc.

In the test for the energy, though there was a reduction in the volume of the hexagonal disc compared to that of the cylindrical one, the S/V ratio was increased by 15 percent. However, even for the same volume hexagon leads to greater surface to volume ratio. In the following Figure 7.17, the variation of surface to volume ratio is presented for a hexagon and a cylinder having equal cross-section and height.

The S/V ratio is high at the lower cross-sectional area for both the hexagon and the cylinder. But for any particular cross-section this ratio is about 5 percent higher for the hexagon.

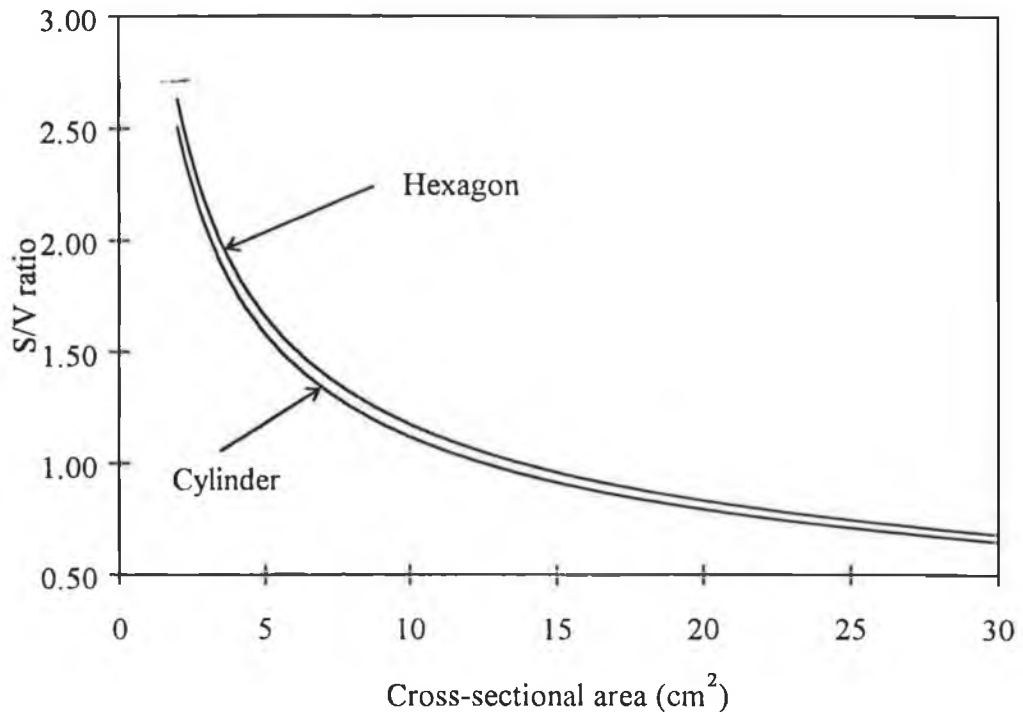


Figure 7.17 S/V ratio of hexagon and cylinder of the same height and volume

7.5.3. SCOPE OF VERSATILITY IN APPLICATION

Presently stack of different height is assembled by placing the cylindrical arrester discs end-to-end for application in the high voltage power line. Fabrication of this type of stack with hexagon should not pose any greater difficulty. In other way, the possibility of side by side assembly with the hexagonal disc can be exploited to adjust the current carrying cross-section.

Now-a-days cylindrical arrester discs are manufactured with different cross-section to fit the current carrying requirements of application. Replacement of different size of cylinder arrester may be possible by a standard hexagonal shape disc. Mass-scale production of a standard hexagonal block should be eventually cost-effective.

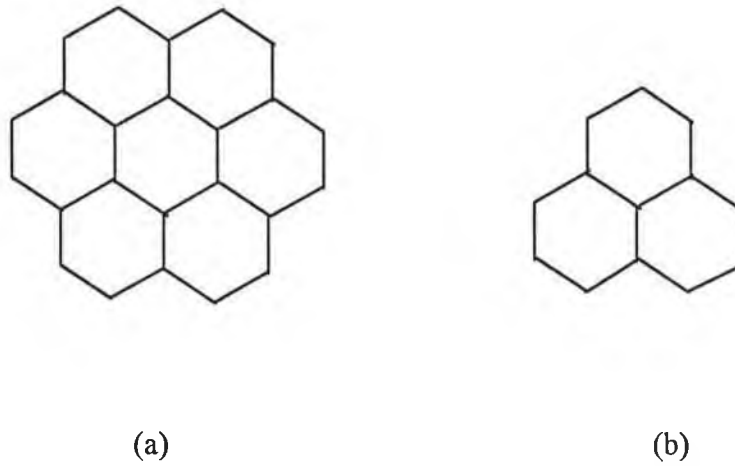


Figure 7.18 Lateral assembly for increasing the cross-section

In the above arrangement the S/V ratio will be further increased compared to that for a cylindrical disc of equivalent cross-section. For arrangements shown in Figure (a) and in (b) the increase in the S/V ratio is respectively more than 19 and 21 percent.

7.6 STRESS WAVE IN HIGH CURRENT IMPULSE

The fracture mechanism of arrester disc in the high current pulse of short duration is different from what is observed in the case of the long pulse. Cracking is the main mode of failure in this case which is unlike the failure by puncture in the long duration (millisecond) pulse (Figure 7.7). Different destruction phenomena were studied by Eda⁴⁴ with impulse durations of 10-15 μs , 100-200 μs and 2ms. He found that pulsed currents having a duration greater than 100 μs caused destruction by the puncture mode while those having a duration less than 50 μs caused destruction by cracking mode.

In the paper, puncture was reported to be thorough (starting from one face to the other) for the discs with a thickness of 1.3 mm. This is caused due to the melting of the Joule heating caused by the concentrated current flow through the preferential

path. In our study with 2 ms pulse there were a few punctures which were thorough in case of the discs with a thickness of 14 mm, however, none was found to be thorough for the taller discs (42 mm thickness). It is understandable that with the increase in thickness or height of the disc the chance of having a preferential current flow path all along the thickness becomes less. For taller discs most of the punctures were located at the periphery accompanied by a split of small chip or chunk. The splitting is attributable to the effect of the stress developed due to the temperature gradient caused by localized heating.

The failure mode of crack or rupture is observed when a high current is passed within a very short time. An attempt was made to explain the cracking mode observed in the case of the short pulse in terms of the thermal relaxation time¹⁰. Heat generated due to passing of a short pulse is thought to be responsible to create a large temperature gradient within the ceramic body which eventually causes failure by cracking. But this supposition is not very well based and can be refuted. The experience that a ceramic container filled with a hot liquid when immersed in cold water generates a fracture by cracking is not uncommon. This is certainly a very slow process compared to the microsecond pulse or a millisecond pulse.

Rupture of an arrester occurring in a short pulse can be better explained in terms of the theory on the stress waves in solid. It is quite likely that when an electrical pulse is imparted, some part of its energy is converted into stress wave. The amplitude of such a stress wave may be assumed to be proportional to that of energy pulse, derived from the instantaneous current and voltage. The energy pulse corresponding to a 100 KA impulse injected into a 5 KV arrester block is shown in Figure 3. This looks slightly steeper than the current pulse.

7.6.1 BRIEF OVERVIEW OF STRESS WAVES IN SOLID

The treatments made in the context of *the rigid dynamics* and *the theory of elasticity* are sufficiently accurate for problems in which the time between the application of a force and the setting up of effective equilibrium is short compared with the times in

which the observations are made¹⁰⁵. But when we consider the effects of forces which are applied for only a very short period of time, or are changing rapidly, the effects must be considered in terms of the propagation of stress waves.

The theory of the propagation of elastic waves in solids was developed during the last century. But this was in many ways in advance of experimental work, as there were then no methods available for observing the passage of stress waves on a laboratory scale. But in recent times due to the advent of electronic techniques to generate and detect elastic waves of high frequency, the field is getting a new boost.

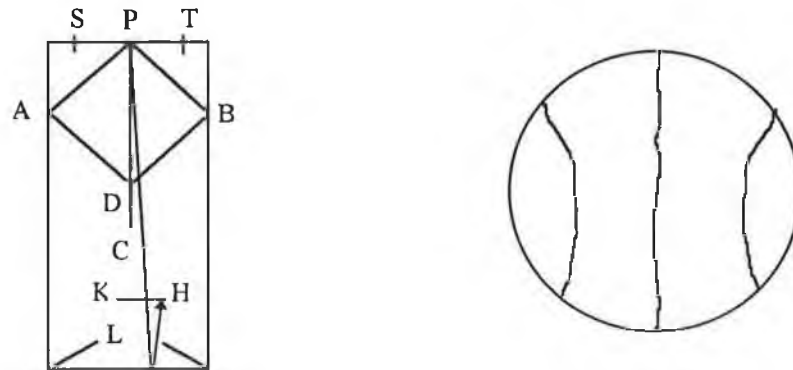
The finite velocity of stress wave in a fluid of density, ρ and the bulk modulus, k can be inferred directly from the equation of motion as $\sqrt{(k/\rho)}$. This is the only type of wave motion which is propagated through a medium which cannot sustain finite shear stresses,. However, in extended isotropic solids, two types of waves may be propagated. These are waves of dilatation (longitudinal wave) and distortion (transverse wave). The wave of dilatation travels with a velocity $\sqrt{[(k+1.33\mu)/\rho]}$, μ being the modulus of rigidity, and wave of distortion travels with a velocity $\sqrt{[\mu/\rho]}$. When a solid medium is deformed, both distortional and dilatational waves are normally generated and propagated.

Fracture Produced by Stress Waves

When a stress pulse of sufficiently large amplitude travels through a solid it may produce fractures. The fractures produced by stress pulses differ from those produced statically. This occurs firstly, because the velocity of crack propagation is considerably lower than the velocity of propagation of the pulse. Secondly, with a short pulse only a small part of the specimen is stressed at any one time and fractures may form in one region of a specimen quite independently of what may be occurring elsewhere. Thirdly, when a compression pulse is incident on a free boundary it gives rise to a reflected tension pulse, while when it is reflected obliquely both a dilatational (longitudinal) and a distortional (transverse) pulses are produced.

7.6.2 COMPARISON OF FRACTURE ORIGINATED BY A STRESS WAVE AND HIGH CURRENT PULSE

When a charge is detonated at the centre of one face of a cylindrical specimen a number of different fracture regions are formed¹⁰⁶ as shown in Figure 7.19 (a). Similar fracture regions are observed for a cylindrical arrester block in high current test, shown in Figure 7.19 (b).



(a) Detonation a charge at point P (b) Effect of HASD pulse on arrester (top view)

Figure 7.19 Comparison of fracture locations produced in the two sources

A circular crack on the top surface a few millimetres from the edge as shown by S and T results from the reflection of the compression pulse at the cylindrical surface of the specimen as a wave of tension. A linear region of fracture extending for some distance down PC, the axis of the cylinder, produced by the wave reflected from the curved surface converging on to the axis of the cylinder so that a very large tension is built. Similar fracture modes are frequently observed in case of the high current test. Though it is subjective to the individual mechanical property of the disc material, a low-volt arrester is not expected to sustain a current more than 9-10 KA/cm². For a high voltage arrester of the same height the current density must be lower to cause fracture as the amplitude of the energy pulse in this case becomes higher for the same level of current.

The geometry of an arrester plays an important role in the failure mechanism. This occurs in arrester blocks having a lower aspect ratio (H/D) are found to be

accompanied by the longitudinal crack as represented by the line PC. But in this case the circular crack at the edges as shown in Figure (b) is very common. Arrester blocks with higher aspect ratio are found to be susceptible to transverse fracture (waist crack). A part's resonant frequencies are determined by its dimensions, the density and the elastic constants of the material. Increasing the length lowers the resonant frequency of the bending mode. The 'waist failure' in case of the arrester discs having a higher aspect ratio appears to originate from the failure due to the first bending mode. In other way, the frequency of the stress wave developed due to the injection of short pulse is very important. Because depending upon this parameter, the mode of vibration of the disc will change. If the excitation frequency matches with the resonant frequency much larger vibrations are generated and can cause earlier failures.

Fracture surfaces in HASD pulse and diametral compression test

The fracture surface generated by the tension in the diametral compression test of an arrester specimen was found to be different than what was observed in case of high current performance test. In the latter case a number of ripples are observed on the fractured surface which resemble to the stress waves propagated through a Perspex specimen¹⁰⁶ as shown in Figure 7.20.

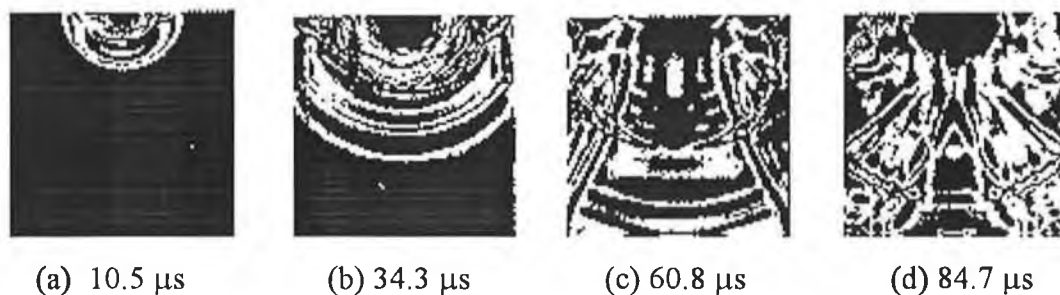
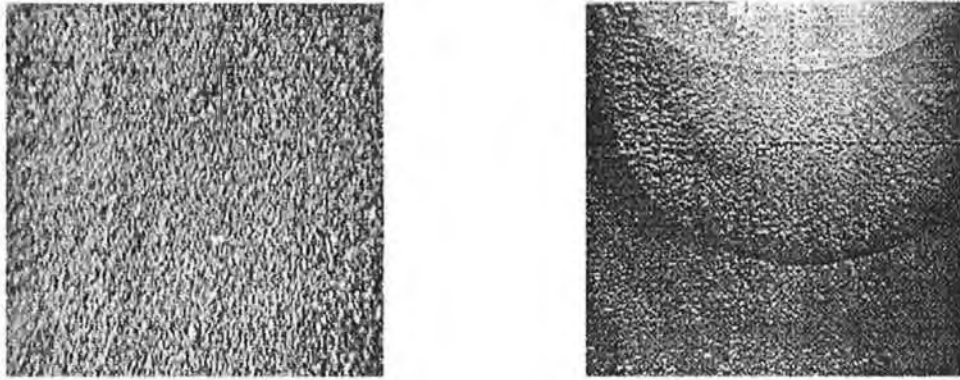


Figure 7.20 Stress waves generated by detonating a charge of lead azide on the centre of upper face of a Perspex parallelepiped specimen

An arrester draws current uniformly throughout the flat face and the centre of the face will be the location of peak stress wave. But if there is any preferential path the

location of resultant stress wave may be shifted. In that context, the fracture locations may be slightly deviated. The fracture surface of a typical failure in HASD test and that in diametral compression test are presented in Figure 7.21.



(a) Diametral Compression test

(b) HASD test

Figure 7.21 Fracture surfaces developed under different test conditions

7.6.3 SPEED OF STRESS WAVE IN ZnO VARISTOR MATERIAL

The general relationship¹⁰⁶ for the speed of stress wave propagation, C consists of the Lamé's constants - λ , μ and the density, ρ of the material. The equation for dilatational wave propagation is as follows:

$$C = \left[\frac{(\lambda + 2\mu)}{\rho} \right]^{\frac{1}{2}} \dots\dots\dots(7.8)$$

This stress wave speed in the metal-oxide varistor material can be estimated on the basis of the elastic properties for ZnO ceramic. Since the bulk of the constituent materials of the varistor is zinc oxide, the result should not deviate too much from the actual value. The Young's modulus, E is derived as a function of Lamé's constants λ and μ . the relationship of which is as follows:

$$E = \frac{\mu(3\lambda + 2\mu)}{(\lambda + \mu)} \dots\dots\dots(7.9)$$

The shear modulus, μ can be expressed in terms of the Young's modulus, E and the Poisson's ratio, ν as in equation (7.10).

$$\mu = \frac{E}{2(1 + \nu)} \dots\dots\dots(7.10)$$

Thus the Poisson's ratio ν can be evaluated by solving the equations (7.9) and (7.10) as a function of λ and μ as

$$\nu = \frac{\lambda}{2(\lambda + \mu)} \dots\dots\dots(7.11)$$

But for a particular material, the Young's modulus decreases with the level of porosity in the material. A relationship between the modulus of elasticity and the porosity volume fraction of the material⁸⁶ is given by:

$$\frac{E}{E_0} = \exp(-\beta p) \dots\dots\dots(7.12)$$

where E_0 = Young's modulus of fully dense material

p = Porosity volume fraction = $1 - (\rho/\rho_0)$

β = Constant ($2 < \beta < 4$)

Now for the pure and fully dense zinc oxide ceramic¹⁰², the density, $\rho_0 = 5.68$ gm/cc, the Young's modulus, $E = 123.5$ GPa and the shear modulus, $\mu = 45.7$ GPa. The Poisson's ratio, ν can be worked out from the equation (7.10) as 0.35.

Now for any assumed density of varistor material, the elastic parameters can be evaluated for a specific value of β . Now taking $\beta = 4$, the velocity of dilatational wave for the ZnO material was calculated by the equation (7.8) as a function of fired density.

By adopting similar method the velocity of dilatational wave for ZnO material was calculated theoretically and plotted against fired density as shown in Figure 7.22.

Analytical and Measured Speed of Stress Wave in ZnO varistor

The non-contact and non-destructive testing method to be developed for detecting the defects or flaws in varistor material is based on the phenomena of imparting opto-acoustical pulses and its propagation in the disc. As part of the DOCERPO goal, an attempt was made to characterize the varistor blocks by a system equipped with CO₂ or YAG laser and a piezo electric sensor. By the laser a single pulse is imparted on the flat surface of the arrester disc and the sensor on the opposite face receives the signal propagated through the disc body. With the elapsed time the speed of propagation of the acoustic wave (celerity) in the ceramic block is determined.

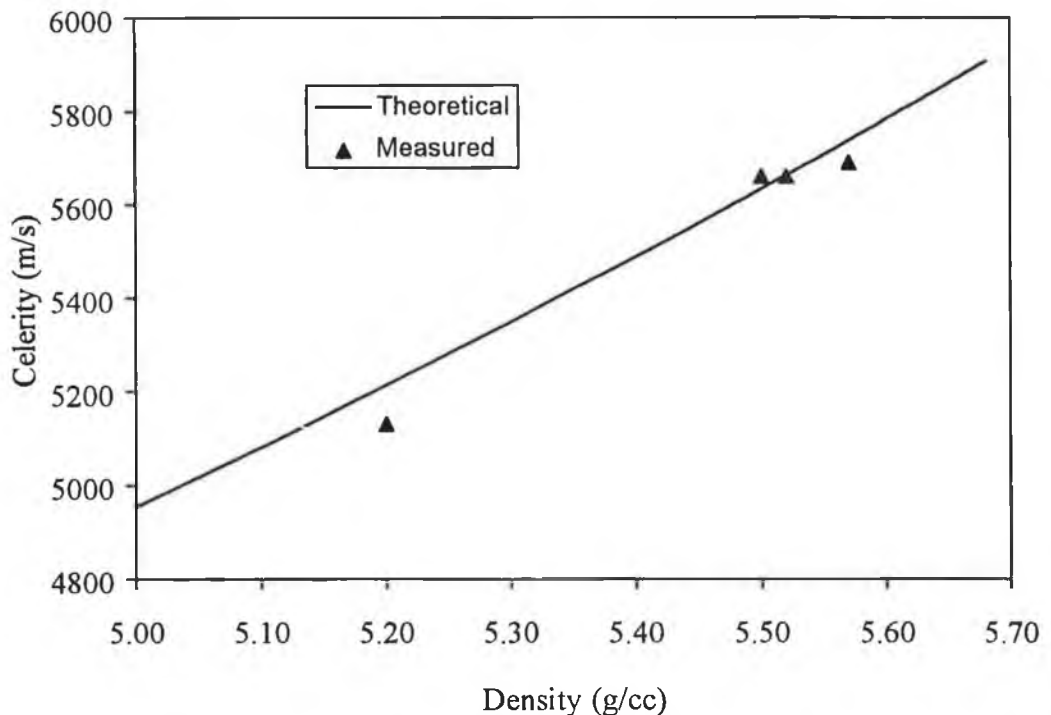


Figure 7.22. Theoretical and measured celerity of ZnO varistor material

The literature suggests that the pulse propagation is dependent on the basic bulk elastic properties and the density of the medium, not on its grain size. The elastic

modulus is also dependent on the porosity - increasing porosity decreases elastic modulus. In Figure 7.22 some of the available measured data [from an internal report] are inserted. The practically determined celerity is found to be in very good agreement with the theoretical results.

The fundamental relationship of the propagation of the stress waves in solids in terms of the elastic constants and density is verified for the zinc oxide varistor material. Grain size of material does not play any significant role. Experimental results obtained in the measurement of celerity are also supportive of this characteristic feature.

7.6.4 REFLECTION OF STRESS WAVES AND OBSERVED INFLUENCE IN HIGH CURRENT PULSE

When an elastic wave reaches a slip free boundary four waves are generated. Two of these are refracted into the second medium and two are reflected back as shown in Figure 7.23.

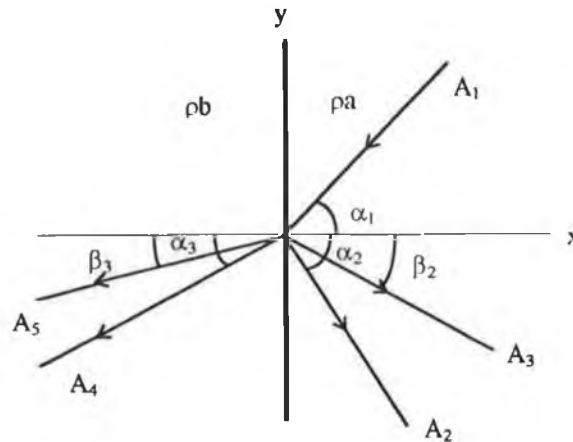


Figure 7.23 Reflection and refraction of incident dilatation wave at plane interface

But the waves of distortion A_3 and A_5 vanish¹⁰⁶, so that only dilatation waves are generated. The solution for the amplitude A_2 of the wave reflected back into the first medium is given by

$$A_2 = \frac{A_1(\rho_b c_3 - \rho_a c_1)}{(\rho_b c_3 + \rho_a c_1)} \dots\dots\dots(7.13)$$

So the amplitude of the reflected stress wave depends on the quantity $(\rho_b c_3 - \rho_a c_1)$ where ρ_a and ρ_b are the densities of the first and second medium and c_1, c_3 are the corresponding velocities of dilatation. It is apparent that no wave will be reflected at normal incidence when the product of the density and velocity is the same for the two media. This product ρc is sometimes known as the characteristic impedance of the medium. An experiment was carried out on the basis of this theory to evaluate the effect of supporting materials in the case of the test for high current. The results were found to be supportive of the prediction from the above proposition.

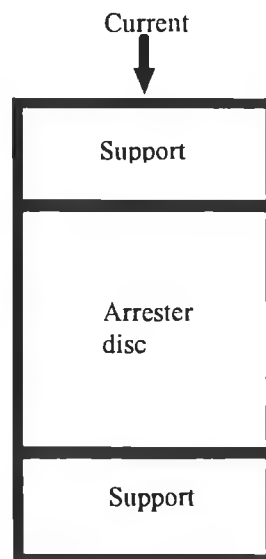


Figure 7.24 Arrangement of arrester block in HASD test

In the HASD test, the supporting blocks as shown in Figure 7.24 are usually made of aluminium, whose characteristic impedance, ρc is $1,706,400 \text{ gm.cm}^{-2}\text{s}^{-1}$. But for mild

steel the impedance is $4,633,200 \text{ gm.cm}^{-2}\text{s}^{-1}$. Now for the varistor material the characteristic impedance is $3,220,000 \text{ gm.cm}^{-2}\text{s}^{-1}$. So in the context of the equation 7.13, when aluminium block is used, the amplitude of reflected wave will change its sign and there will be no change in phase on reflection. But when mild steel will be used the situation will be opposite as its characteristic impedance is higher than that of the varistor material. So a test with mild steel support is expected to generate more reinforced stress wave resulting in more failures.

Test result

Twenty arrester blocks were randomly categorized into two groups - one of which was tested using the aluminium block while the other using the mild steel block as supports [Figure 7.22]. They were subjected to high current tests with increasing rated current until all the discs failed. The rated currents were 94, 99, 103, 105, 106 and 107 KA.

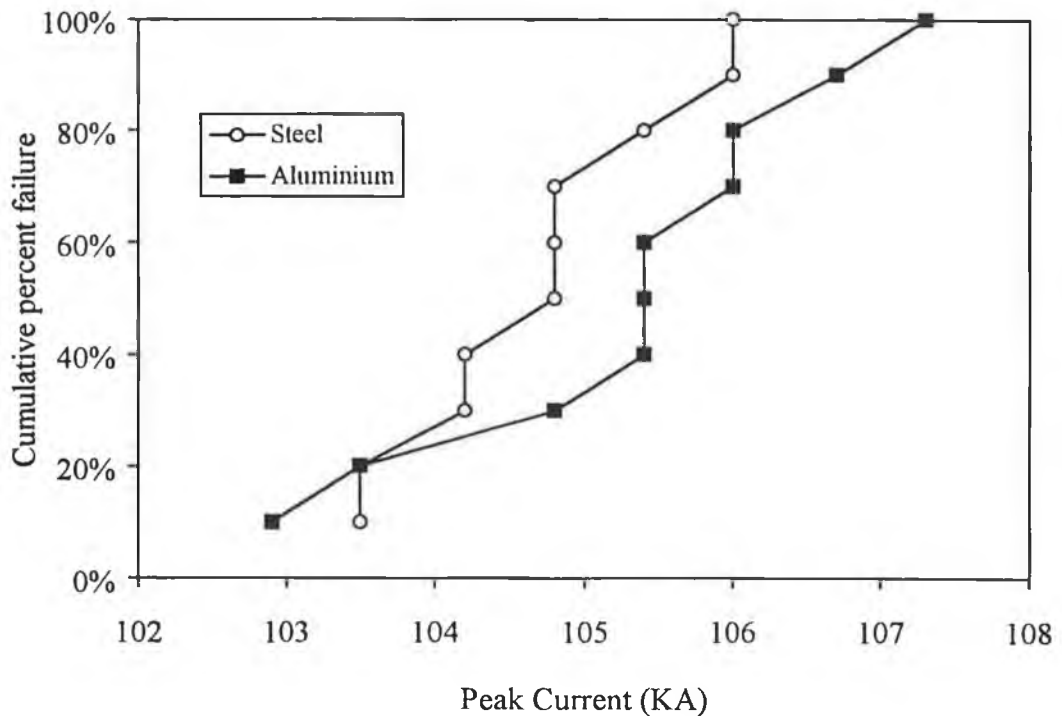


Figure 7.25 Effect of supporting material on the High Current Performance

The plot in Figure 7.25 shows the cumulative percent of failure as function of the actual recorded current at which the discs failed.

Observation and Discussion

The fractures of an arrester block initiated in the high current test may be prevented by adopting measures in the context of stress wave. Some kind of suitable reinforcement can be included in the formulation of the ZnO varistor which will enhance its mechanical strength. The selection of the passivation material should take into account the reflectance criterion.

Materials having a lower reflective index than the presently used glass could be helpful in reducing the amplitude of the reinforced waves reflected from the side surface of the disc. Probably this is one of the reasons for having an improved high current performance from the use of other kinds of passivating material. In terms of the characteristic impedance, choice of aluminium as the supporting block at the end of an arrester assembly stack appears to be appropriate.

Vibrations and other effects of stress wave developed during high current impulse are necessary to be considered to select the geometry of an arrester block. Selection of an arrester geometry should take into account its resonant frequency. Smaller height will maximize the resonant frequency of the disc and can help keep the failure rate in high current test to a minimum. This is actually observed in case of the test on a stack of smaller discs - as practically no failure is found to occur through 'waist failure'.

It is found that superior performance is achievable in HASD test when the arrester blocks are kept under higher pressure by applying load through the contact support. The better gripping or contact between the faces of the support and the arrester block is expected to be helpful in this regard. But there is a disadvantage of this arrangement. Arrester block kept under high pressure will increase the leakage current¹⁰ and eventually its life will be reduced.

Chapter 8

CONCLUSIONS AND RECOMMENDATIONS

8.1 CONCLUSIONS

The concluding remarks outlined here are based on the findings of the study conducted under specified experimental conditions.

8.1.1 COMPACTING PARAMETERS

Three major compacting parameters such as the peak pressure, speed of pressing and duration of dwell were considered. Two separate experiments were conducted - one involving the pressure and speed and the other with the duration of various dwells.

Pressure and Speed

The influence of pressure and speed maintained during compaction of varistor discs was evaluated in terms of the important physical and functional parameters of the varistor. The change of the functional parameters of the varistor due to the changes in the pressing variables is not very significant. The capillary force developed in the liquid phase sintering of the metal-oxide varistor material is very dominant which enhances the diffusion of the material and is attributed to minimize the effect of the green state variation.

Higher green density of the compact obtained by the application of high pressure does not significantly improve the electrical performances of the varistor. But there is a considerable deviation observed in the case of the fired dimension. Though pressing was performed in the same die, the compact having a higher green density led to a higher fired diameter of the disc. It may be mentioned here that due to the springback

effect, the diameter of the green discs pressed with a higher pressure was slightly greater.

Within a very small range of variation, a higher fired density of the discs was achieved as a result of higher pressure and greater speed during compaction. The effect of the pressing speed was found to be opposite for the green and the fired density. A higher pressing speed led to a lower green density but a higher fired density. This observation indicates that the air/oxygen trapped inside the powder due to the rapid pressing plays a positive role in this regard.

Increased fired density of a varistor does not lead to the improvement of all the electrical properties. A positive influence is observed in respect of the energy absorption capability, but with an adverse effect on the leakage characteristics. On the average there is a gain in energy due to the higher fired density. Discs pressed with the lowest pressure could not sustain energy up to the maximum limits attained by the two other categories. In this regard the medium pressure of 66 MPa appears to have a superior performance.

Comparison in terms of the median energy absorption capability shows that the improvement due to the increase in compacting pressure from medium to the high level is not as great as that from the low to the medium level. Therefore, it can be inferred from this observation that after a certain level of pressure (say, 60-80 MPa), the increase in compacting pressure may exhibit a little impact on the energy absorption capability.

In regards to the rate of compression or speed, it appears that neither too low nor too high a speed is appropriate for the improvement of energy absorption capability. The optimum speed range was found to lie between 40-60 mm per minute. However, if there is any dwell in the pressing cycle, the optimum speed range may be different.

Based on the experimental results functional relationships between the response and the input pressing parameters have been developed. Within the experimental limits of

the input parameters, it is possible to estimate the fired diameter and density, the mean energy absorption capability, nominal voltage, clamp ratio, watt-loss, exponent etc. from these predictive relationships.

Duration of Dwell in Pressing cycle

The influence of the dwell time in the pressing cycle is evident on the physical as well as on the electrical properties of arrester blocks. As a result of the variation in dwell the sintered diameter of the arrester blocks was found to vary within a small range but with consistency. The effects on the physical and electrical parameters can be estimated from the developed functional relationship.

Significant influence of different dwells was observed on the electrical parameters of the arrester blocks. However, no particular combination of dwells could lead to the improved performance for all the critical parameters. Among the various test cells, the pressing cycle accompanied by a longer press dwell and an ejection delay was found to be most suitable for energy absorption capability as well as the high current performance. However, under this set condition there is some negative influence observed in terms of the leakage.

In this study individual and interactive effects of the dwells have been estimated from the two-level factorial design of experiment. Pre-press dwell was found to affect negatively on the energy absorption capability. Most of its significant interactive effects were also found to be negative. So in the context of energy absorption capability of arrester it will be beneficial to keep the pre-press dwell to a minimum level that is the pressing cycle should not incorporate any pre-press dwell.

The control cell was pressed under standard conditions incorporating all the three dwells but with shorter duration. The performance of this cell was found to be very poor which can be attributed to the effect of the insufficient duration of dwell.

The preliminary observation of the influence of dwell in the pressing cycle was verified by the replication of two test cells. The trend was found to be supportive of the previous results. Moreover, in this experiment the recorded data on the location of the failure origin provides an additional information on the favourable result of the proper selection of dwell.

The test cell pressed with the optimum dwell did not exhibit any failure from the top face whereas for the other cells more than 45 percent failure took place from the top face. Since the top face is free of being contaminated from contact this difference in failure origin indicates that the superior quality of ceramic is achievable by compacting with an optimum pressing cycle. Thus it is obvious that properly pressed arresters will eventually be more capable if earlier failure from the bottom face can be delayed by some suitable methods.

8.1.2 SINTERING CONFIGURATION

The influence of sintering orientation on the physical properties of varistor was studied and some alternative methods were proposed to eliminate such adverse effects.

Sintering Orientation and Generation of Defects

Defects generated into the arrester blocks due to their sintering orientation have a deeper effect than normally perceived. The adverse effects arising from the bottom face cannot be eradicated by simply removing more materials by grinding. Most of the failures (usually more than two-thirds) were found to originate from the bottom face. Subsequent physical investigation also revealed the inherent weakness of the bottom part of an arrester block.

The discs were found to be harder at the bottom face leading to a poor grindability. Investigation revealed that there was a significant density gradient in the sintered body which could not be correlated with the green body density gradient generated as

a result of die pressing. In this respect the effect of the sintering orientation was very prominent resulting in the lowest density at the central part of the bottom face. The tensile strength by diametral compression was also found to be substantially lower in this location. The microstructural analysis exhibited a higher degree of porosity in this zone but with larger grain. Contamination arising from liquid bismuth during sintering also originate due to this orientation.

Alternative Sintering Configuration

Among the various alternative methods attempted, the smaller support system and the horizontal sintering on Vee-groove using spinel as the liner powder appear to be highly advantageous. Reduced frequency in regrinding from alternative methods is helpful in various aspects such as enhanced grinding wheel life and less material loss. Implementation of these methods will enhance the process capability and should allow to upgrade the rated energy absorption capability and high current performance of the arrester blocks. A solution of the tilting problem with the smaller support will make it even more attractive.

The horizontal sintering technique could prevent earlier failure with less density gradient and better geometry of the arrester discs. Moreover, there is a scope of skipping the grinding operation as the faces are obtained in a very good condition. In this method there will be no possibility of contaminating a disc from liquid bismuth as the inclined liner surface will not accumulate any such liquid. Additionally the liners could possibly be used for more cycles as they are less affected at the contact zone because of their inclined positions. Thus the horizontal sintering technique can be significantly advantageous in terms of process capability as well as cost.

8.1.3 INFLUENCE OF MARGIN ON ELECTRODE

The arresters belonging to BFFE (both face fully electroded) were found to be superior to those belonging to OFFE (one face fully electroded) in terms of the energy absorption capability. Moreover, the performance of the latter category was

better than the CONT group of arresters (both faces are electroded leaving a margin). Thus, the trend of the energy absorption capability as function of the margin in electrode is clear. However, if the passivation is not proper in terms of the quality and thickness, full electrode may result in poor performance. In this case incorporation of full electrode may result in a preferential path of current flow causing earlier failure. This kind of situation may lead to a wrong perception about the effect of full face electroding.

8.1.4 HEXAGON SHAPED DISCS

The increased energy absorption capability of the hexagonal discs processed from the cylindrical discs could be due to the resultant effect of both the removed bismuth coated surface and the increased surface to volume ratio.

In general the hexagonal cross-section of an arrester has two advantages over the cylindrical one. For the same volume of the varistor this geometry will allow more surface to volume ratio and will enable to be assembled both laterally and vertically. A higher surface to volume ratio will improve the stability for life in the steady-state operating condition of a varistor and is expected to have a longer life under the same operating conditions. The scope of lateral assembly will make the hexagonal disc more versatile to adjust the current carrying cross-section for different applications. This lateral assembly will greatly enhance the S/V ratio compared to the cylinder of equivalent cross-section.

With a standard size of hexagonal arrester block it will be possible to minimize the production cost as there will be no cost arising from the tool changing time for different processing operations.

8.1.5 FRACTURE MECHANISM IN HIGH CURRENT

The fracture mechanism of the arrester blocks during the high current test was identified as an effect of the stress wave propagation. High energy injection within a

very short time results in a stress wave with high amplitude. The failure modes observed resemble to those predicted by the theory. This understanding of the influence of stress wave in this regard will be helpful to effectively combat the situation by adopting appropriate measures.

The developed relationship of celerity with the elastic properties of the ZnO varistor material also supports the influence of stress wave. Measurement of the celerity alone by the LASER technique may not be sufficient to detect the defects in the ceramic and identify the defective parts. However, this technique can be suggested for utilization to accurately evaluate the elastic properties of various materials in an easier way.

8.2 THESIS CONTRIBUTION

- Relationship has been developed to predict the important physical and electrical parameters of a varistor as a function of compacting pressure and speed.
- Through a two-level factorial design the influence of dwell in pressing cycle was correlated with the critical parameters of the arrester block.
- Optimum dwell was identified for a particular type of arrester block in terms of the energy absorption capability and high current performance.
- It was established that the extent of the influence of sintering orientation does not remain confined within the shallow depth of the bottom face but it has a far reaching effect than normally anticipated.
- The stress wave theory was indicated to be an appropriate approach in analysing the fracture mechanism observed in case of high current test.
- The analytically evaluated speed of stress wave propagation through ZnO varistor material was closely correlated with the measured celerity by a laser technique.
- An alternative design with hexagonal shape is proposed for the arrester which could be advantageous in various respects.
- A new sintering configuration was attempted, and verified to be an advantageous method over the conventional practice.

- The method of full face electrode (keeping no margin at the periphery) of the arrester block was verified to be conducive to the increased energy absorption capability.
- The density gradient, variation in hardness, difference in mechanical strength, grain size and porosity of the fired disc were found to be a resultant effect of the sintering orientation.

8.3 RECOMMENDATIONS FOR FURTHER WORK

The recommendations proposed here are intended as guidelines for further work to qualify and establish new methods for the improvement of the varistor performance.

8.3.1 COMPACTING PARAMETERS

Future experiments with the compacting parameters can be conducted with a larger sample size. Under the specified condition, there were five discs in a cell for this study. A larger sample size is expected to provide more reliable central values of the investigated parameters.

There were seven levels of pressing speed with three levels of pressure. In future experiment selection of smaller steps with more pressure ranges can be advantageous to locate the optimum level with better resolution.

Some additional compacting parameters can be included for future work. In this respect the aspect ratio of a compact, the use of lubricant in different fractions as pressing aid can be analysed. The variation in performance due to the compacting parameters may be different if the powder is processed using different organic binder other than PVA/PEG. Investigation may be carried out with latex and a number of other binder systems.

The role of green density on the sintering cycle time can be investigated by the rate controlled sintering technique. For a particular shrinkage rate a disc with a higher

green density is expected to require less time to completely shrink for achieving the same target fired density. Thus the total sintering cycle time could be reduced. In this regard application of a higher load for higher green density could be advantageous.

Further investigation with dwell can be carried out to finely tune the duration of dwell with respect to the energy absorption capability and other functional parameters. Moreover, longer duration of dwell can be selected to carry out the experiment. A design of experiment with a second-order response surface methodology can be adopted to investigate the effects of dwell. This will also be helpful in developing more reliable functional relationships.

Dwell in pressing cycle can be optimized for other categories of discs. The volume of powder to be pressed for a disc is considered to be an important factor in selecting the duration of dwell. It is, therefore, recommended to carry out experiment for individual category of arrester blocks to optimize the pressing cycle.

8.3.2 ALTERNATIVE SINTERING CONFIGURATION

The two proposed methods should be verified with a larger sample size for possible implementation. In this respect the design of appropriate sagger geometry could be helpful to place and support the arrester blocks.

8.3.3 HEXAGONAL DISCS

The enhanced performance of the hexagonal discs could be due to the combined effect of the removal of bismuth-rich surface and the higher surface to volume ratio. The extent of the individual effect can be verified. Comparison of the performance of the cylindrical discs and those made from them by removing the surface using cylindrical grinding will reveal the effect of the removal of the skin. The performance of the sintered hexagonal discs processed from a green state using a hexagonal die can be compared with the standard disc to quantify the effect of S/V ratio.

Considering the observed and envisaged benefits from the standard size hexagonal disc an elaborate study is recommended to verify the scope of the proposed assembly.

8.3.4 STRESS WAVE PROPAGATION

The physical dimensions of the arrester blocks should be designed not only on the basis of the current-voltage requirements but also on the basis of their resonant frequencies. Taller discs will have lower frequency of resonance and will be susceptible to waist failure by the first mode of bending. A lower fired density will also reduce the Young's modulus and will initiate earlier failures through this mode.

Passivating materials having lower reflective index should be conducive to suppress the reinforced amplitude of the reflected stress waves from the side. In this respect use of materials having requisite properties can be attempted as more suitable alternatives.

Improving the mechanical strength of the arrester material can be another approach to combat the fracture in high current test. Inclusion of some reinforcement in the metal-oxide power such as SiC or glass frit may be beneficial in this regard. A study can be undertaken to investigate the scope of such enhancement.

REFERENCES

- [1] M. Matsuoka, "Nonohmic Properties of Zinc Oxide Ceramics" *Jpn. J. Appl. Phys.*, Vol. 10, No. 6, pp. 736 - 46, 1971.
- [2] F. Gosauter, R. Perkins, M. Rossinell and F. Schmuckle , "The Metal Oxide Resistor - at the Heart of Modern Surge Arresters" *ABB Review* 1/89, Surge Arresters, Switzerland
- [3] M. Matsuoka, "Progress in Research and Development of Zinc Oxide Varistors" pp. 290 in *Advances in Ceramics, Vol. 1, Grain Boundary Phenomena in Electronic Ceramics*. Edited by L. M. Levinson and D. Hill, Am Ceram Society, Columbus, OH, 1981.
- [4] F. D. Martzloff and L. M. Levinson, "Surge Protective Devices" pp. 274 in *Advances in Ceramics, Vol. 1, Grain Boundary Phenomena in Electronic Ceramics*. Edited by L. M. Levinson and D. Hill, Am Ceram Society, Columbus, OH, 1981.
- [5] K. Eda, "Zinc Oxide Varistors" *IEEE Electrical Insulation Magazine*, Vol. 5, No. 6, pp. 28-41, 1989.
- [6] A. Lagrange, "Present and Future of Zinc Oxide Varistors" *Electronic Ceramics*, Edited by B.C.H. Steele, pp. 1-27, *Elsivier Applied Science*, London and New York
- [7] R Puyan , "Applications and Product Development in Varistor Technology" *J. Material Science*, Vol. 55, pp. 268-277, (1995).
- [8] W C Hart and E W Malone, "Lightning and Lightning Protection", Don White Consultants, Inc, 1988
- [9] "Transient Voltage Suppression Devices 1995", a Databook Published by Harris Semiconductor, Melbourne, FL 32902, USA.
- [10] Tapan K. Gupta, "Application Of Zinc Oxide Varistors" *J. Am. Ceram. Soc.* 73 (7) pp. 1817-1840, 1990.
- [11]. J Fan and R. Freer, "Improvement of the Non-linearity and Degradation Behaviour of ZnO Varistors" *Br. Ceram. Trans.* 92, No 6, pp.221-26, 1993.
- [12] W. C. Richmond, "ZnO based Varistors: AC Model and Characteristics", pp. 425-37, 1981.
- [13] R. Einzinger, "Metal Oxide Varistors" *Ann. Rev. Mater. Sci.* Vol. 17, pp. 299-321, 1987.

- [14] M Matsuoka, T Masuyama and Yoshio Iida, "Nonlinear Electrical Properties of Zinc Oxide Ceramics" Proc. 1st Con. on Solid State Devices , Vol. 39, pp. 94-101, Tokyo, 1969.
- [15] G. E. Pike, "Electronic Properties of ZnO Varistors: A New Model", in "Grain Boundary in Semiconductors", Published by Elsevier Publishing Company, pp. 369-379, 1982.
- [16] G.D. Mahan, "Theory of ZnO Varistors", in "Grain Boundary in Semiconductors", Elsevier Science Publishing Company, Inc., pp. 333-341, 1982.
- [17] V. F. Katkoy, A. I. Ivon, V. O. Makarov, I. M. Chernenko, "Structure Formation in Zinc Oxide Ceramic" Translated from Izvestiya Akademii Nauk SSSR, Neorganicheskie Materialy, Vol. 24, No. 8, pp. 1358-1363, Aug. 1988, 1989 Plenum Publishing Corporation
- [18] Ai Bui, H T Nguyen and A Loubiere, "High-Field ZnO-based Varistors", J. Phys. D: Appl. Phys. Vol. 28 , pp.774-782, 1995. IOP Publishing Ltd.
- [19] T Asokan, G. N. R. Iyengor and G. R. Nagabhushara, "Studies on Microstructure and Density of Sintered ZnO-based Non-linear Resistors" J. Mat. Sc. 22 (1987) 2229-2236.
- [20] T. Takemura, M. Kobayashi, Y. Takada, and K. Sato "Effect of Bismuth Sesquioxide on the Characteristics of ZnO Varistors", J. Am. Ceram. Soc., 69 [5], pp. 430-36, (1986).
- [21] H Kanai, M Imai, "Effects of SiO₂ and Cr₂O₃ on the Formation Process of ZnO Varistors" J. Mat. Sc., Vol. 23, pp. 4379-4382, 1988.
- [22] T. Miyoshi, K Maeda, K. Takahashi and T. Yamazaki, "Effects of Dopants on the Characteristics of Zinc Oxide Varistors" pp. 309 in "Advances in Ceramics", Vol. 1, Grain Boundary Phenomena in Electronic Ceramics. Edited by L. M. Levinson and D. Hill, Am Ceram Society, Columbus, OH, 1981.
- [23] J. M. Driear, J. P. Guertin, T.O. Sokoly and L B Hackney, "Effect of Dopant Valence State on the Microstructure of ZnO Varistors", pp. 317 in "Advances in Ceramics", Vol. 1, Grain Boundary Phenomena in Electronic Ceramics. Edited by L. M. Levinson and D. Hill, Am Ceram Society, Columbus, OH, 1981.
- [24] K. Mukae and I. Nagasawa, "Effect of Praseodymium oxide and Donor Concentration in the Grain Boundary Region of ZnO Varistors", p 331 in "Advances in Ceramics", Vol. 1, Grain Boundary Phenomena in Electronic Ceramics. Edited by L. M. Levinson and D. Hill, Am Ceram Society, Columbus, OH, 1981.

- [25] Y. C. Chen and C. Y. Shen, "Grain Growth Processes in ZnO Varistors with Various Valence States of Manganese and Cobalt", *J. Appl. Phys.*, 69(12), 15 June, 1991.
- [26] T. K. Gupta, "Donor Doping of Ga in ZnO Varistor Grain Boundary" *J. Mater. Res.* Vol. 9, No. 9, pp. 2213-215, Sep 1994.
- [27] T. Takemura, M. Kobayashi, Y. Takada, and K. Sato "Effects of Antimony Oxide on the Characteristics of ZnO Varistors", *J. Am. Ceram. Soc.*, 70 [4], pp. 237-41, (1987).
- [28] W.G. Carlson and T. K. Gupta, "Improved Varistor Non-linearity via Donor Impurity Doping", *J. Appl. Phys.*, Vol. 53, No. 8, pp 5746-5753, August 1982.
- [29] T K Gupta, "Effect of Minor Doping on the High Current Application of the ZnO Varistor", *Ferroelectronics*, Vol. 102, pp 391-396, 1990.
- [30] E. Olsson and G. L. Dunlop, "Development of Intergranular Microstructure in ZnO Varistor Materials" *High Tech Ceramics* edited by P Vincenzini, Elsevier Science Publishers B. V., Amsterdam, 1987, pp 1765-1774
- [31] H. Cerva and W. Russwurm, "Microstructure and Crystal structure of Bismuth Oxide Phases in Zinc Oxide Varistor Ceramics", *J. Am. Ceram. Soc.*, 71 [7], pp. 522-30, (1988)
- [32] E. Olsson, G. Dunlop and R. Osterlund, "Development of Functional Microstructure during sintering of a ZnO Varistor Material", *J. Am. Ceram. Soc.*, 76 [1], pp. 65-71, (1993).
- [33] T. K. Gupta "Influence of Microstructure and Chemistry on the Electrical Characteristics of ZnO Varistors", pp. 493-507, in *Tailoring Multiphase and Composite Ceramics*, Ed. by R. E. Tressler, G. L. Messing, C. G. Pantino and R. E. Newnhan, Plenum, New York, 1986.
- [34] S. Hamsphire and J. Coolican, "Microstructural Characterization of Zinc Oxide Varistors", in "High Tech. Ceramic", Ed. by P. Vincenzini, Elsevier Science Publishers, B. V., Amsterdam, pp. 1833-40, 1987.
- [35] R. A. Sargent, G. L. Dunlop and M. Darveniza, "Effects of Multiple Impulse Currents on the Microstructure and the Electrical Properties Of Metal Oxide Varistor", *IEEE Transactions on Electrical Insulation*, Vol. 27, No. 3, pp. 586-92, June, 1992.
- [36] G. D Mahan, L.M. Levinson and H. R Phillip, "Single Grain Junction Study of ZnO Varistors" *J. Appl. Phys.* Vol 33, No. 9, Nov. 1, pp 830-832, 1978
- [37] J. O. Levine, "Theory of Varistor Electronic Properties", *CRC, Critical Reviews in Solid State Sciences*, Vol. 5, pp 597-608, 1975

- [38] K. Eda, A. Iga, and M. Matsuoka, "Degradation Mechanism of Non-ohmic Zinc Oxide Ceramics", *J. Appl. Phys.* Vol 51, pp 2678-2684, 1980.
- [39] L. Hower, and T.K. Gupta, "A Barrier Model for ZnO Varistors", *J. Appl. Phys.* 50, pp. 2799-812, 1979.
- [40] E. Saksaug, J. Burke and J. Kresge, "IEEE Transactions on Powder Delivery, Vol. 4, No. 4, Oct., 1989.
- [41] W. N. Lawless and T. K. Gupta, "Thermal Properties of Pure and Varistor Zinc Oxide at Low Temperature", *J. Appl. Phys.*, 60 [2], pp. 607-11, 1986.
- [42] J. Ozawa, et al, "IEEE Transaction on Powder Apparatus and Systems", Vol. PAS-102, No. 5, May, 1993.
- [43] N. Amiji, et al., *Advanced Ceramic Materials*, 1[3], pp. 232-36, 1986.
- [44] K. Eda "Destruction Mechanism of ZnO Varistors Due to High Currents", *J. Appl. Phys.*, 56(10), 15 Nov., pp. 2948-55, 1984.
- [45] K. Eda, A. Iga and M. Matsuoka, "Current Creep in Non-ohmic ZnO Ceramics" *Jpn. J. Appl. Phys.*, 18 [5], pp. 997-98, 1979.
- [46] B. Hoffmann and U. Schwing, "Low-Voltage Varistors", pp.343, in *Advances in Ceramics, Vol. 1, Grain Boundary Phenomena in Electronic Ceramics.* Edited by L. M. Levinson and D. Hill, Am Ceram Society, Columbus, OH, 1981.
- [47] N. Shohata, T. Matsumura, K. Utsunao and T. Ohno, "Properties of Multilayer ZnO Ceramic Varistors", pp. 439 in *Advances in Ceramics, Vol. 1, Grain Boundary Phenomena in Electronic Ceramics.* Edited by L. M. Levinson and D. Hill, Am Ceram Society, Columbus, OH, 1981.
- [48] S. Kalpakjian, "Manufacturing Process for Engineering Materials", Addison Wesley Publishing Companies, July, 1985. (1S)
- [49] J. S. Reed, "Introduction to the Principles of Ceramic Processings", John Wiley and Sons, 1988.
- [50] R. A. Haber and P. A. Smith, "Overview of Traditional Ceramics", *Engineered Materials Handbook*, Vol. 4, pp. 3-14, 1991.
- [51] D. C. Craner, "Overview of Technical, Engineering, and Advanced Ceramics", *Engineered Materials Handbook*, Vol. 4, pp. 16-20, 1991.
- [52] O. N Losevic, D. Uskokovic et al., "Synthesis of ZnO Based Varistor Precursor Powders by Reaction Spray Process", Chapman and Hall, PP. 5211-17, 1993.

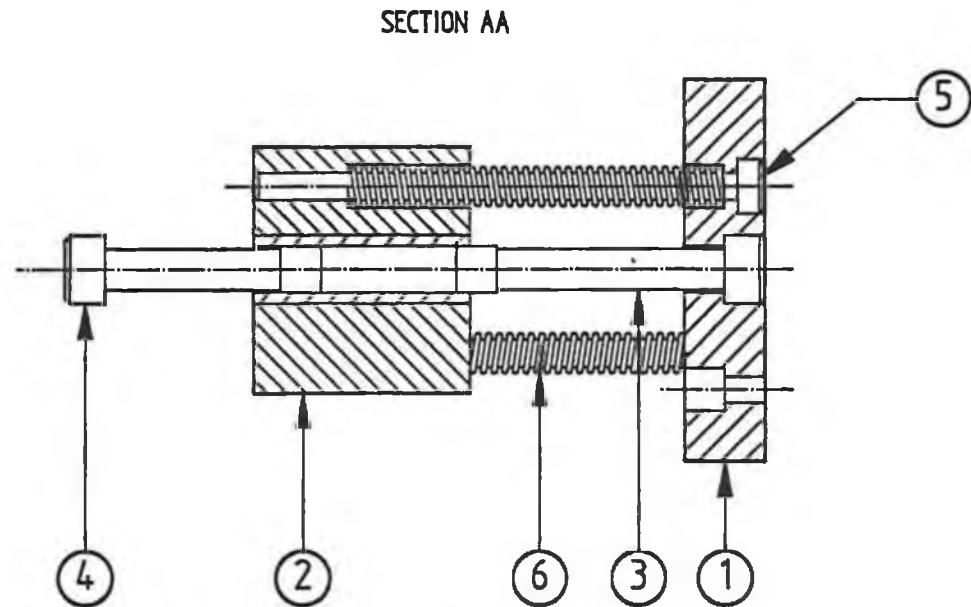
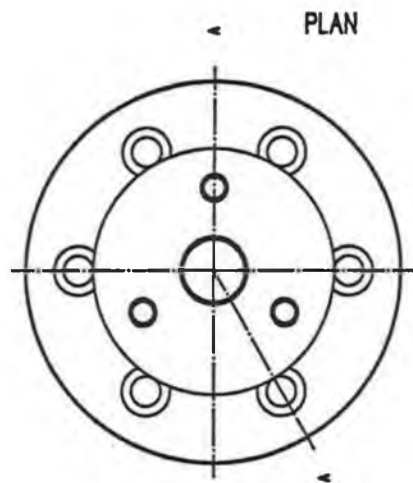
- [53] J. P. Gambino, et al. "Grain Boundary Electronic States in Some Simple ZnO Varistor", *J. Appl. Phys.*, Vol. 61, No. 7, April 1, 1987.
- [54] W. D. Kingery, "Grain Boundary Phenomena in Electronic Ceramics", in "Advance in Ceramics", Vol. 1, pp. 1-22, 1981.
- [55] R. Einzinger, "Grain Boundary Properties in ZnO Varistors", in "Advances in Ceramics", Vol. 1, pp. 359-373, Ed. by L. M. Levinson and D. C. Hill, Columbus, Ohio, 1980.
- [56] H. T. Nguyen, A. Bui and A. Loubiere, "Role of Additives in the High-Field ZnO-Based Varistors", *J. Physc. D: Appl. Phys.*, pp. 601-604, 1995.
- [57] N. Ichinose and Y. Tanno, "Electrical Properties of ZnO Varistors Containing Metallic Zinc" Grain Boundary Phenomena in Electronic Ceramics. Edited by L. M. Levinson and D. Hill, Am Ceram Society, Columbus, OH, 1981.
- [58] T. K. Gupta and A. C. Miller, "Improved Stability of the ZnO Varistor via Donor and Acceptor Doping at the Grain Boundary", *J. Mater. Res.*, 3(4), pp. 745-54, Jul/Aug, 1988.
- [59] T. K. Gupta, "Microstructural Engineering Through Donor and Acceptor Doping in the Grain and Grain Boundary of a Polycrystalline Semi-conducting Ceramic", *J. Mater. Res.*, Vol. 7, No. 12, pp. 3280-3294, Dec., 1992.
- [60] Y. Yano, Y. Takai, and H. Morooka, "Interface States in ZnO Varistor with Mn, Co and Cu Impurities", *J. Mater. Res.*, Vol. 9, No. 1, pp. 112-118, 1994.
- [61] K. Eda, M. Inada and M. Matsuoka, "Grain Growth Control in ZnO Varistors Using Seed Grains", *J. Appl. Physc.*, 54(2), pp. 1095-1099, 1983.
- [62] A Smith, Y. Boyat, J. F. Baumaro, and P. Abelard, "Effect of MgO Addition on a ZnO Varistor Composition", in "Euro-Ceramics" Vol. 2, Edited by G. de With, R. A. Terpstra and R. Metselaar, Elsevier Applied Science, pp. 2.225-2.229, 1989.
- [63] T Asokan and R Freer, "Hot Pressing of Zinc Oxide Varistors", *Br. Ceram. Trans. J.*, 89, 8-12, 1990.
- [64] R M German, "Powder Metallurgy Science", Metal Powder Industries Federation, Princeton, New Jersey, USA, 1984.
- [65] W. Kirsop, "Fundamentals of Tablet Compression", *Supt. No. 19, Aus. J. Pharmacy*, Vol. 45, No. 535, July 30, 1964.
- [66] K. Uematsu, M. Miyashita, J. Kim, Z. Kato and N. Uchida, "Effect of Forming Pressure on the Internal Structure of Alumina Green Bodies Examined with Immersion Liquid Technique", *J. Am. Ceram. Soc.*, 74, [9], pp. 2170-74, 1991.

- [67] J. Van Der Zwan, and C. A. M. Siskens, "The Compaction and Mechanical Properties of Agglomerated Materials", Powder Technology, Netherlands, pp. 43-54, 1982.
- [68] B. Bergman, K. Breder and M. Petersson, "Relationship between Green and Fired Strength of Al₂O₃ with Controlled Defects", Euro-Ceramics, Processing of Ceramics, Edited by G. de With, R. A. Terpstra and R. Metselaar, Vol. 1, Elsevier Applied Science, London and New York.
- [69] K. Kendall, N. McNalford and J. D. Birchall, "The Strength of Green Bodies", Br. Ceram. Proc., No. 37, pp. 255-265, 1988.
- [70] Y. Aketa, Y Tanaka and H Tsuwa, "Studies on Compacting of Metal powder", Tech. Report, Osaka University, 15, pp. 81-94, 1965. (54)
- [71] R. W. Heckel, "Density-Pressure Relationship in Powder Compaction", Trans. Matt. Soc., AIME, Vol. 221, pp. 671-75, Aug., 1961.
- [72] R.G. Frey and J. W. Halloran, "Compaction Behavior of Spray Dried Alumina", J. Am. Ceram. Soc., Vol. 67, No. 3, pp. 199-203, 1984.
- [73] S. Stribos and P. A. Vermer, "Stress and Density Distributions in the Compaction of Powders", Vol. 11, Ed. by M. Palmour III, R. F. Davis, and T. M. Mare, pp. 113-123, 1978.
- [74] A. D. Rosato, T. Vreeland, Jr. and F. B. Prinz, "Manufacture of Powder Compacts", International Material Reviews, Vol. 36, No. 2, pp. 45-61, 1991.
- [75] E. N. Hiestand, "Tablet bond. I. A Theoretical Model", Int. J. Pharm., 67, pp. 221-229, 1991.
- [76] E N Hiestand and D P Smith, "Three Indices for Characterizing the Tableting Performance of Materials", Chemabs, Vol. 9, pp. 47-57, 1984.
- [77] E. Turba, "The Behaviour of Powders Compacted in a Die", Proc. Br. Ceram. Soc., "Fabrication Science", No. 5, Oct., 1965.
- [78] D. Train , M. C. B. Pharm, "Transmission of Forces Through a Powder Mass During the Process of Pelleting", Trans. Instn Chem. Engrs, Vol. 35, pp. 258-266, 1957.
- [79] C. L. Huffine and C. E. Bonilla, "Particle-Size Effects in the Compression of Powders", A. I. Ch.E. Journal, Vol. 8, pp. 490-493, Sep., 1962.
- [80] R. A Dimilia and J S Reed, "Dependence of Compaction on the Glass Transition Temperature of the Binder Phase", Ceram. Buln., Vol. 62, No. 4, pp. 484-488, 1983.(45)

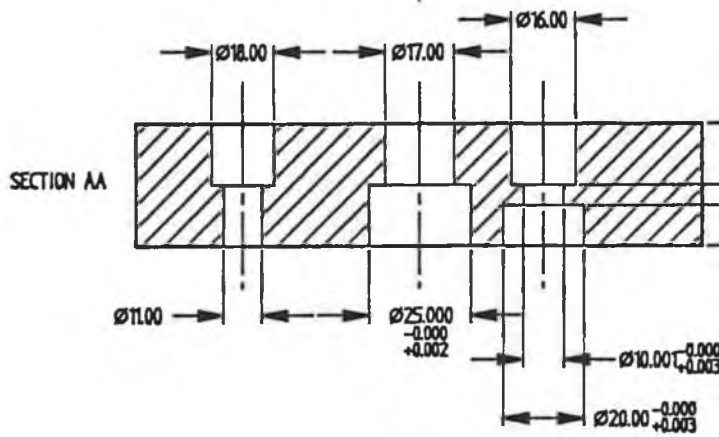
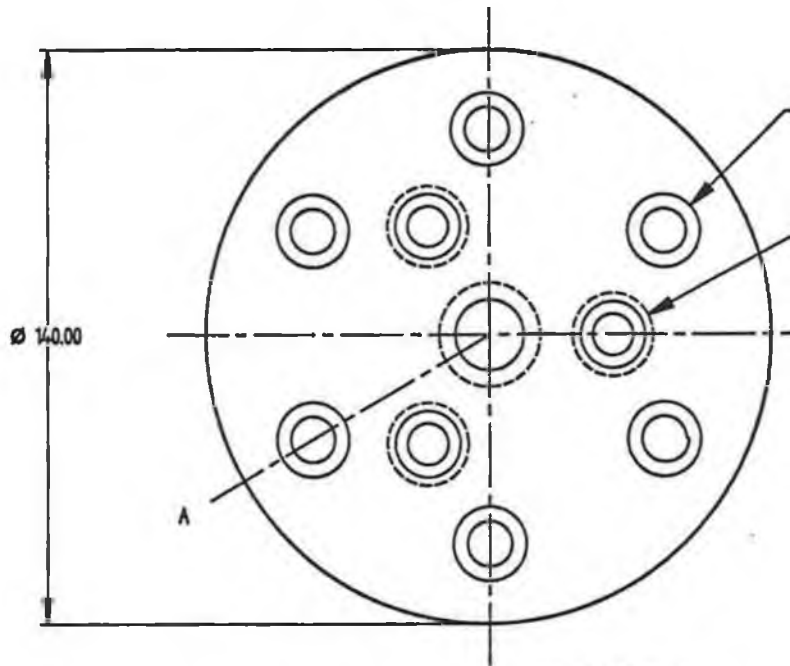
- [81] A. P. S. Reymer, "Dry Pressing of Ceramic Powders", Euro-Ceramics, Processing of Ceramics, Edited by G. de With, R. A. Terpstra and R. Metselaar, Vol. 1, pp. 1.253-1.257, Elsevier Applied Science, London and New York.
- [82] A. R. Cooper Jr, and L. E. Eaton, "Compaction Behaviour of Several Ceramic Powders", J. Am. Ceram. Soc., Vol. 45, NO. 3, pp. 97-101, 1962.
- [83] R. A. Youshaw and J. W. Halloran, "Compaction of Spray-Dried Powders", Ceram. Buln., Vol. 61, NO. 2, pp. 227-230, 1982.
- [84] B. Nyberg, E. Carlström, M. Persson and R. Carlsson, "Uniform Distribution of Pressing Aid", Proc. of 2nd Int. Conf. on Ceramic, pp. 573-80, 1988.
- [85] R. A. Dimilia and J.S. Reed, "Stress Transmission During the Compaction of a Spray-Dried Alumina Powder in a Steel Die", J. Am. Ceram. Soc., Vol. 66, No. 9, pp. 667-72, 1983.(06RP62), (78)
- [86] D. W. Richerson, "Modern Ceramic Engineering-Properties, Processing and Use in Design", Mercel Dekker. Inc., 1982.
- [87] S. Stribos, "Powder-Wall Friction: The Effects of Orientation of Wall Grooves and Wall Lubricants", Powder Tech., 18, pp. 209-214, 1977.
- [88] P. J. Jame, "Powder Metallurgy Review: Fundamental Aspects of the Consolidation of Powder", Powder Mett. Inter., Vol. 4, No. 4, pp. 193-198, 1972.
- [89] G Anderson, "Creep Experiments on Powder", Scand. J. Mett., 12, pp. 312-14, 1983.(82)
- [90] E. Lehfeldt, "The Effect of Ultrasonic Vibrations on the Compacting of Metal Powders", Ultrasonics, pp. 219-223, Oct., 1967.
- [91] E Emeruwa, J Jarrige, J Mexmain, "Ferrite Powder Compaction with Ultrasonic Assistance", Euro-Ceramics, Processing of Ceramics, Edited by G. de With, R. A. Terpstra and R. Metselaar, Vol. 1, pp. 1.249-1.252, Elsevier Applied Science, London and New York(90)
- [92] K. T. Kim and G. Son, "Cyclic Compaction of Ceramic Powders", J. Am. Ceram. Soc., 75 [11], pp. 3157-59, 1992.
- [93] S Clyens and W Johnson, "The Dynamic Compaction of Powdered Materials", Material Science and Engineering, 30, pp. 121-139, 1977. (153)
- [94] M. L. Huckabe, M. J. Paisley and R. L. Russell "RCS-Taking the Mystery out of Densification Profiles", Am. Ceram. Buln., Vol. 73, No. 9, pp. 82-86, 1994.

- [96] R E Walpole, Introduction to Statistics, 3rd edition, Mcmillan Publishing Co., Inc., New York, 1982, p-57
- [97] G. E. P. Box, W. G. Hunter and J. S. Hunter, "Statistics for Experiments-An Introduction to Design, Data Analysis and Model Building", John Wiley and Sons, 1978.
- [98] T. K. Gupta, "Effect of Material and Design Parameters on the Life and Operating Voltage of a ZnO Varistor", J. Mater. Res. 2(2), Mar/Apr 1987, pp 231-238
- [99] X.S. Li, and I.M. Low, "Grinding of Engineering Ceramics with Diamond Wheels", Key Engineering Materials Vols, 53-55, pp.307-312, (1990), Copyright Trans Tech Publications, Switzerland.
- [100] N.J. McCormick, E A. Almond, "Edge Flaking of Brittle Materials", J of Hard Materials, Vol.1, No.1, pp25-51, 1990, UK
- [101] Operating Manual, Leitz Miniload 2, - Microhardness Tester for Vickers, Knoop and Scratch Hardness, Germany.
- [102] I. J. McColm, "Ceramic Hardness", Plenum Press, New York, 1990, p-267
- [103] M. J. Mayo., "Nanoindentation of Nanocrystalline ZnO", J. Mater. Res., Vol. 7, No. 4, pp973-979, 1992.
- [104] R. M. German, "Liquid Phase Sintering", Plenum Press, New York, 1985
- [105] James R Evans, "Statistical Process Control for Quality Improvement", Prentice Hall, Eaglewood Cliffs, New Jersey 07632
- [106] H Kolsky, "Stress Waves in Solids" Dover Publications, Inc.1963.

APPENDIX A
ASSEMBLY DRAWING OF FLOATING DIE



ITEM No.	COMPONENT NAME	MATERIAL	QUANTITY
1.	BASE	D - 2	1
2.	DIE BODY	D - 2 , WC	1
3.	LOWER PUNCH	D - 2 , WC	1
4.	UPPER PUNCH	D - 2 , CW	1
5.	GUIDE PIN	D - 2	3
6.	SPRING		3
7.	EJECTION BLOCK	S/STEEL	1
8.	SINGLE ACTION BLOCK	S/STEEL	2

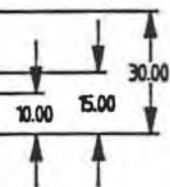


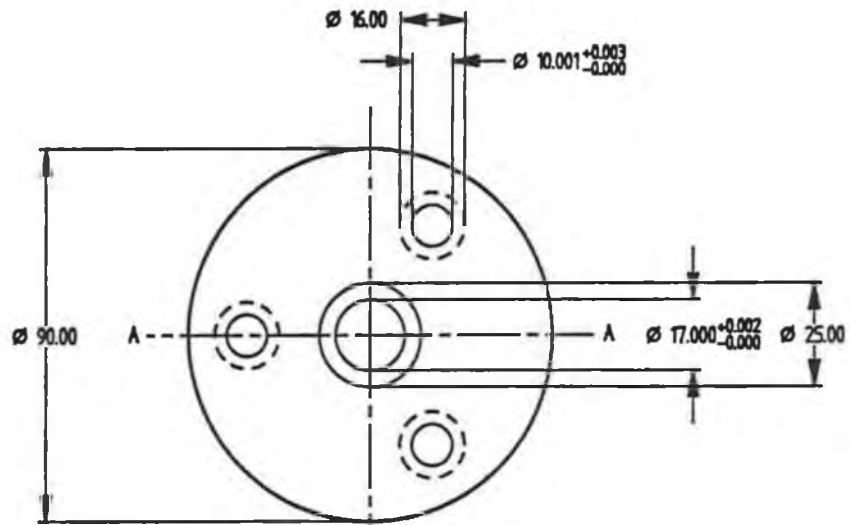
PITCH CENTER RADIUS = 50.50

PITCH CENTER RADIUS = 30.50

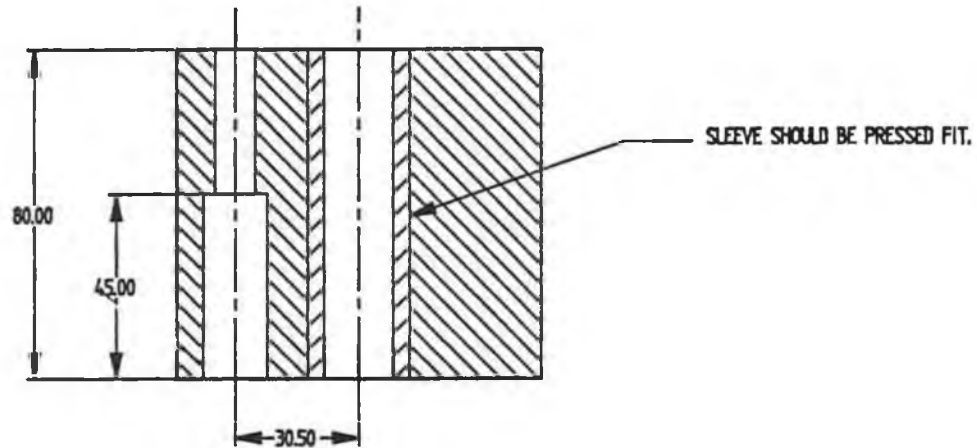
A

PART # 1 - BASE
MATERIAL - D-2
01-01-02
25/91 D-2
T380680-C4
HI - LIFE
ONE PER ASSEMBLY.

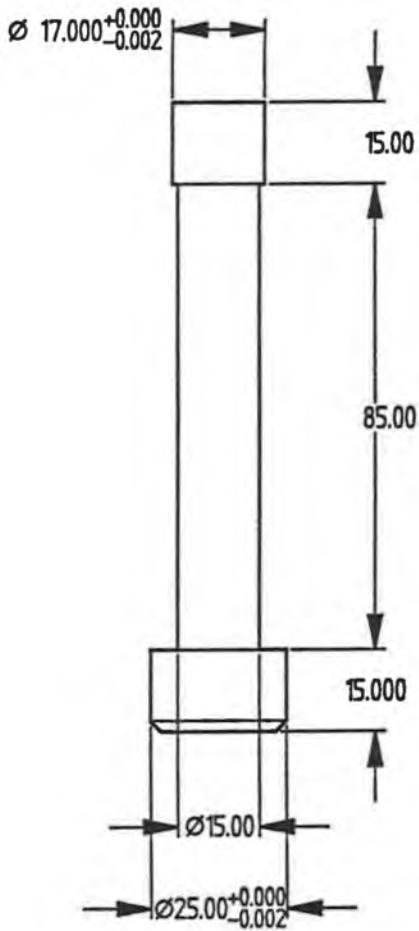




PART #2 - DIE BODY.
 MATERIAL - D-2 FOR BODY
 WC FOR CYLINDRICAL SLEEVE
 ONE PER ASSEMBLY.



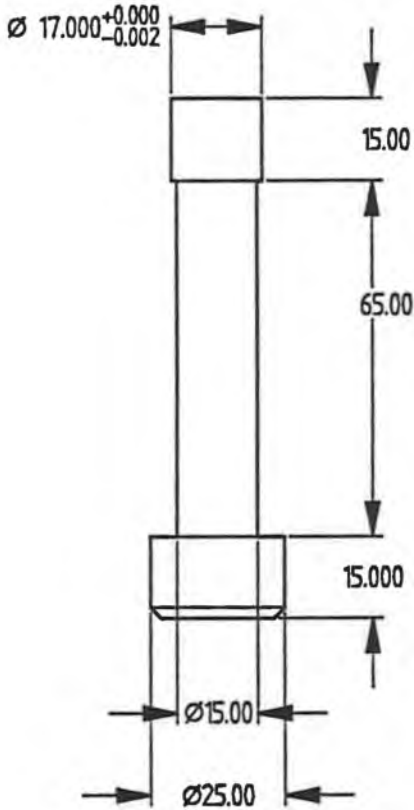
SECTION AA



PART # 3 - LOWER PUNCH
MATERIAL - D-2 FOR BODY
WC FOR INSERT AT TIP.

01-03-04
25/91 D-2
T380682 - 25
HI - LIFE

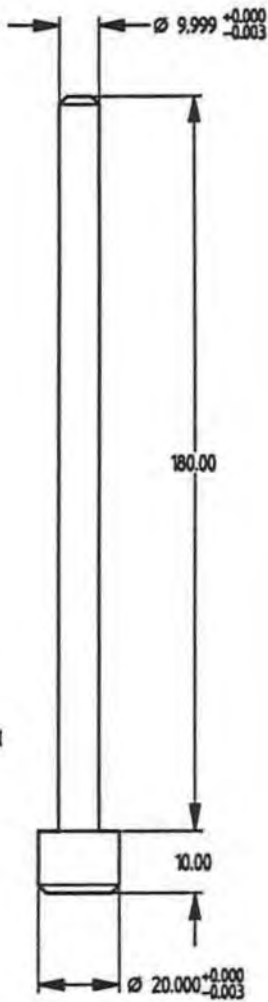
LOWER PUNCH



PART # 4 - UPPER PUNCH
MATERIAL - D-2 FOR BODY
WC FOR INSERT AT TIP.

01-07-0
25/91 D-2
T380682 - C4
HI - LIFE

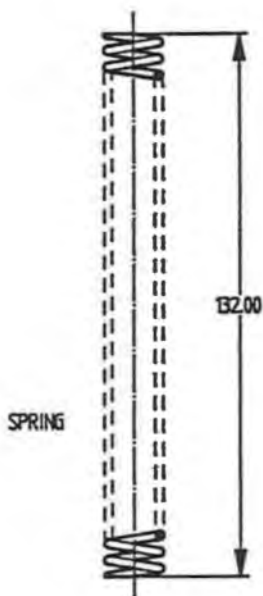
UPPER PUNCH



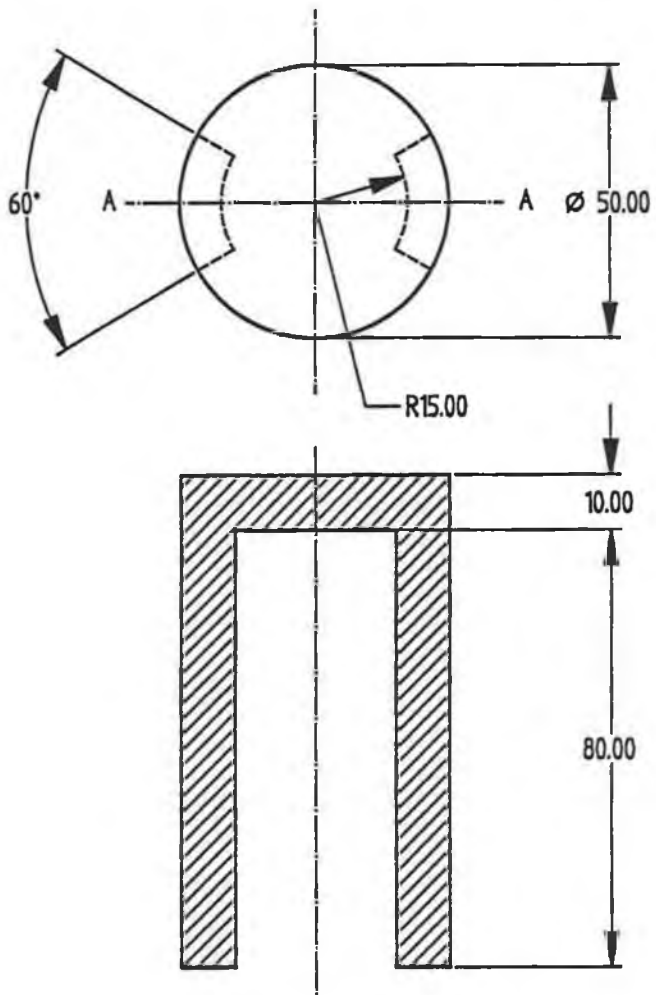
PART # 5 - GUIDE PIN
MATERIAL - D-2

01-02-03
25/91 D-2
T380681 - C4
HI - LIFE

PART # 6 - SPRING



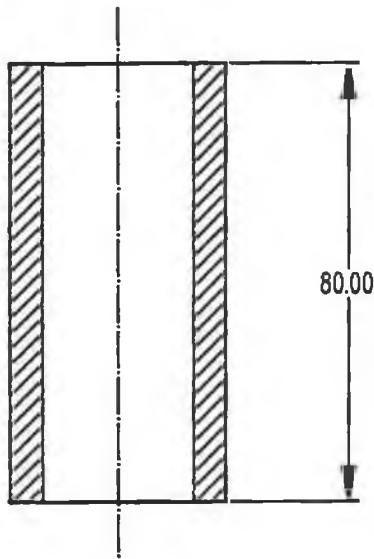
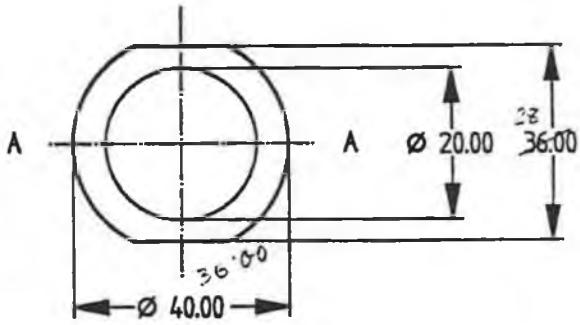
SPRING CONSTANT = 10 N/mm
TURN/cm = 2
WIRE \varnothing = 2mm
OUTSIDE \varnothing = 14.50mm
INSIDE \varnothing = 10.50mm



SECTION AA

PART # 7 - EJECTION TOOL
MATERIAL - STAINLESS STEEL

PART # 8 - SINGLE ACTION BLOCK
MATERIAL - STAINLESS STEEL



APPENDIX B
CALCULATION PROCEDURE FOR RSM

APPENDIX B

B1: Calculation of the coefficient b

The value of the coefficients "b" of the model was computed by least square method, that is, $b = (X^T X)^{-1} X^T y$. The matrix of independent variables X for the nine tests is given below:

$$X = \begin{array}{ccc|c} x_0 & x_1 & x_2 & \text{Trial no.} \\ \hline 1 & -1 & -1 & 1 \\ 1 & 1 & -1 & 2 \\ 1 & -1 & 1 & 3 \\ 1 & 1 & 1 & 4 \\ 1 & 0 & 0 & 5 \\ 1 & 0 & 0 & 6 \\ 1 & 0 & 0 & 7 \\ 1 & 0 & 0 & 8 \\ 1 & 0 & 0 & 9 \end{array}$$

and

$$X^T = \begin{array}{c|cccccccc} & 1 & 1 & 1 & 1 & 1 & 1 & 1 & 1 & 1 \\ \hline -1 & 1 & -1 & 1 & 0 & 0 & 0 & 0 & 0 & 0 \\ -1 & -1 & 1 & 1 & 0 & 0 & 0 & 0 & 0 & 0 \end{array}$$

Hence

$$(X^T X) = \begin{vmatrix} 9 & 0 & 0 \\ 0 & 4 & 0 \\ 0 & 0 & 4 \end{vmatrix}$$

and

$$(X^T X)^{-1} = \begin{vmatrix} 1/9 & 0 & 0 \\ 0 & 1/4 & 0 \\ 0 & 0 & 1/4 \end{vmatrix}$$

B2: Calculation of confidence intervals: First order model

The calculation steps for the error limits are given below:

$$\hat{y} \pm t_{\alpha/2, df} \sqrt{V(\hat{y})}$$

where

$$V(\hat{y}) = C^T s^2$$

Step 1

Estimated error for variance s^2 based on the residual sum of square $S(b)$ is:

$$s^2 = \frac{S(b)}{DF}$$

Step 2

Calculation of the variance-covariance matrix for \mathbf{b} is $(\mathbf{X}^T\mathbf{X})^{-1}s^2$, where $(\mathbf{X}^T\mathbf{X})^{-1}$ is given earlier.

Step 3

Calculation of variance: The variance, $V(\hat{y})$, was as follows:

$$\begin{aligned} V(\hat{y}) &= V(b_0 + b_1x_1 + b_2x_2) \\ &= V(b_0) + x_1^2V(b_1) + x_2^2V(b_2) \\ &= \left(\frac{1}{9} + \frac{1}{4} + \frac{1}{4}\right)s^2 \\ &= \left(\frac{11}{18}\right)s^2 \end{aligned}$$

95 percent confidence interval for \hat{y} is

$$\hat{y} \pm t_{df, \alpha/2} \sqrt{V(\hat{y})}$$

B3: Adequacy of the postulated model:

In order to perform the analysis of variance, the total sum of the square, $\sum y^2$, is usually divided into contributions due to the “zero-order terms”, “first-order terms”, “the lack of fit”, and “pure error”. The sum of square of individual items divided by their respective degrees of freedom give the mean square. The mean square of lack of fit can be compared with the mean square of pure error to test the adequacy of the postulated model by using the F distribution.

The detailed formulae for the analysis of the variance used in this investigation is given in Table 1, where n_o is the number of central points, n_c the number of corner points, N the total number of experimental points, k is the dimension of design (for 2^2

full factorial design the value of k is 2), y_{ni} , the logarithm of observed responses at the central point with mean \bar{y}_o , and (iy) the sum of the cross-products of the columns in the X matrix with the column y of observation.

Table B1: Formulae for the analysis of variance of the first order model

Source	Sum of square (SS)	Degrees of freedom (DF)
Zero-order term	$\left(\sum_{i=1}^N y_i \right)^2 / N = n\bar{y}^2$	1
First-order term	$\sum_{i=1}^k b_i(iy)$	k
Lack of fit	By subtraction	$n_c - k$
Pure error	$\sum_{i=1}^{n_o} (y_{ni} - \bar{y}_o)^2$	$n_o - 1$
Total	$\sum_{i=1}^N y_i^2$	N

APPENDIX C

PUBLICATIONS ON THIS WORK

1. A N M Karim, R Puyané, M A El-Baradie, M S J Hashmi, "Effect of Compaction Parameters on the Physical Properties of Zinc Oxide Varistor Discs", pp 286-291, Proc. Int. Con. on Mechanics of Solids and Mat. Eng., Singapore, June 1995, edited by N L Loh et al,
2. A N M Karim, R Puyané, M A El-Baradie, M S J Hashmi, "Holding Time in Pressing Cycle and Its Influence on the Performance Characteristics of Zinc Oxide Varistor Discs", pp506-511, Proc. Int. Con. on Advances in Mat. & Processing Tech., August, 1995.
3. A N M Karim, R Puyané, M A El-Baradie, M S J Hashmi, "Long and Short Duration Pulse Performance of Zinc Oxide Varistor Compacted with Modified Pressing Cycle", presented and accepted for publication in the Proc. on 1996 World Congress on Powder Metallurgy and Particulate Materials, Washington, D.C.
4. A N M Karim, R Puyané, M A El-Baradie, M S J Hashmi, "Performance Characteristics of Zinc Oxide Varistor Processed Under Different Pressing Conditions" presented and accepted for publication in the Proc. on 1996 World Congress on Powder Metallurgy and Particulate Materials, Washington, D.C